

Topological Fluid Dynamics For Free and Viscous Surfaces

Balci, Adnan; Brøns, Morten

Publication date:
2016

Document Version
Publisher's PDF, also known as Version of record

[Link back to DTU Orbit](#)

Citation (APA):
Balci, A., & Brøns, M. (2016). Topological Fluid Dynamics For Free and Viscous Surfaces. Kgs. Lyngby: Technical University of Denmark (DTU). (DTU Compute PHD-2015; No. 379).

DTU Library

Technical Information Center of Denmark

General rights

Copyright and moral rights for the publications made accessible in the public portal are retained by the authors and/or other copyright owners and it is a condition of accessing publications that users recognise and abide by the legal requirements associated with these rights.

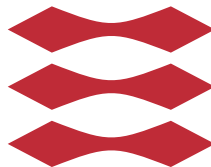
- Users may download and print one copy of any publication from the public portal for the purpose of private study or research.
- You may not further distribute the material or use it for any profit-making activity or commercial gain
- You may freely distribute the URL identifying the publication in the public portal

If you believe that this document breaches copyright please contact us providing details, and we will remove access to the work immediately and investigate your claim.

Topological Fluid Dynamics For Free and Viscous Surfaces

Adnan BALCI

DTU



Kongens Lyngby 2015
PhD-2015-379

Technical University of Denmark
Department of Applied Mathematics and Computer Science
Building 303B, DK-2800 Kongens Lyngby, Denmark
Phone +45 4525 3031, Fax +45 45882673
compute@compute.dtu.dk
www.compute.dtu.dk PhD-2015-379

Summary (English)

In an incompressible fluid flow, streamline patterns and their bifurcations are investigated close to wall for two-dimensional system and close to free and viscous surfaces in three-dimensional system. Expanding the velocity field in a Taylor series, we conduct a local analysis at the given expansion point. Applying the boundary conditions, some relations are obtained among the coefficients of the expansions. Series of coordinate transformations, which preserves the boundary conditions, are used to reduce the number of coefficients. Finally, using the normal form and unfolding theory, the velocity field is analysed structurally and bifurcation diagrams are obtained.

First, two-dimensional viscous flow close to wall for non-simple degenerate critical point is considered depending on three-parameter space. Second, three-dimensional axisymmetric, viscous and steady flow is analysed close to free and viscous surfaces into three situations: Local analysis close to center axis; away from the axis and close to a stationary wall. Next, in the absence of axisymmetric condition, three-dimensional viscous flow is considered close to a free surface.

As an application of the bifurcation diagrams for three-dimensional axisymmetric viscous flow, three different shaped container driven by a rotating top disk is considered. Using a spectral collocation method, a code is constructed to obtain the meridional and swirl velocities. In a result of this code, all structural changes on the streamline patterns are observed and the occurring bifurcations are determined. These bifurcations are compared with the bifurcations obtained from topologically.

Preface

This thesis was prepared at DTU Compute in fulfilment of the requirements for acquiring a Ph.D. in Applied Mathematics and Computer Science.

Thanks to all my colleagues and Danish citizens for providing a very happy and good atmosphere. I am very glad to work with Professor Morten Brøns, especially thanks to him for his encouragement and valuable guidance.

For the external research, I stayed at the Department of Aerospace Engineering and Fluid Mechanics in Seville, Spain. Thanks to Miguel Angel Herrada for his technical help.

Finally, I would like to thank Turkish Military Academy for their meaningful supports in scientific research.

Lyngby, 30-August-2015

A handwritten signature in black ink on a light gray rectangular background. The signature is cursive and appears to read 'Adnan'.

Adnan BALCI

Contents

Summary (English)	i
Preface	iii
1 Introduction	1
2 Topological Fluid Dynamics	5
2.1 Flows and Vector Fields	6
2.2 Topological Equivalence and Structural Stability	9
2.3 Unfolding of degenerate critical points	10
2.4 Normal Forms	10
2.5 Bifurcation Theory for Dynamical Systems	13
2.6 Hamiltonian Systems and Stream Function	14
2.7 Basic Equations and Boundary Conditions for a Steady Flow . .	16
2.7.1 Viscous Surface	19
2.7.2 Free Surface	21
3 Unfolding of Non-simple Degenerate Streamline Patterns Near a No-slip Wall	23
3.1 Normal form for the degenerate case	26
3.2 Unfolding of the degenerate case	27
3.3 Bifurcation analysis of the normal form	29
3.3.0.1 Local bifurcation for on-wall critical points . . .	30
3.3.0.2 Local bifurcation for off-wall critical points . . .	31
3.3.0.3 Global bifurcation associated with on-wall and off-wall critical points	32
3.3.0.4 Global bifurcation associated with off-wall critical points	33
3.4 Application	38

4	Topology of axisymmetric flow near a free surface	43
4.1	Basic Equations and Boundary Conditions for an Axisymmetric Flow	46
4.2	Flow Topology Close to Center Axis	48
4.2.1	Regular Case	52
4.2.2	Co-dimension 1 bifurcation	53
4.2.3	Co-dimension 2 bifurcations	56
4.2.3.1	Case 1	56
4.2.3.2	Case 2	63
4.2.4	Co-dimension 3 bifurcations	68
4.2.4.1	Case 1	68
4.2.4.2	Case 2	80
4.2.4.3	Case 3	85
4.3	Flow Topology Away From The Axis	89
4.3.1	Regular Case	91
4.3.2	Case 1	92
4.3.3	Case 2	98
4.3.4	Case 3	102
4.4	Flow Topology Close to a Stationary Wall	106
4.4.1	Regular Case	107
4.4.2	Co-dimension 1 bifurcation	108
4.4.3	Co-dimension 2 bifurcation	110
4.4.3.1	Case 1	110
4.4.3.2	Case 2	112
4.4.4	Co-dimension 3	114
4.4.4.1	Case 1	115
4.4.4.2	Case 2	118
4.4.4.3	Case 3	120
4.5	Flow Topology Close to a Stationary Wall with a Flat Interface .	123
4.5.1	Regular Case	124
4.5.2	Co-dimension 1 bifurcation	124
4.5.3	Co-dimension 2 bifurcations	127
4.5.3.1	Case (a)	127
4.5.3.2	Case (b)	130
4.6	Conclusion	133
5	Topology of axisymmetric flow near a viscous surface	135
5.1	Flow topology of The Viscous Surface Close To Axis	137
5.1.1	Co-dimension 1 bifurcation on viscous surface	138
5.1.2	Co-dimension 2 bifurcation on viscous surface	139
5.1.2.1	Case (a)	139
5.1.2.2	Case (b)	142
5.2	Flow topology of The Viscous Surface Away From Axis	143
5.3	Flow topology of The Viscous Surface Close To Wall	143

5.3.1	Co-dimension 1 bifurcation	144
5.3.2	Co-dimension 2 bifurcation	145
6	Topology of 3D flow near a free surface	149
6.1	Prerequisites	150
6.1.1	3D Flow Topology In One Fluid	151
6.2	Case 1: $trB = 0$ and $DetB < 0$	155
6.3	Case 2: $trB = 0$ and $DetB > 0$	158
6.4	Case 3: $trB \neq 0$ and $DetB = 0$	164
6.5	Conclusion	166
7	Numerical Investigations of creeping vortex breakdown flows	169
7.1	Problem Formulation	170
7.2	Numerical Procedures	174
7.2.1	Transformation of Equations	174
7.2.2	Linear Problem	174
7.2.3	Discretization	174
7.3	Bifurcation Analysis for LP	176
7.3.1	Topological metamorphoses of air-water flow in the $\alpha = 120$ cone as H_w increases	178
7.3.2	Topological flow metamorphoses in the $\alpha = 60$ cone as H_w increases	180
7.3.3	Conclusion	183
7.4	Bifurcation Analysis for MP	183
7.4.1	Topological metamorphoses of air-water flow in the $\beta = 30$ cone as H_w increases	184
7.4.2	Topological metamorphoses of air-water flow in the $\beta = 45$ and $\beta = 60$ cone as H_w increases	186
7.4.3	Conclusion	187
7.5	Bifurcation Analysis for RP	187
7.5.1	Conclusion	189
7.6	Conclusion	189
	Bibliography	191

Introduction

In fluid mechanics, the type of fluid flow has a major significance to determine the flow motion. Many studies have been published by considering the type of flow. For example, the flow type is stationary if it does not depend on time. One may vary this example in many ways. In this thesis, we mainly focus on two types of fluid flow. One is two-dimensional steady incompressible fluid flow close to a stationary wall, and other is three-dimensional steady incompressible fluid flow close to free and viscous surfaces.

In Chapter 2, we introduce the notion of autonomous dynamical system. Main prerequisites for the forthcoming chapters are given. This chapter includes as a concept, the definition of vector fields and flow, topological conjugacy and equivalence, structural stability of a vector field, normal form and unfolding theory. As a consequence of the unfolding theory, a parameter space is created which we will use in bifurcation analysis. The bifurcation theory and its classification are given. Furthermore, Hamiltonian systems are introduced for two-dimensional and axisymmetric flow. And finally, some boundary conditions for free and viscous surface and Navier-Stokes equations are given for a steady three-dimensional flow.

Chapter 3 is intended to motivate our investigation of two-dimensional viscous flow close to a stationary wall. Revisiting Hartnack's [19] paper, we observe the non-simple degenerate streamline patterns for co-dimension three bifurcation.

The reason is that Hartnack mentions the effect of the Navier-Stokes equations on the streamline topology. In a conclusion of this effect, he declare that it is impossible to see $\tilde{a}_{0,4} = 0$ for a steady flow. Therefore assuming that parameter is zero, the streamline patterns and their bifurcation is analysed in analytical and numerical way. This study is published in

- * A. Balci, M. Andersen, M. C. Thompson and M. Brøns: Codimension three bifurcation of streamline patterns close to a no-slip wall: A topological description of boundary layer eruption. *Physics of Fluids*, 27(5), 2015.

In Chapter 4 and 5, we consider a steady axisymmetric incompressible flow close to free and viscous surfaces, respectively. Since the flow is axisymmetric, the process is closely similar as Chapter 3, due to the existence of stream function. Expanding the velocity field at a specific (after coordinate transformation can be chosen as origin) point, we investigate the streamline patterns and their bifurcations in meridional plane by taking into account the swirl velocity effect. We divide these chapters into three cases:

- (a) close to center axis,
- (b) away from the center axis,
- (c) close to a stationary wall.

These cases are investigated up to the co-dimension three for free surface and up to the co-dimension two for viscous surface.

In Chapter 6, three-dimensional viscous flow is considered close to a free surface. As known, there exist no stream function for three-dimensional flow. Hence we expand the velocity fields separately and investigate the streamline patterns and bifurcations. In Chapters 3 – 6, the normal form transformation is used to simplify the given velocity fields. Obtaining the degenerate and non-degenerate critical points, we investigate the streamline patterns. Since the degenerate critical points are not structurally stable, using the unfolding theory we decide the parameters which will effect the streamline structure. As a final work, the bifurcation theory is used to determine which kind of structural changes occur.

In Chapter 7, we consider a steady axisymmetric flow for two immiscible fluids in three different shaped container in a numerical way. Using the spectral collocation method, the streamline patterns are obtained. We compare these streamline patterns with the streamline patterns in Chapter 4. The results of this numerical analysis contribute to:

- * A. Balci, M. Brøns, M. A. Herrada and V. Shtern : Bifurcations of a creeping air-water flow in a conical container. Submitted for publication. 2015.
- * A. Balci, M. Brøns, M. A. Herrada and V. Shtern : Vortex breakdown in a conical bioreactor. Submitted for publication. 2015.
- * A. Balci, M. Brøns, M. A. Herrada and V. Shtern : Vortex breakdown in a semispherical bioreactor. Submitted for publication. 2015.

CHAPTER 2

Topological Fluid Dynamics

Fluid dynamics generally deals with fluid flow, or the motion of fluids. One can formulate or depict the equations of fluid dynamics in two ways: the Lagrangian and Eulerian description of fluid flow. The Eulerian indicates that in each flow property time and the position vector \vec{x} are the independent variables. Therefore, any flow properties are in the form

$$p = p(\vec{x}, t), \quad \vec{v} = \vec{v}(\vec{x}, t), \quad (2.1)$$

where p is the pressure (scalar field), and v is the velocity (vector field). In the Lagrangian description, instead of the vector fields, an individual fluid particle is considered. The location of the fluid particle is given at a specific point \vec{x}_0 ; and for this approach, the independent variables are \vec{x}_0 and time. Hence, the position of the particle is

$$\vec{x} = \vec{x}(\vec{x}_0, t). \quad (2.2)$$

The Lagrangian description of fluid flow can be considered as an integration of the Eulerian description of fluid flow with the initial conditions. Moreover, one can make these descriptions be related each other by using the substantial (or material) derivative.

The fluid flows can be visualized and described by using streamlines, which are tangent to the velocity field at a given instant of time. In Cartesian coordinate $\tilde{\mathbf{x}} = (x, y, z)$ with corresponding the velocities $\tilde{\mathbf{v}} = (u, v, w)$, the streamline

curves can be obtained by solving the following ordinary differential equations, which are in scalar form,

$$\frac{dx}{u} = \frac{dy}{v} = \frac{dz}{w}, \quad (2.3)$$

with a given initial condition. Defining new variables, we can write any ordinary differential equation as a system. A general system of first order ODEs is simply in the following form

$$\tilde{\mathbf{v}} = \dot{\mathbf{x}} = f(t, \mathbf{x}), \quad (2.4)$$

where f is a smooth function and $\dot{x} = \frac{dx}{dt}$. If f does not depend on time explicitly, the system is called 'autonomous'. Our concern will be this kind of system in this thesis. The following section centers on how the flow can be expressed topologically using autonomous system.

2.1 Flows and Vector Fields

A fluid particle has a position and velocity in a given coordinate system. Let the position vector of the flow be $\mathbf{x} = (x_1, x_2, \dots, x_n) \in \mathbb{R}^n$ and an open set $S \subseteq \mathbb{R}^n$. From the definition of velocity, the derivative of the position vector with respect to time t gives

$$\vec{v}(u_1, u_2, \dots, u_n) = \frac{d\mathbf{x}}{dt} = f(x_1, x_2, \dots, x_n), \quad (2.5)$$

where $f : S \rightarrow \mathbb{R}^n$ is a smooth function and does not explicitly depend on time t . The function f is also named as a velocity field.

A flow $\Phi(x, t) : S \times \mathbb{R} \rightarrow \mathbb{R}^n$ is a differentiable mapping such that

- a) $\Phi(x, 0) = x$, and
- b) for all t and $s \in \mathbb{R}$,

$$\Phi(x, t) \circ \Phi(x, s) = \Phi(x, t + s), \quad (2.6)$$

where \circ is the composition symbol.

The flow can be associated with the vector field, and it is written as

$$\left. \frac{d\Phi(x, t)}{dt} \right|_{t=t_0} = f(x), \quad (2.7)$$

for all $t_0 \in \mathbb{R}$ and $x \in S$. This equation tells us that the flow is a solution of (2.5). From this, the following lemma (see Meiss [1]) derives.

LEMMA 2.1 *Let $\Phi(x, t)$ be a flow, it is then a solution of the I.V.P.*

$$\frac{d\Phi(x_0, t)}{dt} = f(\Phi(x_0, t)), \quad \Phi(x_0, 0) = x_0, \quad (2.8)$$

for (2.5).

For the proof of this lemma and the theorem concerning the existence and uniqueness of solutions, I am pleased to refer Meiss [1].

Orbits or trajectories denoted by $x(t)$ are seen in every dynamical system, and the solutions of (2.8) imply them. If we put all orbits in a set, this set will be a phase portrait. Some of the trajectories in this phase portrait, which fulfill $f(x) = 0$, will be our interest for the reason that the analysis of a streamline starts with a point x_0 which satisfies $f(x_0) = 0$. This point is called a critical point.

The critical point is called 'stable', if for $\forall \epsilon > 0$ there is a $\delta > 0$ such that

$$|\Phi(x, 0) - x_0| < \delta \quad \text{implies} \quad |\Phi(x, t) - x_0| \leq \epsilon \quad \text{for} \quad \forall t \geq 0, \quad (2.9)$$

'asymptotic stable', if the critical point is stable and for some $\delta > 0$

$$|\Phi(x, 0) - x_0| < \delta \quad \text{implies} \quad |\Phi(x, t) - x_0| \rightarrow 0 \quad \text{as} \quad t \rightarrow \infty. \quad (2.10)$$

Any asymptotic stable critical point is also stable, but converse is not correct. If the critical point is not stable, we will call it *unstable*.

Physically, the critical points occur when the velocity is zero. This point has many different names in the literature such as stagnation point, fixed point, equilibrium point. When the function $f(x)$ is infinitely differentiable, one is able to analyse the system in the vicinity of the critical point by using Taylor series expansion. Let us denote the critical point as ' x_0 ', the system (2.5) then has a Taylor expansion at this point

$$\dot{x} = f(x_0) + Df(x_0)(x - x_0) + \mathcal{O}(|x - x_0|^2), \quad (2.11)$$

where D denotes the differential operator and we will call $\dot{x} = Df(x_0)(x - x_0)$ the linearization of (2.5). There is a connection between the linearized system and non-linear one which is provided by Hartman-Grobman Theorem. Prior to giving the theorem, let us first to define some prerequisites which are hyperbolic critical points and topological conjugacy-equivalence.

DEFINITION 2.2 Hyperbolic Critical Points: The critical point is hyperbolic, if the eigenvalues of $Df(x_0)$ have non-zero real part. Otherwise it is non-hyperbolic critical point.

DEFINITION 2.3 Topological Conjugacy Assume that R and T are topological spaces, $\Phi(x, t)$ and $\varphi(x, t)$ two flows. The flows $\Phi : R \times \mathbb{R} \rightarrow R \times \mathbb{R}$ and $\varphi : T \times \mathbb{R} \rightarrow T \times \mathbb{R}$ are conjugate if there is a homeomorphism $h : R \rightarrow T$ such that for each $x \in R$ and all $t \in \mathbb{R}$

$$h(\Phi(x, t)) = \varphi(h(x), t). \quad (2.12)$$

THEOREM 2.4 Hartman-Grobman Theorem

If the velocity field (2.5) with flow $\Phi(x, t)$ has a hyperbolic critical points, then there exist a neighbourhood ϵ such that the non-linear system and the linearized system are topologically conjugate on ϵ .

For the proof of this theorem we consult Meiss [1]. Simply, this theorem states that the linear part of the vector field determines the topology of critical points.

Let λ_i be the eigenvalues of $Df(x_0)$, the hyperbolic critical points for two-dimensional flow can be investigated into four classes:

- (a) sink: if $\forall Re(\lambda_i) < 0$. (Stable Node)
- (b) source: if $\forall Re(\lambda_i) > 0$. (Unstable Node)
- (c) saddle: if at least one $Re(\lambda_i) < 0$, neither a sink nor a source.
- (d) focus: if the eigenvalues are complex and $Re(\lambda_i) \neq 0$. Depending of their stabilities focuses are a sink or a source.

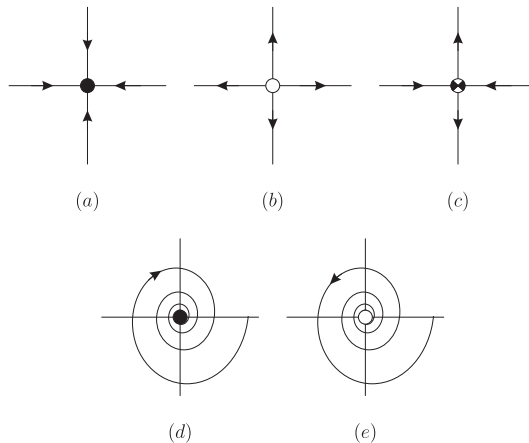


Figure 2.1: The stabilities of the hyperbolic critical points (a) sink (stable node) (b) source (unstable node) (c) saddle (d) sink (stable focus) (e) source (unstable focus).

Until now, the local analysis of the hyperbolic critical points is mainly pointed out by linearising the given velocity field. For the non-hyperbolic critical points we can not use the Hartman-Grobman Theorem. The non-hyperbolic critical points are the degenerate critical points occur when $\det(Df(x_0)) = 0$, which have four cases, see Meiss [1].

2.2 Topological Equivalence and Structural Stability

The structure of streamline patterns is the main interest in this thesis. In a different system the streamline patterns can be alike. Even though topological conjugacy helps us to correspond the each trajectories of flows $\Phi(x, t)$ and $\varphi(x, t)$, it is too restrictive to make the trajectories same in phase portrait. However the next theorem will protect to shape and direction of flows which will make two streamline patterns alike:

DEFINITION 2.5 Topological Equivalence Assume that R and T are topological spaces, $\Phi(x, t)$ and $\varphi(x, t)$ two flows. The flows $\Phi : R \times \mathbb{R} \rightarrow R \times \mathbb{R}$ and $\varphi : T \times \mathbb{R} \rightarrow T \times \mathbb{R}$ are equivalent if there is a homeomorphism $h : R \rightarrow T$, that maps the streamlines of $\Phi(x, t)$ onto the streamlines of $\varphi(x, t)$ (preserving the direction of time).

Since our concern is just investigating a flow in a local area, defining h in a subset of the flow domain, we can say $\Phi(x, t)$ and $\varphi(x, t)$ are locally topological equivalent.

The question is why we need that equivalence. A small perturbations in the flow field may result a structural difference or not in the streamline patterns. If the phase portrait of flows is not effected by a small perturbations, we will call the system is structurally stable. The following definition will give us the main idea.

DEFINITION 2.6 Structurally stability Suppose $v(x)$ is a continuously differentiable vector field. If all perturbations $v(x) + \epsilon(x)$ are topologically equivalent to $v(x)$ where $\epsilon(x)$ is sufficiently small, the vector field $v(x)$ is structurally stable.

Note that this depends on the class of perturbations, hence we will discuss this in Hamiltonian case separately. The structural stability of the hyperbolic

critical points can be directly obtained by implicit function theorem, see details Kuznetsov [2].

DEFINITION 2.7 Implicit Function Theorem: Let us consider an open set $S \subset \mathbb{R}^n \times \mathbb{R}^k$, and T is continuously differentiable function in (S, \mathbb{R}^n) . Assume a point $(x_0, c_0) \in S$ such that $T(x_0; c_0) = \tau$ and $D_x T(x_0; c_0)$ is a non-singular matrix. Then there are open sets $U \subset \mathbb{R}^n$ and $V \subset \mathbb{R}^k$ and a unique continuously differentiable function $f(c) : U \rightarrow V$ for which $x_0 = f(c_0)$ and $T(f(c); c) = \tau$.

If one needs to locate bifurcation, the degenerate critical points need to be investigated. Because these critical points are structurally unstable, they can be affected by a small perturbation.

2.3 Unfolding of degenerate critical points

A small perturbation in the velocity field creates a bifurcation for the degenerate critical points. This perturbation can be called an unfolding of the degenerate critical points. Creating a new small parameters by using unfolding, a new structure for the velocity field may arise.

Mathematically, let us consider the system (2.7). Assume that the origin is a degenerate critical point. We can define the unfolding of this degenerate critical point as:

DEFINITION 2.8 Unfolding A family of vector fields $f(x; \mu)$, at origin $f(x; 0) = f(x)$, is said to be an unfolding of given degenerate critical point .

The implicit function theorem sheds light on focusing on a neighbourhood of a given parameter value. To make a local bifurcation analysis, one needs to investigate a local degenerate structure. The degeneracy degree of this structure will be expressed by the number of parameter. Depending on these parameters we will make a bifurcation analysis.

2.4 Normal Forms

The most important process in a way to analyse bifurcations in multidimensional systems is to simplify a dynamical system as much as possible. We will restrict

our attention to find the simplest system by using a near identity transformation. Let the autonomous system is given as

$$\dot{\mathbf{x}} = A\mathbf{x} + f_2(\mathbf{x}) + f_3(\mathbf{x}) + \dots \quad (2.13)$$

where $\mathbf{x} \in \mathbb{R}^n$, A is an $n \times n$ matrix and f_i homogeneous vector polynomials with the order i . The terms of f_i are a linear combination of the following form

$$x_1^{i_1} x_2^{i_2} \dots x_n^{i_n} \quad \text{with} \quad \sum_{j=1}^n i_j = i. \quad (2.14)$$

To simplify the vector field (2.13), let a near identity transformation be given as

$$\mathbf{x} = \xi + h(\xi) \quad (2.15)$$

where h is a sum of h_i which have the same property as f_i . Differentiation of (2.15) is

$$\dot{\mathbf{x}} = \left(I + \frac{\partial h(\xi)}{\partial \xi} \right) \dot{\xi} \quad (2.16)$$

where $\frac{\partial h(\xi)}{\partial \xi}$ is the Jacobian of $h(\xi)$. Applying the transformation (2.15) into the dynamical system (2.13), we have

$$\left(I + \frac{\partial h(\xi)}{\partial \xi} \right) \dot{\xi} = A(\xi + h(\xi)) + f_2(\xi + h(\xi)) + f_3(\xi + h(\xi)) + \dots \quad (2.17)$$

The continuity of the Jacobian and $\det \left| I + \frac{\partial h(\xi)}{\partial \xi} \right| \neq 0$ ensures that we can multiply both sides with the inverse of $\left(I + \frac{\partial h(\xi)}{\partial \xi} \right)$ which gives

$$\dot{\xi} = \left(I + \frac{\partial h(\xi)}{\partial \xi} \right)^{-1} (A(\xi + h(\xi)) + f_2(\xi + h(\xi)) + f_3(\xi + h(\xi)) + \dots) \quad (2.18)$$

where the inverse matrix expansion is

$$\left(I + \frac{\partial h(\xi)}{\partial \xi} \right)^{-1} = I - \frac{\partial h_2(\xi)}{\partial \xi} - \frac{\partial h_3(\xi)}{\partial \xi} + \left(\frac{\partial h_2(\xi)}{\partial \xi} \right)^2 + \dots \quad (2.19)$$

Thus, eq. (2.18) can be written as

$$\begin{aligned} \dot{\xi} = & A\xi + \left(Ah_2(\xi) - \frac{\partial h_2(\xi)}{\partial \xi} A\xi + \tilde{f}_2(\xi) \right) \\ & + \left(Ah_3(\xi) - \frac{\partial h_3(\xi)}{\partial \xi} A\xi + \tilde{f}_3(\xi, h_2(\xi)) \right) + \mathcal{O}(\xi^4), \end{aligned} \quad (2.20)$$

where

$$\tilde{f} = \left(I + \frac{\partial h(\xi)}{\partial \xi} \right)^{-1} f(\xi + h(\xi)) + \left(\frac{\partial h_2(\xi)}{\partial \xi} \right)^2 A\xi - \frac{\partial h_2(\xi)}{\partial \xi} Ah_2(\xi) + \dots \quad (2.21)$$

If we want to remove the quadratic terms from (2.20), the following needs to be solved

$$\left(Ah_2(\xi) - \frac{\partial h_2(\xi)}{\partial \xi} A\xi + f_2(\xi) \right) = 0. \quad (2.22)$$

This is called the homological equation for h_2 . We need to choose h_2 such that it will simplify the given dynamical systems as much as possible and we will call that simplified dynamical system is normal form. Note that when A is the zero matrix, h_2 disappears from (2.22) and it can never be solved. In many cases in this thesis, this is actually the case. Nevertheless, near-identity transformations can be used to obtain simplifications as we shall see in the following chapters.

Let us illustrate the method with an example.

EXAMPLE 2.1 *Let us consider an one-dimensional system whose Taylor expansion is*

$$\dot{x} = \gamma_1 x + \gamma_2 x^2 + \gamma_3 x^3 + \mathcal{O}(x^4) \quad (2.23)$$

Let us represent a near identity transformation

$$x = \xi + \alpha_2 \xi^2 + \alpha_3 \xi^3 + \mathcal{O}(\xi^4). \quad (2.24)$$

We want to choose the α_i to simplify (2.23). Differentiating (2.24) and substituting into (2.23) we obtain

$$\dot{\xi}(1 + 2\alpha_2 \xi + 3\alpha_3 \xi^2 + \mathcal{O}(\xi^3)) = \gamma_1 \xi + (\gamma_2 + \alpha_2 \gamma_1) \xi^2 + \mathcal{O}(\xi^3). \quad (2.25)$$

Dividing both sides by $(1 + 2\alpha_2 \xi + 3\alpha_3 \xi^2 + \mathcal{O}(\xi^3))$ and expanding in power series, one can obtain

$$\dot{\xi} = \gamma_1 \xi + (\gamma_2 - \alpha_2 \gamma_1) \xi^2 + \mathcal{O}(\xi^3). \quad (2.26)$$

Assuming $\gamma_1 \neq 0$ and choosing

$$\alpha_2 = \frac{\gamma_2}{\gamma_1} \quad (2.27)$$

it is possible to eliminate the quadratic term.

It will be worth pointing out that the normal form of the velocity field is locally topologically equivalent to the given velocity field.

2.5 Bifurcation Theory for Dynamical Systems

The unfolding of a degenerate critical points create some new parameters in the system. Let us define this system as

$$\dot{x} = f(x; \mu_i), \quad i \geq 1 \quad (2.28)$$

where μ_i is a set of parameters. In fluid structure, these parameters can be gravity, Reynolds number, viscosity etc. A small perturbation of these parameters may affect the system and change the structure of flow. The structurally changes on the system can be called bifurcations.

The next example may clarify the main idea:

EXAMPLE 2.2 *Let us consider a special unfolding for a one-dimensional flow*

$$\dot{x} = \mu + x^2. \quad (2.29)$$

The critical points, which can be obtained by solving $\dot{x} = 0$, are $x = -\sqrt{\mu}$ and $x = \sqrt{\mu}$. Depending on the sign of μ , the number of critical point may vary. The creation and destruction of critical point can be seen in Fig. 2.2.

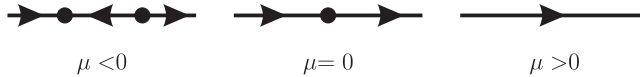


Figure 2.2: Creation and destruction the critical point, arrows demonstrate the direction of velocity.

$\mu = 0$ is called a bifurcation point, due to the fact that the creation starts at that point. This bifurcation type is a well-known bifurcation which is called saddle-node bifurcation. However we will call this kind of bifurcations, more generally, co-dimension one bifurcation because the number of parameter, needed to display the bifurcation, is just one.

Changing the stability of a critical point is known as local bifurcation, or it is a structurally change in the neighbourhood of a degenerate critical points.

There are also global bifurcations. These bifurcations are more difficult to analyse than local ones. Homo-clinic and hetero-clinic bifurcations can be given as examples for global bifurcations. To clarify, see Fig. 2.3.

In the following chapters, we will have bifurcation diagrams which will give us information about the critical points. In the bifurcation diagrams, one will

see the local and global bifurcations which show the structural changes in streamline patterns.

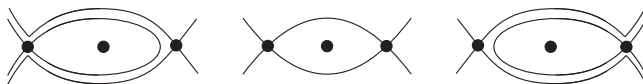


Figure 2.3: A hetero-clinic connection between two saddle points, broken in a global bifurcation.

Until now, we consider the general structure and system. From now on, we will specify the flow by considering the boundary conditions, total energy, continuity etc.

2.6 Hamiltonian Systems and Stream Function

Modelling a dynamical system by taking account no energy loss, the system is then called Hamiltonian, or conservative. The mathematical definition is:

DEFINITION 2.9 Hamiltonian System A dynamical system on \mathbb{R}^2 is Hamiltonian if the system expressed in the form

$$\dot{x} = \frac{\partial H}{\partial y}, \quad \dot{y} = -\frac{\partial H}{\partial x}, \quad (2.30)$$

where $H(x, y) \in C^2$.

Along the trajectories, the total derivative can be written as

$$\frac{dH}{dt} = \frac{\partial H}{\partial x} \frac{dx}{dt} + \frac{\partial H}{\partial y} \frac{dy}{dt} = 0, \quad (2.31)$$

from chain rule and (2.30). Hence, H is constant and the trajectories can be found as the contours defined by $H = \text{constant}$.

For an incompressible 2D flows or 3D axisymmetric flow, the stream function is defined and it is useful to plot streamlines. Incompressibility of the flows makes the velocity field divergence free, $\nabla \cdot \vec{v} = 0$. In a Cartesian coordinate system (x, y) , it follows a stream function $\psi(x, y)$ exists such that

$$u(x, y) = \frac{\partial \psi}{\partial y}, \quad v(x, y) = -\frac{\partial \psi}{\partial x}, \quad (2.32)$$

where $\vec{v} = (u, v)$. In cylindrical coordinate (r, θ, z) for axisymmetric flow, the stream function $\psi(r, z)$ exists (again due to the incompressibility) such that

$$u(r, z) = \frac{1}{r} \frac{\partial \psi}{\partial z}, \quad w(r, z) = -\frac{1}{r} \frac{\partial \psi}{\partial r}, \quad (2.33)$$

where $\vec{v} = (u, w)$.

The velocity field (2.5) in Cartesian coordinate system (x, y) can be written as

$$\dot{x} = \frac{\partial \psi}{\partial y}, \quad \dot{y} = -\frac{\partial \psi}{\partial x}, \quad (2.34)$$

and in cylindrical coordinate system (for axisymmetric flow) (r, θ, z) , it is in the form

$$\dot{x} = \frac{\partial \psi}{\partial z}, \quad \dot{y} = -\frac{\partial \psi}{\partial q}, \quad (2.35)$$

where $q = \frac{r^2}{2}$, which are Hamiltonian systems.

For Hamiltonian system, one can observe two kind of critical points which are *saddle* and *center*. Type of the critical points can be determined by the determinant of Jacobian matrix J of given Hamiltonian system,

* If $|J| < 0$, the critical point is *saddle*,

* If $|J| > 0$, the critical point is *center*,

where the Jacobian matrix is

$$J = \begin{pmatrix} \frac{\partial}{\partial x} \frac{\partial \psi}{\partial y} & \frac{\partial}{\partial y} \frac{\partial \psi}{\partial y} \\ -\frac{\partial}{\partial x} \frac{\partial \psi}{\partial x} & -\frac{\partial}{\partial y} \frac{\partial \psi}{\partial x} \end{pmatrix}. \quad (2.36)$$

Note that in general linear center is not structurally stable (non-hyperbolic) but for Hamiltonian system it is.

When $|J| = 0$, the critical point is *degenerate*, divided into two cases:

- (a) Simple degenerate critical point: J is not the zero matrix with zero being an eigenvalue with algebraic multiplicity two and geometric multiplicity one.
- (b) Non-simple degenerate critical point: J is the zero matrix with zero being an eigenvalue with algebraic and geometric multiplicity two.

A Taylor expansion of the stream function at any point (x_0, y_0) is written

$$\psi = \sum_{n,m} (x - x_0)^n (y - y_0)^m. \quad (2.37)$$

Depending on the flow conditions, one can reduce the number of coefficient from the given stream function. Hence, we will give some boundary conditions in the next section, which are used in this thesis.

2.7 Basic Equations and Boundary Conditions for a Steady Flow

In this section, we allude to some essential prerequisites to use in forthcoming chapters. Prior to investigation of the topological aspect, it will be useful to define the boundary conditions and the Navier-Stokes equations in order to reduce the number of coefficients in the velocity field.

Note that in this thesis, we assume that the flow is *steady, incompressible* and *viscous*.

In Cartesian coordinates (x, y, z) with the corresponding velocity components $\mathbf{v} = (u, v, w)$, the steady Navier-Stokes equation is written as

$$\rho(\mathbf{v} \cdot \nabla \mathbf{v}) = -\nabla p + \mu \nabla^2 \mathbf{v} + f, \quad (2.38)$$

$$\nabla \cdot \mathbf{v} = 0, \quad (2.39)$$

where ρ , p , μ and f are the density, pressure, dynamic viscosity and the other body forces acting on fluid, respectively. The body forces could be gravity force g , but this force can be included into pressure.

It is possible to find the Navier-Stokes equation for all coordinate systems in fluid mechanics textbooks. From one of them, Landau and Lifshitz [3] expressed (2.38) and (2.39) in cylindrical coordinates (r, θ, z) with corresponding velocity

component (u, v, w) as

$$\frac{1}{r} \frac{\partial(ru)}{\partial r} + \frac{1}{r} \frac{\partial v}{\partial \theta} + \frac{\partial w}{\partial z} = 0, \quad (2.40a)$$

$$\rho \left(\gamma \cdot \nabla u - \frac{v^2}{r} \right) = \mu \left(\nabla^2 u - \frac{u}{r^2} - \frac{2}{r^2} \frac{\partial v}{\partial \theta} \right) - \frac{\partial p}{\partial r}, \quad (2.40b)$$

$$\rho \left(\gamma \cdot \nabla v + \frac{uv}{r} \right) = \mu \left(\nabla^2 v - \frac{v}{r^2} + \frac{2}{r^2} \frac{\partial u}{\partial \theta} \right) - \frac{1}{r} \frac{\partial p}{\partial \theta}, \quad (2.40c)$$

$$\rho (\gamma \cdot \nabla w) = \mu \nabla^2 w - \frac{\partial p}{\partial z}, \quad (2.40d)$$

where

$$\nabla^2 = \frac{1}{r} \frac{\partial}{\partial r} \left(r \frac{\partial}{\partial r} \right) + \frac{1}{r^2} \frac{\partial^2}{\partial \theta^2} + \frac{\partial^2}{\partial z^2} \quad \text{and} \quad \gamma = \left(u, \frac{v}{r}, w \right). \quad (2.41)$$

In the forthcoming chapters, we investigate the flow close to a surface. On the surface, we have three kinds boundary conditions; kinematic, tangential stress and normal stress boundary conditions. Prior to introducing these boundary conditions, we need to give some basic tools.

Normal and tangential vector

The normal vector \mathbf{n} and the tangential vectors \mathbf{t}_1 and \mathbf{t}_2 of the surface $z = F(r, \theta)$ for the cylindrical coordinate (r, θ, z) are

$$\mathbf{n} = \left(1 + F_r^2 + \frac{1}{r^2} F_\theta^2 \right)^{-1/2} \left(-F_r, -\frac{1}{r} F_\theta, 1 \right), \quad (2.42a)$$

$$\mathbf{t}_1 = (1 + F_r^2)^{-1/2} (1, 0, F_r), \quad (2.42b)$$

$$\mathbf{t}_2 = \left(1 + \frac{1}{r^2} F_\theta^2 \right)^{-1/2} \left(0, 1, \frac{1}{r} F_\theta \right), \quad (2.42c)$$

where $F_r = \frac{\partial F}{\partial r}$ and $F_\theta = \frac{\partial F}{\partial \theta}$. For the Cartesian coordinate (x, y, z) , they are on the surface $z = F(x, y)$,

$$\mathbf{n} = (1 + F_x^2 + F_y^2)^{-1/2} (-F_x, -F_y, 1), \quad (2.43a)$$

$$\mathbf{t}_1 = (1 + F_x^2)^{-1/2} (1, 0, F_x), \quad (2.43b)$$

$$\mathbf{t}_2 = (1 + F_y^2)^{-1/2} (0, 1, F_y), \quad (2.43c)$$

where $F_x = \frac{\partial F}{\partial x}$ and $F_y = \frac{\partial F}{\partial y}$. These vectors are illustrated in Fig. 2.4. In *Wolfram* website [4], one can find detailed explanation of these vectors.

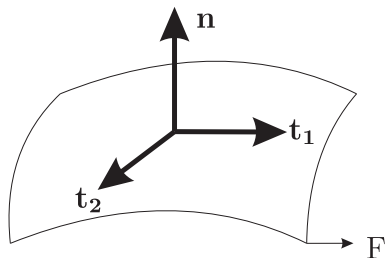


Figure 2.4: A surface F with the normal and tangential vectors.

We note that the kinematic and tangential stress boundary conditions help us to reduce the number of coefficients from (2.37), however, the normal stress boundary condition not. It just give us some physical relations between the coefficients of pressure expansion and the coefficients of velocity expansion. Therefore, we will consider them separately and taking into account the free and viscous surface.

For a viscous surface, we need to consider two immiscible fluids and for a free surface just one fluid.

Let us to use m , ($m = 1, 2$), subscript to separate given fluid. For instance, the velocity component u is u_1 for fluid 1 and u_2 for fluid 2.

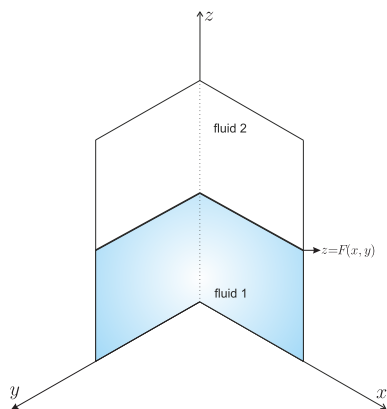


Figure 2.5: Two immiscible fluids with viscous surface.

2.7.1 Viscous Surface

It will be useful to express the radii of curvature, which we will use when we introduce the boundary conditions.

The sum of the principal radii of curvature

In three dimensional coordinate systems, more than one curvature at a given point exist. Each plane through this point containing the normal line to the surface cuts the surface in a plane. At this point, infinitely many planes exist, and they all have the normal. The curvature can be found by the relation of these planes with the surface.

Let consider the maximum and minimum of the set of curvatures R_1 and R_2 . They can be directly obtained by the differential geometry books, for instance [5]. However, our interest is only to find the average of the principal curvatures. That can be obtained from the mean curvature, because the mean curvature is in the form

$$H = \frac{1}{2} \left(\frac{1}{R_1} + \frac{1}{R_2} \right). \quad (2.44)$$

Hence, in the sequel our concern will be about obtaining the analysis of $2H$ (total curvature) of a given surface.

The mean curvature can be obtained by several approaches or formulas. We prefer the following formula,

$$2H = -\nabla \cdot \mathbf{n} = \frac{1}{R_1} + \frac{1}{R_2}, \quad (2.45)$$

where \mathbf{n} is the normal vector at a given point. This equality has been proved by Peters [6] and Henson [7].

Using the expression (2.45), the sum of radii of curvature of the surface $z = F(r, \theta)$ in cylindrical coordinates (r, θ, z) is written as

$$\frac{1}{R_1} + \frac{1}{R_2} = -\nabla \cdot \mathbf{n} = -\frac{1}{r} \left[\frac{\partial}{\partial r} \left(\frac{r}{M} F_r \right) + \frac{\partial}{\partial \theta} \left(\frac{1}{rM} F_\theta \right) \right], \quad (2.46)$$

where $M = \left(1 + (F_r)^2 + \frac{1}{r^2} (F_\theta)^2 \right)^{1/2}$ and \mathbf{n} is directed into fluid 1, and in Cartesian coordinate (x, y, z)

$$\frac{1}{R_1} + \frac{1}{R_2} = \frac{2F_{xy}F_xF_y - F_{yy}(F_x^2 + 1) - F_{xx}(F_y^2 + 1)}{(1 + F_x^2 + F_y^2)^{3/2}} \quad (2.47)$$

where the surface equation is $z = F(x, y)$.

Kinematic and Tangential Stress Boundary Conditions

The kinematic boundary condition states that the velocity field is parallel to the interface or surface, that means

$$\mathbf{n} \cdot \vec{v}_m = 0, \quad (2.48)$$

where $\vec{v}_m = (u_m(x, y, F(x, y)), v_m(x, y, F(x, y)), w_m(x, y, F(x, y)))$ is velocity field in Cartesian coordinate (x, y, z) and $\vec{v}_m = (u_m(r, F(r)), w_m(r, F(r)))$ in cylindrical coordinate (r, θ, z) with the axisymmetric flow.

Due to the motion of two immiscible fluids, we must take into account the surface tension. When the surface tension coefficient is a constant, the boundary condition for a general three dimensional flow of two immiscible viscous fluids is given by Landau and Lifshitz [3] as

$$n_j(\Upsilon_{2ij} - \Upsilon_{1ij}) = \sigma \left(\frac{1}{R_1} + \frac{1}{R_2} \right) n_i, \quad (2.49)$$

which express the balance of the forces of viscous friction on the surface between fluids. In here, Υ_{mij} is the stress tensor, σ is the surface tension, and R_1 and R_2 are the principal radii of curvature at a given point of the surface, respectively. The stress tensor is defined as

$$\Upsilon_{ij} = -p\delta_{ij} + \tau_{ij}, \quad (2.50)$$

where p , δ_{ij} and τ_{ij} are the pressure, Kronecker's delta and viscous stress tensor, respectively. The viscous tensor is defined by Landau and Lifshitz [3] for an incompressible flow in Cartesian coordinate (x, y, z) as

$$\tau_{ij} = \mu \left(\frac{\partial u_i}{\partial x_j} + \frac{\partial u_j}{\partial x_i} \right), \quad (2.51)$$

where μ is the viscosity. The stress tensor is in the form

$$\Upsilon = \begin{pmatrix} -p + 2\mu \left(\frac{\partial u}{\partial x} \right) & \mu \left(\frac{\partial v}{\partial x} + \frac{\partial u}{\partial y} \right) & \mu \left(\frac{\partial w}{\partial x} + \frac{\partial u}{\partial z} \right) \\ \mu \left(\frac{\partial v}{\partial x} + \frac{\partial u}{\partial y} \right) & -p + 2\mu \left(\frac{\partial v}{\partial y} \right) & \mu \left(\frac{\partial v}{\partial z} + \frac{\partial w}{\partial y} \right) \\ \mu \left(\frac{\partial w}{\partial x} + \frac{\partial u}{\partial z} \right) & \mu \left(\frac{\partial v}{\partial z} + \frac{\partial w}{\partial y} \right) & -p + 2\mu \left(\frac{\partial w}{\partial z} \right) \end{pmatrix}, \quad (2.52)$$

where (u, v, w) are the velocities. In cylindrical coordinates (r, θ, z) with the velocity component (u, v, w) , the stress tensor is written as

$$\Upsilon = \begin{pmatrix} -p + 2\mu \left(\frac{\partial u}{\partial r} \right) & \mu \left(r \frac{\partial(v/r)}{\partial r} + \frac{1}{r} \frac{\partial u}{\partial \theta} \right) & \mu \left(\frac{\partial w}{\partial r} + \frac{\partial u}{\partial z} \right) \\ \mu \left(r \frac{\partial(v/r)}{\partial r} + \frac{1}{r} \frac{\partial u}{\partial \theta} \right) & -p + 2\mu \left(\frac{1}{r} \frac{\partial v}{\partial \theta} + \frac{u}{r} \right) & \mu \left(\frac{\partial v}{\partial z} + \frac{1}{r} \frac{\partial w}{\partial \theta} \right) \\ \mu \left(\frac{\partial w}{\partial r} + \frac{\partial u}{\partial z} \right) & \mu \left(\frac{\partial v}{\partial z} + \frac{1}{r} \frac{\partial w}{\partial \theta} \right) & -p + 2\mu \left(\frac{\partial w}{\partial z} \right) \end{pmatrix}. \quad (2.53)$$

The balance of the tangential stress at a viscous surface can be obtained from the dot product of (2.49) and t_i

$$n_j(\Upsilon_{2ij} - \Upsilon_{1ij})t_i = \sigma \left(\frac{1}{R_1} + \frac{1}{R_2} \right) n_i t_i. \quad (2.54)$$

Since $n_i \cdot t_i = 0$, we have

$$n_j(\Upsilon_{2ij} - \Upsilon_{1ij})t_i = 0. \quad (2.55)$$

Note that this gives us two boundary conditions, as it must be used for two linearly independent tangential vectors.

Normal Stress Boundary Condition

The balance of the normal stress at a viscous surface can be obtained from the dot product of (2.49) and n_i

$$n_j(\Upsilon_{2ij} - \Upsilon_{1ij})n_i = \sigma \left(\frac{1}{R_1} + \frac{1}{R_2} \right) n_i n_i. \quad (2.56)$$

Since $n_i \cdot n_i = 1$, we have

$$n_j(\Upsilon_{2ij} - \Upsilon_{1ij})n_i = \sigma \left(\frac{1}{R_1} + \frac{1}{R_2} \right). \quad (2.57)$$

2.7.2 Free Surface

If the surface of a fluid has both zero normal stress and parallel shear stress, the surface is called "free surface", such as the boundary between air and water. The boundary conditions for a free surface can be obtained by neglecting one of the stress in the fluid.

The kinematic boundary condition is

$$\mathbf{n} \cdot \vec{v} = 0. \quad (2.58)$$

The tangential stress boundary condition is

$$n_j(\Upsilon_{ij})t_i = 0, \quad (2.59)$$

and the normal stress boundary condition is

$$n_j(\Upsilon_{ij})n_i = \sigma \left(\frac{1}{R_1} + \frac{1}{R_2} \right). \quad (2.60)$$

CHAPTER 3

Unfolding of Non-simple Degenerate Streamline Patterns Near a No-slip Wall

In fluid dynamics, there exist many challenges in analysing the flow motion analytically, numerically and experimentally. Many scientists have wondered the behaviour and structure of flow in different flow situations. As we know the flow can be laminar or turbulent; stationary or non-stationary; viscous or not. Depending on these situations many researches have been conducted over long periods. Using the Eulerian or Lagrangian approaches, the equations for fluid dynamics formulated, and to analyse these equations, many method have been introduced and explored to visualize the flow motion.

In this chapter, we consider two-dimensional viscous flow and wonder which streamline patterns can be observed near a no-slip wall. As a way to obtain these streamline patterns, possibly the most elementary approach to identification of structures in flows is considered, which is the topology of the streamlines

$$\dot{\mathbf{x}} = \mathbf{v}(\mathbf{x}) \tag{3.1}$$

where \mathbf{v} is the velocity field. As we mention before that the *critical points* defined

by $\mathbf{v} = 0$ organize the phase portrait of an autonomous system like (3.1). The analysis of streamline topology has a long history with pioneering work by Dean [8], Legendre [9, 10, 11] and Delery [12], followed by many others [13, 14, 15, 16]. The main idea of all these studies is to expand the velocity field or stream function in Taylor series. Dean [8] considered these expansions as a solution of the Navier-Stokes equation and investigated the flow situations, which are attached and separated to solid boundaries. Depending on the situation of flow many studies developed by using this idea.

As known, the flow can be characterized by a Froude, Weber, Reynolds number, geometric properties, time (for unsteady flow) and so on. We will call them all as a parameter which are effecting the flow. The question may arise what happens to the flow structure when these parameters vary. Bifurcation theory can be applied to characterize the changes in streamline pattern. A general bifurcation theory for streamline patterns has been developed by several authors [16, 17, 18, 19, 20, 21]. The possible bifurcations of two dimensional flow close to a stationary linear wall have been investigated by Bakker [16]. In this study, he discussed changes in flow topology by considering the bifurcations of critical points. Using normal forms, this study is revisited by Hartnack [19]. The non-linear fixed wall and the time dependence of the streamlines is considered. Up to codimension three, possible bifurcations have been observed for a simple degenerate critical points. He also observed the bifurcations for a non-simple degeneracy up to codimension two and investigated the effect of the Navier-Stokes equations. Our study is an extension of Hartnack's study. The non-simple case is revisited and extended up to codimension three. The results in this chapter are published in [22].

Let us commence to introduce some phenomena from this study. A two dimensional incompressible flow close to fixed wall ($y = 0$) is considered. The local structure of the streamlines close to a point which we take to be the origin, can be found from a Taylor expansion of the stream function. Under the assumption of zero-flux and no-slip conditions, one can write the stream function as

$$\psi = y^2 \sum_{n,m=0}^{\infty} a_{n,m+2} x^n y^m, \quad (3.2)$$

and the velocity field is

$$u = \frac{\partial \psi}{\partial y}, \quad v = -\frac{\partial \psi}{\partial x}. \quad (3.3)$$

Up to the orders five, a Taylor expansion of the stream function is in the form

$$\psi = y^2(a_{0,2} + a_{1,2}x + a_{0,3}y + a_{2,2}x^2 + a_{1,3}xy + a_{0,4}y^2) + \mathcal{O}(|x, y|^5). \quad (3.4)$$

If $a_{0,2} = 0$, the origin is a critical point and the type of the point is given by

the eigenvalues of the Jacobian matrix

$$J = \begin{pmatrix} u_x & u_y \\ v_x & v_y \end{pmatrix} = \begin{pmatrix} 2a_{1,2} & 3a_{0,3} \\ 0 & -a_{1,2} \end{pmatrix}. \quad (3.5)$$

If $a_{1,2} \neq 0$, the eigenvalues are real and non-zero, such that the critical point is a regular point of separation or attachment. If, however, $a_{1,2} = 0$ the critical point is degenerate, and a small variation of the coefficients $a_{n,m}$ may result in a qualitative change of the local streamline pattern, that is, a bifurcation. A bifurcation analysis is efficiently approached by obtaining a normal form, where as many higher-order terms as possible in (3.4) are removed by non-linear coordinate transformations. The number of bifurcation parameters which remain in the normal form is the co-dimension of the degenerate critical point. Under the non-degeneracy condition $a_{0,3} \neq 0$ normal forms and bifurcation diagrams of co-dimension up to three has been obtained in [16, 19, 20]. This is known as the simple case, while the case $a_{0,3} = 0$ is non-simple. The most basic non-simple situation has co-dimension two under the non-degeneracy conditions

$$a_{2,2} \neq 0, \quad \tilde{a}_{0,4} = a_{0,4} - \frac{a_{1,3}^2}{4a_{2,2}} \neq 0 \quad (3.6)$$

which is studied in [16, 19]. Here, we scale the definition of $\tilde{a}_{0,4}$ by multiplying $a_{2,2}$. Two different bifurcation diagrams have been obtained from this normal form, depending on the value of σ , where

$$\sigma = \begin{cases} +1 & \text{for } a_{2,2}/\tilde{a}_{0,4} > 0 \\ -1 & \text{for } a_{2,2}/\tilde{a}_{0,4} < 0 \end{cases},$$

and $c_{0,2}$ and $c_{0,3}$ are sufficiently small transformed parameters.

The case where the first condition is violated, together with other non-degeneracy conditions,

$$a_{0,2} = a_{1,2} = a_{0,3} = a_{2,2} = 0, \quad a_{1,3} \neq 0, \quad a_{3,2} \neq 0, \quad (3.7)$$

has codimension three [23, 24].

Hartnack [19] also mentions the effect of the Navier-Stokes equations on the streamline topology. According to his results, it is impossible to have $\tilde{a}_{0,4} = 0$ for a steady flow, that is, this condition just need to be seen for unsteady flow. Our interest is that which kind of bifurcations can be obtained for an unsteady flow. Hence we break the other condition instead of $a_{2,2}$

$$a_{0,2} = a_{1,2} = a_{0,3} = \tilde{a}_{0,4} = 0, \quad a_{2,2} \neq 0. \quad (3.8)$$

In the rest of thesis, we will obtain the normal form and the bifurcation diagram associated with this degeneracy under a further non-degeneracy condition of the

form $\tilde{a}_{0,5}$, which will be given in the next section, is a parameter which appears in the course of the analysis. In the application section, we will show that the bifurcation diagram is the relevant one for the vortex-driven flow. With this analysis, all topological bifurcation diagrams for flows close to a no-slip wall with codimension up to three have been obtained.

3.1 Normal form for the degenerate case

In this section, we perform a series of coordinate transformations in an attempt to simplify the streamfunction (3.2) by using the assumptions (3.8). Since $a_{0,2} = a_{1,2} = a_{0,3} = 0$, equation (3.2) is written as

$$\begin{aligned} \psi = y^2 & (a_{2,2}x^2 + a_{1,3}xy + a_{0,4}y^2 + a_{3,2}x^3 + a_{2,3}x^2y \\ & + a_{1,4}xy^2 + a_{0,5}y^3 + \mathcal{O}(|x, y|^4)). \end{aligned} \quad (3.9)$$

Following Hartnack [19], we introduce the new variable $\xi = x + \frac{a_{1,3}}{2a_{2,2}}y$ to eliminate the term $a_{1,3}xy^3$. As a consequence of assumption $\tilde{a}_{0,4} = 0$, the streamfunction then reads

$$\psi = y^2 (a_{2,2}\xi^2 + a_{3,2}\xi^3 + \tilde{a}_{2,3}\xi^2y + \tilde{a}_{1,4}\xi y^2 + \tilde{a}_{0,5}y^3 + \mathcal{O}(|\xi, y|^4)), \quad (3.10)$$

where

$$\begin{aligned} \tilde{a}_{2,3} &= a_{2,3} - \frac{3a_{3,2}a_{1,3}}{2a_{2,2}}, \\ \tilde{a}_{1,4} &= a_{1,4} - \frac{a_{2,3}a_{1,3}}{a_{2,2}} + \frac{3a_{3,2}a_{1,3}^2}{4a_{2,2}^2}, \\ \tilde{a}_{0,5} &= a_{0,5} - \frac{a_{1,4}a_{1,3}}{2a_{2,2}} + \frac{a_{2,3}a_{1,3}^2}{4a_{2,2}^2} - \frac{a_{3,2}a_{1,3}^3}{8a_{2,2}^3}. \end{aligned} \quad (3.11)$$

Further simplifications can be obtained from non-linear coordinate transformations. Define a near-identity transformation such that the wall $y = 0$ is mapped $\eta = 0$ by

$$\xi = \chi + r_{2,0}\chi^2 + r_{1,1}\chi\eta + r_{0,2}\eta^2, \quad y = \eta + s_{1,1}\chi\eta + s_{0,2}\eta^2. \quad (3.12)$$

The transformed streamfunction is written as

$$\begin{aligned} \psi = \eta^2 & (a_{2,2}\chi^2 + (2a_{2,2}r_{2,0} + 2s_{1,1}a_{2,2} + a_{3,2})\chi^3 \\ & + (2a_{2,2}r_{1,1} + 2s_{0,2}a_{2,2} + \tilde{a}_{2,3})\chi^2\eta \\ & + (2a_{2,2}r_{0,2} + \tilde{a}_{1,4})\chi\eta^2 + \tilde{a}_{0,5}\eta^3 + \mathcal{O}(|\chi, \eta|^4)). \end{aligned} \quad (3.13)$$

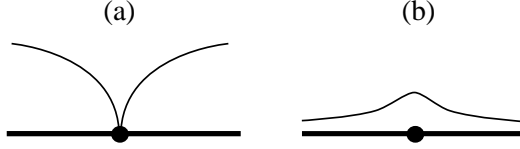


Figure 3.1: Streamline patterns close to the degenerate critical point for the normal form (3.15). (a): $\sigma = 1$, (b): $\sigma = -1$.

The terms $\chi^3\eta^2$, $\chi^2\eta^3$ and $\chi\eta^4$ can be eliminated by choosing $r_{2,0} = 0$, $r_{1,1} = 0$, $r_{0,2} = -\frac{\tilde{a}_{1,4}}{2a_{2,2}}$, $s_{1,1} = -\frac{a_{3,2}}{2a_{2,2}}$ and $s_{0,2} = -\frac{\tilde{a}_{2,3}}{2a_{2,2}}$ and we get

$$\psi = \eta^2 (a_{2,2}\chi^2 + \tilde{a}_{0,5}\eta^3 + \mathcal{O}(|\chi, \eta|^4)). \quad (3.14)$$

Finally, we scale time by dividing the stream function by $\tilde{a}_{0,5}$ and scale χ by substituting $\chi = \sqrt{\frac{\tilde{a}_{0,5}}{a_{2,2}}}|x'$ and obtain

$$\psi = \eta^2 (\sigma x'^2 + \eta^3 + \mathcal{O}(|x', \eta|^4)). \quad (3.15)$$

where

$$\sigma = \frac{a_{2,2}}{\tilde{a}_{0,5}} \left| \frac{\tilde{a}_{0,5}}{a_{2,2}} \right| = \begin{cases} +1 & \text{for } a_{2,2}/\tilde{a}_{0,5} > 0 \\ -1 & \text{for } a_{2,2}/\tilde{a}_{0,5} < 0 \end{cases},$$

and we have assumed $\tilde{a}_{0,5} \neq 0$. To analyse the topology of the flow close to the critical point $(0,0)$ of (3.15), we look for possible separatrices (dividing streamlines) by solving $\psi = 0$. Disregarding the \mathcal{O} -term, the solutions are

$$\eta = 0, \quad \eta = (-\sigma x'^2)^{1/3}, \quad (3.16)$$

where the first solution corresponds to the wall and the latter forms a cusp which is in the fluid domain $\eta > 0$ only if $\sigma = -1$. The possible streamline patterns are shown in Fig. 3.1.

Again note that the stream function (3.9) cannot occur in a steady flow. Hence, the analysis of this paper is relevant only for unsteady flow.

3.2 Unfolding of the degenerate case

The degenerate case is structurally unstable. Small perturbations of the parameters away from the degenerate value may result in different streamline patterns. Following the approach from the previous section, we will now derive a normal

form to simplify the bifurcation analysis. We define again the new variable $\xi = x + \frac{a_{1,3}}{2a_{2,2}}y$ and substituting this into Eqn. (3.2), we get

$$\begin{aligned} \psi = y^2(\epsilon_1 + \epsilon_2\xi + \epsilon_3y + \epsilon_4y^2 + a_{2,2}\xi^2 \\ + a_{3,2}\xi^3 + \tilde{a}_{2,3}\xi^2y + \tilde{a}_{1,4}\xi y^2 + \tilde{a}_{0,5}y^3 + \mathcal{O}(|\xi, y|^4)), \end{aligned} \quad (3.17)$$

where

$$a_{0,2} = \epsilon_1, \quad a_{1,2} = \epsilon_2, \quad a_{0,3} - \frac{a_{1,3}a_{1,2}}{2a_{2,2}} = \epsilon_3, \quad a_{0,4} - \frac{a_{1,3}^2}{4a_{2,2}} = \epsilon_4, \quad (3.18)$$

are small parameters and $\tilde{a}_{2,3}, \tilde{a}_{1,4}, \tilde{a}_{0,5}$ are given in (3.11).

To further simplify the stream function, we apply the near-identity transformation

$$\xi = \chi + r_{0,2}\eta^2, \quad y = \eta + s_{1,1}\chi\eta + s_{0,2}\eta^2. \quad (3.19)$$

As in the degenerate case, we aim at removing the χ^3y^2 , χ^2y^3 and χy^4 -terms. The coefficients for these terms in the transformed stream function are

$$\begin{aligned} f(\epsilon_2, s_{1,1}) &= s_{1,1}^2\epsilon_2 + a_{3,2} + 2s_{1,1}a_{2,2}, \\ g(\epsilon_2, \epsilon_3, s_{0,2}) &= 2s_{0,2}a_{2,2} + 2s_{1,1}s_{0,2}\epsilon_2 + \tilde{a}_{2,3} + 3s_{1,1}^2\epsilon_3, \\ h(\epsilon_2, \epsilon_3, \epsilon_4, r_{0,2}) &= 6s_{1,1}\epsilon_3s_{0,2} + 4s_{1,1}r_{0,2}\epsilon_2 + 4\epsilon_4s_{1,1} \\ &\quad + \tilde{a}_{1,4} + 2a_{2,2}r_{0,2} + s_{0,2}^2\epsilon_2, \end{aligned} \quad (3.20)$$

respectively. Since

$$\begin{aligned} f(0, -\frac{a_{3,2}}{2a_{2,2}}) &= 0, \\ \frac{\partial f}{\partial s_{1,1}}(0, -\frac{a_{3,2}}{2a_{2,2}}) &= 2a_{2,2} \neq 0, \end{aligned} \quad (3.21)$$

it follows from the implicit function theorem that there exists a function $s_{1,1}(\epsilon_2)$ with $s_{1,1}(0) = -\frac{a_{3,2}}{2a_{2,2}}$ such that $f(\epsilon_2, s_{1,1}(\epsilon_2)) = 0$, for ϵ_2 sufficiently small.

Similarly, we find functions $s_{0,2}(\epsilon_2, \epsilon_3)$ and $r_{0,2}(\epsilon_2, \epsilon_3, \epsilon_4)$ which solve $g = 0$ and $h = 0$, respectively. Again, we only use the assumption $a_{2,2} \neq 0$ and the implicit function theorem. This yields the stream function

$$\psi = \eta^2 (\epsilon_1 + \hat{\epsilon}_2\chi + \hat{\epsilon}_3\eta + \hat{a}_{2,2}\chi^2 + \hat{\epsilon}_4\chi\eta + \hat{\epsilon}_5\eta^2 + \hat{a}_{0,5}\eta^3), \quad (3.22)$$

where the $\hat{\epsilon}$ are transformed small parameters and $\hat{a}_{2,2} = \tilde{a}_{2,2} + \mathcal{O}(\hat{\epsilon})$, $\hat{a}_{0,5} = \tilde{a}_{0,5} + \mathcal{O}(\hat{\epsilon})$. Further, by a scaling of the time by dividing the stream function by $\hat{a}_{0,5}$, we obtain

$$\psi = \eta^2 \left(\epsilon_1 + \tilde{\epsilon}_2\chi + \tilde{\epsilon}_3\eta + \frac{\hat{a}_{2,2}}{\hat{a}_{0,5}}\chi^2 + \tilde{\epsilon}_4\chi\eta + \tilde{\epsilon}_5\eta^2 + \eta^3 + \mathcal{O}(|\chi, \eta|^4) \right), \quad (3.23)$$

and, finally, to eliminate the $\chi\eta^2$ and $\chi\eta^3$ -terms, we apply a final simplification by introducing new variables

$$\chi = a + bx_1 + cy_1, \quad \eta = y_1. \quad (3.24)$$

Choosing the coefficients as

$$a = -\frac{\tilde{\epsilon}_2 \hat{a}_{0,5}}{2\hat{a}_{2,2}}, \quad b = \left| \frac{\hat{a}_{0,5}}{\hat{a}_{2,2}} \right|^{1/2}, \quad c = -\frac{\tilde{\epsilon}_4 \hat{a}_{0,5}}{2\hat{a}_{2,2}}, \quad (3.25)$$

the simplified stream function is then written as

$$\psi = y_1^2(c_{0,0} + c_{0,1}y_1 + c_{0,2}y_1^2 + y_1^3 + \sigma x_1^2 + \mathcal{O}(|x_1, y_1|^4)) \quad (3.26)$$

where

$$\begin{aligned} c_{0,0} &= \epsilon_1 - \frac{\tilde{\epsilon}_2^2 \hat{a}_{0,5}}{4\hat{a}_{2,2}}, & c_{0,1} &= \tilde{\epsilon}_3 - \frac{\tilde{\epsilon}_2 \tilde{\epsilon}_4 \hat{a}_{0,5}}{2\hat{a}_{2,2}} \\ c_{0,2} &= \tilde{\epsilon}_5 - \frac{\tilde{\epsilon}_4^2 \hat{a}_{0,5}}{4\hat{a}_{2,2}}, & \sigma &= \frac{\hat{a}_{2,2}}{\hat{a}_{0,5}} \left| \frac{\hat{a}_{0,5}}{\hat{a}_{2,2}} \right|, \end{aligned} \quad (3.27)$$

$c_{0,0}$, $c_{0,1}$ and $c_{0,2}$ are small parameters. Note that the definition of σ agrees with that for the degenerate case. When the bifurcation parameters are sufficiently small $a_{2,2}$ and $\hat{a}_{2,2}$ are of the same sign, as is the case for $a\tilde{a}_{0,5}$ and $\hat{a}_{0,5}$.

We summarize our findings in

THEOREM 3.1 *Let $a_{0,2}$, $a_{1,2}$, $a_{0,3}$ and $\tilde{a}_{0,4}$ be small parameters. Assuming the non-degeneracy conditions $a_{2,2} \neq 0$ and $\tilde{a}_{0,5} \neq 0$ the normal form for the streamfunction (3.2) is*

$$\psi = y^2(c_{0,0} + c_{0,1}y + c_{0,2}y^2 + y^3 + \sigma x^2 + \mathcal{O}(|x, y|^4)), \quad (3.28)$$

where

$$\sigma = \begin{cases} +1 & \text{for } \tilde{a}_{2,2}/\tilde{a}_{0,5} > 0 \\ -1 & \text{for } \tilde{a}_{2,2}/\tilde{a}_{0,5} < 0 \end{cases},$$

$c_{0,0}$, $c_{0,1}$, $c_{0,2}$ are small transformed parameters.

3.3 Bifurcation analysis of the normal form

In this section, we analyze the bifurcations in the dynamical system defined by the normal form (3.28). Different values for σ , we decide the bifurcation diagrams and analyze the topology of the flow field both on-wall and off-wall

critical points. Truncating the \mathcal{O} -term in (3.28), the dynamical system is in the form (time-scaled by y)

$$\begin{aligned}\dot{x} &= 2c_{0,0} + 3c_{0,1}y + 4c_{0,2}y^2 + 5y^3 + 2\sigma x^2 \\ \dot{y} &= -2\sigma yx\end{aligned}\tag{3.29}$$

with the determinant of the Jacobian

$$|J| = 6\sigma c_{0,1}y + 16\sigma c_{0,2}y^2 - 8x^2 + 30\sigma y^3.\tag{3.30}$$

Remember that the critical points are called "saddle" when $|J| < 0$, "center" when $|J| > 0$ and "degenerate" when $|J| = 0$.

We have four different kinds of bifurcation for this system. They are:

- Local bifurcation for on-wall critical points
- Local bifurcation for off-wall critical points
- Global bifurcation associated with off-wall critical points
- Global bifurcation associated with on-wall and off-wall critical points.

Local bifurcations associated with degenerate critical points and global bifurcations associated with the hetero-clinic connection of critical points. Simply, a global bifurcation appears when the value of ψ at different critical points of saddle type coincide.

3.3.0.1 Local bifurcation for on-wall critical points

To find the local bifurcation curve for on-wall critical points, we insert $y = 0$ (on-wall condition) into (3.29),

$$\dot{x} = 2c_{0,0} + 2\sigma x^2, \quad \dot{y} = 0.\tag{3.31}$$

From this, one finds that $(\sqrt{-\sigma c_{0,0}}, 0)$ and $(-\sqrt{-\sigma c_{0,0}}, 0)$ are critical points. This shows that there are two on-wall critical points when $\sigma c_{0,0} < 0$, and no critical points when $\sigma c_{0,0} > 0$. Hence, a local bifurcation occurs on the line $c_{0,0} = 0$.

3.3.0.2 Local bifurcation for off-wall critical points

To find local bifurcation for off-wall critical points, we substitute $x = 0$ into (3.29) and (3.30). The local bifurcation curve can be obtained by using "resultant" command in "Maple". Eliminating y from $\dot{x} = 0$ and $|J| = 0$, one finds

$$c_{0,0}(128c_{0,0}c_{0,2}^3 - 36c_{0,1}^2c_{0,2}^2 - 540c_{0,0}c_{0,1}c_{0,2} + 135c_{0,1}^3 + 675c_{0,0}^2) = 0. \quad (3.32)$$

We are not interested in the line $c_{0,0}$ any more since it is already a local bifurcation curve. The second factor of (3.32) is quadratic for $c_{0,0}$, hence we solve it with respect to $c_{0,0}$. The discriminant of (3.32) is $4(16c_{0,2}^2 - 45c_{0,1})^3$. We use $\Delta = 16c_{0,2}^2 - 45c_{0,1}$ as a more convenient parameter instead of $c_{0,1}$ since it determines the number of critical points. From now on, as a parameter space, we will use $(c_{0,0}, c_{0,2}, \Delta)$. The local bifurcation for off-wall points occurs on the curves ($\Delta \geq 0$),

$$\Gamma^\pm : c_{0,0(1,2)} = \frac{32}{675} c_{0,2}^3 - \frac{2}{225} \Delta c_{0,2} \pm \frac{1}{675} \sqrt{\Delta^3}. \quad (3.33)$$

These curves, however, shows the bifurcation for all the critical points which are under and above the wall. We are just interested in the critical points above wall (or positive 'y'). To separate the under-wall critical points, we need to examine $\dot{x} = 0$ for $x = 0$. The critical points can be found by solving

$$2c_{0,0} + 3c_{0,1}y + 4c_{0,2}y^2 + 5y^3 = 0. \quad (3.34)$$

Using the substitutions $c_{0,1} = \frac{16c_{0,2}^2 - \Delta}{45}$ and (3.33) into (3.34), we have

$$5y^3 + 4c_{0,2}y^2 + \frac{16c_{0,2}^2}{15}y - \frac{\Delta}{15}y + \frac{64c_{0,2}^3}{675} - \frac{4\Delta c_{0,2}}{225} \pm \frac{2\Delta^{3/2}}{675} = 0. \quad (3.35)$$

Solving this equation with respect to 'y', we obtain

$$y_1 = -\frac{2\sqrt{\Delta}}{15} - \frac{4c_{0,2}}{15}, \quad y_{2,3} = \frac{\sqrt{\Delta}}{15} - \frac{4c_{0,2}}{15} \quad \text{for } \Gamma^+, \quad (3.36)$$

$$y_1 = \frac{2\sqrt{\Delta}}{15} - \frac{4c_{0,2}}{15}, \quad y_{2,3} = -\frac{\sqrt{\Delta}}{15} - \frac{4c_{0,2}}{15} \quad \text{for } \Gamma^-. \quad (3.37)$$

These roots show us that the positive roots have occurred when $c_{0,2} < 0$ for $\Delta = 0$. For $\Delta > 0$, we have the following relations: For Γ^+ ;

$$c_{0,2} < -\frac{\sqrt{\Delta}}{2} \Rightarrow y_{1,2,3} > 0, \quad (3.38)$$

$$-\frac{\sqrt{\Delta}}{2} < c_{0,2} < \frac{\sqrt{\Delta}}{4} \Rightarrow y_1 < 0, \quad y_{2,3} > 0, \quad (3.39)$$

$$c_{0,2} > \frac{\sqrt{\Delta}}{4} \Rightarrow y_{1,2,3} < 0, \quad (3.40)$$

and for Γ^- ;

$$c_{0,2} < -\frac{\sqrt{\Delta}}{4} \Rightarrow y_{1,2,3} > 0, \quad (3.41)$$

$$-\frac{\sqrt{\Delta}}{4} < c_{0,2} < \frac{\sqrt{\Delta}}{2} \Rightarrow y_1 > 0, \quad y_{2,3} < 0, \quad (3.42)$$

$$c_{0,2} > \frac{\sqrt{\Delta}}{2} \Rightarrow y_{1,2,3} < 0. \quad (3.43)$$

From these relations, we can decide the normal form of the local bifurcation curves Γ^\pm . Since the roots of (3.34) must be positive, we have to eliminate the curves in (3.40) for Γ^+ and the curves in (3.43) for Γ^- . In addition, the local bifurcation occurs under the wall for the condition (3.42), therefore, we have also eliminated it.

3.3.0.3 Global bifurcation associated with on-wall and off-wall critical points

There exists also a possibility of the saddle-saddle connection between the off-wall and the on-wall critical points. This type global bifurcation corresponds to the stream function attaining the on-wall value of zero in an off-wall critical point. It occurs when we eliminate y from $\psi = 0$ and $\dot{x} = 0$ by using "resultant" command in "Maple" and obtain

$$c_{0,0} (4c_{0,0}c_{0,2}^3 - c_{0,1}^2c_{0,2}^2 - 18c_{0,0}c_{0,1}c_{0,2} + 4c_{0,1}^3 + 27c_{0,0}^2) = 0. \quad (3.44)$$

This equation is also quadratic for $c_{0,0}$, and can be solved with respect to $c_{0,0}$. The discriminant of (3.44) is $16(c_{0,2}^2 - 3c_{0,1})^3$. In here, we choose $E = c_{0,2}^2 - 3c_{0,1}$ as a parameter instead of $c_{0,1}$, due to the same reason of choosing Δ . The global bifurcation for on-wall and off-wall saddle critical points occurs

$$\gamma^\pm : c_{0,0(1,2)} = \frac{1}{27}c_{0,2}^3 - \frac{1}{9}Ec_{0,2} \pm \frac{2}{27}\sqrt{E^3}. \quad (3.45)$$

It is suitable to write $E = \frac{\Delta - c_{0,2}^2}{15}$. It implies that when $-\sqrt{\Delta} < c_{0,2} < \sqrt{\Delta}$ we have two solutions for $c_{0,0}$. This bifurcation only occurs when $c_{0,0} < 0$ since the on-wall critical points only appear for $c_{0,0} < 0$. We also observed that for $\sigma = 1$, just γ^2 and for $\sigma = -1$, just γ^1 has a significance since coinciding points must be only saddle.

3.3.0.4 Global bifurcation associated with off-wall critical points

Finally, one should consider the heteroclinic bifurcation among the off-wall critical points. Such connections happen when the streamfunction attains the same values at two saddle critical points. We can find this bifurcation by eliminating y_1 and y_2 from

$$\dot{x}(0, y_1) = 5 y_1^3 + 4 c_{0,2} y_1^2 + 3 c_{0,1} y_1 + 2 c_{0,0} = 0, \quad (3.46a)$$

$$\dot{x}(0, y_2) = 5 y_2^3 + 4 c_{0,2} y_2^2 + 3 c_{0,1} y_2 + 2 c_{0,0} = 0, \quad (3.46b)$$

$$\begin{aligned} \psi(0, y_1) - \psi(0, y_2) = & (-y_2 + y_1) (c_{0,2} y_1^3 + c_{0,2} y_1^2 y_2 + c_{0,2} y_1 y_2^2 + c_{0,2} y_2^3 \\ & + y_1^4 + y_1^3 y_2 + y_1^2 y_2^2 + y_1 y_2^3 + y_2^4 + c_{0,1} y_1^2 + c_{0,1} y_1 y_2 \\ & + c_{0,1} y_2^2 + c_{0,0} y_1 + c_{0,0} y_2) = 0, \end{aligned} \quad (3.46c)$$

where $y_1 \neq y_2$. The resultant of eq. (33b) and eq. (33c) with respect to y_2 gives an expression, after that again construction the resultant between this expression and (33a) with respect to y_1 gives the following equation

$$128 c_{0,0} c_{0,2}^3 - 36 c_{0,1}^2 c_{0,2}^2 - 540 c_{0,0} c_{0,1} c_{0,2} + 135 c_{0,1}^3 + 675 c_{0,0}^2 = 0 \quad (3.47)$$

where we again have removed factors which correspond to bifurcations studied above. Providing the global bifurcations for off-wall critical points, we substitute $c_{0,1} = \frac{16c_{0,2}^2 - \Delta}{45}$ into (3.47) and solve it for $c_{0,0}$ yields

$$\begin{aligned} \zeta^\pm : c_{0,0\pm} = & \frac{94}{225} c_{0,2}^3 - \frac{7}{225} \Delta c_{0,2} \\ & \pm \frac{2}{675} \sqrt{15625 c_{0,2}^6 - 1875 \Delta c_{0,2}^4 + 75 \Delta^2 c_{0,2}^2 - \Delta^3}. \end{aligned} \quad (3.48)$$

The global bifurcation between off-wall and off-wall saddle points only occurs when the conditions $\sigma = -1$ and $\Delta > 0$ are fulfilled. In addition, we need to have at least three critical point. Since we just only observe three critical points between the local bifurcation curves and for $c_{0,0} < 0$, we eliminate all the other parts of this curve.

In Fig. 3.2 and 3.3, we only have the local bifurcation for the on-wall critical points. Physically, for $\sigma = 1$ and $\Delta < 0$, while there is no flow for $c_{0,0} > 0$, a separation bubble occurs for $c_{0,0} < 0$.

In the following figures, the full lines are local bifurcation curves $c_{0,0} = 0$ and Γ^\pm , the dotted lines are the global bifurcation curves γ^\pm , and the dash-dotted line is the global bifurcation curve ζ^+ . The points *A–E* mark where different bifurcation curves meet.

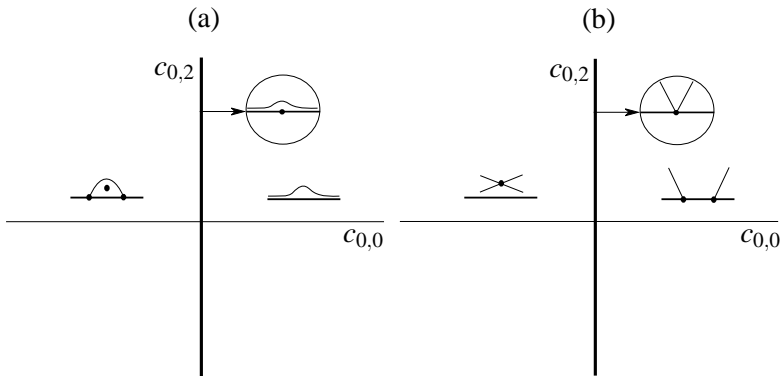


Figure 3.2: Bifurcation diagrams for the normal form (3.15) for $\Delta < 0$. (a): $\sigma = 1$, (b): $\sigma = -1$.

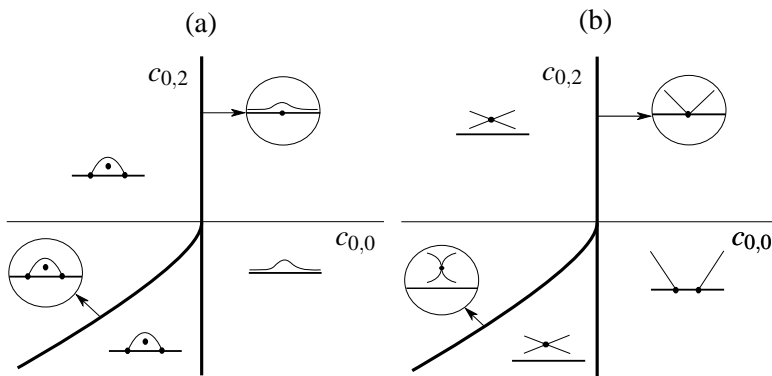


Figure 3.3: Bifurcation diagrams for the normal form (3.15) for $\Delta = 0$. (a): $\sigma = 1$, (b): $\sigma = -1$.

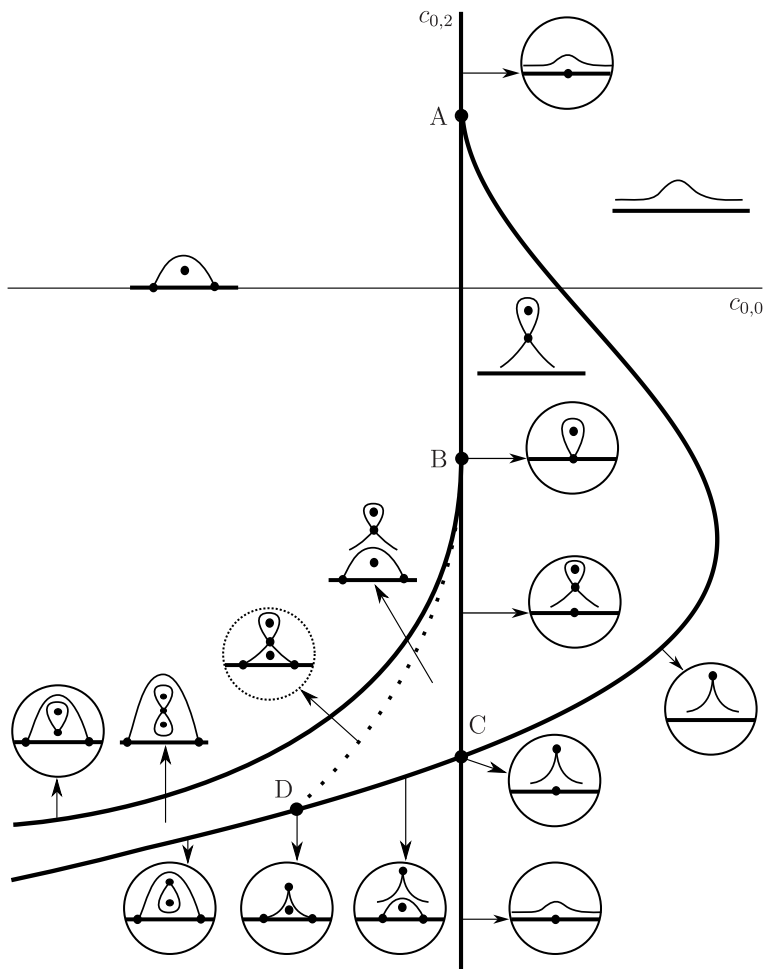


Figure 3.4: Bifurcation diagrams for the normal form (3.15) for $\Delta > 0$ and $\sigma = 1$.

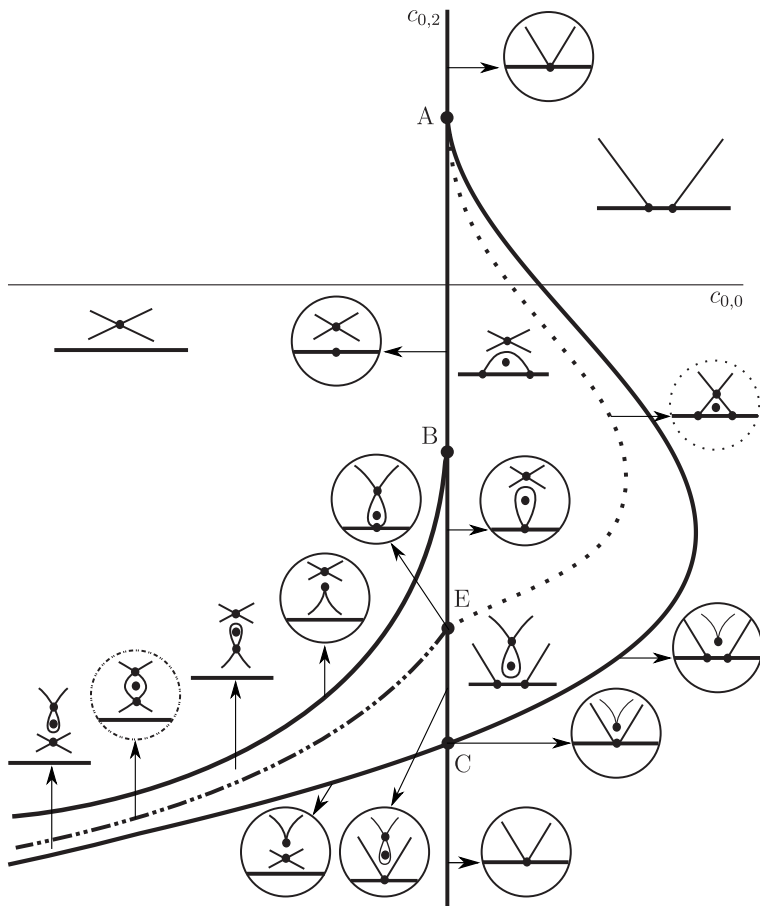


Figure 3.5: Bifurcation diagrams for the normal form (3.15) for $\Delta > 0$ and $\sigma = -1$.

Since we just consider the existence of a stream function, all possible streamline patterns have been observed. The advantage of obtaining these patterns is to see and realize the process of flow movement.

3.4 Application

As an application, we consider a vortex convected close to a stationary wall which induces a viscous response from the wall boundary layer in Fig. 3.6. This section is a short review of [22], and the figures are all from that paper.

For a sufficiently high Reynolds number vorticity from the boundary layer is ejected into the surrounding fluid, resulting in secondary vortex structures. This phenomenon is called *eruption* of the boundary layer. Our starting point is the analysis by Kudela and Malecha [25, 26] who showed numerically how the streamline pattern changes through several stages as a vortex erupts from the boundary layer. In [22], we provide further numerical simulations to understand the process in more detail when the Reynolds number and time vary.

Kudela and Malecha [25, 26] observed various different streamlines during the eruption process by using a fixed wall from the configuration as in Fig. 3.6. A Gaussian vortex with core radius a , which is circulating clock-wise with strength $-\Gamma$ and the distance d from a flat wall is considered at $t = 0$. This is then evolved for a short relation time with a free-slip wall boundary to smooth out transient oscillations, allowing the flow to adjust. When the initial oscillations are reduced, the wall boundary condition is instantaneously switched to a no-slip wall and the computation is continued. The equations were solved in a coordinate system where the vortex is initially at rest. The equations are non-dimensionalized by the length scale $L = d$ and time scale $T = 2\pi ad/\Gamma$. The Reynolds number is defined by $Re = \frac{L^2}{T\nu}$. The flow equations are solved by a well-established finite-element code using *GLL quadrature* and *Lagrange polynomials*. Standard domain and resolution studies were performed to ensure the reliability of predictions, and very good agreement with the results by Kudela and Malecha [26] is obtained. For the computational details please see [27].

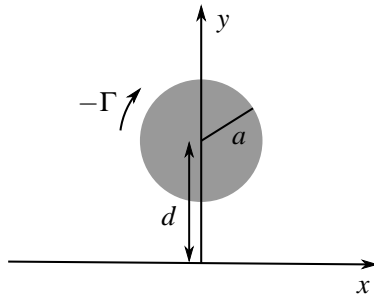


Figure 3.6: Initial configuration of the eruption process. A Gaussian vortex with core radius a and negative circulation $-\Gamma$ is placed at $(0, d)$.

Increasing the value of Re , the streamline patterns are observed in a sequence of time. We realize that the bifurcation diagrams obtained in the topological section for $\sigma = 1$ contains all the bifurcations we have observed in the eruption flow. In Fig. 3.7, we re-sketch the Fig 3.4 without streamline patterns. In this figure, the roman numeral in each of regions are the ones to use the classify the flow topology. Note that the regions II and II' are really one region as they are connected through the part where $\Delta < 0$.

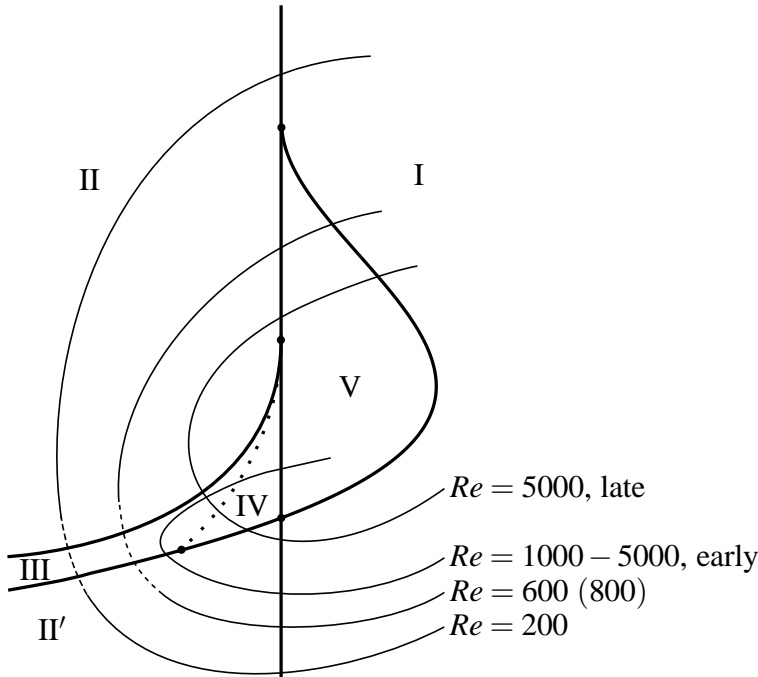


Figure 3.7: The bifurcation diagram for the normal form (3.28) for $\sigma > 0$. A slice with $\Delta > 0$ is shown. The thin lines are time traces for the eruption flow shown in Figs. 3.8–3.12. The dashed part represent parts where the path goes through the region with $\Delta < 0$. The trace for $Re = 800$ is identical to that for $Re = 600$ except that the dashed part is a full line such that the path goes through region III.

For $Re = 200$, a separation zone occurs at the wall between $t = 3$ and $t = 6$ and disappears between $t = 6$ and $t = 10.6875$. (see Fig. 3.8)

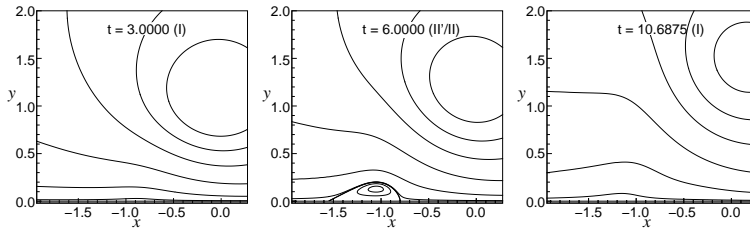


Figure 3.8: Numerically obtained streamlines for the vortex-induced flow for $Re = 200$. In each panel the dimensionless time and the topological classification according to the bifurcation diagram in Fig. 3.7 is shown.

For $Re = 600$, a separation zone again occurs at the wall between $t = 2.75$ and $t = 7.5$, but rather than shrinking while attached to the wall it pinches off, creating a saddle point in the fluid. The dividing streamlines of the saddle enclose a region with closed streamlines around a center type critical point. This can be considered a vortex structure which is not yet erupted. However, soon after, between $t = 11.3625$ and $t = 11.3813$, the vortex structure starts to shrink and disappears as the saddle and the center merge in a saddle-center bifurcation before it has left the wall. (see Fig. 3.9)

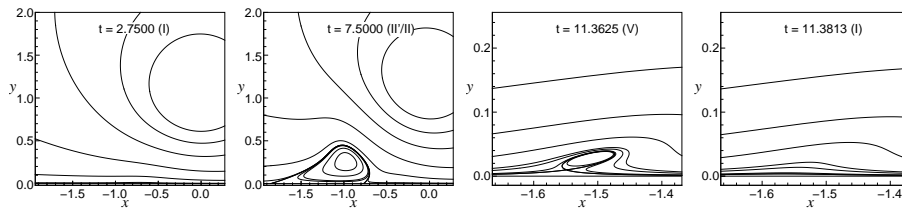


Figure 3.9: As Fig. 3.8, but for $Re = 600$.

For $Re = 800$, a saddle-center bifurcation occurs inside the attached separation zone. This creates a figure-eight structure visible at $t = 10.3125$. Shortly thereafter, another saddle-center bifurcation occurs where the lower center and the saddle disappear, leaving only a single center inside the separation zone. (see Fig. 3.10)

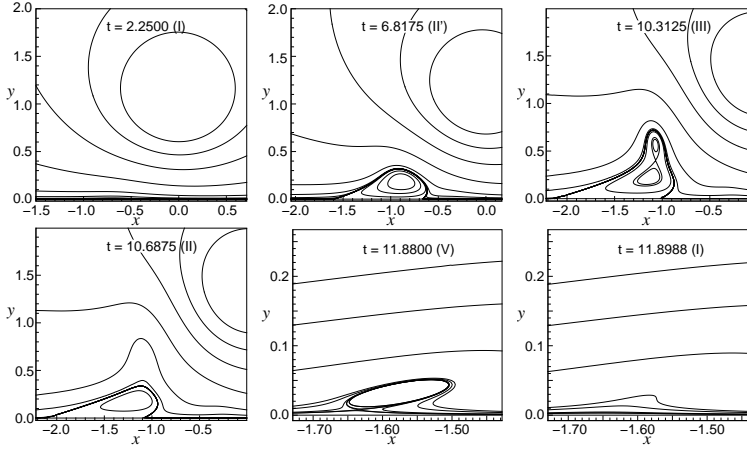


Figure 3.10: As Fig. 3.8, but for $Re = 800$.

For the early stages of $Re = 5000$, eruption takes place following sequence of events which we show in Fig. 3.11. Again a figure eight is created inside the separation zone at $t = 13.3225$, but now the top center and the saddle pinch off in a global bifurcation, leaving a separation zone attached to the wall and an erupted vortex structure at $t = 13.8975$. The separation zone shrinks and disappears, while the erupted vortex leaves the boundary layer as it rotates around the main vortex.

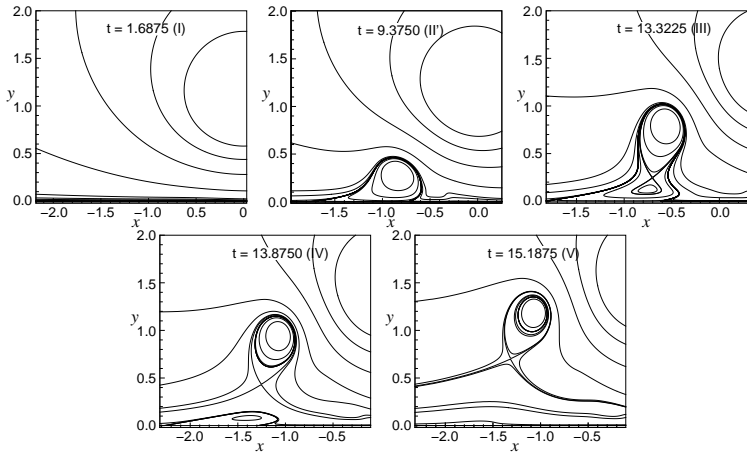


Figure 3.11: As Fig. 3.8, but for $Re = 5000$, early stages.

At later stages further topological changes may occur if Re is sufficiently high.

We illustrate this for $Re = 5000$ in Fig. 3.12. Here an attached separation zone is again created, and a little later a vortex structure appears above it in a saddle-center bifurcation. It does not erupt but merges with the separation zone which subsequently disappears in a few bifurcations. For higher values of Re these secondary topological changes may lead to eruption [26] and generate more complex streamline patterns which are outside the scope of the present study.

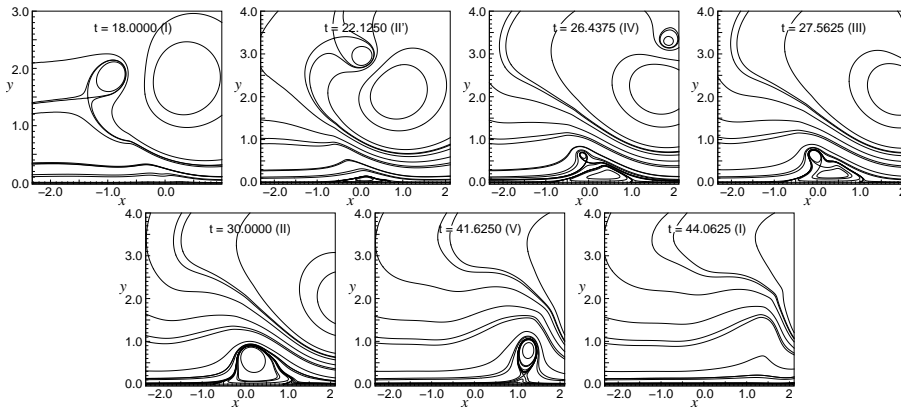


Figure 3.12: As Fig. 3.8, but for $Re = 5000$, later stages.

In a conclusion, all possible streamline patterns for the eruption process from a boundary layer have been obtained. We have shown that the bifurcation diagram 3.4 describes the basic changes of streamline topology in the eruption process from a boundary layer. The creation of a secondary vortex erupting from the boundary layer is associated with the *pinching off* a saddle-center pair of streamlines in a global bifurcation. The bifurcation diagram associated with the singularity we study here is the simplest which can account for both creation of the recirculation zone on the wall and the pinching off, as no other bifurcation diagram with three parameters or less allows both these transitions.

CHAPTER 4

Topology of axisymmetric flow near a free surface

In this chapter, we investigate a steady incompressible axisymmetric flow on a free surface via topological aspect.

The analysis of inter-facial flows is a vast topic in many areas (environment, engineering etc.) and have generated many interests recently. The most prevalent example is the surface between two immiscible (not mixed) fluids. All these kind of surfaces are found in nature such as ocean and the air in the Earth's atmosphere. From a physical viewpoint, a free surface may be referred as a constant normal stress and no shear stresses. Mathematically, if the existence of a continuum is insignificant with the zero viscosity and density above the interface, the free surface occurs. Scientists find flows on surface interesting and develop mathematical models to analyze them using some boundary conditions, such as the kinematic and dynamic boundary conditions on the free surface. It can be found many studies to investigate these kind of flows in analytically, numerically and experimentally . As an analytical study, Lugt [28, 29] considered a topological description of flows in the vicinity of viscous and free surface. His work is revisited by Brøns [17], by including non-constant curvature of the interface and gradients of surface tension. Including the fourth-order normal form, Deliceoglu [21] extended Brøns's study and obtained the streamline patterns for two-dimensional incompressible flow up to co-dimension three by using bifurcation theory.

The question then may arise: is there any effect of angular velocity? To see this, we need to consider three-dimensional flow, which can be classified as axisymmetric (which we consider in this chapter) or not.

The emergence of a local circulation region in a swirling flow, often referred to as vortex breakdown (VB) had been investigated by Brøns and *et al.* [30] in a cylinder with rotating bottom and a free surface. Considering the Reynolds number and the aspect ratio of cylinder as bifurcation parameters, they obtained possible bifurcations of streamline patterns for an axisymmetric flow up to co-dimension two. Their local analysis was close to both the vortex axis (center axis) and the interface. In here, the surface tension and the curvature of the interface were not taken into account.

Previous studies have focused on the topology in the meridional plane, that is, the topology of the level curves of the stream function ψ . However, there is an interaction between ψ and the swirl velocity v through the boundary conditions and the Navier-Stokes equation. We will consider this as well. We can say that this chapter is indeed a combination of [30] and [17], due to considering the surface tension and the curvature effects on the interface by taking into account the existence of swirl velocity. Additionally, the flow is also considered close to wall. Our aim is to elucidate which kind of possible streamline patterns on the interface can occur

- (a) close to the center axis,
- (b) away from the center axis, and
- (c) close to a stationary wall. (see Fig. 4.1)

All these analyses will be given up to co-dimension three.

We consider a three-dimensional axisymmetric incompressible flow in cylindrical coordinates (r, θ, z) with corresponding velocities $(u = \dot{r}, v = r\dot{\theta}, w = \dot{z})$. Since the flow is axisymmetric and incompressible, a stream function $\psi(r, z)$ exist and can be defined as (see eq. (2.33))

$$u(r, z) = \dot{r} = \frac{1}{r} \frac{\partial \psi}{\partial z}, \quad w(r, z) = \dot{z} = -\frac{1}{r} \frac{\partial \psi}{\partial r}. \quad (4.1)$$

Likewise the previous chapter, we can expand the stream function in a Taylor series at the point (r_{00}, z_{00}) as

$$\psi = \sum_{m+n=0}^{\infty} a_{m,n} (r - r_{00})^m (z - z_{00})^n, \quad (4.2)$$

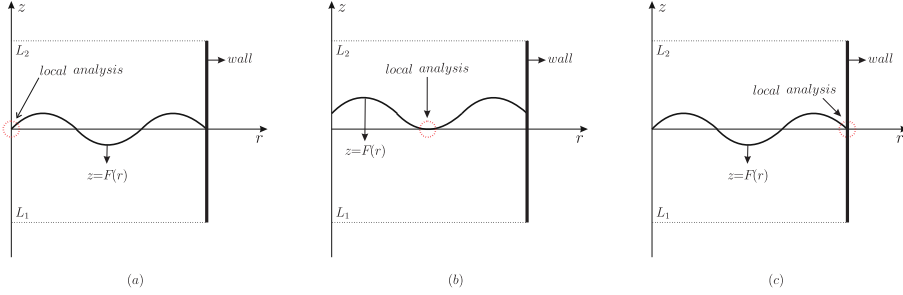


Figure 4.1: The local analysis will be investigated (a) on axis, (b) away from axis and (c) on wall. The interface is translated such that (a) $F(0) = 0$, (b) $F(r_0) = 0$ and (c) $F(r_w) = 0$, where expansion will be taken at origin, r_0 and r_w , respectively.

and the interface $z = F(r)$ is smooth and expanded at the point r_{00} as

$$F(r) = \sum_{i=1}^{\infty} k_i (r - r_{00})^i. \quad (4.3)$$

In the following procedure, we will also need to investigate the swirl velocity and pressure gradient, hence we also expand them

$$p = \sum_{m+n=0}^{\infty} p_{m,n} (r - r_{00})^m (z - z_{00})^n, \quad (4.4)$$

$$v = \sum_{m+n=0}^{\infty} b_{m,n} (r - r_{00})^m (z - z_{00})^n. \quad (4.5)$$

As boundary conditions, which we will use to reduce the number of coefficients from the given vector field and to see the relations among the coefficients $a_{m,n}$, $b_{m,n}$ and $p_{m,n}$, we have the kinematic boundary condition (2.58), tangential stress boundary condition (2.59) and normal stress boundary condition (2.60). As a next step, we consider the Navier-Stokes equations (2.40a)-(2.40d) to see the existence of more simplification and the relations among the coefficients.

Using the given boundary conditions and some non-linear transformations, the normal form of the given velocity field is obtained. The unfolding theory and the process to obtain the bifurcation diagrams are exactly same as in the previous chapter.

4.1 Basic Equations and Boundary Conditions for an Axisymmetric Flow

In Chapter 2, we introduce the boundary conditions for the free surface in a cylindrical coordinate system (r, θ, z) . In this chapter, since the flow is axisymmetric we will re-consider them.

Firstly, we introduce the normal vector, tangential vectors, radii of curvature, stress tensor and expansion of interface prior to the examination of the boundary conditions due to the fact that they are prerequisites.

For an axisymmetric flow, the normal \mathbf{n} and tangential vectors $\mathbf{t}_1, \mathbf{t}_2$ (2.42) at $(r, F(r))$ are

$$\mathbf{n} = N^{-1}(-F_r, 0, 1), \quad (4.6a)$$

$$\mathbf{t}_1 = N^{-1}(1, 0, F_r), \quad (4.6b)$$

$$\mathbf{t}_2 = N^{-1}(0, 1, 0), \quad (4.6c)$$

where $N = \left(1 + \left(\frac{\partial F}{\partial r}\right)^2\right)^{1/2}$ and the radii of curvature is

$$\frac{1}{R_1} + \frac{1}{R_2} = -\nabla \cdot \mathbf{n} = \frac{1}{r} \left[\frac{\partial}{\partial r} \left(\frac{r}{N} F_r \right) \right] = \frac{F_r^3 + r F_{rr} + F_r}{r (F_r^2 + 1)^{3/2}}. \quad (4.7)$$

For an axisymmetric flow, the stress tensor (2.57) is in the form

$$\Upsilon = \begin{pmatrix} -p + 2\mu \left(\frac{\partial u}{\partial r}\right) & \mu \left(r \frac{\partial(v/r)}{\partial r}\right) & \mu \left(\frac{\partial w}{\partial r} + \frac{\partial u}{\partial z}\right) \\ \mu \left(r \frac{\partial(v/r)}{\partial r}\right) & -p + 2\mu \left(\frac{u}{r}\right) & \mu \left(\frac{\partial v}{\partial z}\right) \\ \mu \left(\frac{\partial w}{\partial r} + \frac{\partial u}{\partial z}\right) & \mu \left(\frac{\partial v}{\partial z}\right) & -p + 2\mu \left(\frac{\partial w}{\partial z}\right) \end{pmatrix}. \quad (4.8)$$

The general case of the Navier-Stokes equations for a steady flow of a viscous incompressible fluids was given in (2.40a)-(2.40d). Since our study based on the axisymmetric flow, all variables are independent of θ . Therefore, we rewrite

4.1 Basic Equations and Boundary Conditions for an Axisymmetric Flow 47

them as

$$\frac{1}{r} \frac{\partial(ru)}{\partial r} + \frac{\partial w}{\partial z} = 0, \quad (4.9a)$$

$$\rho \left(u \frac{\partial u}{\partial r} + w \frac{\partial u}{\partial z} - \frac{v^2}{r} \right) = \mu \left(\nabla^2 u - \frac{u}{r^2} \right) - \frac{\partial p}{\partial r}, \quad (4.9b)$$

$$\rho \left(u \frac{\partial v}{\partial r} + w \frac{\partial v}{\partial z} + \frac{uv}{r} \right) = \mu \left(\nabla^2 v - \frac{v}{r^2} \right), \quad (4.9c)$$

$$\rho \left(u \frac{\partial w}{\partial r} + w \frac{\partial w}{\partial z} \right) = \mu \nabla^2 w - \frac{\partial p}{\partial z}, \quad (4.9d)$$

where $\nabla^2 = \frac{1}{r} \frac{\partial}{\partial r} \left(r \frac{\partial}{\partial r} \right) + \frac{\partial^2}{\partial z^2}$.

For the axisymmetric flow, the following boundary conditions occur on the free surface which is given in Chapter 2:

The kinematic boundary condition : We rewrite eq. (2.58) by considering the velocity field (u, v, w) and normal vector (4.6a) for an axisymmetric flow as

$$F_r u = w. \quad (4.10)$$

The tangential stress boundary conditions: We rewrite Eq. (2.59) by considering the velocity field (u, v, w) , normal vector (4.6a), tangential vector (4.6b) and stress tensor (4.8) for an axisymmetric flow as

$$\mu(1 - F_r^2) \left(\frac{\partial w}{\partial r} + \frac{\partial u}{\partial z} \right) - 2\mu F_r \left(\frac{\partial u}{\partial r} - \frac{\partial w}{\partial z} \right) = 0, \quad (4.11)$$

and for the tangential vector (4.6c),

$$F_r \frac{\partial v}{\partial r} - F_r \frac{v}{r} - \frac{\partial v}{\partial z} = 0. \quad (4.12)$$

The normal stress boundary conditions: We rewrite eq. (2.60) by considering the velocity field (u, v, w) , normal vector (4.6a) and stress tensor (4.8) for an axisymmetric flow as

$$\begin{aligned} -p(r, z)(1 + F_r^2) - 2\mu F_r \left(\frac{\partial u}{\partial z} + \frac{\partial w}{\partial r} \right) + 2\mu \left(F_r^2 \frac{\partial u}{\partial r} + \frac{\partial w}{\partial z} \right) = \\ -\sigma \frac{F_r^3 + r F_{rr} + F_r}{r (F_r^2 + 1)^{1/2}}. \end{aligned} \quad (4.13)$$

4.2 Flow Topology Close to Center Axis

In the meridional plane, we translate the coordinate system such that $F(0) = 0$. Therefore, at the axis the free surface is moved to the origin (see Fig. (4.2)). Using the Taylor expansion of a stream function, we will be able to investigate the streamlines with given boundary conditions. Taking into account the surface tension, kinematic and tangential stress boundary condition, our aim is to obtain the normal form of the stream function in the vicinity of origin.

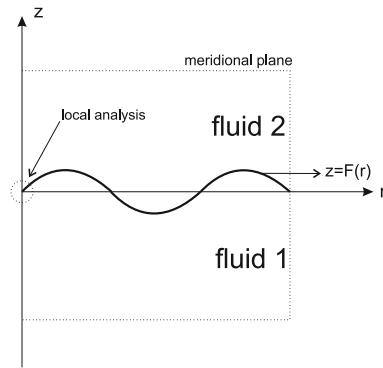


Figure 4.2: Translated meridional plane.

Since the expansion point is chosen as the *origin* ($r_{00} = 0$), we can write the stream function (4.2) as

$$\psi(r, z) = \sum_{m+n=0}^{\infty} a_{mn} r^m z^n. \quad (4.14)$$

The interface $F(r)$ must be an even function due to the axisymmetry. To provide the smoothness of (4.3), we need to say $\frac{d^{2n+1}F}{dr^{2n+1}} = 0$ where $n = 0, \dots$. With this, the interface becomes (since $r_{00} = 0$)

$$F(r) = \sum_{i=1}^{\infty} k_{2i} r^{2i}. \quad (4.15)$$

The center axis is a streamline, hence the stream function fulfils $\psi(r, z) = 0$ at $r = 0$, this means the coefficients $a_{0n} = 0$ for $n = 0, 1, \dots$. Furthermore, due to the axisymmetric assumption, the stream function is symmetric about

the center axis ($\psi(r, z) = \psi(-r, z)$). From this, we also have $a_{2m-1, n} = 0$ for $m = 1, 2, \dots$. By substituting these equalities, the stream function becomes

$$\psi(r, z) = r^2 \sum_{m+n=0}^{\infty} a_{2m+2, n} r^{2m} z^n, \quad (4.16)$$

where the velocity field is in the form (4.1).

Applying the kinematic (4.10) and tangential stress boundary conditions (4.11) to the stream function (4.16), the number of coefficients can be reduced. These substitutions effect the meridional plane.

Applying the tangential (4.12) and normal stress boundary condition (4.13) to the given stream function, the relations for azimuthal velocity and pressure will be observed. Hence, we will consider the boundary conditions into two way:

- (i) The boundary conditions which are effecting the stream function,
- (ii) The boundary conditions which are effecting angular velocity and pressure.

Using the velocities in equation (4.1), the kinematic boundary condition (4.10) can be written as

$$-F_r \frac{\partial \psi}{\partial z} = \frac{\partial \psi}{\partial r}. \quad (4.17)$$

Inserting the interface (4.15) and (4.1) into the kinematic boundary condition yields for the lowest-order coefficients

$$a_{2,0} = 0, \quad a_{4,0} = -k_2 a_{2,1}, \quad a_{6,0} = -k_2^2 a_{2,2} - k_4 a_{2,1} - k_2 a_{4,1}, \dots \quad (4.18)$$

and from the tangential stress condition (4.11),

$$a_{2,2} = 2 k_2 a_{2,1}, \quad a_{4,2} = 24 k_2^3 a_{2,1} - 3 k_2 a_{2,3} + 6 k_2 a_{4,1}, \dots \quad (4.19)$$

Note that, if the interface is flat, all $a_{2n,0} = 0$. The process can be found in the Maple worksheet [31]. It is useful to apply the transformation $r = x$ and $z = y + F(r)$ which makes the interface flat. Substituting these variables and the coefficients obtained from the boundary conditions into the stream function, we have

$$\begin{aligned} \psi = & a_{2,1} x^2 y + 2 a_{2,1} k_2 x^2 y^2 + a_{2,3} x^2 y^3 + (4 a_{2,1} k_2^2 + a_{4,1}) x^4 y \\ & + a_{2,4} x^2 y^4 + (24 a_{2,1} k_2^3 + 6 k_2 a_{4,1}) x^4 y^2 \\ & + a_{2,5} x^2 y^5 + (4 a_{2,4} k_2 + a_{4,3}) x^4 y^3 + (4 a_{2,1} k_2 k_4 + 3 a_{2,3} k_2^2) \\ & + 2 (24 a_{2,1} k_2^3 - 3 a_{2,3} k_2 + 6 k_2 a_{4,1}) k_2 + a_{6,1} x^6 y + a_{2,6} x^2 y^6 \\ & + (5 a_{2,5} k_2 + a_{4,4}) x^4 y^4 + (384 a_{2,1} k_2^5 + 120 a_{2,1} k_2^2 k_4 - 30 a_{2,3} k_2^3 \\ & + 104 a_{4,1} k_2^3 - 6 k_6 a_{2,1} + 8 k_4 a_{4,1} + 10 k_2 a_{6,1}) x^6 y^2 + \mathcal{O}(|x, y|^9). \end{aligned} \quad (4.20)$$

It is possible to see the relations between the coefficients from the normal stress boundary condition (4.13). Prior to doing this, we need to simplify some of the coefficients from the pressure and the velocity v . To make these, the Navier-Stokes equations (5.6) and the tangential stress (4.12) are used.

Due to the fact that the velocity u is odd and w even, it can be obtained from the Navier-Stokes equation (2.38) that the pressure is an even and velocity v is an odd function of the radial variable. Hence we rewrite the pressure (4.4) and the velocity v (4.5) by taking account of $p(r, z) = p(-r, z)$ and $v(r, z) = -v(-r, z)$ at the origin as

$$p = \sum_{m+n=0}^{\infty} p_{2m,n} r^{2m} z^n, \quad (4.21)$$

$$v = \sum_{m+n=0}^{\infty} b_{2m+1,n} r^{2m+1} z^n. \quad (4.22)$$

Firstly, to determine the relations between the coefficients of the velocity v , we insert the equation (4.22) into (4.12) and obtain the following relations

$$b_{1,1} = 0, \quad b_{3,1} = -2k_2 b_{1,2} + 4b_{3,0} k_2, \dots \quad (4.23)$$

As a next step, we use the azimuthal component of Navier-Stokes equation (5.6c) and obtain

$$b_{1,3} = 4k_2 b_{1,2}, \quad b_{3,0} = -\frac{-\rho a_{2,1} b_{1,0} + \mu b_{1,2}}{4\mu}, \dots \quad (4.24)$$

To see all relations, please look at the Maple worksheet [31]. Using all these substitutions, the velocity v can be written up to the fifth-order terms as

$$\begin{aligned} v = & b_{1,0} r + b_{1,2} r z^2 - \frac{(-\rho a_{2,1} b_{1,0} + \mu b_{1,2}) r^3}{4\mu} + 4k_2 b_{1,2} r z^3 \\ & + \left(-2k_2 b_{1,2} - \frac{(-\rho a_{2,1} b_{1,0} + \mu b_{1,2}) k_2}{\mu} \right) r^3 z + \mathcal{O}(|r, z|^5). \end{aligned} \quad (4.25)$$

Secondly, the relations between the coefficients of the pressure equation (4.21) can be obtained by using the Navier-Stokes equations (5.6b) and (5.6d). From these equations, one can find some relations between the coefficients of pressure and velocities. Substituting this relations into the pressure expansion (4.21) we

obtain, (up to the fourth-order terms)

$$\begin{aligned}
p &= p_{0,0} + 8\mu a_{2,1}k_2z - (2\rho a_{2,1}^2 + 6\mu a_{2,3} + 8\mu a_{4,1})z^2 \\
&+ \left(\frac{\rho b_{1,0}^2 - \rho a_{2,1}^2}{2} + 3\mu a_{2,3} + 4\mu a_{4,1} \right) r^2 \\
&+ (-128\mu a_{2,1}k_2^3 - 8\rho a_{2,1}^2k_2 + 16\mu a_{2,3}k_2 - 32\mu a_{4,1}k_2 - 8\mu a_{2,4})z^3 \\
&+ (96\mu a_{2,1}k_4 + 24\mu a_{2,3}k_2 + 48\mu a_{4,1}k_2) r^2z + \mathcal{O}(|r, z|^4). \tag{4.26}
\end{aligned}$$

From eq. (5.6b), we obtain the relations for $\frac{\partial p}{\partial r}$ and from eq. (5.6d) $\frac{\partial p}{\partial z}$. We see that $\frac{\partial p}{\partial r}$ and $\frac{\partial p}{\partial z}$ have some same coefficients. For example, from $\frac{\partial p}{\partial r}$, the coefficient $p_{2,1}$ is in the form

$$p_{2,1} = 96\mu a_{2,1}k_4 + 24\mu a_{2,3}k_2 + 48\mu a_{4,1}k_2, \tag{4.27}$$

and from $\frac{\partial p}{\partial z}$, $p_{2,1}$ is

$$p_{2,1} = 192\mu a_{2,1}k_2^3 - 24\mu a_{2,3}k_2 + 48\mu a_{4,1}k_2 + 12\mu a_{2,4}. \tag{4.28}$$

Since (4.27) and (4.28) are same, eliminating $p_{2,1}$ from them, we obtain

$$a_{2,4} = -16a_{2,1}k_2^3 + 8k_4a_{2,1} + 4a_{2,3}k_2. \tag{4.29}$$

There exist also other coefficients like $p_{2,1}$. However they include the coefficients of swirl velocity, which is not useful for meridional plane. For example, $p_{2,2}$ is also common coefficient of $\frac{\partial p}{\partial r}$ and $\frac{\partial p}{\partial z}$, eliminating $p_{2,2}$ like $p_{2,1}$, we obtain that

$$a_{4,3} = -\frac{3\rho a_{2,1}a_{2,3} + 4\rho a_{2,1}a_{4,1} + \rho b_{1,0}b_{1,2} + 30\mu a_{2,5} + 48\mu a_{6,1}}{24\mu}. \tag{4.30}$$

It is very significant to underline that the flow must be steady, if not, this relations can not be observed.

Alternatively, from the vorticity transport equation

$$\nabla \times \vec{N}S = 0 \tag{4.31}$$

where $\vec{N}S$ is the Navier-Stokes equations (5.6b)-(5.6d), from the second component we observe the same results (details can be found in [31])

$$\begin{aligned}
r^3z^0 &: -384\mu a_{2,1}k_2^3 + 192\mu k_4a_{2,1} + 96\mu k_2a_{2,3} - 24\mu a_{2,4} = 0, \\
r^3z^1 &: -12\rho a_{2,1}a_{2,3} - 16\rho a_{2,1}a_{4,1} - 4\rho b_{1,0}b_{1,2} - 120\mu a_{2,5} - 96\mu a_{4,3} \\
&- 192\mu a_{6,1} = 0. \tag{4.32}
\end{aligned}$$

Inserting the pressure and the stream function into the normal stress boundary condition (4.13), we obtain some relations between the coefficients of stream function and pressure equation, for example, $a_{2,1} = -\frac{4\sigma k_2 + p_{0,0}}{4\mu}$. Since the other relations $a_{4,1}, a_{6,1}$ include too many terms, we will not write all of them here, they can be again found from the Maple worksheet [31]. Note that $a_{4,1}$ and $a_{6,1}$ include some coefficients from the swirl velocity v . In the following process, these relations seem to be not very useful. However, they give us some physical expressions. For example, the equation

$$a_{2,1} = -\frac{4\sigma k_2 + p_{0,0}}{4\mu} \quad (4.33)$$

expresses that the pressure is $-4\sigma k_2 - 4\mu a_{2,1}$ at the origin. That means if $a_{2,1} = -\frac{\sigma k_2}{\mu}$, the pressure is 'zero' at the origin.

The velocity v and pressure p are not very effective to change the topology. They help us to find some physical informations and especially to obtain the relations for $a_{2,4}$. It can be said that for the steady flow when $a_{2,1} = 0$ and $a_{2,3} = 0$, then $a_{2,4} = 0$ as well. Since we will consider the topology of fluids in the meridional plane, the importance of velocity v and pressure p is low.

4.2.1 Regular Case

The origin is a critical or singular point due to the velocity u and w (4.1) by using the stream function (5). The linearised system is written as

$$\begin{pmatrix} \dot{x} \\ \dot{y} \end{pmatrix} = J \begin{pmatrix} x \\ y \end{pmatrix}, \quad (4.34)$$

where J is the Jacobian matrix

$$J = \begin{pmatrix} a_{2,1} & 0 \\ 0 & -2a_{2,1} \end{pmatrix}. \quad (4.35)$$

The eigenvalues for this matrix are $-a_{2,1}$ and $2a_{2,1}$. Firstly, we assume that $a_{2,1} < 0$, the origin is a saddle with the stable direction on the interface, which is the eigenvector $(1, 0)$ and unstable direction on the center axis, which is the other eigenvector $(0, 1)$. For $a_{2,1} > 0$, only the stable and unstable direction reversed. (see Fig. 4.3) If $a_{2,1} = 0$, higher order terms must be investigated in order to determine the flow topology. This condition physically indicates that the first coefficient of pressure $p_{0,0}$ equals $-4\sigma k_2$. That means, at the origin the pressure depends on the surface tension and the second derivative of given interface. Physically, it gives us the pressure is zero if the interface is flat at the origin.

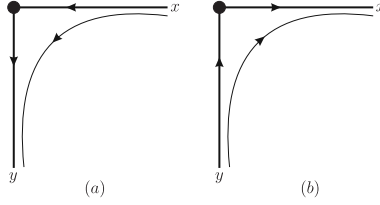


Figure 4.3: Streamlines in the vicinity of origin for the non-degenerate critical point with $a_{2,1} \neq 0$ (a) $a_{2,1} < 0$ (b) $a_{2,1} > 0$.

4.2.2 Co-dimension 1 bifurcation

Assuming $a_{2,1} = 0$, the stream function is in the following form

$$\psi = a_{2,3}x^2y^3 + a_{4,1}x^4y + \mathcal{O}(|x, y|^6). \quad (4.36)$$

Factoring the coefficient $a_{2,3}$ and substituting $x = A\tilde{x}$ and $y = B\tilde{y}$, the *truncated* stream function can be written as

$$\psi = a_{4,1}A^2B\tilde{x}^2\tilde{y} \left(B^2 \frac{a_{2,3}}{a_{4,1}} \tilde{y}^2 + A^2 \tilde{x}^2 \right). \quad (4.37)$$

Scaling the stream function by dividing by $a_{4,1}A^2B$ and substituting $B = \left| \frac{a_{4,1}}{a_{2,3}} \right|^{1/2}$ and $A = 1$, we have

$$\psi = \tilde{x}^2\tilde{y}(\sigma\tilde{y}^2 + \tilde{x}^2), \quad (4.38)$$

where

$$\sigma = \frac{a_{2,3}}{a_{4,1}} \left| \frac{a_{4,1}}{a_{2,3}} \right| = \begin{cases} +1 & \text{for } a_{2,3}/a_{4,1} > 0 \\ -1 & \text{for } a_{2,3}/a_{4,1} < 0 \end{cases},$$

and we have assumed $a_{2,3} \neq 0$ and $a_{4,1} \neq 0$. For (4.38), we can find the possible dividing streamlines by solving $\psi = 0$. This yields

$$\tilde{x} = 0 \quad \text{or} \quad \tilde{y} = 0 \quad \text{or} \quad \tilde{y} = \pm\sqrt{-\sigma\tilde{x}}. \quad (4.39)$$

The latter represents separatrices when $\sigma = -1$. However the positive case is outside the physical domain, so only the solution $\tilde{y} = -\sqrt{-\sigma\tilde{x}}$ is of interest. (see Fig. 4.4).

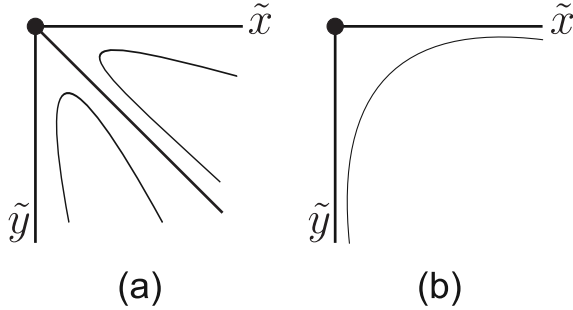


Figure 4.4: Streamlines in the vicinity of the origin in case of a degenerate critical point with $a_{2,1} = 0$ for (a) $\sigma = -1$ (b) $\sigma = 1$.

The unfolding of the degenerate case (4.38) is, including terms up to order five

$$\psi = \epsilon_1 x^2 y + 2 \epsilon_1 k_2 x^2 y^2 + a_{2,3} x^2 y^3 + (4 \epsilon_1 k_2^2 + a_{4,1}) x^4 y, \quad (4.40)$$

where $\epsilon_1 = a_{2,1}$ is a small parameter. To simplify this equation, we introduce a transformation which preserves the boundary conditions ($x = 0$ is mapped to $\xi = 0$) and the symmetry condition ($(x(-\xi, \eta), y(-\xi, \eta)) = (-x(\xi, \eta), y(\xi, \eta))$) (for detailed expression please look at [32])

$$x = \xi + m_{1,1} \xi \eta, \quad y = \eta + l_{0,2} \eta^2. \quad (4.41)$$

Choosing $l_{0,2} = 0$ and $m_{1,1} = -k_2$, we have

$$\psi = \xi^2 \eta (\epsilon_1 + \tilde{a}_{2,3} \eta^2 + \tilde{a}_{4,1} \xi^2), \quad (4.42)$$

where $\tilde{a}_{2,3} = -3 \epsilon_1 k_2^2 + a_{2,3}$ and $\tilde{a}_{4,1} = 4 \epsilon_1 k_2^2 + a_{4,1}$. Factoring the coefficient $\tilde{a}_{4,1}$ and substituting $\xi = A \tilde{\xi}$ and $\eta = B \tilde{\eta}$, we have

$$\psi = \tilde{a}_{4,1} A^2 B \tilde{\eta} \tilde{\xi}^2 \left(\epsilon_1 + B^2 \frac{\tilde{a}_{2,3}}{\tilde{a}_{4,1}} \tilde{\eta}^2 + A^2 \tilde{\xi}^2 \right). \quad (4.43)$$

Scaling the stream function by dividing by $\tilde{a}_{4,1} A^2 B$ and choosing $B = \left| \frac{\tilde{a}_{2,3}}{\tilde{a}_{4,1}} \right|^{1/2}$ and $A = 1$, the stream function becomes

$$\psi = \tilde{\eta} \tilde{\xi}^2 \left(\epsilon_1 + \sigma \tilde{\eta}^2 + \tilde{\xi}^2 \right), \quad (4.44)$$

where $\sigma = \frac{\tilde{a}_{2,3}}{\tilde{a}_{4,1}} \left| \frac{\tilde{a}_{4,1}}{\tilde{a}_{2,3}} \right|$. We can summarize this in

THEOREM 4.1 *Let $a_{2,1}$ be a small parameter. Assuming the non-degeneracy conditions $\tilde{a}_{4,1} \neq 0$ and $\tilde{a}_{2,3} \neq 0$ the normal form for the streamfunction (4.36) is*

$$\psi = x^2 y (c_{0,0} + x^2 + \sigma y^2 + \mathcal{O}(|x, y|^3)), \quad (4.45)$$

where

$$\sigma = \begin{cases} +1 & \text{for } \tilde{a}_{2,3}/\tilde{a}_{4,1} > 0 \\ -1 & \text{for } \tilde{a}_{2,3}/\tilde{a}_{4,1} < 0 \end{cases},$$

and $c_{0,0}$ is a small transformed parameter.

The velocity field of (4.45) is

$$\begin{aligned} u &= \frac{1}{x} \frac{\partial \psi}{\partial y} = x(x^2 + 3\sigma y^2 + c_{0,0}), \\ w &= -\frac{1}{x} \frac{\partial \psi}{\partial x} = -2y(2x^2 + \sigma y^2 + c_{0,0}), \end{aligned} \quad (4.46)$$

with the determinant of the Jacobian

$$J = -12x^4 + 18x^2y^2\sigma - 10x^2c_{0,0} - 18y^4 - 12y^2\sigma c_{0,0} - 2c_{0,0}^2 \quad (4.47)$$

On the interface, the critical points can be obtained by substituting $y = 0$ into the velocity field,

$$u(x, 0) = x(x^2 + c_{0,0}) \quad \text{and} \quad v(x, 0) = 0, \quad (4.48)$$

and for the center axis, we substitute $x = 0$ into the velocity field,

$$u(0, x) = 0 \quad \text{and} \quad v(0, y) = -2y(\sigma y^2 + c_{0,0}). \quad (4.49)$$

These show us that the sign of the $c_{0,0}$ is a significant parameter to change the number of critical points. Hence, $c_{0,0} = 0$ is the bifurcation point for this case.

The critical points for away from the boundaries can be found by solving

$$x^2 + 3\sigma y^2 + c_{0,0} = 0 \quad \text{and} \quad 2x^2 + \sigma y^2 + c_{0,0} = 0. \quad (4.50)$$

If we eliminate x from the given equations, we obtained that

$$5\sigma y^2 + c_{0,0} = 0, \quad (4.51)$$

which has a solution when $c_{0,0}\sigma < 0$. We observe two kinds of bifurcations here, which are *corner bubble creation* and *corner crossing* can be seen in Fig. 4.5. These bifurcations and the streamline patterns are also obtained by Brøns [30]. Even though the surface tension and curvature of the interface were not considered in [30], the co-dimension one bifurcations looks like similar.

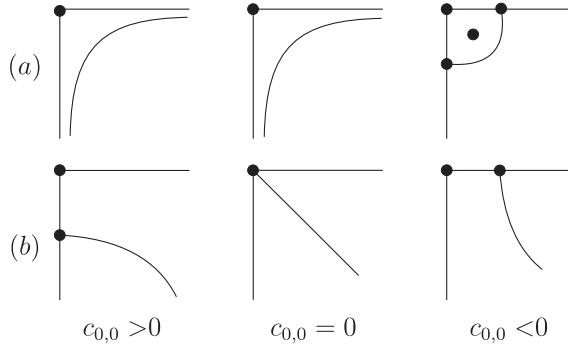


Figure 4.5: Bifurcation diagrams for the normal form (4.45). (a) $\sigma = 1$ (b) $\sigma = -1$.

4.2.3 Co-dimension 2 bifurcations

We have assumed that for the co-dimension one bifurcation, $a_{4,1}$ and $a_{2,3}$ non-zero. Hence, the question may arise: what happens if we break one of the assumptions?

The higher order terms determine the flow topology and the co-dimension two bifurcation occurs. In this section we consider new non-degeneracy conditions which are

- $a_{2,1} = 0$, $a_{2,3} = 0$, $a_{4,1} \neq 0$ and $a_{2,5} \neq 0$,
- $a_{2,1} = 0$, $a_{2,3} \neq 0$, $a_{4,1} = 0$ and $-3a_{2,3}k_2^2 + a_{6,1} \neq 0$.

4.2.3.1 Case 1

The first degeneracy condition is that $a_{2,1} = 0$, $a_{2,3} = 0$, $a_{4,1} \neq 0$ and $a_{2,5} \neq 0$. For steady flow, from (4.29) we have $a_{2,4} = 0$. By using these assumptions, the extended and truncated stream function (4.36) including terms up to order 7, becomes

$$\begin{aligned} \psi = & a_{4,1}x^4y + 6k_2a_{4,1}x^4y^2 + a_{2,5}x^2y^5 + a_{4,3}x^4y^3 \\ & + (12k_2^2a_{4,1} + a_{6,1})x^6y. \end{aligned} \quad (4.52)$$

To obtain the normal form of this equation, we introduce a near-identity transformation such that $x = 0$ and $y = 0$ is mapped $\xi = 0$ and $\eta = 0$, respectively,

and preserves the symmetry condition by

$$\begin{aligned} x &= \xi + m_{1,1}\xi\eta + m_{3,0}\xi^3 + m_{1,2}\xi\eta^2, \\ y &= \eta + l_{0,2}\eta^2 + l_{0,3}\eta^3 + l_{2,1}\xi^2\eta. \end{aligned} \quad (4.53)$$

After substitutions (see details in Maple worksheet [31]), we choose $m_{1,1} = m_{1,2} = m_{3,0} = 0$, $l_{0,2} = -6k_2$, $l_{2,1} = -\frac{a_{6,1}+12a_{4,1}k_2^2}{a_{4,1}}$ and $l_{0,3} = -\frac{a_{4,3}-72a_{4,1}k_2^2}{a_{4,1}}$ the stream function becomes

$$\psi = a_{4,1}\xi^4\eta + a_{2,5}\xi^2\eta^5. \quad (4.54)$$

Factoring the coefficient $a_{4,1}$ and substituting $\xi = A\xi$ and $\eta = B\eta$ into the previous stream function

$$\psi = a_{4,1}A^2B\xi^2\eta \left(A^2\xi^2 + B^4\frac{a_{2,5}}{a_{4,1}}\eta^4 \right), \quad (4.55)$$

and scaling it by dividing by $a_{4,1}A^2B$, and substituting $A = 1$ and $B = \left| \frac{a_{4,1}}{a_{2,5}} \right|^{1/4}$ we obtain

$$\psi = \xi^2\eta(\xi^2 + \sigma\eta^4), \quad (4.56)$$

where

$$\sigma = \frac{a_{2,5}}{a_{4,1}} \left| \frac{a_{4,1}}{a_{2,5}} \right| = \begin{cases} +1 & \text{for } a_{2,5}/a_{4,1} > 0 \\ -1 & \text{for } a_{2,5}/a_{4,1} < 0 \end{cases},$$

and we have assumed $a_{2,5} \neq 0$. For $\sigma = 1$, the separatrices are $\eta = 0$ and $\xi = 0$; for $\sigma = -1$ there exist also a parabolic separatrix $\xi = \sqrt{-\sigma\eta^2}$. (see Fig. 4.6)

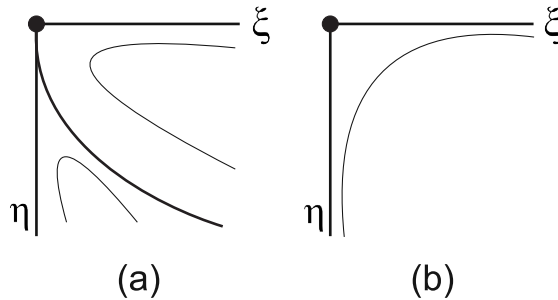


Figure 4.6: Possible streamlines in the vicinity of origin for the degenerate case (4.56). (a) $\sigma = -1$ (b) $\sigma = 1$.

The unfolding for this case, which is truncated after the seventh-order terms, is

$$\begin{aligned} \psi &= \epsilon_1 x^2 y + 2 \epsilon_1 k_2 x^2 y^2 + \epsilon_2 x^2 y^3 + (4 \epsilon_1 k_2^2 + a_{4,1}) x^4 y + a_{2,4} x^2 y^4 \\ &+ (24 \epsilon_1 k_2^3 + 6 k_2 a_{4,1}) x^4 y^2 + a_{2,5} x^2 y^5 \\ &+ (4 (-16 \epsilon_1 k_2^3 + 8 \epsilon_1 k_4 + 4 \epsilon_2 k_2) k_2 + a_{4,3}) x^4 y^3 \\ &+ (4 \epsilon_1 k_2 k_4 + 3 \epsilon_2 k_2^2 + 2 (24 \epsilon_1 k_2^3 + 6 k_2 a_{4,1} - 3 \epsilon_2 k_2) k_2 + a_{6,1}) x^6 y \quad (4.57) \end{aligned}$$

where $\epsilon_1 = a_{2,1}$, $\epsilon_2 = a_{2,3}$ and $a_{2,4} = -16 \epsilon_1 k_2^3 + 8 \epsilon_1 k_4 + 4 \epsilon_2 k_2$ from (4.29). This unfolding can be simplified by applying the near identity transformation (4.53) as well. Prior to applying this transformation, we will investigate this case into three sub-cases which make the process much easier,

- $k_2 \neq 0$, $k_4 \neq 0$ or $k_4 = 0$
- $k_2 = 0$, $k_4 \neq 0$,
- $k_2 = 0$, $k_4 = 0$.

For the case of the co-dimension 2 bifurcation, we will use sub-scripts to make clear the previous three cases from now on, unless explicitly stated. (e.g. ψ_1 instead of ψ)

Case 1.1: $k_2 \neq 0$, $k_4 \neq 0$ or $k_4 = 0$

Choosing $m_{3,0} = -3l_{2,1}$, $l_{0,2} = -\frac{2k_2}{5}$, $m_{1,1} = -\frac{7k_2}{5}$ and $m_{1,2} = \frac{504k_2^3 - 75k_2 l_{0,3} - 500k_4}{25k_2}$, the stream function reads as

$$\begin{aligned} \psi_1 &= \epsilon_1 \xi^2 \eta + \gamma \epsilon_1 \xi^2 \eta^2 + \tilde{\epsilon}_2 \xi^2 \eta^3 + \tilde{a}_{4,1} \eta \xi^4 + \tilde{a}_{2,5} \xi^2 \eta^5 \\ &+ f(\epsilon_1, \epsilon_2, l_{0,3}) \xi^4 \eta^3 + g(\epsilon_1, \epsilon_2, l_{2,1}) \eta \xi^6 \quad (4.58) \end{aligned}$$

where

$$\begin{aligned} \tilde{a}_{4,1} &= a_{4,1} + \mathcal{O}(\epsilon_1), \quad \tilde{a}_{2,5} = a_{2,5} + \mathcal{O}(\epsilon_1, \epsilon_2), \quad \gamma = -\frac{6k_2}{5} \\ f(\epsilon_1, \epsilon_2, l_{0,3}) &= a_{4,3} + \frac{1406 k_2^2 a_{4,1}}{25} - 11 a_{4,1} l_{0,3} - \frac{80 k_4 a_{4,1}}{k_2} + \mathcal{O}(\epsilon_1, \epsilon_2), \quad (4.59) \\ g(\epsilon_1, \epsilon_2, l_{2,1}) &= a_{6,1} + 12 a_{4,1} k_2^2 - 11 a_{4,1} l_{2,1} + \mathcal{O}(\epsilon_1, \epsilon_2). \end{aligned}$$

Since

$$g\left(0, 0, \frac{a_{6,1} + 12 a_{4,1} k_2^2}{11 a_{4,1}}\right) = 0, \quad \frac{\partial}{\partial l_{2,1}} g\left(0, 0, \frac{a_{6,1} + 12 a_{4,1} k_2^2}{11 a_{4,1}}\right) = -11 a_{4,1} \neq 0,$$

it follows from the implicit function theorem that there exists a function $l_{2,1}(\epsilon_1, \epsilon_2)$ with $l_{2,1}(0, 0) = \frac{a_{6,1} + 12 a_{4,1} k_2^2}{11 a_{4,1}}$ such that $g(\epsilon_1, \epsilon_2, l_{2,1}(\epsilon_1, \epsilon_2)) = 0$, for ϵ_1 and ϵ_2

sufficiently small. Similarly, one can also find functions $l_{0,3}(\epsilon_1, \epsilon_2)$ which solves $f = 0$. The stream function reads as,

$$\xi^2 \eta (\epsilon_1 + \gamma \epsilon_1 \eta + \tilde{\epsilon}_2 \eta^2 + \tilde{a}_{4,1} \xi^2 + \tilde{a}_{2,5} \eta^4). \quad (4.60)$$

Likewise the process of obtaining the normal form, we substitute $\xi = A\tilde{\xi}$ and $\eta = B\tilde{\eta}$ and collect the coefficient $\tilde{a}_{4,1}A^2$ outside the parenthesis and obtain

$$\tilde{a}_{4,1}A^4B\tilde{\xi}^2\tilde{\eta} \left(\frac{\epsilon_1}{A^2} + \frac{B\gamma\epsilon_1}{A^2}\tilde{\eta} + \frac{B^2\tilde{\epsilon}_2}{A^2}\tilde{\eta}^2 + \tilde{\xi}^2 + \frac{B^4\tilde{a}_{2,5}}{A^2\tilde{a}_{4,1}}\tilde{\eta}^4 \right). \quad (4.61)$$

Choosing $B = \frac{1}{\gamma}$ and $A = \left| \frac{\tilde{a}_{4,1}B^4}{\tilde{a}_{2,5}} \right|^{1/2}$, next scaling the stream function by dividing by $\tilde{a}_{4,1}A^4B$ we obtain

$$\tilde{\xi}^2\tilde{\eta} (\epsilon_1 + \epsilon_1\tilde{\eta} + \tilde{\epsilon}_2\tilde{\eta}^2 + \tilde{\xi}^2 + \sigma\tilde{\eta}^4), \quad (4.62)$$

where $\sigma = \frac{\tilde{a}_{2,5}}{\tilde{a}_{4,1}} \left| \frac{\tilde{a}_{4,1}}{\tilde{a}_{2,5}} \right|$. From this process, the following theorem arises.

THEOREM 4.2 *Let $a_{2,1}, a_{2,3}$ be small parameters and k_2 non-zero. Assuming the non-degeneracy conditions $a_{4,1} \neq 0$ and $a_{2,5} \neq 0$ the normal form for the streamfunction (4.56) is*

$$\psi_1 = x^2y (c_{0,0} + c_{0,0}y + c_{0,2}y^2 + x^2 + \sigma y^4). \quad (4.63)$$

where

$$\sigma = \begin{cases} +1 & \text{for } \tilde{a}_{2,5}/\tilde{a}_{4,1} > 0 \\ -1 & \text{for } \tilde{a}_{2,5}/\tilde{a}_{4,1} < 0 \end{cases},$$

$c_{0,0}$ and $c_{0,2}$ are small transformed parameters.

Case 1.2: $k_2 = 0, k_4 \neq 0$

Due to the similar process of the Case 1.1, we will skip to write more detail in this case and Case 1.3. For detailed expressions please look the Maple worksheet [31]. Choosing $l_{0,3} = -\frac{a_{4,3}}{a_{4,1}} + \mathcal{O}(\epsilon_1, \epsilon_2)$, $l_{0,2} = m_{1,1} = m_{3,0} = m_{1,2} = 0$ and $l_{2,1} = -\frac{a_{6,1}}{a_{4,1}} + \mathcal{O}(\epsilon_1, \epsilon_2)$, and following the similar process as in the Case 1.1, the following theorem arises.

THEOREM 4.3 *Let $a_{2,1}, a_{2,3}$ be small parameters and $k_2 = 0$ and $k_4 \neq 0$. Assuming the non-degeneracy conditions $a_{4,1} \neq 0$ and $a_{2,5} \neq 0$ the normal form for the streamfunction (4.56) is*

$$\psi_2 = x^2y (c_{0,0} + c_{0,2}y^2 + x^2 + c_{0,0}y^3 + \sigma y^4). \quad (4.64)$$

where

$$\sigma = \begin{cases} +1 & \text{for } \tilde{a}_{2,5}/\tilde{a}_{4,1} > 0 \\ -1 & \text{for } \tilde{a}_{2,5}/\tilde{a}_{4,1} < 0 \end{cases},$$

$c_{0,0}$ and $c_{0,2}$ are small transformed parameters.

Case 1.3: $k_2 = 0, k_4 = 0$

Choosing $l_{0,3} = -\frac{a_{4,3}}{a_{4,1}} + \mathcal{O}(\epsilon_1, \epsilon_2)$, $l_{0,2} = m_{1,1} = m_{3,0} = m_{1,2} = 0$ and $l_{2,1} = -\frac{a_{6,1}}{a_{4,1}} + \mathcal{O}(\epsilon_1, \epsilon_2)$, and following the similar process as in the Case 1.1, the following theorem arises.

THEOREM 4.4 *Let $a_{2,1}, a_{2,3}$ be small parameters and $k_2 = 0$ and $k_4 = 0$. Assuming the non-degeneracy conditions $a_{4,1} \neq 0$ and $a_{2,5} \neq 0$ the normal form for the streamfunction (4.56) is*

$$\psi_3 = x^2 y (c_{0,0} + c_{0,2} y^2 + x^2 + \sigma y^4). \quad (4.65)$$

where

$$\sigma = \begin{cases} +1 & \text{for } \tilde{a}_{2,5}/\tilde{a}_{4,1} > 0 \\ -1 & \text{for } \tilde{a}_{2,5}/\tilde{a}_{4,1} < 0 \end{cases},$$

$c_{0,0}$ and $c_{0,2}$ are small transformed parameters.

When we make a bifurcation analysis of the given stream function into three cases, it is observed that there is no difference among them. Hence, we will just consider one of the stream function from them. (Let it be Case 1.1) The reason will be explained in the following process.

From now on, using the velocity field and determinant of Jacobian, we will create the bifurcation diagrams.

The velocity field for (4.63) is

$$\begin{aligned} u_1 &= x (c_{0,0} + 2 y c_{0,0} + 3 y^2 c_{0,2} + x^2 + 5 \sigma y^4), \\ w_1 &= -2 y (c_{0,0} + y c_{0,0} + y^2 c_{0,2} + 2 x^2 + \sigma y^4), \end{aligned} \quad (4.66)$$

with the determinant of the Jacobian

$$\begin{aligned} J_1 &= -50 \sigma^2 y^8 - 60 \sigma y^6 c_{0,2} + 110 \sigma x^2 y^4 - 40 \sigma y^5 c_{0,0} - 20 \sigma y^4 c_{0,0} \\ &\quad - 18 y^4 c_{0,2}^2 + 18 x^2 y^2 c_{0,2} - 24 y^3 c_{0,1} c_{0,2} - 12 x^4 - 4 x^2 y c_{0,0} \\ &\quad - 12 y^2 c_{0,0} c_{0,2} - 8 y^2 c_{0,0}^2 - 10 x^2 c_{0,0} - 8 y c_{0,0} c_{0,1} - 2 c_{0,0}^2. \end{aligned} \quad (4.67)$$

On the interface, the number of critical points can be found when we substitute $y = 0$ into the velocity field. The velocity w directly vanishes by using this substitution. Hence the velocity u determines the number of critical points on the interface,

$$u_1 = x(c_{0,0} + x^2) = 0. \quad (4.68)$$

When $c_{0,0} < 0$ there are two critical points and when $c_{0,0} > 0$ there is one critical point on the interface. Since $c_{0,0}$ is a bifurcation point for the critical point on the interface. This is valid for all three cases. (Case 1.1, 1.2 and 1.3)

For the critical points on the center axis, we need to substitute $x = 0$ into the velocity field. Here, the velocity w determines the number of critical points,

$$w_1 = c_{0,0} + y c_{0,0} + y^2 c_{0,2} + \sigma y^4. \tag{4.69}$$

The local bifurcation curve for the critical points on the center axis can be obtained by taking the resultant of $J(0, y)$ and $w(0, y)$ with respect y . This curve is

$$\begin{aligned} LCOC_1 : c_{0,0}(256c_{0,0}^2 - 27\sigma c_{0,0}^3 + 144\sigma c_{0,0}^2 c_{0,2} - 128\sigma c_{0,0} c_{0,2}^2 - \\ - 4c_{0,0} c_{0,2}^3 + 16c_{0,2}^4) \end{aligned} \tag{4.70}$$

For the cases 1.2 and 1.3,

$$\begin{aligned} LCOC_2 : c_{0,0}\sigma(256\sigma c_{0,0}^2 - 128c_{0,0} c_{0,2}^2 + 144\sigma c_{0,0}^3 c_{0,2} + 16\sigma c_{0,2}^4 \\ - 27c_{0,0}^5 - 4c_{0,0}^2 c_{0,2}^3) = 0 \end{aligned} \tag{4.71}$$

$$LCOC_3 : 16c_{0,0} (4\sigma c_{0,0} - c_{0,2}^2)^2 = 0 \tag{4.72}$$

The bifurcation diagram and the bifurcation process for Case 1.1 and Case 1.2 are similar, however for Case 1.3 is different, see Fig. 4.7. In this figure, we can eliminate curve B and C , because of the fact that curve B changes the number of critical points for just upper-side of interface and curve C does not change anything. Therefore, we just need to curves A and D , for the on-going process. Though the bifurcation diagrams seem different, curve A and D have the same property for the lower-side of interface. Hence we conclude that the bifurcation diagrams are similar.

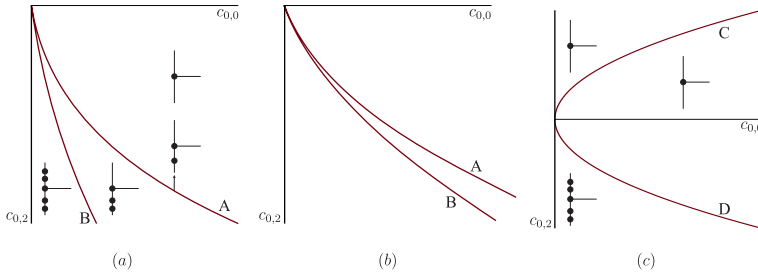


Figure 4.7: The local bifurcation curves for (a) $LCOC_1$ (b) $LCOC_2$ and (c) $LCOC_3$ which are drawn using Maple.

The other bifurcation curves, which are local bifurcation curve for away from the boundaries and global bifurcation curves, have also the similar properties for the cases 1 – 3. Therefore we will just consider one case (Case 1) from now on.

Away from the center axis and the interface, the local bifurcation curve for the critical points can be found from substituting $x^2 = -5\sigma y^4 - 3y^2 c_{0,2} - 2y c_{0,0} - c_{0,0}$ into the velocity w ,

$$w = -9\sigma y^4 - 5y^2 c_{0,2} - 3y c_{0,0} - c_{0,0}. \quad (4.73)$$

Using this substitution into J_1 (4.67) as well, we find the resultant of J and w with respect to y and obtain

$$\begin{aligned} LCOF_1 : 20736\sigma^2 c_{0,0}^2 - 19683\sigma c_{0,0}^3 + 58320\sigma c_{0,0}^2 c_{0,2} \\ - 28800\sigma c_{0,0} c_{0,2}^2 - 4500 c_{0,0} c_{0,2}^3 + 10000 c_{0,2}^4 = 0. \end{aligned} \quad (4.74)$$

Note that this result normally includes the equation ' $LCOC_1$ ' as a factor, however we directly eliminate it due to the fact that we have already used it as a local bifurcation curve. The obtained streamline patterns and the bifurcation diagrams are also observed by Brøns [30]. That makes us to ask a question about the boundary conditions for free surface, and the shape of the interface are really important or not.

For $\sigma = 1$, we observed that $LCOF_1$ has no significance for the physical region $y < 0$.

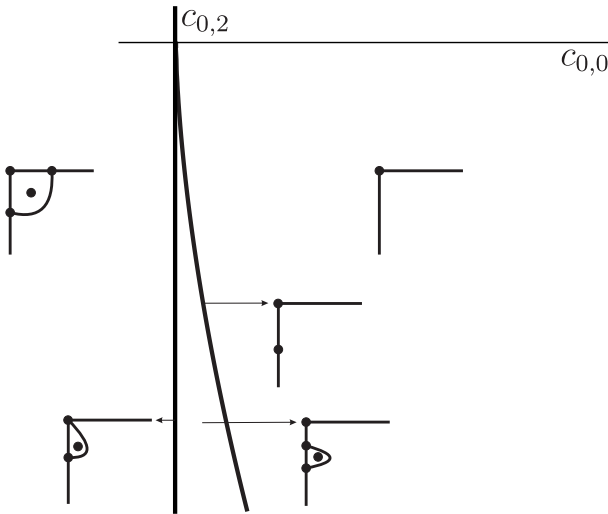


Figure 4.8: Bifurcation diagram for the normal forms (4.63)-(4.65) for $\sigma = 1$.

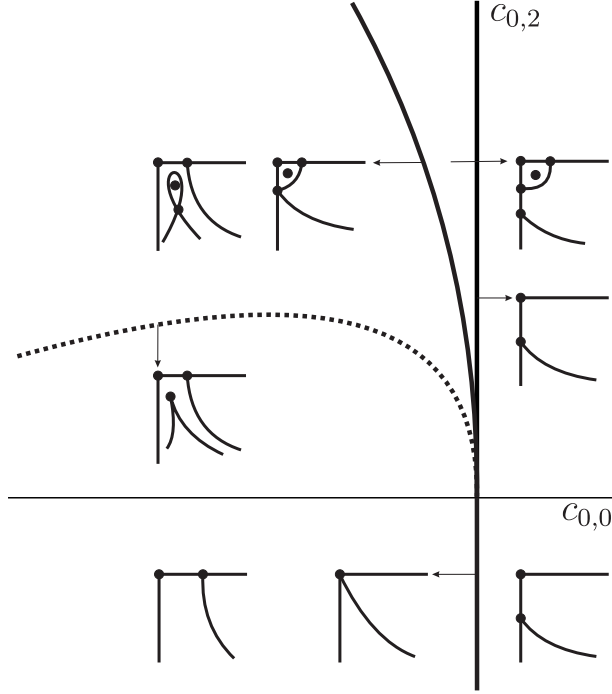


Figure 4.9: Bifurcation diagram for the normal forms (4.63)-(4.65) for $\sigma = -1$. Dashed curve is $LCOF_1$.

4.2.3.2 Case 2

The second degeneracy condition is $a_{2,3} \neq 0$ and $a_{4,1} = 0$. For steady flow, from (4.29) we have $a_{2,4} = 4a_{2,3}k_2$. For this condition, the extended and truncated stream function (4.36) is

$$\begin{aligned} \psi = & a_{2,3}x^2y^3 + 4a_{2,3}k_2x^2y^4 + a_{2,5}x^2y^5 + (16a_{2,3}k_2^2 + a_{4,3})x^4y^3 \\ & + (-3a_{2,3}k_2^2 + a_{6,1})x^6y. \end{aligned} \quad (4.75)$$

We can simplify this stream function by using the non-linear transformation (4.53). Choosing $l_{0,2} = l_{0,3} = l_{2,1} = 0$, $m_{1,1} = -2k_2$, $m_{3,0} = -\frac{16a_{2,3}k_2^2 + a_{4,3}}{2a_{2,3}}$ and $m_{1,2} = \frac{12a_{2,3}k_2^2 - a_{2,5}}{2a_{2,3}}$ the stream function becomes

$$\psi = a_{2,3}\eta^3\xi^2 + \tilde{a}_{6,1}\eta\xi^6 \quad (4.76)$$

where $\tilde{a}_{6,1} = (-3a_{2,3}k_2^2 + a_{6,1})$. To make more simplification, we substitute $\xi = A\tilde{\xi}$ and $\eta = B\tilde{\eta}$ and factorize the equation as the following

$$\psi = \tilde{a}_{6,1}A^2B\tilde{\xi}^2\tilde{\eta} \left(A^4\tilde{\xi}^4 + \frac{a_{2,3}B^2}{\tilde{a}_{6,1}}\tilde{\eta}^2 \right), \quad (4.77)$$

and choosing $A = 1$ and $B = \left| \frac{\tilde{a}_{6,1}}{a_{2,3}} \right|^{1/2}$, we scale the stream function by dividing $\tilde{a}_{6,1}A^2B$ and obtain

$$\psi = \tilde{\xi}^2\tilde{\eta}(\tilde{\xi}^4 + \sigma\tilde{\eta}^2), \quad (4.78)$$

where

$$\sigma = \frac{a_{2,3}}{\tilde{a}_{6,1}} \left| \frac{\tilde{a}_{6,1}}{a_{2,3}} \right| = \begin{cases} +1 & \text{for } \tilde{a}_{6,1}/a_{2,3} > 0 \\ -1 & \text{for } \tilde{a}_{6,1}/a_{2,3} < 0 \end{cases},$$

and we have assumed $\tilde{a}_{6,1} \neq 0$. For $\sigma = 1$, the separatrices are $\tilde{\eta} = 0$ and $\tilde{\xi} = 0$; for $\sigma = -1$ there exist also a parabolic separatrix $\tilde{\eta} = \sqrt{-\sigma}\tilde{\xi}^2$, see Fig. 4.10.

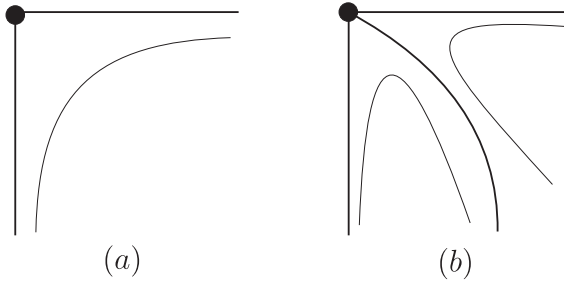


Figure 4.10: Possible streamlines in the vicinity of origin for the degenerate normal form (4.78). (a) $\sigma = 1$ (b) $\sigma = -1$.

The unfolding for this case is

$$\begin{aligned} \psi = & \epsilon_1 x^2 y + 2 \epsilon_1 k_2 x^2 y^2 + a_{2,3} x^2 y^3 + (4 \epsilon_1 k_2^2 + \epsilon_2) x^4 y + a_{2,5} x^2 y^5 \\ & + (-16 \epsilon_1 k_2^3 + 4 a_{2,3} k_2 + 8 \epsilon_1 k_4) x^2 y^4 + (24 \epsilon_1 k_2^3 + 6 k_2 \epsilon_2) x^4 y^2 \\ & + (-64 \epsilon_1 k_2^4 + 16 a_{2,3} k_2^2 + 32 \epsilon_1 k_2 k_4 + a_{4,3}) x^4 y^3 \\ & + (4 \epsilon_1 k_2 k_4 + 3 a_{2,3} k_2^2 + 2 (24 \epsilon_1 k_2^3 - 3 a_{2,3} k_2 + 6 k_2 \epsilon_2) k_2 + a_{6,1}) x^6 y, \end{aligned} \quad (4.79)$$

where $\epsilon_1 = a_{2,1}$, $\epsilon_2 = a_{4,1}$. This equation can be simplified by applying the near identity transformation (4.53). Since this transformation includes too many

terms please see the transformed stream function in [31]. Choosing

$$\begin{aligned} l_{0,2} &= -\frac{2k_2}{5}, \quad l_{2,1} = \frac{a_{4,3} + 16a_{2,3}k_2^2}{3a_{2,3}}, \quad l_{0,3} = 0, \\ m_{1,1} &= -\frac{7k_2}{5} + \mathcal{O}(\epsilon_1), \quad m_{3,0} = -\frac{a_{4,3} + 16a_{2,3}k_2^2}{a_{2,3}} + \mathcal{O}(\epsilon_1, \epsilon_2), \\ m_{1,2} &= \frac{1}{2a_{2,3}} \left(-a_{2,5} + \frac{59a_{2,3}k_2^2}{5} \right) + \mathcal{O}(\epsilon_1, \epsilon_2), \end{aligned} \quad (4.80)$$

we observe that $m_{1,1}$, $m_{3,0}$ and $m_{1,2}$ eliminate the terms $\xi^2\eta^4$, $\xi^2\eta^5$ and $\xi^4\eta^3$ by using implicit function theorem like in the previous case, respectively. The idea is same, however, to clarify the process let us give an example. In the previous section, to eliminate the coefficient $f(\epsilon_1, \epsilon_2, l_{0,3})$ of $\xi^4\eta^3$ term, we use the implicit function theorem and say that a function $l_{0,3}(\epsilon_1, \epsilon_2)$ exist which solves $f = 0$. Similarly, we can say there exists a function $m_{1,1}(\epsilon_1)$ which solves the coefficients of $\xi^2\eta^4$ term. Thus, the stream function is written as

$$\psi = \epsilon_1\xi^2\eta + \gamma\epsilon_1\xi^2\eta^2 + \epsilon_2\xi^4\eta + \tilde{a}_{2,3}\eta^3\xi^2 + \tilde{a}_{6,1}\xi^6\eta, \quad (4.81)$$

where the ϵ are transformed small parameters and

$$\tilde{a}_{2,3} = a_{2,3} + \mathcal{O}(\epsilon_1), \quad \tilde{a}_{6,1} = a_{6,1} + \mathcal{O}(\epsilon_1, \epsilon_2), \quad \gamma = -\frac{6k_2}{5}. \quad (4.82)$$

Finally, we substitute $\xi = A\tilde{\xi}$ and $\eta = B\tilde{\eta}$ to make more simplification, and factorizing the stream function into $A^6B\tilde{a}_{6,1}\tilde{\xi}^2\tilde{\eta}$ we have

$$A^6B\tilde{a}_{6,1}\tilde{\xi}^2\tilde{\eta} \left(\frac{\epsilon_1}{A^4} + \frac{B\gamma\epsilon_1\eta}{A^4} + \frac{\epsilon_2\tilde{\xi}^2}{A^2} + \tilde{\xi}^4 + \frac{B^2\tilde{a}_{2,3}}{A^4\tilde{a}_{6,1}}\eta^2 \right). \quad (4.83)$$

Depending on whether $\gamma = 0$ or not, we can investigate this case into two cases. However, we will just consider the case for $\gamma \neq 0$ for the same reason as in the previous case. To see the similarities between $\gamma = 0$ and $\gamma \neq 0$ please see [33].

Choosing $B = \frac{1}{\gamma}$ and $A = \left(\frac{B^2\tilde{a}_{2,3}}{\tilde{a}_{6,1}} \right)^{1/4}$, we scale the stream function by dividing by $A^6B\tilde{a}_{6,1}$ and the following theorem arises.

THEOREM 4.5 *Let $a_{2,1}$, $a_{4,1}$ be small parameters. Assuming the non-degeneracy conditions $a_{2,3} \neq 0$ and $\tilde{a}_{6,1} \neq 0$ the normal form for the stream function (4.78) is*

$$\psi = x^2y (c_{0,0} + c_{0,0}y + c_{2,0}x^2 + \sigma y^2 + x^4), \quad (4.84)$$

where

$$\sigma = \begin{cases} +1 & \text{for } \tilde{a}_{6,1}/\tilde{a}_{2,3} > 0 \\ -1 & \text{for } \tilde{a}_{6,1}/\tilde{a}_{2,3} < 0 \end{cases},$$

$c_{0,0}$ and $c_{2,0}$ are small transformed parameters.

The velocity field for (4.84) is,

$$\begin{aligned} u &= x (c_{0,0} + 2 y c_{0,0} + x^2 c_{2,0} + 3 \sigma y^2 + x^4), \\ w &= -2 y (c_{0,0} + y c_{0,0} + 2 x^2 c_{2,0} + \sigma y^2 + 3 x^4), \end{aligned} \quad (4.85)$$

with the determinant of the Jacobian

$$\begin{aligned} J &= -30 x^8 + 96 \sigma x^4 y^2 - 38 x^6 c_{2,0} - 18 \sigma^2 y^4 + 18 \sigma x^2 y^2 c_{2,0} + 16 x^4 y c_{0,0} \\ &\quad - 12 x^4 c_{2,0}^2 - 24 \sigma y^3 c_{0,0} - 16 x^4 c_{0,0} - 4 x^2 y c_{0,0} c_{2,0} - 12 \sigma y^2 c_{0,0} \\ &\quad - 10 x^2 c_{0,0} c_{2,0} - 8 y^2 c_{0,0}^2 - 8 y c_{0,0}^2 - 2 c_{0,0}^2 \end{aligned} \quad (4.86)$$

On the interface ($y = 0$), the velocity field becomes

$$u = x(c_{0,0} + c_{2,0}x^2 + x^4), \quad w = 0, \quad (4.87)$$

and the solutions of $u = 0$ determine the number of critical points on the interface and their type can be found from the determinant of the Jacobian

$$J = -30 x^8 - 38 x^6 c_{2,0} - 12 x^4 c_{2,0}^2 - 16 x^4 c_{0,0} - 10 x^2 c_{0,0} c_{2,0} - 2 c_{0,0}^2. \quad (4.88)$$

To find the local bifurcation curve for the critical points on the interface, we take the resultant of J (4.88) and u (4.87) with respect to x in an attempt to obtain the local bifurcation curve which is

$$LCOI : c_{2,0}^2 - 4 c_{0,0} = 0. \quad (4.89)$$

Similarly, to find the local bifurcation curve for the critical points on the center axis we substitute $x = 0$ in the velocity field

$$u = 0, \quad w = -2y(c_{0,0} + y c_{0,0} + \sigma y^2), \quad (4.90)$$

and the solutions of $w = 0$ are

$$y^\pm = \frac{-c_{0,0} \pm \sqrt{c_{0,0}^2 - 4c_{0,0}}}{2\sigma} \approx \frac{-c_{0,0} \pm \sqrt{-4c_{0,0}}}{2\sigma}, \quad (4.91)$$

since $c_{0,0}$ is small. For $c_{0,0} < 0$ there are two solutions (one positive and one negative) and for $c_{0,0} > 0$, no solution exists.

For the critical points which are away from both the center axis and interface, firstly we eliminate y from the velocity $\frac{u}{x}$ and $-\frac{w}{2y}$ and obtain

$$\begin{aligned} LcO : \sigma (64 \sigma x^8 + 80 \sigma x^6 c_{2,0} + 25 \sigma x^4 c_{2,0}^2 + 32 \sigma x^4 c_{0,0} - 5 x^4 c_{0,0}^2 \\ + 20 \sigma x^2 c_{0,0} c_{2,0} - 3 x^2 c_{0,0}^2 c_{2,0} + 4 \sigma c_{0,0}^2 - c_{0,0}^3) = 0. \end{aligned} \quad (4.92)$$

Secondly, we eliminate x from $-\frac{dLcO}{dx}$ and LcO , and obtain the local bifurcation curve which is indicated by dashed curves in the figures,

$$\begin{aligned}
 LBCO : & -2500 \sigma c_{2,0}^6 + 1125 c_{0,0} c_{2,0}^6 + 22800 \sigma c_{0,0} c_{2,0}^4 \\
 & - 15420 c_{0,0}^2 c_{2,0}^4 + 2358 \sigma c_{0,0}^3 c_{2,0}^4 - 67584 \sigma c_{0,0}^2 c_{2,0}^2 \\
 & + 58848 c_{0,0}^3 c_{2,0}^2 - 15420 \sigma c_{0,0}^4 c_{2,0}^2 + 1125 c_{0,0}^5 c_{2,0}^2 + 65536 \sigma^3 c_{0,0}^3 \\
 & - 67584 c_{0,0}^4 + 22800 \sigma c_{0,0}^5 - 2500 c_{0,0}^6 = 0.
 \end{aligned}
 \tag{4.93}$$

Remember that, the bifurcation diagrams and the streamline patterns in the previous case look like similar with the bifurcation diagrams obtained by Brøns [30]. However, in this case new structures and bifurcation diagrams have been observed for co-dimension two bifurcation, means only case 1 was considered in [30].

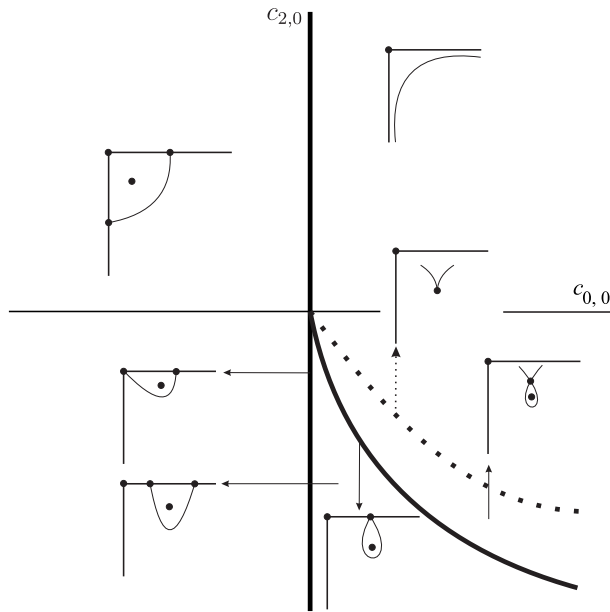


Figure 4.11: Possible streamlines for the normal form (4.84) for $\sigma = 1$.

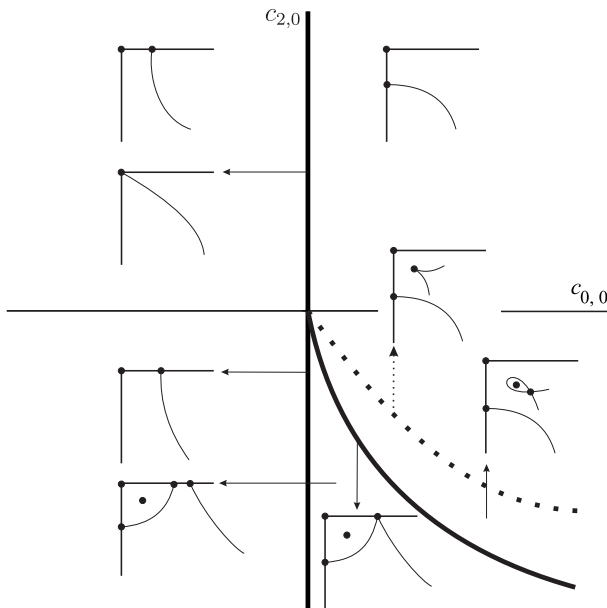


Figure 4.12: Possible streamlines for the normal form (4.84) for $\sigma = -1$.

4.2.4 Co-dimension 3 bifurcations

As a further investigation, we break the non-degenerate conditions in the co-dimension two bifurcations. Creating new non-degenerate conditions we attempt to analyse the co-dimension three bifurcation in this section which can be divided into three cases

- $a_{2,1} = 0, a_{2,3} = 0, a_{4,1} = 0, a_{2,5} \neq 0, a_{6,1} \neq 0,$
- $a_{2,1} = 0, a_{2,3} = 0, a_{4,1} \neq 0, a_{2,5} = 0, a_{2,6} \neq 0$ and
- $a_{2,1} = 0, a_{2,3} \neq 0, a_{4,1} = 0, a_{6,1} = 3a_{2,3}k_2^2, a_{2,6} \neq 0$

4.2.4.1 Case 1

If we apply the first degeneracy condition into the extended and truncated stream function (4.36), we have

$$\psi = a_{2,5}x^2y^5 + a_{4,3}x^4y^3 + a_{6,1}x^6y. \quad (4.94)$$

We substitute $x = Ax$ and $y = By$ into (4.94) in an attempt to simplify,

$$a_{2,5}A^2B^5x^2y^5 + a_{4,3}A^4B^3x^4y^3 + a_{6,1}A^6Bx^6y. \quad (4.95)$$

Choosing $B = 1$ and $A = \left| \frac{a_{2,5}}{a_{6,1}} \right|^{1/4}$, and scaling the stream function by dividing $a_{6,1}A^6B$, we obtain the normal form as

$$\psi = x^2y(\sigma y^4 + \omega x^2y^2 + x^4), \quad (4.96)$$

where $\sigma = \frac{a_{2,5}}{a_{6,1}} \left| \frac{a_{6,1}}{a_{2,5}} \right| = \pm 1$ and $\omega = \frac{a_{4,3}}{a_{6,1}} \left| \frac{a_{6,1}}{a_{2,5}} \right|^{1/2}$. We significantly emphasize that when $\omega = -2$ and $\sigma = 1$, the stream function becomes

$$\psi = x^2y(x^2 - y^2)^2, \quad (4.97)$$

which is not a normal form. For $\omega = -2$ and $\sigma = 1$, one needs to investigate the higher order terms. Streamline patterns close to the degenerate critical point for the normal form (4.96) are illustrated in Fig. 4.13.

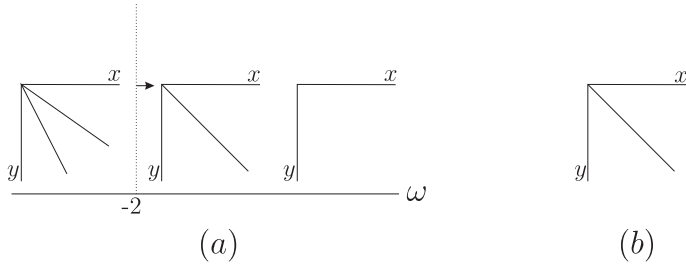


Figure 4.13: Dividing streamlines for equation (4.96) in the vicinity of origin for (a) $\sigma = 1$ (b) $\sigma = -1$.

The unfolding of the normal form (4.96) is in the form

$$\begin{aligned} \psi = & \epsilon_1 x^2 y + 2 \epsilon_1 k_2 x^2 y^2 + \epsilon_2 x^2 y^3 + (4 \epsilon_1 k_2^2 + \epsilon_3) x^4 y + a_{2,5} x^2 y^5 \\ & + (-16 \epsilon_1 k_2^3 + 8 \epsilon_1 k_4 + 4 \epsilon_2 k_2) x^2 y^4 + (24 \epsilon_1 k_2^3 + 6 \epsilon_3 k_2) x^4 y^2 \\ & + (4 (-16 \epsilon_1 k_2^3 + 8 \epsilon_1 k_4 + 4 \epsilon_2 k_2) k_2 + a_{4,3}) x^4 y^3 \\ & + (4 \epsilon_1 k_2 k_4 + 3 \epsilon_2 k_2^2 + 2 (24 \epsilon_1 k_2^3 - 3 \epsilon_2 k_2 + 6 \epsilon_3 k_2) k_2 + a_{6,1}) x^6 y, \end{aligned} \quad (4.98)$$

where $a_{2,1} = \epsilon_1$, $a_{2,3} = \epsilon_2$ and $a_{4,1} = \epsilon_3$. Using the non-linear transformation (4.53), included fourth-order terms, we simplified the stream function as (for the process please look at the Maple worksheet [31])

$$\eta \zeta^2 \epsilon_1 + \gamma \epsilon_1 \eta^2 \zeta^2 + \epsilon_2 \eta^3 \zeta^2 + \epsilon_3 \eta \zeta^4 + \zeta^2 \eta^5 a_{2,5} + a_{4,3} \eta^3 \zeta^4 + \tilde{a}_{6,1} \zeta^6 \eta \quad (4.99)$$

where $\gamma = -\frac{6k_2}{5}$ and $\tilde{a}_{6,1} = a_{6,1} + \mathcal{O}(\epsilon_1, \epsilon_2)$.

This stream function can be investigated in two situations, which are $k_2 = 0$ and $k_2 \neq 0$. If $k_2 \neq 0$, one is able to scale the stream function by using $\xi = \left| \frac{a_{2,5}}{\gamma^4 \tilde{a}_{6,1}} \right|^{1/4} x$ and $\eta = \frac{1}{\gamma} y$ and dividing then the stream function by $A^6 B \tilde{a}_{6,1}$. After these scalings, the following theorem arises:

THEOREM 4.6 *Let $a_{2,1}$, $a_{4,1}$ and $a_{2,3}$ be small parameters and $k_2 \neq 0$. Assuming the non-degeneracy conditions $a_{2,5} \neq 0$ and $\tilde{a}_{6,1} \neq 0$ the normal form for the stream function (4.96) is*

$$\psi = x^2 y (c_{0,0} + y c_{0,0} + y^2 c_{0,2} + x^2 c_{2,0} + x^4 + \omega x^2 y^2 + \sigma y^4), \quad (4.100)$$

where

$$\sigma = \begin{cases} +1 & \text{for } \tilde{a}_{6,1}/\tilde{a}_{2,5} > 0 \\ -1 & \text{for } \tilde{a}_{6,1}/\tilde{a}_{2,5} < 0 \end{cases},$$

$c_{0,0}$, $c_{2,0}$ and $c_{0,2}$ are small transformed parameters. If $k_2 = 0$, the stream function can be written as,

$$\psi = x^2 y (c_{0,0} + y^2 c_{0,2} + x^2 c_{2,0} + x^4 + \omega x^2 y^2 + \sigma y^4). \quad (4.101)$$

Like the previous section, there is no difference choosing the value of k_2 . Hence we will use the stream function (4.100) from now on, please see the similarities between $k_2 = 0$ and $k_2 \neq 0$ in [34].

The velocity field of (4.100) is

$$\begin{aligned} u &= x (c_{0,0} + c_{0,0} y + 3 y^2 c_{0,2} + x^2 c_{2,0} + x^4 + 3 \omega x^2 y^2 + 5 \sigma y^4), \\ w &= -2 y (c_{0,0} + c_{0,0} y + y^2 c_{0,2} + 2 x^2 c_{2,0} + 3 x^4 + 2 \omega x^2 y^2 + \sigma y^4), \end{aligned} \quad (4.102)$$

with the determinant of Jacobian matrix

$$\begin{aligned} |J| &= -60 \omega^2 x^4 y^4 + 10 \omega \sigma x^2 y^6 - 50 \sigma^2 y^8 + 30 \omega x^6 y^2 + 400 \sigma x^4 y^4 \\ &\quad - 24 \omega x^4 y^2 c_{2,0} - 42 \omega x^2 y^4 c_{0,2} + 110 \sigma x^2 y^4 c_{2,0} - 60 \sigma y^6 c_{0,2} - 30 x^8 \\ &\quad - 44 \omega x^2 y^3 c_{0,0} - 40 \sigma y^5 c_{0,0} - 38 x^6 c_{2,0} + 96 x^4 y^2 c_{0,2} - 30 \omega x^2 y^2 c_{0,0} \\ &\quad - 20 \sigma y^4 c_{0,0} + 16 x^4 y c_{0,0} - 12 x^4 c_{2,0}^2 + 18 x^2 y^2 c_{0,2} c_{2,0} - 18 y^4 c_{0,2}^2 \\ &\quad - 16 x^4 c_{0,0} - 4 x^2 y c_{0,0} c_{2,0} - 24 y^3 c_{0,0} c_{0,2} - 10 x^2 c_{0,0} c_{2,0} - 8 y^2 c_{0,0}^2 \\ &\quad - 12 y^2 c_{0,0} c_{0,2} - 8 y c_{0,0}^2 - 2 c_{0,0}^2 \end{aligned} \quad (4.103)$$

The local bifurcation curve for the critical points on interface

The critical points on the interface can be obtained by applying $y = 0$ into the velocity field ,

$$u = x(x^4 + c_{2,0}x^2 + c_{0,0}), \quad w = 0, \quad (4.104)$$

Solving $u = 0$ with respect to x , we have

$$x_{1,2,3,4} = \pm 1/2 \sqrt{\pm 2 \sqrt{c_{2,0}^2 - 4c_{0,0}} - 2c_{2,0}}, \quad \text{or} \quad x = 0. \quad (4.105)$$

To determine the number of critical points, $\Delta = -c_{2,0}^2 + 4c_{0,0}$ has more significance than $c_{0,0}$. Hence, instead of parameter $c_{0,0}$, we will use Δ as a parameter. The number of critical points are illustrated in Fig. 4.14.

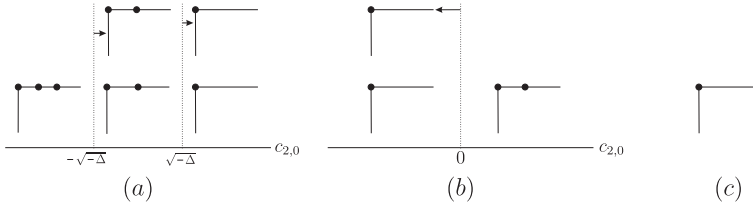


Figure 4.14: The number of critical points on the interface for (a) $\Delta < 0$ (b) $\Delta = 0$ (c) $\Delta > 0$.

The local bifurcation curve for the critical points on center axis

Substituting $x = 0$ into the velocity field and the determinant of Jacobian, the critical points and their type on the center axis can be determined by eliminating y from them. The local bifurcation curve for this critical points is

$$\begin{aligned} LCOC : 256c_{0,0}^2 - 27\sigma c_{0,0}^3 + 144\sigma c_{0,0}^2 c_{0,2} - 128\sigma c_{0,0} c_{0,2}^2 \\ - 4c_{0,0} c_{0,2}^3 + 16c_{0,2}^4 = 0 \end{aligned} \quad (4.106)$$

Substituting $c_{0,0} = \frac{\Delta + c_{2,0}^2}{4}$ into (4.106), we have

$$\begin{aligned} \tau : 16\sigma^2 \Delta^2 - \frac{27\sigma \Delta^3}{64} + 9\sigma c_{0,2} \Delta^2 - 32\sigma c_{0,2}^2 \Delta - c_{0,2}^3 \Delta + 16c_{0,2}^4 \\ + \left(32\sigma^2 \Delta - \frac{81\sigma \Delta^2}{64} + 18\sigma c_{0,2} \Delta - 32\sigma c_{0,2}^2 - c_{0,2}^3 \right) c_{2,0}^2 \\ + \left(16\sigma^2 - \frac{81\Delta \sigma}{64} + 9\sigma c_{0,2} \right) c_{2,0}^4 - \frac{27\sigma}{64} c_{2,0}^6 \end{aligned} \quad (4.107)$$

The curve τ can be seen in Fig. 4.15 and 4.16.

From the figure, one can say that the bifurcation can be estimated by the sign of $c_{0,2}$. This can be proved analytically by finding the roots of (4.107) as well. Reducing the order of $c_{2,0}$ by substituting $c_{2,0}^2 = x$ into (4.107), a cubic equation is obtained. The discriminant of this cubic equation is

$$\frac{262144c_{0,2}^5(\sigma + c_{0,2})(128\sigma + 3c_{0,2})^3}{14348907}. \quad (4.108)$$

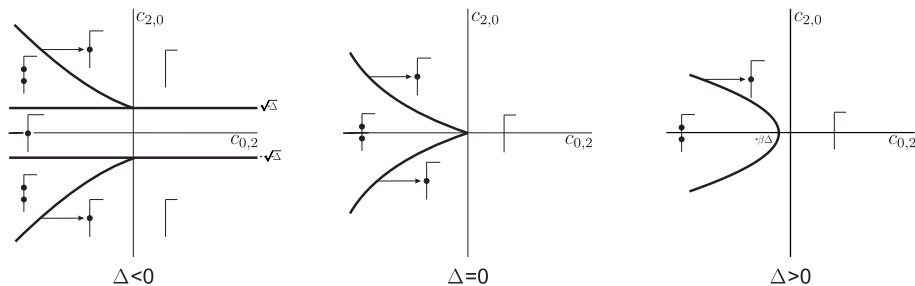


Figure 4.15: The local bifurcation curves for the critical points on the center axis for $\sigma = 1$

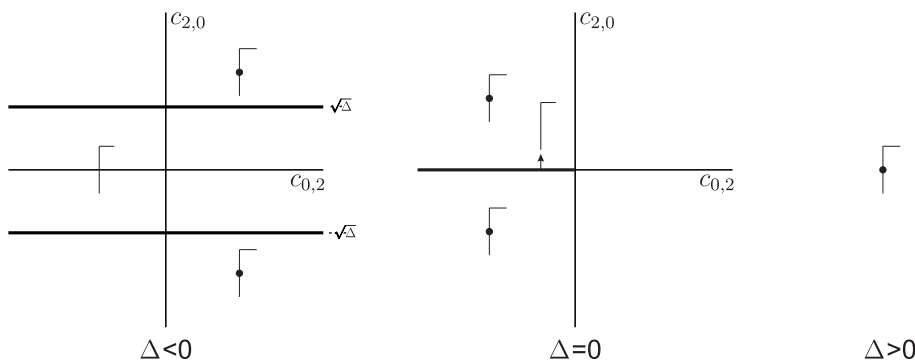


Figure 4.16: The local bifurcation curves for the critical points on the center axis for $\sigma = -1$

Since $\sigma = \pm 1$, and $c_{0,2}$ is sufficiently small, the sign of the $c_{0,2}$ determines the number of critical points. Therefore, we consider $c_{0,2}$ into three case which are $c_{0,2} < 0$, $c_{0,2} = 0$ and $c_{0,2} > 0$, to decrease the number of unknown variable. In the following process, the bifurcation diagram will depend on just ω and $c_{2,0}$, hence this local curve will be a line on this diagram which is called *LW*.

The local bifurcation curve for the critical points away from boundaries-LBC

To obtain the local bifurcation curve for the critical points away from boundaries, firstly we eliminate x from u/x and $-w/2y$ by using resultant command in 'Maple'. Secondly, we eliminate y from the previous result and its derivative with respect to y . The equation for this curve includes too many terms hence we kindly refer to the Maple worksheet [34] to see this curve.

In this study, it is also possible to see the heteroclinic connection between the saddle critical points. We have four kind global bifurcation curves which are:

The global bifurcation curve for the saddle critical points on-axis, on-interface and away from the boundaries-GBC1

This curve can be obtained by eliminating x and y from

$$\frac{u(x, y)}{x} = 0, \quad \frac{w(x, y)}{2y} = 0, \quad \text{and} \quad \frac{\psi(x, y)}{x^2y} = 0 \quad (4.109)$$

The global bifurcation curve for the saddle critical points on the axis and away from the axis-GBC2

Let consider (x_1, y_1) is a critical point in flow, and $(0, y_2)$ is a critical point on the axis. For these critical points if the following equations are valid, the global bifurcation curve can be seen,

$$\begin{aligned} u(x_1, y_1) &= 0, & w(x_1, y_1) &= 0, \\ u(0, y_2) &= 0, & w(0, y_2) &= 0, \\ |J(x_1, y_1)| &< 0, & |J(0, y_2)| &< 0, \\ \psi(x_1, y_1) &= \psi(0, y_2). \end{aligned} \quad (4.110)$$

To obtain this curve, by using 'Maple'(resultant or Groebner[Basis] command) we can eliminate x_1 , y_1 and y_2 . We kindly refer to the Maple worksheet [34] to whole process.

The global bifurcation curve for the saddle critical points on the interface and away from the interface-GBC3

Let consider (x_1, y_1) is a critical point in flow, and $(x_2, 0)$ is a critical point on the interface. For these critical points if the following equations are valid, the global bifurcation curve can be seen,

$$\begin{aligned} u(x_1, y_1) &= 0, & w(x_1, y_1) &= 0, \\ u(x_2, 0) &= 0, & w(x_2, 0) &= 0, \\ |J(x_1, y_1)| &< 0, & |J(x_2, 0)| &< 0, \\ \psi(x_1, y_1) &= \psi(x_2, 0). \end{aligned} \quad (4.111)$$

The global bifurcation curve for the saddle critical points away from the boundaries-GBC4

Let consider (x_1, y_1) and (x_2, y_2) are critical points in flow. For these critical points if the following equations are valid, the global bifurcation curve can be seen,

$$\begin{aligned} u(x_1, y_1) &= 0, & w(x_1, y_1) &= 0, \\ u(x_2, y_2) &= 0, & w(x_2, y_2) &= 0, \\ |J(x_1, y_1)| &< 0, & |J(x_2, y_2)| &< 0, \\ \psi(x_1, y_1) &= \psi(x_2, y_2). \end{aligned} \quad (4.112)$$

Obtaining this curve in Maple is very difficult. Hence we write a Matlab code for this curve. The process can be summarized as:

- Firstly, we eliminate x from the velocity field. It gives us a equation which depends on $y, \sigma, \Delta, c_{2,0}$ and $c_{0,2}$.
- We fixed $\sigma, c_{0,2}$ and Δ , and obtained the y solutions. We are considering the under the interface region, hence the solutions must be in the physical domain $y < 0$ and $x > 0$. At least three solutions must be observed for the heteroclinic connection.
- We put the y values into the velocity field, and obtain x values.
- We put (x, y) variables into the determinant of Jacobian to see which critical points are saddle points.
- Finally, we put these saddle points into the stream function and set the their difference smaller than $1E-6$, or more precisely $|\psi(x_1, y_1) - \psi(x_2, y_2)| < 1E - 6$.

In the end of this process, we observed which values for ω and $c_{2,0}$ are satisfying these conclusions.

Normally, we have four parameters in this study. However, we are able to construct the bifurcation diagram using two parameters which are ω and $c_{2,0}$ with the following cases:

1. $\sigma = 1$;
 - a. $\Delta > 0$; (a1) $c_{0,2} > 0$ (a2) $c_{0,2} = 0$ (a3) $c_{0,2} < 0$
 - b. $\Delta = 0$; (b1) $c_{0,2} > 0$ (b2) $c_{0,2} = 0$ (b3) $c_{0,2} < 0$
 - c. $\Delta < 0$; (c1) $c_{0,2} > 0$ (c2) $c_{0,2} = 0$ (c3) $c_{0,2} < 0$
2. $\sigma = -1$;
 - d. $\Delta > 0$; (d1) $c_{0,2} > 0$ (d2) $c_{0,2} = 0$ (d3) $c_{0,2} < 0$
 - e. $\Delta = 0$; (e1) $c_{0,2} > 0$ (e2) $c_{0,2} = 0$ (e3) $c_{0,2} < 0$
 - f. $\Delta < 0$; (f1) $c_{0,2} > 0$ (f2) $c_{0,2} = 0$ (f3) $c_{0,2} < 0$

Let begin by considering the case 2d, $\Delta > 0$ and $\sigma = -1$. One can observe that there is no critical point on the interface from Fig. 4.14, and one critical point exist on the center axis from Fig.4.16. No local bifurcation exists for the critical points away from the boundaries for this case and the sign of $c_{0,2}$ has no significance. By using Maple, we sketch the streamline patterns numerically to be sure the process is correct or not. As an example, the streamline pattern

4.17 is a numerical result from Maple by using 'contourplot' command. This streamline pattern is same as the case $e1$ for $c_{2,0} > 0$ which we show in Fig. 4.24. Choosing a specific values of the parameters, which holds the conditions in the cases the bifurcation diagrams and the streamline patterns are obtained. For Fig. 4.17, we choose $\Delta = 0.01$ with any choices for $c_{0,2}$, that is, whatever you choose for $c_{0,2}$ the streamline pattern 4.17 will be obtained. To see whole process please look in Maple worksheet [34].

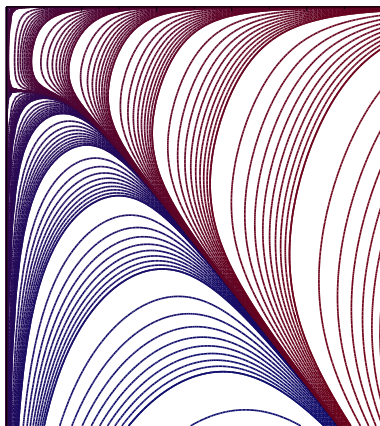


Figure 4.17: The streamline pattern for the normal form (4.100) when $\sigma = -1$ and $\Delta > 0$ (d1, d2, d3).

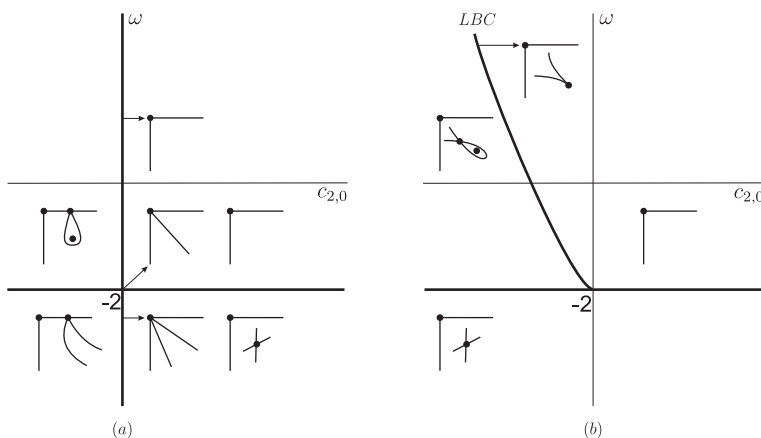


Figure 4.18: The bifurcation diagrams for the normal form (4.100) when $\sigma = 1$, (a) $\Delta > 0$ and $c_{0,2} \geq 0$ (a1, a2) and (b) $\Delta = 0$ and $c_{0,2} \geq 0$ (b1, b2).

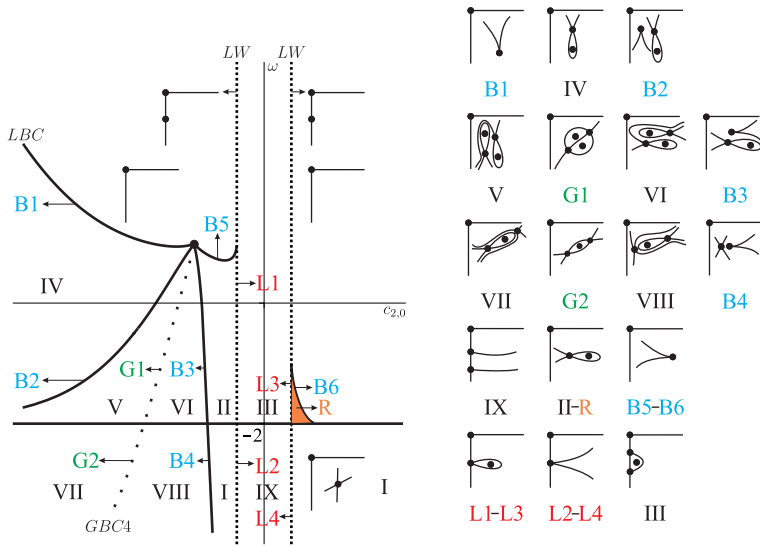


Figure 4.19: $\sigma = 1, \Delta > 0$ and $c_{0,2} < 0$ (a3).

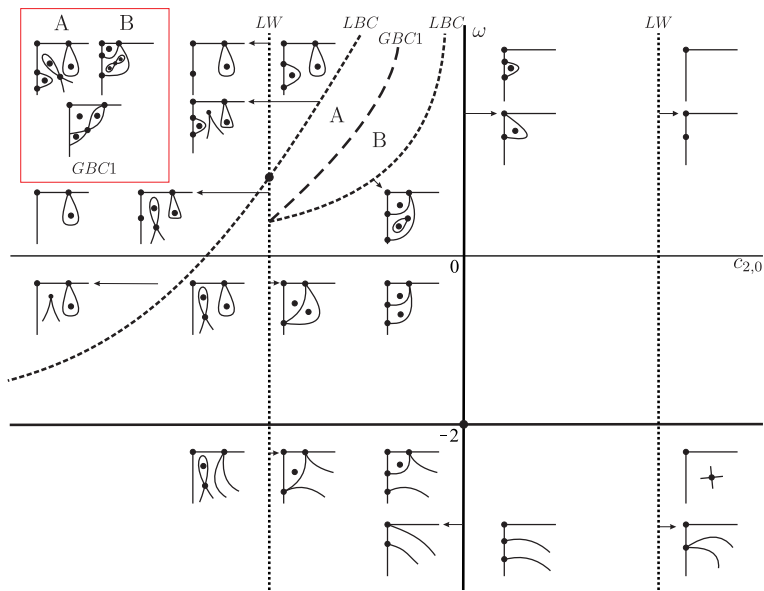


Figure 4.20: $\sigma = 1, \Delta = 0$ and $c_{0,2} < 0$ (b3).

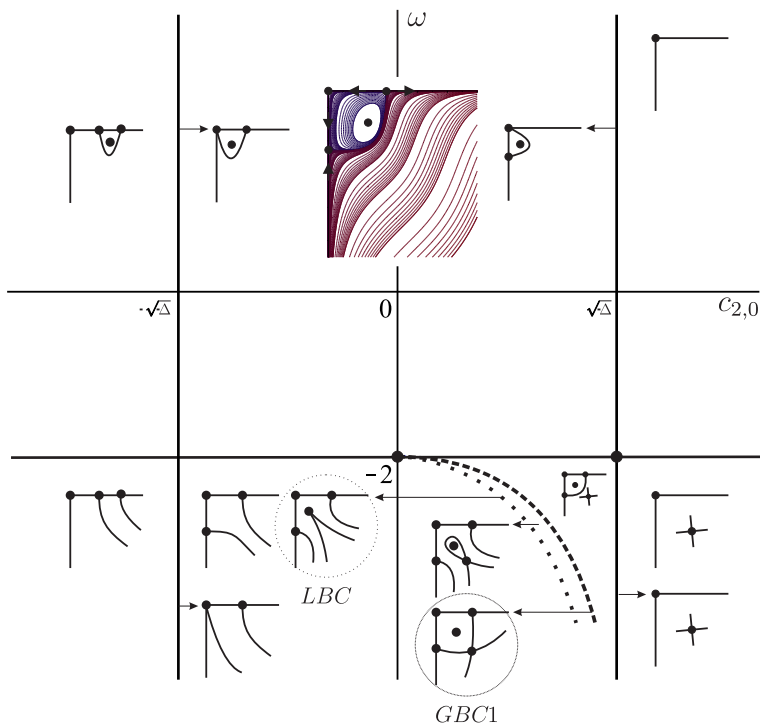


Figure 4.21: $\sigma = 1$, $\Delta < 0$ and $c_{0,2} \geq 0$ (c_1, c_2). Numerical result is just to show how a contourplot actually looks like.

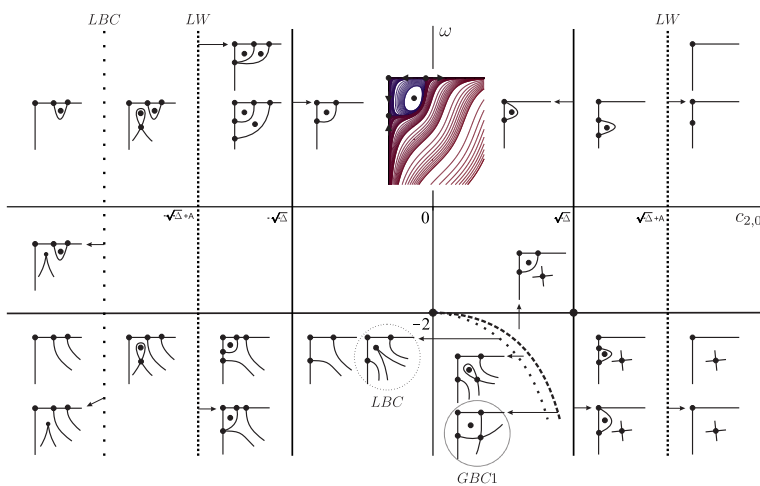


Figure 4.22: $\sigma = 1$, $\Delta < 0$ and $c_{0,2} < 0$ (c_3).

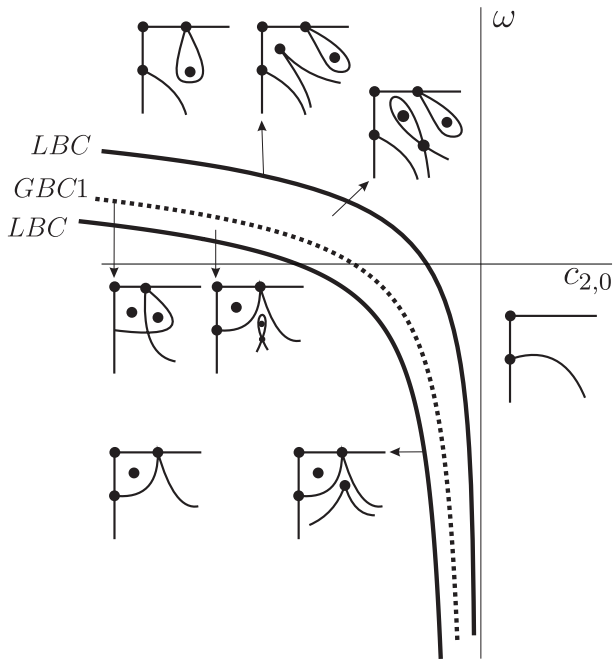


Figure 4.23: $\sigma = -1$, $\Delta = 0$ and $c_{0,2} > 0$ (e1) .

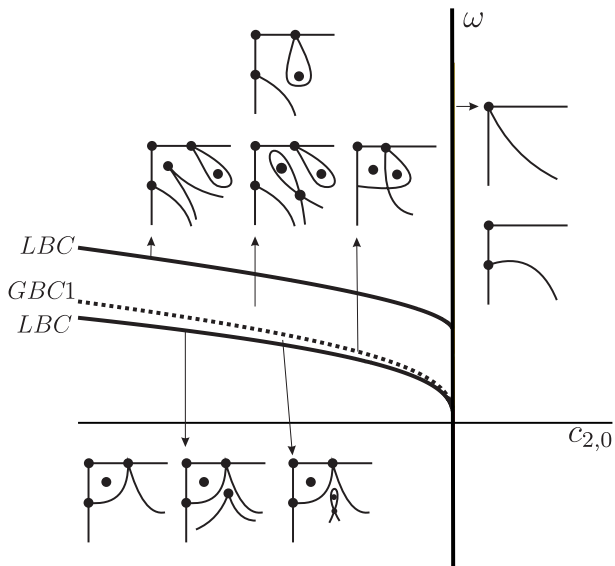


Figure 4.24: $\sigma = -1$, $\Delta = 0$ and $c_{0,2} = 0$ (e2) .

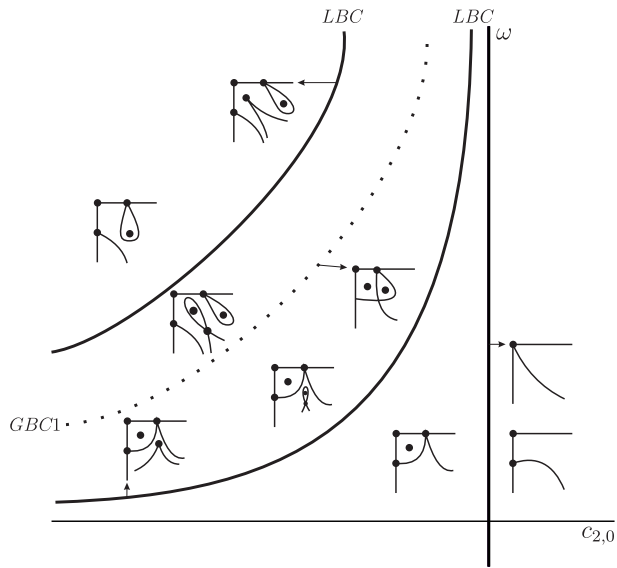


Figure 4.25: $\sigma = -1$, $\Delta = 0$ and $c_{0,2} < 0$ (e3) .

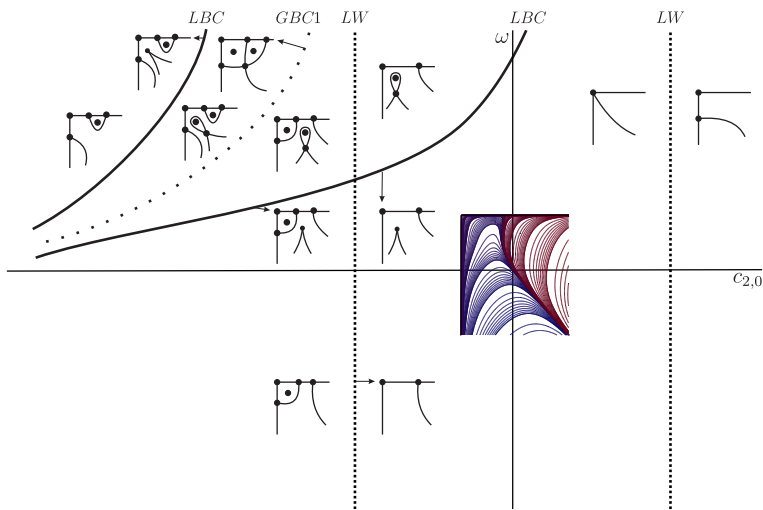


Figure 4.26: $\sigma = -1$ and $\Delta < 0$ (f1, f2, f3) .

4.2.4.2 Case 2

Using the second degeneracy condition, the stream function (4.36) becomes

$$\begin{aligned} \psi = & a_{4,1}x^4y + 6k_2a_{4,1}x^4y^2 + a_{4,3}x^4y^3 + (12k_2^2a_{4,1} + a_{6,1})x^6y + a_{2,6}x^2y^6 \\ & + a_{4,4}x^4y^4 + (104a_{4,1}k_2^3 + 8k_4a_{4,1} + 10k_2a_{6,1})x^6y^2. \end{aligned} \quad (4.113)$$

This can be simplified as (to see detailed simplification we kindly refer to Maple worksheet "Near Axis NormalFormandUnfoldings.mw" in [31])

$$a_{2,6}\eta^6\xi^2 + \eta\xi^4a_{4,1}. \quad (4.114)$$

Using our assumption $a_{4,1} \neq 0$, it is convenient to write (4.114) as

$$a_{4,1}\xi^2\eta\left(\frac{a_{2,6}}{a_{4,1}}\eta^5 + \xi^2\right). \quad (4.115)$$

More simplification is available for this equation by substituting $\xi = Ax$ and $\eta = By$. Choosing $A = 1$ and $B = \left(\frac{a_{4,1}}{a_{2,6}}\right)^{1/5}$, and scaling the stream function by dividing $a_{4,1}A^4B$, we have

$$x^2y(y^5 + x^2). \quad (4.116)$$

This degenerate case is shown in Fig. 4.27.

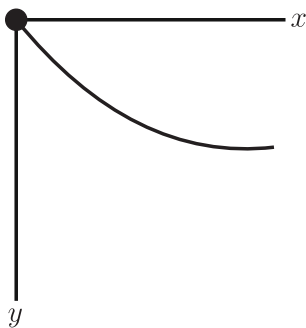


Figure 4.27: The degenerate case for the normal form (4.116).

The unfolding of degenerate case (4.116) is

$$\begin{aligned}
\psi = & \epsilon_1 x^2 y + 2 \epsilon_1 k_2 x^2 y^2 + \epsilon_2 x^2 y^3 + (4 \epsilon_1 k_2^2 + a_{4,1}) x^4 y + (5 \epsilon_3 k_2 + a_{4,4}) x^4 y^4 \\
& + (-16 \epsilon_1 k_2^3 + 8 \epsilon_1 k_4 + 4 \epsilon_2 k_2) x^2 y^4 + (24 \epsilon_1 k_2^3 + 6 k_2 a_{4,1}) x^4 y^2 + \epsilon_3 x^2 y^5 \\
& + (4 (-16 \epsilon_1 k_2^3 + 8 \epsilon_1 k_4 + 4 \epsilon_2 k_2) k_2 + a_{4,3}) x^4 y^3 + a_{2,6} x^2 y^6 \\
& + (4 \epsilon_1 k_2 k_4 + 3 \epsilon_2 k_2^2 + 2 (24 \epsilon_1 k_2^3 + 6 k_2 a_{4,1} - 3 \epsilon_2 k_2) k_2 + a_{6,1}) x^6 y \\
& + (384 \epsilon_1 k_2^5 + 104 a_{4,1} k_2^3 + 120 \epsilon_1 k_2^2 k_4 - 30 \epsilon_2 k_2^3 + 8 k_4 a_{4,1} \\
& + 10 k_2 a_{6,1} - 6 \epsilon_1 k_6) x^6 y^2
\end{aligned} \tag{4.117}$$

To obtain the normal form of the unfolding, it is convenient to use the non-linear transformation (4.53) with the fourth ordered terms. The simplified stream function can be written as

$$\psi = \epsilon_1 \xi^2 \eta + \gamma \epsilon_1 \xi^2 \eta^2 + \epsilon_2 \xi^2 \eta^3 + \tilde{a}_{4,1} \xi^4 \eta + \epsilon_3 \xi^2 \eta^5 + \tilde{a}_{2,6} \xi^2 \eta^6. \tag{4.118}$$

where $\gamma = -\frac{6k_2}{5}$, $\tilde{a}_{4,1} = a_{4,1} + \mathcal{O}(\epsilon_1)$ and $\tilde{a}_{2,6} = a_{2,6} + \mathcal{O}(\epsilon_1, \epsilon_2, \epsilon_3)$. This case also can be considered into two cases which are $k_2 = 0$ or not. Like the previous section, there is no difference between them, however analysis of $k_2 \neq 0$ is more difficult than $k_2 = 0$. Hence, we choose $k_2 = 0$ instead of $k_2 \neq 0$, in here. Please see the similarities between these two cases in [35]. As a next step, substituting $\xi = Ax$ and $\eta = \left(\frac{\tilde{a}_{2,6}}{\tilde{a}_{4,1}}\right)^{1/5} y$ into (4.118), and scaling the stream function by dividing $\tilde{a}_{4,1} A^4 B$, the next theorem arises.

THEOREM 4.7 *Let $a_{2,1}$, $a_{2,5}$ and $a_{2,3}$ be small parameters and $k_2 = 0$. Assuming the non-degeneracy conditions $a_{2,6} \neq 0$ and $a_{4,1} \neq 0$ the normal form for the stream function (4.96) is*

$$\psi = x^2 y (y^5 + y^4 c_{0,4} + y^2 c_{0,2} + x^2 + c_{0,0}) \tag{4.119}$$

where $c_{0,0}$, $c_{0,2}$ and $c_{0,4}$ are small transformed parameters.

The velocity field for the stream function (4.119) is

$$\begin{aligned}
u &= x (6y^5 + 5y^4 c_{0,4} + 3y^2 c_{0,2} + x^2 + c_{0,0}), \\
w &= -2y (y^5 + y^4 c_{0,4} + y^2 c_{0,2} + 2x^2 + c_{0,0}),
\end{aligned} \tag{4.120}$$

with the determinant of Jacobian matrix

$$\begin{aligned}
|J| = & -120y^9 c_{0,4} - 72y^{10} - 50y^8 c_{0,4}^2 - 72y^7 c_{0,2} + 180x^2 y^5 - 60y^6 c_{0,2} c_{0,4} \\
& - 24y^5 c_{0,0} + 110x^2 y^4 c_{0,4} - 20y^4 c_{0,0} c_{0,4} - 18y^4 c_{0,2}^2 + 18x^2 y^2 c_{0,2} - 12x^4 \\
& - 12y^2 c_{0,0} c_{0,2} - 10x^2 c_{0,0}^2 - 2c_{0,0}^2.
\end{aligned} \tag{4.121}$$

On the interface, the critical points can be obtained by solving

$$u = x(x^2 + c_{0,0}). \quad (4.122)$$

This equation yields that there exist the critical point when $c_{0,0} < 0$ and when $c_{0,0} > 0$ they do not exist. That makes $c_{0,0} = 0$ a bifurcation point.

To find the critical points on the center axis, we substitute $x = 0$ into the velocity field and obtain

$$u = 0, \quad w = -2y(y^5 + c_{0,4}y^4 + c_{0,2}y^2 + c_{0,0}). \quad (4.123)$$

The local bifurcation curve for the critical points on the center axis can be found by eliminating y from $J(0, y)$ and $w(0, y)$ which is

$$\begin{aligned} LCOC : & 256c_{0,0}^2c_{0,4}^5 - 128c_{0,0}c_{0,2}^2c_{0,4}^4 + 16c_{0,2}^4c_{0,4}^3 \\ & + 2000c_{0,0}^2c_{0,2}c_{0,4}^2 - 900c_{0,0}c_{0,2}^3c_{0,4} + 108c_{0,2}^5 + 3125c_{0,0}^3 = 0, \end{aligned} \quad (4.124)$$

and the local bifurcation curve for the critical points away from the boundaries can be found by firstly substituting $x^2 = -6y^5 - 5y^4c_{0,4} - 3y^2c_{0,2} - c_{0,0}$ into w and J , and secondly eliminating y from these equations, which is

$$\begin{aligned} LCAX : & 15116544c_{0,0}^2c_{0,4}^5 - 20995200c_{0,0}c_{0,2}^2c_{0,4}^4 + 7290000c_{0,2}^4c_{0,4}^3 \\ & + 98010000c_{0,0}^2c_{0,2}c_{0,4}^2 - 122512500c_{0,0}c_{0,2}^3c_{0,4} + 40837500c_{0,2}^5 \\ & + 45753125c_{0,0}^3 = 0. \end{aligned} \quad (4.125)$$

These bifurcation curves are cubic for $c_{0,0}$. Hence, we can obtain which values of $c_{0,0}$ solve *LCOC* and *LCAX* by finding the sign of discriminant of (4.124) and (4.125).

The discriminant of *LCOC* with respect to $c_{0,0}$ is

$$\Delta_1 = -16c_{0,2}^5(4c_{0,4}^3 + 25c_{0,2})^2(128c_{0,4}^3 + 675c_{0,2})^3, \quad (4.126)$$

and the discriminant of *LCAX* is

$$\Delta_2 = -c_{0,2}^5(2916c_{0,4}^3 + 15125c_{0,2})^2(3456c_{0,4}^3 + 15125c_{0,2})^3. \quad (4.127)$$

These discriminants yield that the number of $c_{0,0}$, which solve *LCOC*, depends on $c_{0,2}$ and $128c_{0,4}^3 + 675c_{0,2}$ and the number of $c_{0,0}$, which solve *LCAX*, depends on $c_{0,2}$ and $3456c_{0,4}^3 + 15125c_{0,2}$.

We will follow a different strategy for this case because all variables are important and can not be assumed a fixed value. If we follow the process as in the previous cases, it is very hard to see all occurring bifurcations.

In this case, we do not reduce the dimension of parameter space. Instead of it, firstly, we sketch the curves $128c_{0,4}^3 + 675c_{0,2} = 0$ (red curve) and $3456c_{0,4}^3 + 15125c_{0,2} = 0$ (blue curve) in Fig. 4.28, that gives the number of $c_{0,0}$ which solves the local bifurcation curves.

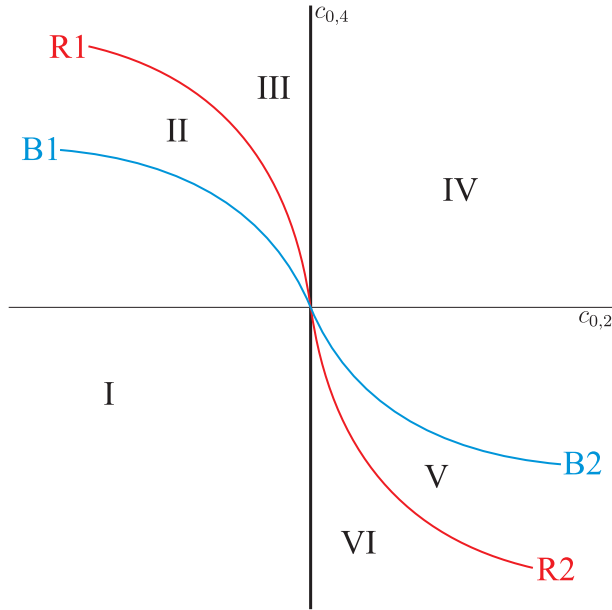


Figure 4.28: This diagram expresses the number of $c_{0,0}$ values which solves *LCOC* and *LCAX*.

Let us say $c_{0,0}^*[i]$ are solutions of *LCAX* and $c_{0,0}[i]$ solutions of *LCOC* where $i = 1, 2, 3$ due to the fact that the maximum number of solution of given curves is three.

In Region *I* and *IV*, there exist just one $c_{0,0}$ which solves *LCOC* and *LCAX*, which are $c_{0,0} = c_{0,0}[1]$ and $c_{0,0} = c_{0,0}^*[1]$, respectively. In these regions

On blue curves *B1* and *B2*, the solutions for *LCAX* becomes three, such that two of them are same. They are $c_{0,0} = c_{0,0}^*[1] = \frac{1306368c_{0,4}^5}{45753125}$ and $c_{0,0} = c_{0,0}^*[2, 3] = \frac{2985984c_{0,4}^5}{45753125}$. Depending on the sign of $c_{0,4}$, the sign of solutions $c_{0,0}^*[i]$ may vary on the blue curves. For *LCOC*, there is still one solution.

In Region *II* and *V*, there are three different solutions for *LCAX* and there is one solution for *LCOC*.

On red curves *R1* and *R2*, the solutions for *LCOC* becomes three, such that two of them are same. They are $c_{0,0}[1] = \frac{1792c_{0,4}^5}{253125}$ and $c_{0,0}[2,3] = \frac{4096c_{0,4}^5}{253125}$. Depending on the sign of $c_{0,4}$, the sign of solutions $c_{0,0}[i]$ may vary on the red curves. For *LCAX*, three different solutions exist.

In Region *III* and *VI*, both curves have three different solutions.

Finally, on the line $c_{0,2} = 0$, the solutions for *LCOC* are $c_{0,0} = c_{0,0}[1] = \frac{-256c_{0,4}^5}{3125}$ and $c_{0,0} = c_{0,0}[2,3] = 0$, the solutions for *LCAX* are $c_{0,0} = c_{0,0}^*[1] = \frac{-15116544c_{0,4}^5}{45753125}$ and $c_{0,0} = c_{0,0}^*[2,3] = 0$.

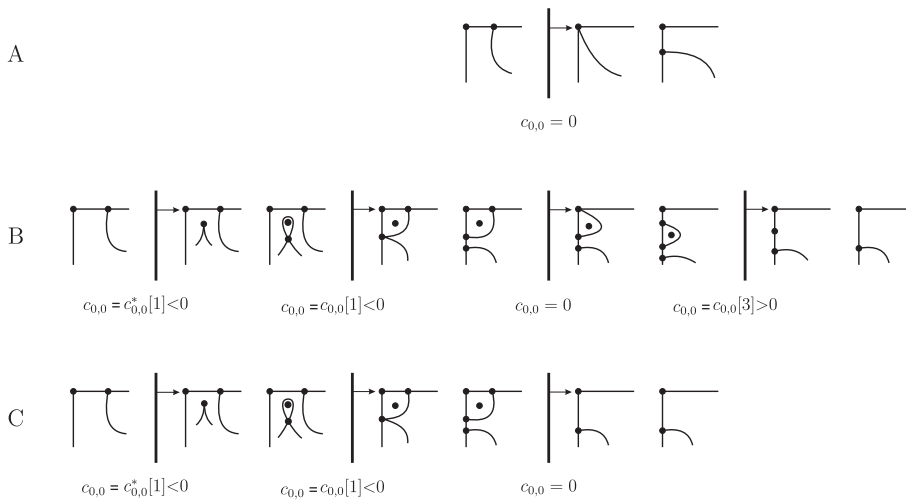


Figure 4.29: This figure shows us the bifurcations of the streamlines in different regions of Fig. 4.28. $c_{0,0}$ increases as one moves to the right.

In Region *I* and *II* in Fig. 4.28, a corner crossing bifurcation has been observed. We show this process as *A* in Fig. 4.29.

In Region *III*, we observed four different bifurcations such that one of them is occurring on the local bifurcation curve for away from the axis and the others on the local bifurcation curve for on the axis. This process is shown as *B* in Fig. 4.29.

And the final process which is shown as C in 4.29, is occurring in the regions IV, V and VI . The detailed observations and analysis can be found in Maple worksheet [35].

No global bifurcation has been observed for this case.

4.2.4.3 Case 3

Using the third degeneracy condition, the normal form of the stream function (4.36) is (details can be found in "Near Axis NormalFormandUnfoldings.mw" in [31])

$$a_{2,3}\eta^3\xi^2 + \tilde{a}_{8,1}\xi^8\eta, \quad (4.128)$$

where $\tilde{a}_{8,1} = -32k_2^4a_{2,3} - 6k_2k_4a_{2,3} - 3k_2^2a_{4,3} + a_{8,1}$. Using our assumption $a_{2,3} \neq 0$, it is convenient to write it as

$$a_{2,3}\xi^2\eta \left(\frac{\tilde{a}_{8,1}}{a_{2,3}}\xi^6 + \eta^2 \right). \quad (4.129)$$

More simplification is available for this equation by substituting $\xi = Ax$ and $\eta = By$. Choosing $B = 1$ and $A = \left(\frac{a_{2,3}}{\tilde{a}_{8,1}} \right)^{1/6}$, and scaling the stream function by dividing $a_{2,3}A^4B^4$, we have

$$x^2y(\sigma x^6 + y^2). \quad (4.130)$$

where $\sigma = \frac{a_{2,3}}{\tilde{a}_{8,1}} \left| \frac{\tilde{a}_{8,1}}{a_{2,3}} \right| = \pm 1$. This degenerate case can be figured as in Fig. 4.30.

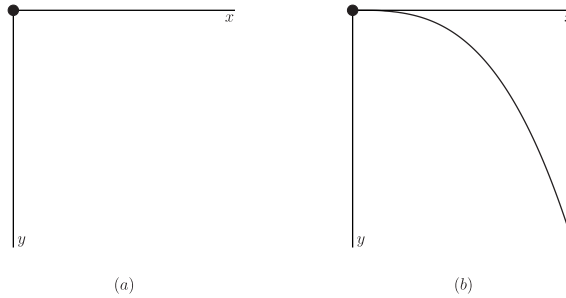


Figure 4.30: The degenerate case for (a) $\sigma = 1$, (b) $\sigma = -1$.

The unfolding of the degenerate case includes too many terms, therefore we kindly refer to [31] to see the unfolding and its elimination process. At the end of the process, the next theorem arise:

THEOREM 4.8 *Let $a_{2,1}$, $a_{4,1}$ and $a_{6,1}$ be small parameters and $k_2 \neq 0$. Assuming the non-degeneracy conditions $a_{2,3} \neq 0$ and $a_{8,1} \neq 0$ the normal form for the stream function (4.96) is*

$$\psi = x^2 y (\sigma x^6 + c_{4,0} x^4 + c_{2,0} x^2 y + c_{2,0} x^2 + y^2 + 2 c_{0,0} y + c_{0,0}) \quad (4.131)$$

where

$$\sigma = \begin{cases} +1 & \text{for } \tilde{a}_{8,1}/\tilde{a}_{2,3} > 0 \\ -1 & \text{for } \tilde{a}_{8,1}/\tilde{a}_{2,3} < 0 \end{cases},$$

$c_{0,0}$, $c_{2,0}$ and $c_{4,0}$ are small transformed parameters. If $k_2 = 0$,

$$\psi = x^2 y (\sigma x^6 + c_{4,0} x^4 + c_{2,0} x^2 + y^2 + c_{0,0}). \quad (4.132)$$

In the following analysis, we observe that the local bifurcation curves for the critical points on-center axis and interface are closely similar for cases $k_2 \neq 0$ and $k_2 = 0$. However, the local bifurcation curve for the critical points away from boundaries is completely different. Making bifurcation analysis for $k_2 \neq 0$ is more difficult, since reducing the parameter space is not possible as in the previous cases. However, for case $k_2 = 0$ is possible. Therefore, in this section we decide to continue with the stream function (4.132). Please see the analyses for cases $k_2 = 0$ and $k_2 \neq 0$ in [36].

The velocity field for the stream function (4.132) is

$$\begin{aligned} u &= x (\sigma x^6 + x^4 c_{4,0} + x^2 c_{2,0} + 3 y^2 + c_{0,0}), \\ w &= -2 y (4 \sigma x^6 + 3 x^4 c_{4,0} + 2 x^2 c_{2,0} + y^2 + c_{0,0}), \end{aligned} \quad (4.133)$$

with the determinant of Jacobian matrix

$$\begin{aligned} |J| &= -56 x^{12} - 82 \sigma x^{10} c_{4,0} - 52 \sigma x^8 c_{2,0} - 30 x^8 c_{4,0}^2 + 222 \sigma x^6 y^2 \\ &\quad - 22 \sigma x^6 c_{0,0} - 38 x^6 c_{2,0} c_{4,0} + 96 x^4 y^2 c_{4,0} - 16 x^4 c_{0,0} c_{4,0} - 12 x^4 c_{2,0}^2 \\ &\quad + 18 x^2 y^2 c_{2,0} - 10 x^2 c_{0,0} c_{2,0} - 18 y^4 - 12 y^2 c_{0,0} - 2 c_{0,0}^2. \end{aligned} \quad (4.134)$$

To find the critical points on the center axis, we substitute $x = 0$ into the velocity field and obtain

$$u = 0, \quad w = -2 y (y^2 + c_{0,0}). \quad (4.135)$$

Depending on the sign of $c_{0,0}$, the number of critical points on the axis varies. Hence $c_{0,0} = 0$ is a bifurcation point for the center axis.

The number of critical points away from the boundaries depends on the following equation obtained from the resultant of the velocities u , w and the determinant

of Jacobian $|J|$,

$$LCAX : -1149984 \sigma c_{0,0}^2 + 1393920 c_{0,0} c_{2,0} c_{4,0} - 484000 c_{2,0}^3 - 360448 \sigma c_{0,0} c_{4,0}^3 + 140800 \sigma c_{2,0}^2 c_{4,0}^2 = 0. \quad (4.136)$$

This equation is quadratic for $c_{0,0}$ and its discriminant is

$$Disc = -495616(165\sigma c_{2,0} - 64c_{4,0}^2)^3. \quad (4.137)$$

We introduce $\Delta = 165\sigma c_{2,0} - 64c_{4,0}^2$ to use instead of $c_{2,0}$ as a parameter since Δ has much more significance than $c_{2,0}$. From now on, the parameter space will be $(\Delta, c_{0,0}, c_{4,0})$.

On the interface, the critical points can be obtained by solving

$$u = x(\sigma x^6 + c_{4,0}x^4 + c_{2,0}x^2 + c_{0,0}) = 0. \quad (4.138)$$

The local bifurcation curve for the critical points on the interface can be found by eliminating x from (4.134) and u ,

$$LCOA : 27c_{0,0}^2 - 18\sigma c_{0,0}c_{2,0}c_{4,0} + 4\sigma c_{2,0}^3 + 4c_{0,0}c_{4,0}^3 - c_{2,0}^2c_{4,0}^2 = 0. \quad (4.139)$$

Substituting $c_{2,0} = \frac{64c_{4,0}^2 - \Delta}{165\sigma}$ into $LCOA$, we can write it in $(\Delta, c_{0,0}, c_{4,0})$ space. Depending on the sign of Δ , we will give the bifurcation diagrams. In the diagrams the red curves are $LCOA$ and the blue curves are $LCAX$.

Sketching the bifurcation curves, we decide which part of given curves are of our interest. We observe that some bifurcations occur in the upper-side of physical plane, therefore we eliminate them. Between the bifurcation curves, regions are created. As a further step, region by region, (region means the area between the curves, such as region *II* in the Fig. 4.32), we investigate the streamlines and the stream function. Firstly, we find the number of critical points and then decide the topology of them by considering determinant of Jacobian. To make sure, the given stream function is sketched by using 'contourplot' command in Maple. In a conclusion, we have obtained the following bifurcation diagrams.

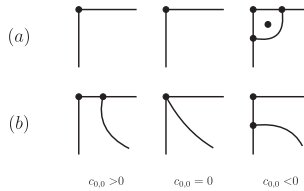


Figure 4.31: The bifurcation diagram and the possible streamline patterns for the normal form (4.131) when $\Delta \leq 0$ and (a) $\sigma = 1$ (b) $\sigma = -1$.

In Fig. 4.32 and 4.33, $R2 - R3$ implies the region between $R2$ and $R3$. There exist no global bifurcation for this case.

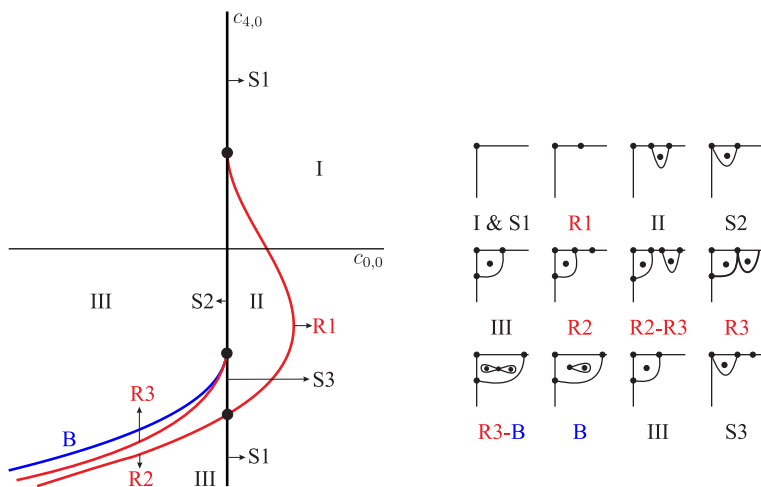


Figure 4.32: The bifurcation diagram and the possible streamline patterns for the normal form (4.131) when $\Delta > 0$ and $\sigma = 1$.

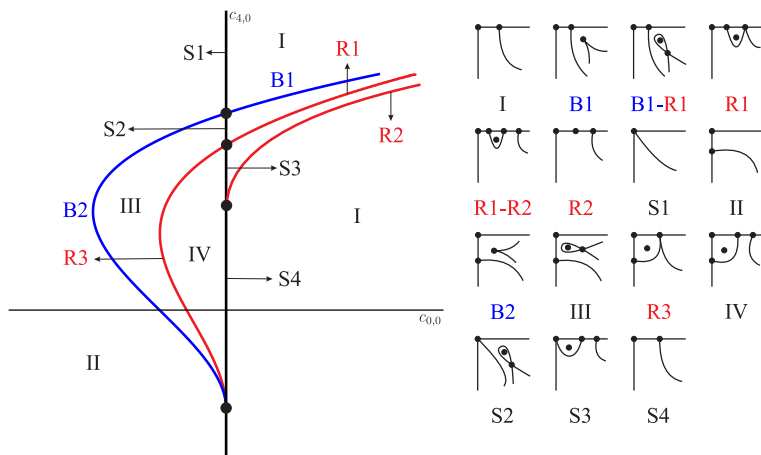


Figure 4.33: The bifurcation diagram and the possible streamline patterns for the normal form (4.131) when $\Delta > 0$ and $\sigma = -1$.

4.3 Flow Topology Away From The Axis

In the meridional plane (r, z) , we translate the coordinate system such that $F(r_0) = 0$, see Fig. 4.34.

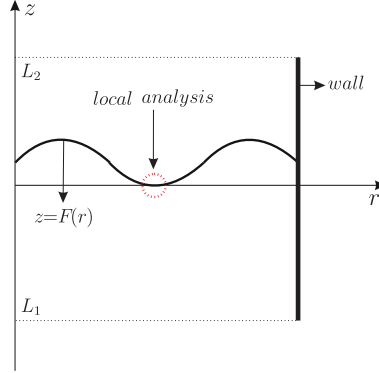


Figure 4.34: Translated meridional plane.

Away from the axis, the stream function (4.2) and the smooth interface (4.3) are expanded at r_0 . Since we observe the fluid motion on the interface, physics allow us to introduce $s = r - r_0$ and $\eta = z - F(s)$, hence the stream function and smooth interface can be written in the following form

$$\psi(s, \eta) = \sum_{m+n=0}^{\infty} a_{m,n} s^m \eta^n, \quad (4.140)$$

$$F(s) = \sum_{m=1}^{\infty} k_m s^m. \quad (4.141)$$

Applying the kinematic boundary condition (4.10), we obtain the following relations

$$a_{i,0} = 0 \quad i = 1, 2, 3, 4, \dots \quad (4.142)$$

and from tangential stress boundary condition (4.11),

$$a_{0,2} = a_{0,2}(a_{0,1}, a_{1,1}, r_0, k_1, k_2), \quad (4.143)$$

$$a_{1,2} = a_{0,2}(a_{0,1}, a_{1,1}, a_{2,1}, r_0, k_1, k_2, k_3), \quad (4.144)$$

$$a_{2,2} = a_{0,2}(a_{0,1}, a_{1,1}, a_{2,1}, a_{3,1}, r_0, k_1, k_2, k_3, k_4), \quad (4.145)$$

the relations $a_{i,2}$ have been obtained. Since they includes too many terms, we kindly refer to Maple worksheet [35] to see the details. With these relations and back substitution $s = x$ and $z = y + F(s)$, the stream function is written

$$\begin{aligned} \psi(x, y) = & a_{0,0} + a_{0,1}y + a_{0,2}y^2 + a_{1,1}xy + a_{0,3}y^3 + a_{1,2}xy^2 + a_{2,1}x^2y \\ & + a_{0,4}y^4 + a_{1,3}xy^3 + a_{2,2}x^2y^2 + a_{3,1}x^3y + \mathcal{O}(|x, y|^5), \end{aligned} \quad (4.146)$$

where $a_{0,2}$, $a_{1,2}$ and $a_{2,2}$ are obtained from tangential stress boundary conditions. The truncated velocity field can be written as

$$\begin{aligned} u = & \frac{1}{x+r_0} \frac{\partial \psi}{\partial y} = \frac{a_{0,1}}{r_0} + \left(\frac{a_{1,1}}{r_0} - \frac{a_{0,1}}{r_0^2} \right) x + \frac{2a_{0,2}}{r_0} y + \left(\frac{a_{2,1}}{r_0} - \frac{a_{1,1}}{r_0^2} + \frac{a_{0,1}}{r_0^3} \right) x^2 \\ & + \left(\frac{2a_{1,2}}{r_0} - \frac{2a_{0,2}}{r_0^2} \right) yx + \frac{3a_{0,3}}{r_0} y^2 + \left(\frac{a_{3,1}}{r_0} - \frac{a_{2,1}}{r_0^2} - \frac{a_{0,1}}{r_0^4} + \frac{a_{1,1}}{r_0^3} \right) x^3 \\ & + \left(\frac{2a_{2,2}}{r_0} - \frac{2a_{1,2}}{r_0^2} + \frac{2a_{0,2}}{r_0^3} \right) yx^2 + \left(\frac{3a_{1,3}}{r_0} - \frac{3a_{0,3}}{r_0^2} \right) y^2x + \frac{4a_{0,4}}{r_0} y^3, \end{aligned} \quad (4.147)$$

$$\begin{aligned} w = & -\frac{1}{x+r_0} \frac{\partial \psi}{\partial x} = -\frac{a_{1,1}}{r_0} y + \left(-\frac{2a_{2,1}}{r_0} + \frac{a_{1,1}}{r_0^2} \right) yx - \frac{a_{1,2}}{r_0} y^2 \\ & + \left(-\frac{3a_{3,1}}{r_0} + \frac{2a_{2,1}}{r_0^2} - \frac{a_{1,1}}{r_0^3} \right) yx^2 + \left(-\frac{2a_{2,2}}{r_0} + \frac{a_{1,2}}{r_0^2} \right) y^2x - \frac{a_{1,3}}{r_0} y^3. \end{aligned} \quad (4.148)$$

Like the previous section, we expand the pressure equation (4.4) and azimuthal velocity (4.5) at r_0 . Applying the tangential stress boundary condition (4.12) and using Navier-Stokes equations, we reduce the number of coefficients from the azimuthal velocity and pressure. As a next step, the normal stress boundary condition (4.13) is investigated and we obtain the pressure at the origin for (s, z) coordinate system as

$$p_{0,0} = -\frac{2\mu\sqrt{\Upsilon}(2k_1a_{0,1}k_2 + a_{1,1}\Upsilon) + \sigma(k_1^3 + 2k_2r_0 + k_1)}{(\Upsilon)^{3/2}r_0}, \quad (4.149)$$

where $\Upsilon = k_1^2 + 1$. The normal stress boundary condition gives us just physical expressions. We observe that the normal stress and tangential stress (4.12) have no effect on the meridional plane. Hence, we skip to give details about them from now on and again we kindly refer to Maple worksheet [35] to see all details about them.

4.3.1 Regular Case

The linearised system matrix of (4.147) is

$$\begin{pmatrix} u \\ w \end{pmatrix} = \begin{pmatrix} \frac{a_{0,1}}{r_0} \\ 0 \end{pmatrix} + \begin{pmatrix} \frac{a_{1,1}}{r_0} - \frac{a_{0,1}}{r_0^2} & \frac{2a_{0,2}}{r_0} \\ 0 & -\frac{a_{1,1}}{r_0} \end{pmatrix} \begin{pmatrix} x \\ y \end{pmatrix}. \quad (4.150)$$

If $a_{0,1} = 0$, the origin (for xy-coordinate system) is a critical point. In this system, the Jacobian matrix is given by

$$J = \begin{pmatrix} \frac{a_{1,1}}{r_0} & \frac{2a_{0,2}}{r_0} \\ 0 & -\frac{a_{1,1}}{r_0} \end{pmatrix}, \quad (4.151)$$

where $a_{0,2} = 2r_0a_{1,1}k_1(k_1^2 + 1)$ (from tangential stress condition). The eigenvalues for this matrix are $\tilde{a}_{1,1} = \frac{a_{1,1}}{r_0}$ and $-\tilde{a}_{1,1}$. For $\tilde{a}_{1,1} < 0$, the origin is a saddle and the eigenvector $(1, 0)$ is the stable direction and the another eigenvector $(a_{0,2}, -a_{1,1})$ is the unstable direction. For $\tilde{a}_{1,1} > 0$ just the flow reversed. (Non-degenerate point, $\tilde{a}_{1,1} \neq 0$).

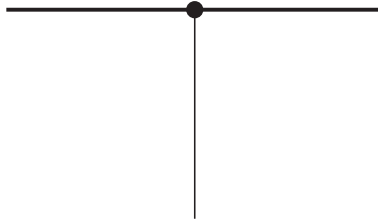


Figure 4.35: Dividing streamline on the free surface for non-degenerate critical point with $\tilde{a}_{1,1} \neq 0$.

If $a_{0,1} = a_{1,1} = 0$, we need to examine the higher order terms in order to determine the flow topology. The origin now is a degenerate critical point. From the tangential stress boundary condition, we have $a_{0,2} = 0$ and $a_{1,2} = \frac{2a_{2,1}k_1}{k_1^2 + 1}$ since $a_{0,1} = a_{1,1} = 0$. Substituting these coefficients into the stream function, we have

$$\psi(x, y) = a_{0,3}y^3 + \frac{2a_{2,1}k_1}{k_1^2 + 1}xy^2 + a_{2,1}x^2y + \mathcal{O}(|x, y|^4). \quad (4.152)$$

To eliminate the term xy^2 , we introduce a linear transformation

$$x = \xi + A\eta, \quad y = \eta. \quad (4.153)$$

where $A = -\frac{k_1}{k_1^2+1}$. With this transformation, the stream function becomes

$$\psi(\xi, \eta) = a_{2,1}\xi^2\eta + \tilde{a}_{0,3}\eta^3 + \mathcal{O}(|\xi, \eta|^4), \quad (4.154)$$

where $\tilde{a}_{0,3} = -\frac{k_1^2 a_{2,1}}{(k_1^2+1)^2} + a_{0,3}$. If $\frac{\tilde{a}_{0,3}}{a_{2,1}} > 0$, no separatrix has been observed except the interface. If $\frac{\tilde{a}_{0,3}}{a_{2,1}} < 0$, there exist two separatrices. The dividing streamlines are in the following directions

$$\eta = \pm \sqrt{\frac{\tilde{a}_{0,3}}{a_{2,1}}}\xi \quad \text{and} \quad \eta = 0. \quad (4.155)$$

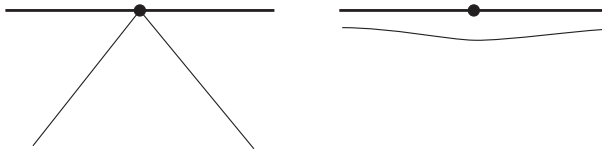


Figure 4.36: Dividing streamline on the free surface for degenerate critical point with $\frac{\tilde{a}_{0,3}}{a_{2,1}} < 0$ (left pattern) and $\frac{\tilde{a}_{0,3}}{a_{2,1}} > 0$ (right pattern).

These degenerate points and their unfoldings are also investigated by [17] and [37], although in these studies two-dimensional (non-axisymmetric) flow is considered.

In the following, we extend the degenerate conditions using the following assumptions.

Case (i) $a_{0,1} = 0$, $a_{1,1} = 0$, $a_{2,1} = 0$, $\tilde{a}_{0,3} \neq 0$, $a_{3,1} \neq 0$,

Case (ii) $a_{0,1} = 0$, $a_{1,1} = 0$, $a_{2,1} \neq 0$, $\tilde{a}_{0,3} = 0$ and

Case (iii) $a_{0,1} = 0$, $a_{1,1} = 0$, $a_{2,1} = 0$, $\tilde{a}_{0,3} = 0$.

4.3.2 Case 1

Applying the first assumption into (4.152) and extending the stream function up to the fifth order we have

$$\psi(x, y) = a_{0,3}y^3 + a_{0,4}y^4 + a_{1,3}xy^3 + a_{2,2}x^2y^2 + a_{3,1}x^3y + \mathcal{O}(|x, y|^5), \quad (4.156)$$

where $a_{2,2} = \frac{3a_{3,1}k_1}{k_1^2+1}$. We can simplify the stream function using the near-identity transformation which preserves the boundary condition such that $y = 0$

is mapped to $\eta = 0$,

$$x = \tilde{\xi} + m_{0,1}\eta + m_{2,0}\tilde{\xi}^2 + m_{1,1}\tilde{\xi}\eta + m_{0,2}\eta^2, \quad y = \eta + l_{1,1}\tilde{\xi}\eta + l_{0,2}\eta^2. \quad (4.157)$$

Choosing

$$\begin{aligned} m_{0,1} &= -\frac{k_1}{k_1^2 + 1}, \quad m_{2,0} = m_{1,1} = m_{0,2} = 0, \\ l_{1,1} &= -\frac{a_{1,3}}{3a_{0,3}} + \frac{a_{3,1}k_1^2}{(k_1^2 + 1)^2 a_{0,3}}, \\ l_{0,2} &= -\frac{a_{0,4}}{3a_{0,3}} + \frac{a_{1,3}k_1}{(k_1^2 + 1)a_{0,3}} - \frac{2a_{3,1}k_1^3}{3(k_1^2 + 1)^3 a_{0,3}}, \end{aligned} \quad (4.158)$$

the stream function becomes

$$\psi(\tilde{\xi}, \eta) = a_{0,3}\eta^3 + a_{3,1}\eta\tilde{\xi}^3 + \mathcal{O}(|\tilde{\xi}, \eta|^5). \quad (4.159)$$

This equation can be simplified as well, by using the transformation $\tilde{\xi} = A\xi$, yields

$$a_{0,3} \left(\eta^3 + A^3 \frac{a_{3,1}}{a_{0,3}} \xi^3 \eta + \mathcal{O}(|\xi, \eta|^5) \right). \quad (4.160)$$

Scaling this equation by dividing $a_{0,3}$ and substituting $A = \left(\frac{a_{0,3}}{a_{3,1}} \right)^{1/3}$, we obtain

$$\eta(\xi^3 + \eta^2) + \mathcal{O}(|\xi, \eta|^5). \quad (4.161)$$

The dividing streamlines are in the following directions

$$\eta = \pm \sqrt{-\xi^3} \quad \text{and} \quad \eta = 0. \quad (4.162)$$

which is seen in Fig. 4.37.

A small perturbation make some differences in flow structure. Hence assuming $a_{0,1} = \epsilon_1$, $a_{1,1} = \epsilon_2$ and $a_{2,1} = \epsilon_3$, the unfolding of the degenerate case (4.161) can be written as (truncated after fourth ordered terms)

$$\begin{aligned} \psi &= \epsilon_1 y + a_{0,2} y^2 + \epsilon_2 x y + a_{0,3} y^3 + a_{1,2} x y^2 + \epsilon_3 x^2 y + a_{0,4} y^4 + a_{3,1} x^3 y \\ &\quad + a_{2,2} x^2 y^2 + a_{1,3} x y^3. \end{aligned} \quad (4.163)$$

This equation can be simplified by using the same transformation like the de-

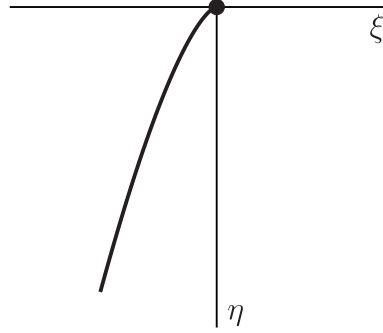


Figure 4.37: The dividing streamline for the degenerate case (4.161)

generate case, including the quadratic terms. Choosing the relations as

$$\begin{aligned}
 m_{0,1} &= -\frac{k_1}{k_1^2 + 1} + \mathcal{O}(\epsilon_1, \epsilon_2, \epsilon_3), \quad m_{2,0} = m_{1,1} = m_{0,2} = 0, \\
 l_{1,1} &= -\frac{a_{1,3}}{3a_{0,3}} + \frac{a_{3,1}k_1^2}{(k_1^2 + 1)^2 a_{0,3}} + \mathcal{O}(\epsilon_1, \epsilon_2, \epsilon_3), \\
 l_{0,2} &= -\frac{a_{0,4}}{3a_{0,3}} + \frac{a_{1,3}k_1}{(k_1^2 + 1)a_{0,3}} - \frac{2a_{3,1}k_1^3}{3(k_1^2 + 1)^3 a_{0,3}} + \mathcal{O}(\epsilon_1, \epsilon_2, \epsilon_3), \\
 l_{1,2} &= \frac{(2r\theta k_1^2 k_2 - k_1^3 - 2r\theta k_2 - k_1) a_{1,3}}{3a_{0,3}r\theta (k_1^2 + 1)^2} \\
 &\quad - \frac{a_{3,1}k_1^2 (2r\theta k_1^2 k_2 - k_1^3 - 2r\theta k_2 - k_1)}{a_{0,3}r\theta (k_1^2 + 1)^4} \\
 &\quad - \frac{6r\theta^2 k_1^4 k_3 - 8r\theta^2 k_1^3 k_2^2 + 2r\theta k_1^4 k_2 + 24r\theta^2 k_1 k_2^2 + k_1^5}{2r\theta^2 (k_1^2 + 1)^3} \\
 &\quad - \frac{6r\theta^2 k_3 - 2k_1^3 + 2r\theta k_2 - k_1}{2r\theta^2 (k_1^2 + 1)^3}, \\
 m_{1,2} &= \frac{1}{3a_{0,3}} \left(a_{0,4} - \frac{a_{3,1}k_1^3}{(k_1^2 + 1)^3} \right) + \frac{2r\theta k_1^2 k_2 + k_1^3 - 2r\theta k_2 + k_1}{2r\theta (k_1^2 + 1)^2}, \quad (4.164)
 \end{aligned}$$

we obtain

$$\begin{aligned}
 \psi &= \epsilon_1 \eta + \tilde{\epsilon}_2 \eta \tilde{\xi} + \gamma \tilde{\epsilon}_1 \eta^2 + \tilde{a}_{0,3} \eta^3 + \tilde{\epsilon}_3 \tilde{\xi}^2 \eta + \tilde{a}_{3,1} \tilde{\xi}^3 \eta + f(m_{0,1}, \epsilon_1, \epsilon_2, \epsilon_3) \tilde{\xi}^2 \eta^2 \\
 &\quad + g(l_{1,1}, \epsilon_1, \epsilon_2, \epsilon_3) \tilde{\xi} \eta^3 + h(l_{0,2}, \epsilon_1, \epsilon_2, \epsilon_3) \eta^4 \quad (4.165)
 \end{aligned}$$

where

$$\begin{aligned}
f(m_{0,1}, \epsilon_1, \epsilon_2, \epsilon_3) &= 3 \frac{(m_{0,1}k_1^2 + k_1 + m_{0,1})a_{3,1}}{k_1^2 + 1} + \mathcal{O}(\epsilon_1, \epsilon_2, \epsilon_3), \\
g(l_{1,1}, \epsilon_1, \epsilon_2, \epsilon_3) &= 3a_{0,3}l_{1,1} + a_{1,3} - 3 \frac{a_{3,1}k_1^2}{(k_1^2 + 1)^2} + \mathcal{O}(\epsilon_1, \epsilon_2, \epsilon_3), \\
h(l_{0,2}, \epsilon_1, \epsilon_2, \epsilon_3) &= 3a_{0,3}l_{0,2} + a_{0,4} + 2 \frac{a_{3,1}k_1^3}{(k_1^2 + 1)^3} - \frac{a_{1,3}k_1}{k_1^2 + 1} + \mathcal{O}(\epsilon_1, \epsilon_2, \epsilon_3), \\
\tilde{a}_{0,3} &= a_{0,3} + \mathcal{O}(\epsilon_1, \epsilon_2, \epsilon_3), \quad \tilde{a}_{3,1} = a_{3,1} + \mathcal{O}(\epsilon_1, \epsilon_2, \epsilon_3), \\
\tilde{\epsilon}_i &= \epsilon_i + \mathcal{O}(\epsilon_1, \epsilon_2, \epsilon_3), \\
\gamma &= l_{0,2} + \frac{k_2(k_1^2 - 1)}{(k_1^2 + 1)^2} - \frac{k_1}{(k_1^2 + 1)r_0}. \tag{4.166}
\end{aligned}$$

Since

$$f\left(-\frac{k_1}{k_1^2 + 1}, 0, 0, 0\right) = 0, \quad \frac{\partial}{\partial m_{0,1}} f\left(-\frac{k_1}{k_1^2 + 1}, 0, 0, 0\right) = 3a_{3,1} \neq 0, \tag{4.167}$$

it follows from IFT. that there exists a function $m_{0,1}(\epsilon_1, \epsilon_2, \epsilon_3)$ with $m_{0,1}(0) = -\frac{k_1}{k_1^2 + 1}$ such that $f(m_{0,1}(\epsilon_1, \epsilon_2, \epsilon_3), \epsilon_1, \epsilon_2, \epsilon_3) = 0$, for ϵ_1, ϵ_2 and ϵ_3 sufficiently small. Similarly, one can also find functions $l_{1,1}(\epsilon_1, \epsilon_2, \epsilon_3)$ and $l_{0,2}(\epsilon_1, \epsilon_2, \epsilon_3)$ which solve $g = 0$ and $h = 0$, respectively. More simplification is possible by replacing $\xi = \xi - \frac{\tilde{\epsilon}_3}{3a_{3,1}}$ which eliminates the term $\xi^2\eta$. With this transformation the stream function (4.165) becomes

$$\psi = \tilde{\epsilon}_1\eta + \tilde{\epsilon}_2\eta\tilde{\xi} + \gamma\tilde{\epsilon}_1\eta^2 + \tilde{a}_{0,3}\eta^3 + \tilde{a}_{3,1}\tilde{\xi}^3\eta. \tag{4.168}$$

Finally, we substitute $\tilde{\xi} = A\xi$ and $\eta = B\tilde{\eta}$ to make more simplification. The stream function now can reads

$$\tilde{a}_{0,3}B^3 \left(\frac{\tilde{a}_{3,1}A^3\xi^3\tilde{\eta}}{\tilde{a}_{0,3}B^2} + \tilde{\eta}^3 + \frac{\gamma\tilde{\epsilon}_1\tilde{\eta}^2}{\tilde{a}_{0,3}B} + \frac{\tilde{\epsilon}_2\tilde{\eta}A\xi}{\tilde{a}_{0,3}B^2} + \frac{\tilde{\epsilon}_1\tilde{\eta}}{\tilde{a}_{0,3}B^2} \right). \tag{4.169}$$

If $\gamma \neq 0$, we scale the stream function by dividing $\tilde{a}_{0,3}B^3$ and choosing $B = \frac{1}{\gamma}$ and $A = \frac{\tilde{a}_{0,3}}{\gamma^2\tilde{a}_{3,1}}$ and for $\gamma = 0$ choosing $B = 1$ and $A = \frac{\tilde{a}_{0,3}}{\tilde{a}_{3,1}}$, the next theorem arises by labelling the coordinates as (x, y) .

THEOREM 4.9 *Let $a_{0,1}, a_{1,1}$ and $a_{2,1}$ be small parameters and $\gamma \neq 0$. Assuming the non-degeneracy conditions $\tilde{a}_{0,3} \neq 0$ and $a_{3,1} \neq 0$ the normal form for the stream function (4.146) is*

$$\psi = y(c_{0,0} + c_{0,0}y + c_{1,0}x + y^2 + x^3), \tag{4.170}$$

where $c_{0,0}$ and $c_{1,0}$ are small transformed parameters. If $\gamma = 0$, the stream function is written in the following form

$$\psi = y(c_{0,0} + c_{1,0}x + y^2 + x^3). \quad (4.171)$$

The velocity field for the stream function (4.170) is (multiplied by $(x + r_0)$)

$$\begin{aligned} u &= x^3 + xc_{1,0} + 3y^2 + 2c_{0,0}y + c_{0,0}, \\ w &= -y(3x^2 + c_{1,0}). \end{aligned} \quad (4.172)$$

and for the stream function (4.171) is

$$\begin{aligned} u &= x^3 + xc_{1,0} + 3y^2 + c_{0,0}, \\ w &= -y(3x^2y + c_{1,0}). \end{aligned} \quad (4.173)$$

To find the critical points on the interface, we substitute $y = 0$ into the velocity field and obtain (cases $\gamma = 0$ and $\gamma \neq 0$ are same)

$$u = x^3 + xc_{1,0} + c_{0,0}, \quad w = 0. \quad (4.174)$$

The solution of velocity $u = 0$ determines the number of critical point on the interface. The local bifurcation curve can be obtained by eliminating x from $u(x, 0)$ and $|J(x, 0)$, which is

$$4c_{1,0}^3 + 27c_{0,0}^2 = 0. \quad (4.175)$$

To obtain the critical points away from the interface (for $y \neq 0$), we eliminate x and y from the velocity field and $|J|$, and we obtain

$$\begin{aligned} 3c_{0,0}^4 - 18c_{0,0}^3 + 4c_{1,0}^3 + 27c_{0,0}^2 &= 0, & \gamma \neq 0, \\ 4c_{1,0}^3 + 27c_{0,0}^2 &= 0 & \gamma = 0. \end{aligned} \quad (4.176)$$

Finally, we are ready to make a bifurcation diagram with these local bifurcation curves. It is worth pointing out that there exist no global bifurcation for this case.

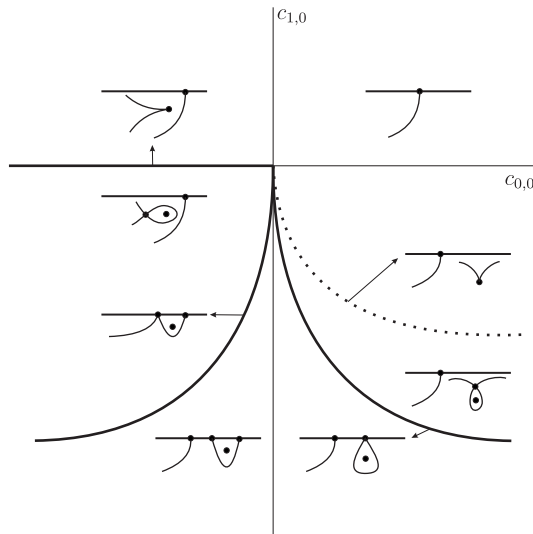


Figure 4.38: The streamline patterns and bifurcation diagram for the normal form (4.170).

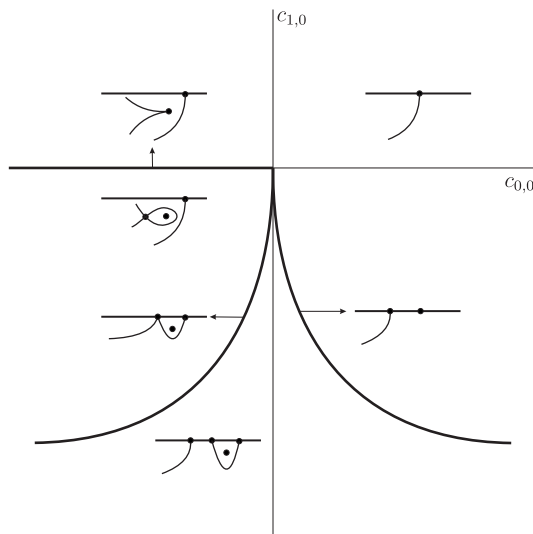


Figure 4.39: The streamline patterns and bifurcation diagram for the normal form (4.171).

Despite the similarity of degenerate case which is obtained by A. Deliceoglu [37], the unfolding and the bifurcation diagrams do not look similar. The reason is

that he consider $\gamma\epsilon_1$ as a new parameter.

4.3.3 Case 2

Substituting the second assumption into (4.152) and extend the stream function up to the fifth order we have

$$\begin{aligned} \psi(x, y) = & a_{1,2}xy^2 + a_{2,1}x^2y + a_{0,4}y^4 + a_{1,3}xy^3 + a_{2,2}x^2y^2 + a_{3,1}x^3y \\ & + \mathcal{O}(|x, y|^5), \end{aligned} \quad (4.177)$$

where $a_{1,2}$ and $a_{2,2}$ are related the other coefficients due to the tangential stress boundary condition. Using the transformation (4.157), we can simplify the stream function by choosing

$$\begin{aligned} l_{0,2} = 0, \quad l_{1,1} = 0, \quad m_{1,0} = -\frac{k_1}{k_1^2 + 1}, \quad m_{2,0} = -\frac{a_{3,1}}{2a_{2,1}}, \\ m_{1,1} = \frac{6r_0k_1^2k_2 + k_1^3 - 6r_0k_2 + k_1}{4r_0(k_1^2 + 1)^2}, \\ m_{0,2} = \frac{3a_{3,1}k_1^2}{2(k_1^2 + 1)^2} - \frac{a_{1,3}}{2} - \frac{k_1(6r_0k_1^2k_2 + k_1^3 - 6r_0k_2 + k_1)}{2r_0(k_1^2 + 1)^3}, \end{aligned} \quad (4.178)$$

then the stream function (4.177) becomes

$$\psi = a_{2,1}\tilde{\xi}^2\eta + \tilde{a}_{0,4}\eta^4 + \mathcal{O}(|\tilde{\xi}, \eta|^5), \quad (4.179)$$

where

$$\begin{aligned} \tilde{a}_{0,4} = & a_{0,4} - \frac{a_{2,1}k_1^2(6r_0k_1^2k_2 + k_1^3 - 6r_0k_2 + k_1)}{2r_0(k_1^2 + 1)^4} \\ & + \frac{2a_{3,1}k_1^3}{(k_1^2 + 1)^3} - \frac{a_{1,3}k_1}{k_1^2 + 1}. \end{aligned} \quad (4.180)$$

To make more simplification, we scale time by dividing the stream function by $\tilde{a}_{0,4}$ and using the transformation $\tilde{\xi} = \left| \frac{\tilde{a}_{0,4}}{a_{2,1}} \right|^{1/2} \xi$, we obtain

$$\psi = \eta(\sigma\xi^2 + \eta^3), \quad (4.181)$$

where $\sigma = \frac{a_{2,1}}{\tilde{a}_{0,4}} \left| \frac{\tilde{a}_{0,4}}{a_{2,1}} \right| = \pm 1$. The dividing streamline can be obtained by $\psi = 0$, which are

$$\eta = 0, \quad \xi = \pm \sqrt{-\sigma\eta^3}. \quad (4.182)$$

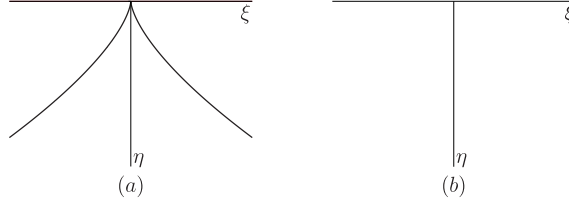


Figure 4.40: The dividing streamline for the degenerate case (4.181) for (a) $\sigma = 1$, (b) $\sigma = -1$.

They are seen in Fig. 4.40.

Like the previous section, let us introduce small parameters $a_{0,1} = \epsilon_1$, $a_{1,1} = \epsilon_2$ and $\tilde{a}_{0,3} = \epsilon_3$. Using these parameters, the unfolding of the degenerate case can be written as

$$\begin{aligned} \psi = & \epsilon_1 z + \hat{a}_{2,0} z^2 + \epsilon_2 s z + \epsilon_3 z^3 + \hat{a}_{1,2} s z^2 + a_{2,1} s^2 z \\ & + a_{0,4} z^4 + a_{1,3} s z^3 + \hat{a}_{2,2} s^2 z^2 + a_{3,1} s^3 z, \end{aligned} \quad (4.183)$$

where $\hat{a}_{i,j}$ is in the form $a_{i,j} + \epsilon$. Using a non-linear transformation

$$\begin{aligned} s = & \xi - \frac{k_1}{k_1^2 + 1} \eta + m_{2,0} \xi^2 + m_{1,1} \xi \eta + m_{0,2} \eta^2 + m_{3,0} \xi^3 + m_{2,1} \xi^2 \eta \\ & + m_{1,2} \xi \eta^2 + m_{0,3} \eta^3, \\ z = & \eta + l_{0,2} \eta^2 + l_{1,1} \xi \eta + l_{2,1} \xi^2 \eta + l_{1,2} \xi \eta^2 + l_{0,3} \eta^3, \end{aligned} \quad (4.184)$$

we can simplify the given stream function by choosing

$$\begin{aligned} l_{0,2} = & -\frac{2 r_0 k_1^2 k_2 - k_1^3 - 2 r_0 k_2 - k_1}{2 r_0 (k_1^2 + 1)^2}, \quad l_{1,1} = m_{1,2} = 0, \\ l_{1,2} = & -\frac{6 r_0^2 k_1^4 k_3 - 8 r_0^2 k_1^3 k_2^2 + 2 r_0 k_1^4 k_2 + 24 r_0^2 k_1 k_2^2 + k_1^5}{2 (k_1^2 + 1)^3 r_0^2} \\ & + \frac{6 r_0^2 k_3 - 2 k_1^3 + 2 r_0 k_2 - k_1}{2 (k_1^2 + 1)^3 r_0^2}. \end{aligned} \quad (4.185)$$

The stream function now can read as

$$\begin{aligned} \psi = & \epsilon_1 \eta + \tilde{\epsilon}_2 \eta \xi + \epsilon_3 \eta^3 + \tilde{a}_{2,1} \xi^2 \eta + \tilde{a}_{0,4} \eta^4 + f(m_{0,2}, \epsilon_1, \epsilon_2, \epsilon_3) \xi \eta^3 \\ & + g(m_{1,1}, \epsilon_1, \epsilon_2, \epsilon_3) \xi^2 \eta^2 + h(m_{2,0}, \epsilon_1, \epsilon_2, \epsilon_3) \xi^3 \eta, \end{aligned} \quad (4.186)$$

where

$$\begin{aligned} f(m_{0,2}, \epsilon_1, \epsilon_2, \epsilon_3) &= \Theta(m_{0,2}) + \mathcal{O}(\epsilon_1, \epsilon_2, \epsilon_3), \\ g(m_{1,1}, \epsilon_1, \epsilon_2, \epsilon_3) &= \Theta(m_{1,1}) + \mathcal{O}(\epsilon_1, \epsilon_2, \epsilon_3), \\ h(m_{2,0}, \epsilon_1, \epsilon_2, \epsilon_3) &= \Theta(m_{2,0}) + \mathcal{O}(\epsilon_1, \epsilon_2, \epsilon_3), \\ \tilde{a}_{0,4} &= a_{0,4} + \mathcal{O}(\epsilon_1, \epsilon_2, \epsilon_3), \quad \tilde{a}_{2,1} = a_{2,1} + \mathcal{O}(\epsilon_1, \epsilon_2, \epsilon_3), \end{aligned} \quad (4.187)$$

$\Theta()$ implies the equations in (4.178). Like the process in the previous case, by using I.F.T., one can find functions $m_{0,2}(\epsilon_1, \epsilon_2, \epsilon_3)$, $m_{1,1}(\epsilon_1, \epsilon_2, \epsilon_3)$ and $m_{2,0}(\epsilon_1, \epsilon_2, \epsilon_3)$ which solve $f = 0$, $g = 0$ and $h = 0$, respectively. To make more simplification, we can translate the origin by replacing $\xi = \xi - \frac{\epsilon_2}{2a_{2,1}}$ (the term $\xi\eta$ will be eliminated) and following the similar strategy in the degenerate case, such as scaling and the substituting $\xi = A\tilde{\xi}$ and $\eta = B\tilde{\eta}$, the next theorem arises:

THEOREM 4.10 *Let $a_{0,1}$, $a_{1,1}$ and $\tilde{a}_{0,3}$ be small parameters. Assuming the non-degeneracy conditions $a_{2,1} \neq 0$ and $\tilde{a}_{0,4} \neq 0$ the normal form for the stream function (4.179) is*

$$\psi = y(c_{0,0} + c_{0,2}y^2 + y^3 + \sigma x^2), \quad (4.188)$$

where

$$\sigma = \begin{cases} +1 & \text{for } \tilde{a}_{0,4}/\tilde{a}_{2,1} > 0 \\ -1 & \text{for } \tilde{a}_{0,4}/\tilde{a}_{2,1} < 0 \end{cases},$$

$c_{0,0}$ and $c_{0,2}$ are small transformed parameters.

The velocity field for the stream function (4.188) is (multiplication by $(x + r_0)$)

$$\begin{aligned} u &= \sigma x^2 + 4y^3 + 3y^2 c_{0,2} + c_{0,0}, \\ w &= -2\sigma xy. \end{aligned} \quad (4.189)$$

To find the critical points on the interface, we substitute $y = 0$ into the velocity field and obtain

$$u = \sigma x^2 + c_{0,0} = 0, \quad w = 0. \quad (4.190)$$

The critical points on the interface depend on the solutions of the velocity u , and its solutions exist when $-\sigma c_{0,0} \leq 0$. To find the critical points away from the interface ($y \neq 0$), we substitute $x = 0$ into the velocity u and J ,

$$\begin{aligned} u &= 4y^3 + 3y^2 c_{0,2} + c_{0,0} = 0, \\ J &= 24\sigma y^3 + 12\sigma y^2 c_{0,2}. \end{aligned} \quad (4.191)$$

The resultant of these equations with respect to y , gives us the local bifurcation curve for the critical points away from interface which is

$$-c_{0,0}^2 \sigma (c_{0,2}^3 + 4c_{0,0}) = 0. \quad (4.192)$$

It is possible to see global bifurcation curves for this case. This bifurcation appears when the following condition holds;

$$\begin{aligned} u(x_1, y_1) = 0, \quad u(x_2, 0) = 0, \quad w(x_1, y_1) = 0, \quad w(x_2, 0) = 0, \\ \psi(x_1, y_1) = \psi(x_2, 0), \quad \text{where } J(x_1, y_1) < 0, \quad J(x_2, 0) < 0, \end{aligned} \quad (4.193)$$

which gives the intersection of the saddle points for away from and on the interface. The global bifurcation curve is

$$c_{0,2}^3 + 8c_{0,0} = 0, \quad (4.194)$$

and is denoted as dashed lines in the figures.

The bifurcation diagram can be figured as in Fig. 4.41 for $\sigma = 1$ and Fig. 4.42 for $\sigma = -1$.

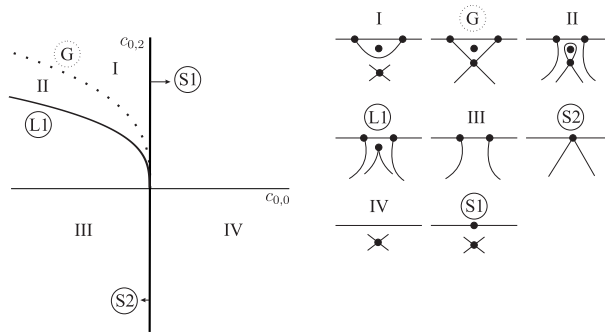


Figure 4.41: The bifurcation diagram and the streamline patterns for the normal form (4.188) with $\sigma = 1$.

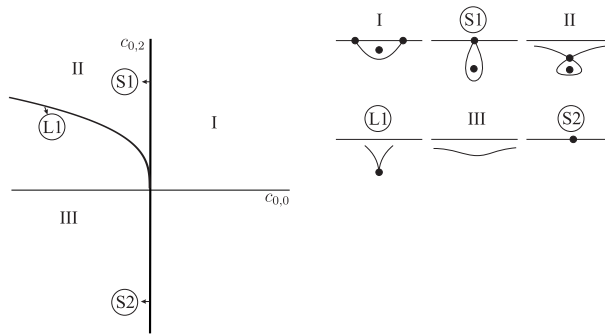


Figure 4.42: The bifurcation diagram and the streamline patterns for the normal form (4.188) with $\sigma = -1$.

4.3.4 Case 3

We first consider the vorticity transport equation

$$\nabla \times \vec{N}\vec{S} = 0 \quad (4.195)$$

where $\vec{N}\vec{S}$ is the Navier-Stokes equations in cylindrical coordinate system. As known, this result is in vectorial form. The second component of this form gives us by applying the assumptions for this case

$$\begin{aligned} r^2 z^0 : 12 \mu r_0 a_{0,4} + \frac{r_0 \rho b_{0,0} b_{1,0} k_1 + 18 \mu r_0 a_{3,1} k_1 - \rho b_{0,0}^2 k_1}{k_1^2 + 1} &= 0, \\ r^0 z^2 : a_{2,2} &= 0, \\ r^1 z^1 : \mu r_0 a_{1,3} &= 0. \end{aligned} \quad (4.196)$$

According the term $r^0 z^2$, $a_{2,2}$ must be equal 'zero' for a steady flow. The vorticity transport equation under the given assumptions makes $a_{1,3} = 0$ and $a_{2,2} = 0$. Using the assumptions for the third case and $a_{1,3} = a_{2,2} = 0$, the stream function is written (up to the fifth order term) as

$$\psi = a_{3,1} s^3 z + a_{0,4} z^4 + \mathcal{O}(|s, z|^5). \quad (4.197)$$

Dividing the stream function by $a_{0,4}$, and scaling $s \rightarrow \left(\frac{a_{0,4}}{a_{3,1}}\right)^{\frac{1}{3}} x$ and $z \rightarrow y$, ψ can be simplified as by truncating higher order terms

$$\psi = y(x^3 + y^3). \quad (4.198)$$

The dividing streamlines can be obtained by solving $\psi = 0$, which are

$$y = 0, \quad x^3 = -y^3. \quad (4.199)$$

They are seen in Fig. 4.43.

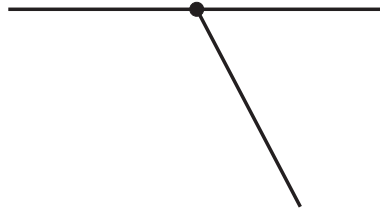


Figure 4.43: Non-simple degenerate critical point on the interface with the given conditions.

To unfold the degenerate case, we have assumed $a_{0,1} = \epsilon_1$, $a_{1,1} = \epsilon_2$, $a_{2,1} = \epsilon_3$ and $a_{0,3} = \epsilon_4$ are small parameters. The unfolding of the degenerate case includes too much terms, hence we kindly refer to Maple worksheet [35] to see the whole process. After using non-linear transformation the simplified stream function becomes

$$\psi = \tilde{a}_{0,4}\eta^4 + \tilde{a}_{3,1}\eta\xi^3 + \epsilon_4\eta^3 + \epsilon_3\eta\xi^2 + \epsilon_2\eta\xi + \epsilon_1\eta, \quad (4.200)$$

where $\tilde{a}_{0,4} = a_{0,4} + \mathcal{O}(\epsilon_1, \epsilon_2, \epsilon_3, \epsilon_4)$ and $\tilde{a}_{3,1} = a_{3,1} + \mathcal{O}(\epsilon_1, \epsilon_2, \epsilon_3, \epsilon_4)$. The $\xi^2\eta$ term can be eliminated by applying the linear transformation $\xi = -\frac{\epsilon_3}{3a_{3,1}} + \tilde{\xi}$ into (4.200), and obtained

$$\hat{a}_{0,4}\eta^4 + \hat{a}_{3,1}\eta\tilde{\xi}^3 + \hat{\epsilon}_4\eta^3 + \hat{\epsilon}_2\eta\tilde{\xi} + \hat{\epsilon}_1\eta. \quad (4.201)$$

More simplification can be made by dividing the stream function by $\hat{a}_{0,4}$ and scaling by $\tilde{\xi} \rightarrow \left(\frac{\hat{a}_{0,4}}{\hat{a}_{3,1}}\right)^{\frac{1}{3}}x$ and $\eta \rightarrow y$, then the following theorem arises:

THEOREM 4.11 *Let $a_{0,1}$, $a_{1,1}$, $a_{2,1}$ and $a_{0,3}$ be small parameters. Assuming the non-degeneracy conditions $a_{0,4} \neq 0$ and $a_{3,1} \neq 0$, the normal form is*

$$\psi = y(c_{0,1} + c_{1,1}x + c_{0,3}y^2 + x^3 + y^3) \quad (4.202)$$

where $c_{0,1}$, $c_{1,1}$ and $c_{0,3}$ are small transformed parameters.

The differential equations for the streamlines are,

$$\begin{aligned} \dot{x} = u &= x^3 + 4y^3 + 3y^2c_{0,3} + xc_{1,1} + c_{0,1}, \\ \dot{y} = w &= -y(3x^2 + c_{1,1}). \end{aligned} \quad (4.203)$$

The critical points on the interface which are the solutions of

$$x^3 + xc_{1,1} + c_{0,1} = 0, \quad (4.204)$$

may vary when the discriminant of (4.204), which is $4c_{1,1}^3 + 27c_{0,1}^2$, changes.

For the critical points away from the interface, the local bifurcation curve can be obtained by taking the resultant of the velocities which is

$$c_{1,1}^9 (27c_{0,3}^6 + 216c_{0,1}c_{0,3}^3 + 64c_{1,1}^3 + 432c_{0,1}^2) = 0. \quad (4.205)$$

However, the number of critical points for away from the interface mainly depends on the sign of $c_{1,1}$ since $w = 3x^2 + c_{1,1} = 0$. Therefore, we determine investigating this case into three sub-cases which depends on the sign of $c_{1,1}$.

It is possible to see two kinds of global bifurcation for this case which are:

1. Global bifurcation associated with the critical points on and away from the interface. To find this bifurcation curve, the main idea is akin to the Case 2. The curve written as

$$432 c_{0,3}^6 + 5832 c_{0,1} c_{0,3}^3 + 2916 c_{1,1}^3 + 19683 c_{0,1}^2 = 0. \quad (4.206)$$

2. Global bifurcation associated with the critical points away from the interface. To find this bifurcation curve, the following conditions must hold:

$$\begin{aligned} \psi(x_1, y_1) &= \psi(x_2, y_2), & J(x_1, y_1) &< 0, & J(x_2, y_2) &< 0, \\ u(x_1, y_1) &= u(x_2, y_2) = w(x_1, y_1) = w(x_2, y_2) = 0. \end{aligned} \quad (4.207)$$

This global bifurcation curve can be obtained by eliminating x_1 , x_2 , y_1 and y_2 from the previous conditions. Note that this bifurcation can just be seen for $c_{1,1} < 0$.

$c_{1,1} > 0$: The number of critical points on the interface is just one, and away from the interface no critical point exists. The streamline pattern is figured as in Fig. 4.44.

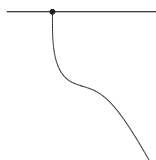


Figure 4.44: Streamline pattern for the normal form (4.200) with $c_{1,1} > 0$.

$c_{1,1} = 0$: The number of critical points on the interface depends on the value of $c_{0,1}$, and away from the interface depends on the curve $c_{0,3}^3 + 4c_{0,1}$. Hence, the streamline patterns and bifurcation diagram are figured as in Fig. 4.45.

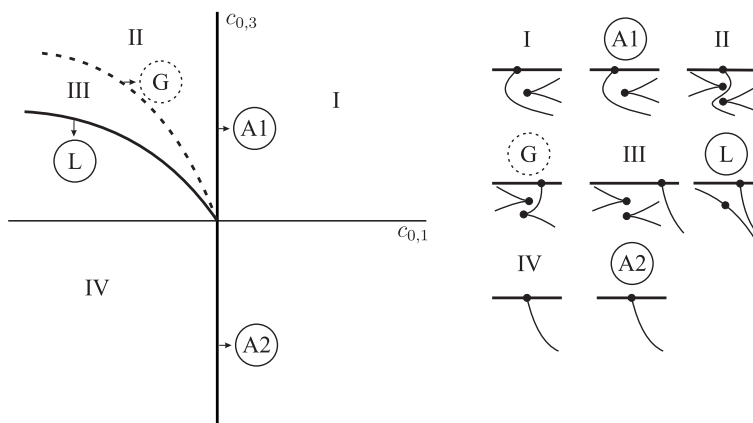


Figure 4.45: Streamline pattern for the normal form (4.200) with $c_{1,1} = 0$.

$c_{1,1} < 0$: In Fig. 4.46, the red curve denotes the local bifurcation curve for away from axis; the blue curve is for the global bifurcation curve associated with the critical points which are on and away from the interface; and dashed curve is for the global bifurcation curve associated with the critical points which are away from the interface.

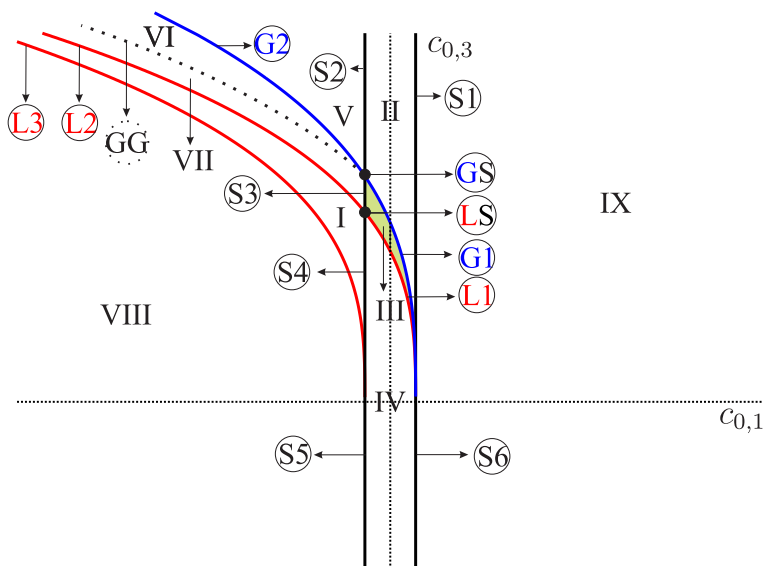


Figure 4.46: Streamline pattern for the normal form (4.200) with $c_{1,1} < 0$.

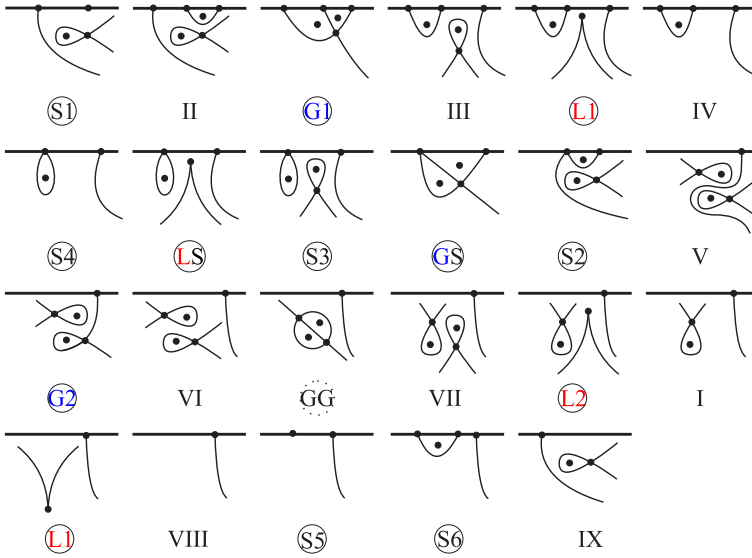


Figure 4.47: The streamline patterns occurring in Fig. 4.46.

We analyse the degenerate case and its unfolding for an axisymmetric flow close to the free surface. In this case, co-dimension three bifurcation is observed. The topology of 2D flows close to the free surface had been studied by A. Deliceoglu [37] for similar case. We observed similar dividing streamline for the degenerate case, however the unfolding of the degenerate case and bifurcation diagram look different. The reason is that we could not eliminate $a_{0,4}$ as he did because of the swirl velocity effect.

4.4 Flow Topology Close to a Stationary Wall

The process for this section is almost similar as the previous section. In this section, we will focus on the streamline patterns in the vicinity of the intersection point of a stationary wall

$$s = \sum_{i=1}^{\infty} d_i z^i, \tag{4.208}$$

and the interface $F(s)$. (see in Fig. 4.48)

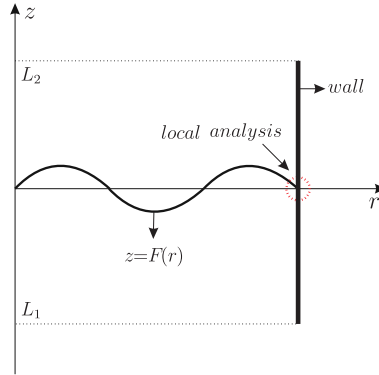


Figure 4.48: The local analysis of a flow close to intersection of wall and interface. The interface is translated $F(r_0) = 0$.

The process obtaining the stream function (4.146) is similar for this case as well. Additionally, we have extra boundary conditions $u = w = 0$ on the wall. The relations, which are obtained from this boundary conditions, can be found into Maple worksheet [38].

4.4.1 Regular Case

The lowest order of the stream function for this case is obtained as (up to the fifth order term)

$$\psi = a_{3,1}s^3z + 3\Gamma a_{3,1}z^2s^2 + \mathcal{O}(|s, z|^5), \quad (4.209)$$

where $\Gamma = \frac{k_1}{k_1^2+1}$ when wall is $s = 0$ and $\Gamma = \frac{d_1k_1^2+d_1+k_1}{k_1^2+1}$ when wall is in form (4.208). Firstly, we have assumed that $a_{3,1} \neq 0$ and $\Gamma \neq 0$. The stream function is scaled by dividing by $a_{3,1}$. Depending on the sign of Γ , the dividing streamline can be figured as Fig. 4.49.

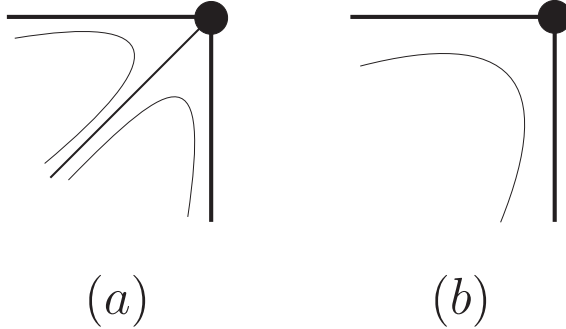


Figure 4.49: The dividing streamline and non-simple degenerate points for (a) $\Gamma > 0$ and (b) $\Gamma < 0$.

If we break this non-degenerate condition, we need to examine higher order terms. As one see that this non-degeneracy can break by assuming $\Gamma = 0$, that means $k_1 = 0$ when wall is $s = 0$ and $d_1 = -\frac{k_1}{k_1^2+1}$ when wall is in the form (4.208).

4.4.2 Co-dimension 1 bifurcation

The higher degree of the stream function need to be investigated when $\Gamma = 0$. The stream function (4.209) extended up to the sixth order by applying $\Gamma = 0$ and written as

$$\psi = 5k_2a_{3,1}z^2s^3 + a_{4,1}s^4z + a_{2,3}s^2z^3 + a_{3,1}s^3z + \mathcal{O}(|s, z|^6). \quad (4.210)$$

To reduce the number of coefficients, we define a near identity transformation which preserves the boundary conditions,

$$s = \xi + m_{2,0}\xi^2 + m_{1,1}\xi\eta, \quad z = \eta + l_{0,2}\eta^2 + l_{1,1}\xi\eta. \quad (4.211)$$

After applying this transformation into the given stream function (see details in [38]), we choose $m_{2,0} = m_{1,1} = 0$, $l_{1,1} = -\frac{a_{4,1}}{a_{3,1}}$ and $l_{0,2} = -5k_2$, the stream function is simplified as

$$\psi = a_{2,3}\xi^2\eta^3 + a_{3,1}\xi^3\eta + \mathcal{O}(|\xi, \eta|^6). \quad (4.212)$$

Further simplification can be made by scaling the $(\xi\eta)$ -coordinate system as a form $\xi \rightarrow A\xi$ and dividing stream function by $Aa_{3,1}$ where $A = \frac{a_{3,1}}{b_{2,3}}$. The corresponding stream function becomes

$$\psi = \xi^2\eta(\eta^2 + \xi) + \mathcal{O}(|\xi, \eta|^6). \quad (4.213)$$

The dividing streamline can be found by solving $\psi = 0$, which are in the direction $\xi = -\eta^2$, $\xi = 0$ and $\eta = 0$ seen as Fig. 4.50.

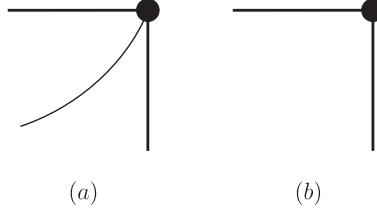


Figure 4.50: The dividing streamline for the degenerate case (4.213) for $\Gamma = 0$.

Introducing the small parameter $\Gamma = \epsilon_1$, the unfolding of the degenerate case (4.213) is given by (truncated after fifth-order terms)

$$\begin{aligned} \psi = & a_{3,1}s^3z + 3\frac{a_{3,1}\epsilon_1s^2z^2}{\epsilon_1^2 + 1} + a_{2,3}s^2z^3 + a_{4,1}s^4z \\ & + \frac{(10r_0k_2a_{3,1} + \mathcal{O}(\epsilon_1))z^2s^3}{2r_0(\epsilon_1^4 + 2\epsilon_1^2 + 1)}. \end{aligned} \quad (4.214)$$

Using the transformation (6.44) and by choosing

$$\begin{aligned} m_{2,0} = 0, \quad m_{1,1} = -l_{0,2}, \quad l_{1,1} = -\frac{a_{4,1}}{a_{3,1}}, \\ l_{0,2} = -5k_2 + \mathcal{O}(\epsilon_1), \end{aligned} \quad (4.215)$$

one can obtain

$$\psi = a_{2,3}\xi^2\eta^3 + a_{3,1}\epsilon_1\xi^2\eta^2 + a_{3,1}\xi^3\eta. \quad (4.216)$$

Scaling the coordinate system like the degenerate case, the next theorem arises:

THEOREM 4.12 *Let Γ be a small parameter. Assuming the non-degeneracy conditions $a_{3,1} \neq 0$ and $a_{2,3} \neq 0$ the normal form is*

$$\psi = \eta\xi^2(\eta^2 + \eta c_{0,1} + \xi) \quad (4.217)$$

where $c_{0,1}$ is small parameter.

The differential equations for the streamlines are, after a scaling of the time by ξ ,

$$\begin{aligned} \dot{\xi} = u = \xi(3\eta^2 + 2\eta c_{0,1} + \xi), \\ \dot{\eta} = w = -\eta(2\eta^2 + 2\eta c_{0,1} + 3\xi). \end{aligned} \quad (4.218)$$

The critical points on the wall can be found by substituting $\xi = 0$ into the velocity field,

$$-\eta (2\eta^2 + 2\eta c_{0,1}) = 0. \quad (4.219)$$

which are $(0, 0)$ and $(0, -c_{0,1})$.

For the critical points on interface, we need to substitute $\eta = 0$ into the velocity field. It is observed that $(0, 0)$ is only the critical point on the interface.

Depending on the value of $c_{0,1}$, the streamlines are figured in Fig. 4.51.

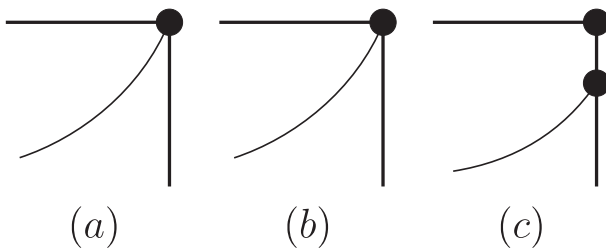


Figure 4.51: The streamline patterns for the normal form (4.217) where (a) $c_{0,1} < 0$, (b) $c_{0,1} = 0$ and (c) $c_{0,1} > 0$.

4.4.3 Co-dimension 2 bifurcation

As non-degenerate conditions we have assumed that $a_{3,1} \neq 0$ or $a_{2,3} \neq 0$, previously. If we assume that $a_{3,1} = 0$ or $a_{2,3} = 0$, co-dimension 2 bifurcation has been occurred and the higher order terms need to be investigated. In this section, we will analyse the following two cases:

- $\Gamma = 0, a_{3,1} = 0, a_{2,3} \neq 0, a_{4,1} \neq 0,$
- $\Gamma = 0, a_{2,3} = 0, a_{3,1} \neq 0, a_{2,4} \neq 0.$

4.4.3.1 Case 1

Applying the first assumptions into the stream function (4.209) which is extended up to the sixth-order terms, we have

$$\psi = a_{4,1}s^4z + a_{2,3}s^2z^3. \quad (4.220)$$

This can be written as

$$s^2 z (\sigma z^2 + s^2), \tag{4.221}$$

when we scale the stream function by dividing $a_{4,1}$ and scaling the coordinate system. In here, $\sigma = \frac{a_{2,3}}{a_{4,1}} \left| \frac{a_{4,1}}{a_{2,3}} \right| = \pm 1$. Depending on the sign of σ , the dividing streamline is figured in Fig. 4.52.

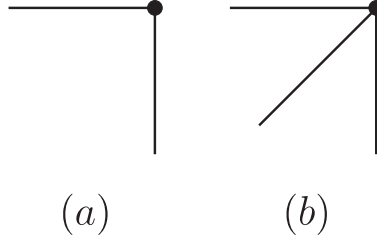


Figure 4.52: The dividing streamlines for the degenerate case (4.221) with (a) $\sigma = 1$, (b) $\sigma = -1$.

Simplified unfolding of the degenerate normal form is in the form

$$\psi = 4 a_{4,1} \epsilon_1 \xi^3 \eta^2 + a_{4,1} \xi^4 \eta + a_{2,3} \xi^2 \eta^3 + 3 \epsilon_2 \epsilon_1 \xi^2 \eta^2 + \epsilon_2 \xi^3 \eta, \tag{4.222}$$

where $\epsilon_2 = a_{3,1}$ and $\epsilon_1 = \Gamma$ by using the near identity transformation (6.44), see details in Maple worksheet [38]. To make more simplification, we scale $\eta \rightarrow B\eta$ by choosing $B = \left| \frac{a_{4,1}}{a_{2,3}} \right|^{\frac{1}{2}}$, and scaling the stream function by dividing by $Ba_{4,1}$, the following theorem arises:

THEOREM 4.13 *Let $a_{3,1}$ and k_1 be small parameters. Assuming the non-degeneracy conditions $a_{4,1} \neq 0$ and $a_{2,3} \neq 0$, the normal form is in the form*

$$\psi = x^2 y (\sigma y^2 + 4 c_{0,2} x y + 3 c_{0,1} c_{0,2} y + x^2 + c_{0,1} x) \tag{4.223}$$

where

$$\sigma = \begin{cases} +1 & \text{for } a_{4,1}/a_{2,3} > 0 \\ -1 & \text{for } a_{4,1}/a_{2,3} < 0 \end{cases},$$

$c_{0,1}$ and $c_{0,2}$ are small parameters.

The velocity field of (4.223) is

$$\begin{aligned} u &= x (3 \sigma y^2 + 8 x y c_{0,2} + 6 y c_{0,1} c_{0,2} + x^2 + x c_{0,1}), \\ w &= -y (2 \sigma y^2 + 12 x y c_{0,2} + 6 y c_{0,1} c_{0,2} + 4 x^2 + 3 x c_{0,1}). \end{aligned} \tag{4.224}$$

The critical points on the wall can be found by substituting $x = 0$ into the velocity field

$$u = 0, \quad w = -2y^2(\sigma y + c_{0,1}c_{0,2}). \quad (4.225)$$

The solutions of velocity w give us the critical points which are $(0, 0)$ and $(0, -\frac{c_{0,1}c_{0,2}}{\sigma})$. $c_{0,1} = 0$ and $c_{0,2} = 0$ are bifurcation points for the on-wall critical points.

On-interface critical points can be obtained by substituting $y = 0$ into the velocity field,

$$u = x^2(x + c_{0,1}), \quad w = 0. \quad (4.226)$$

Hence the critical points on the interface are $(0, 0)$ and $(-c_{0,1}, 0)$. $c_{0,1} = 0$ is the bifurcation point for the critical points on interface. $c_{0,1} = 0$ and $c_{0,2} = 0$ are also bifurcation points for the critical points away from boundaries. The streamline patterns and bifurcation diagrams can be figured as in Fig. 4.53.

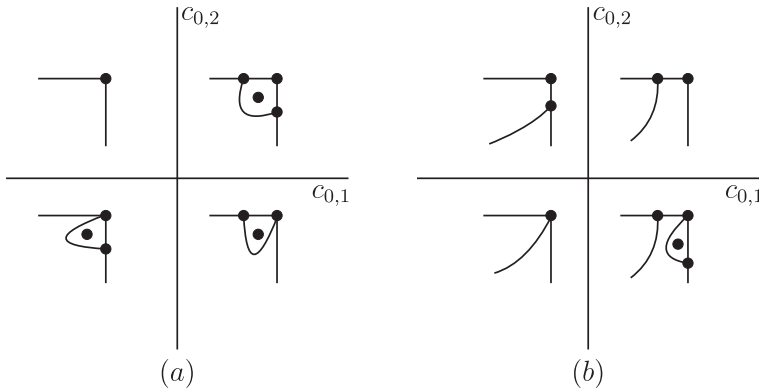


Figure 4.53: The streamline patterns for the normal form (4.223) (a) $\sigma = 1$ and (b) $\sigma = -1$.

4.4.3.2 Case 2

Applying the second assumptions into the stream function (4.209) which is extended up to the seventh-order terms, we have

$$\begin{aligned} \psi = & a_{3,1}s^3z + 5k_2a_{3,1}z^2s^3 + a_{4,1}s^4z + a_{3,3}s^3z^3 + a_{2,4}s^2z^4 + a_{5,1}s^5z \\ & + \frac{(6r_0^2a_{3,1}k_3 + 7r_0^2a_{4,1}k_2 - r_0k_2a_{3,1})z^2s^4}{r_0^2}. \end{aligned} \quad (4.227)$$

Using the near identity transformation (6.44), one can simplify the stream function as (details in [38])

$$\psi = \xi^2 \eta (a_{2,4} \eta^3 + a_{3,1} \xi). \quad (4.228)$$

Scaling the stream function by dividing $a_{2,4}$, and $\xi \rightarrow \frac{a_{2,4}}{a_{3,1}} \xi$ the simplified stream function is written as

$$\psi = \xi^2 \eta (\eta^3 + \xi). \quad (4.229)$$

The dividing streamlines of the critical point occurs when $\psi = 0$, or

$$\xi = 0, \quad \eta = 0, \quad \xi = -\eta^3. \quad (4.230)$$

There exist no dividing streamline for this case. The degenerate case for this non-simple critical point can be figured as Fig. 4.52 (a).

The unfolding of this degenerate case and its simplification process can be found in [38]. The following theorem arises in the end of this process:

THEOREM 4.14 *Let $a_{2,3}$ and Γ be small parameters. Assuming the non-degeneracy conditions $a_{3,1} \neq 0$ and $a_{2,4} \neq 0$, the normal form is in the form*

$$\psi = x^2 y (c_{0,1} y + x + c_{0,2} y^2 + y^3) \quad (4.231)$$

where $c_{0,1}$ and $c_{0,2}$ are sufficiently small parameters.

The velocity field of (4.231) is

$$\begin{aligned} u &= x (2 c_{0,1} y + x + 3 c_{0,2} y^2 + 4 y^3), \\ w &= -y (2 c_{0,1} y + 3 x + 2 c_{0,2} y^2 + 2 y^3). \end{aligned} \quad (4.232)$$

The critical points on the wall can be found by substituting $x = 0$ into the velocity field, which is

$$u = 0, \quad w = -2 y^2 (c_{0,1} + c_{0,2} y + y^2). \quad (4.233)$$

The solutions of $w = 0$ are the critical points. Therefore its discriminant is a local bifurcation curve for the critical points on the wall.

The critical point on the interface can be obtained by substituting $y = 0$ into velocity field, yields

$$u = x^2, \quad w = 0, \quad (4.234)$$

means the critical point is only 'origin'.

The local bifurcation curve for the critical points away from boundaries can be obtained by eliminating x and y from velocity field and the determinant of Jacobian, which is

$$-49c_{0,2}^2 + 160c_{0,1} = 0. \quad (4.235)$$

This curve, however, is just changing the critical points right-hand side of wall. Hence it has no importance.

The bifurcation diagram for the normal form (4.231) is figured in Fig. 4.54.

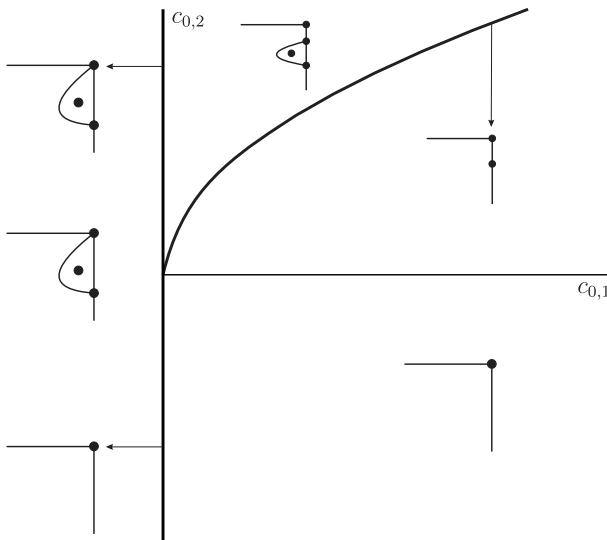


Figure 4.54: The streamline patterns and bifurcation diagram for the normal form (4.231).

4.4.4 Co-dimension 3

In this section, we extend the degenerate conditions as the following three cases which will be analysed:

- $\Gamma = 0, a_{3,1} = 0, a_{2,3} = 0, a_{2,4} \neq 0, a_{3,3} \neq 0, a_{4,1} \neq 0,$
- $\Gamma = 0, a_{2,3} = 0, a_{2,4} = 0, a_{3,1} \neq 0, a_{2,5} \neq 0,$
- $\Gamma = 0, a_{3,1} = 0, a_{4,1} = 0, a_{2,3} \neq 0, a_{5,1} \neq 0.$

From now on, we will just write the simplified degenerate cases and the normal form of their unfolding directly due to avoiding writing long-terms equations. Whole process can be found in the Maple worksheet [38].

4.4.4.1 Case 1

Under the given assumption, we use a series of transformation into the stream function (4.209) which is extended up to the seventh-order terms. We obtain the degenerate case as

$$\psi = x^2 y (xy^2 + y^3 + x^2). \quad (4.236)$$

The dividing streamline is figured in Fig. 4.55.

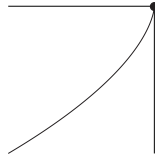


Figure 4.55: The dividing streamlines for (4.236).

The unfolding for the degenerate case (4.236) is simplified by applying series of transformation. After all, the following theorem arises:

THEOREM 4.15 *Let $a_{2,3}$, $a_{3,1}$ and Γ be small parameters. Assuming the non-degeneracy conditions $a_{3,3} \neq 0$, $a_{4,1} \neq 0$ and $a_{2,4} \neq 0$, the normal form is in the form*

$$\psi = x^2 y (3c_{0,1}c_{1,1}y + c_{1,1}x + c_{0,2}y^2 + 4c_{0,1}xy + x^2 + y^3 + xy^2) \quad (4.237)$$

where $c_{0,1}$, $c_{1,1}$ and $c_{0,2}$ are sufficiently small parameters.

The velocity field of (4.237) is

$$\begin{aligned} u &= x (6c_{0,1}c_{1,1}y + c_{1,1}x + 3c_{0,2}y^2 + 8c_{0,1}xy + x^2 + 4y^3 + 3xy^2), \\ w &= -y (6c_{0,1}c_{1,1}y + 3c_{1,1}x + 2c_{0,2}y^2 + 12c_{0,1}xy + 4x^2 + 2y^3 + 3xy^2). \end{aligned} \quad (4.238)$$

The critical points on the wall can be found by solving

$$w(0, y) = -2y^2(y^2 + yc_{0,2} + 3c_{0,1}c_{1,1}) = 0. \quad (4.239)$$

The solutions of this equation may vary depending on the sign of its discriminant which is $-12 c_{0,1}c_{1,1} + c_{0,2}^2$.

The critical points on the interface are the solutions of

$$u(x, 0) = x^2(x + c_{1,1}) = 0. \tag{4.240}$$

And the critical points away from boundaries can be obtained by taking the resultant of the velocities u and w , with respect to x , and again taking the resultant of the previous equation and its derivative with respect to y . The equation includes too many terms, hence we do not write this bifurcation curve in here, please see it in [33].

The dimension of parameter space is three. However we can reduce the dimension two due to the all local bifurcation curve just depend on the sign of $c_{1,1}$. Therefore considering the sign of $c_{1,1}$, we briefly sketch the bifurcation diagrams in Fig. 4.56, 4.57 and 4.58.

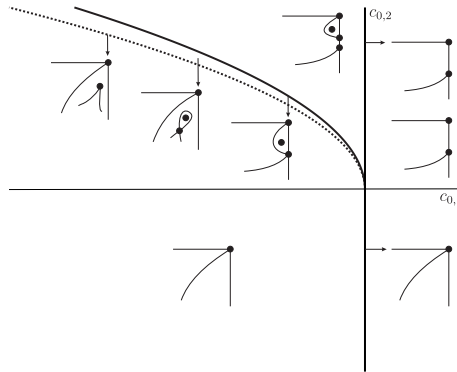


Figure 4.56: Bifurcation diagram for $c_{1,1} < 0$. The dashed curve is the local bifurcation curve away from the boundaries.

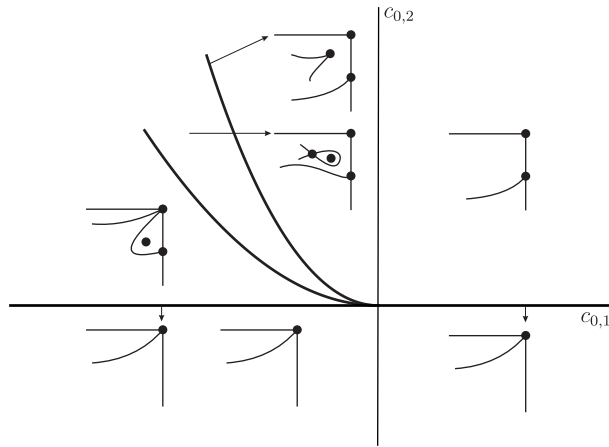


Figure 4.57: Bifurcation diagram for $c_{1,1} = 0$.

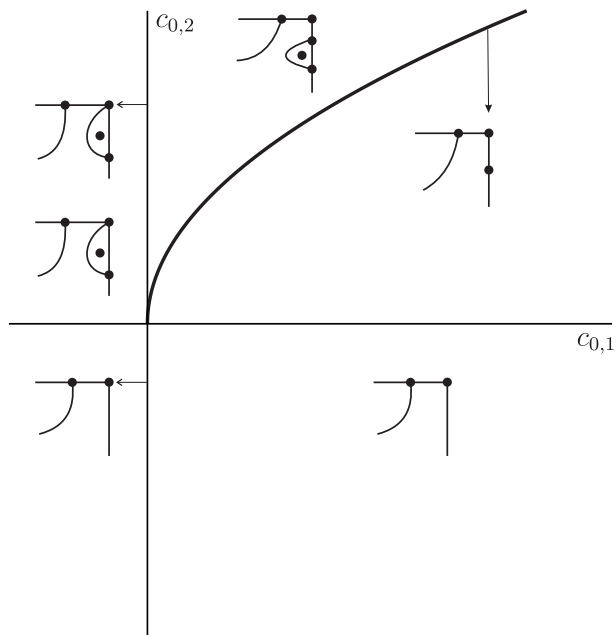


Figure 4.58: Bifurcation diagram for $c_{1,1} > 0$.

4.4.4.2 Case 2

Using the assumptions for this case, we use a series of transformation into the stream function (4.209) which is extended up to the eight-order terms. The degenerate case is obtained as

$$\psi = x^2 y (y^4 + x). \quad (4.241)$$

The dividing streamline is figured in Fig. 4.59.

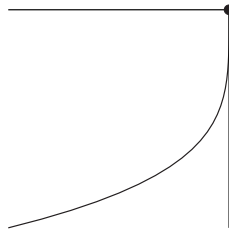


Figure 4.59: The dividing streamlines for the degenerate case (4.241).

The unfolding for the degenerate case (4.241) is simplified by applying series of transformation. In conclusion, the following theorem arise:

THEOREM 4.16 *Let $a_{2,3}$, $a_{2,4}$ and k_1 be small parameters. Assuming the non-degeneracy conditions $a_{3,1} \neq 0$ and $a_{2,5} \neq 0$, the normal form is in the form*

$$\psi = x^2 y (c_{0,1} y + x + c_{0,2} y^2 + c_{0,3} y^3 + y^4) \quad (4.242)$$

where $c_{0,1}$, $c_{0,2}$ and $c_{0,3}$ are sufficiently small parameters.

The velocity field of (4.242) is

$$\begin{aligned} u &= x (2 c_{0,1} y + x + 3 c_{0,2} y^2 + 4 c_{0,3} y^3 + 5 y^4), \\ w &= -y (2 c_{0,1} y + 3 x + 2 c_{0,2} y^2 + 2 c_{0,3} y^3 + 2 y^4). \end{aligned} \quad (4.243)$$

The critical points on the wall can be obtained by substituting $x = 0$ into the velocity field

$$u = 0, \quad w = -2y^2 (c_{0,1} + c_{0,2} y + c_{0,3} y^2 + y^3). \quad (4.244)$$

The solutions of $w = 0$ are the critical points on the wall. The local bifurcation curve for these critical points is obtained by taking the resultant of w and J with respect to y when $x = 0$, which is given

$$LC : 4 c_{0,1} c_{0,3}^3 - c_{0,2}^2 c_{0,3}^2 - 18 c_{0,1} c_{0,2} c_{0,3} + 4 c_{0,2}^3 + 27 c_{0,1}^2 = 0. \quad (4.245)$$

This curve is a quadratic for $c_{0,1}$ can solvable. The discriminant of it with respect to $c_{0,1}$ is

$$\Delta = c_{0,3}^2 - 3c_{0,2}. \tag{4.246}$$

Instead of $c_{0,2}$, we can use Δ as a parameter due to the fact that the significance of Δ is higher than $c_{0,2}$.

The critical points on the interface is just $(0, 0)$. For the critical points away from the boundaries, the local bifurcation curve is obtained by eliminating x from the velocities u and w ,

$$39y^2 + 20yc_{0,3} + 7c_{0,2} = 0, \tag{4.247}$$

next, eliminating y from (4.247) and its derivative

$$\begin{aligned} LCAW : -75920 c_{0,1}c_{0,3}^3 + \frac{40768 c_{0,3}^6}{27} - \frac{104468 c_{0,3}^4 \Delta}{9} + \frac{56056 c_{0,3}^2 \Delta^2}{3} \\ + 283920 c_{0,1}c_{0,3} \Delta - \frac{231868 \Delta^3}{27} + 949104 c_{0,1}^2 = 0. \end{aligned} \tag{4.248}$$

No global bifurcation has been seen in this case.

Depending on the sign of Δ , we sketched the bifurcation diagram as in Fig. 4.60 and 4.61.

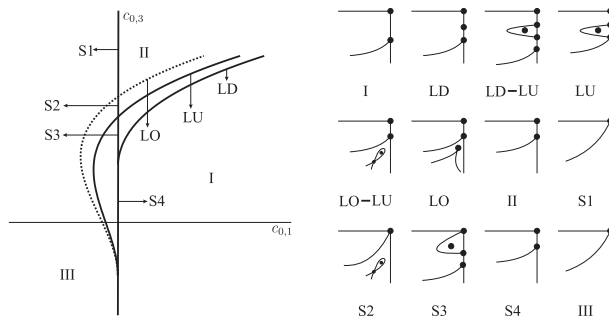


Figure 4.60: Bifurcation diagram for $\Delta > 0$. The dashed curve denoted the local bifurcation curve for the critical points away from boundaries.

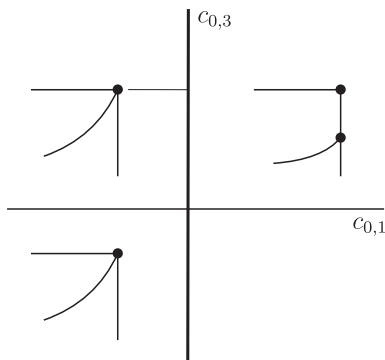


Figure 4.61: Bifurcation diagram for $\Delta \leq 0$.

4.4.4.3 Case 3

Applying the given assumptions in the final case and again using a series of transformation, the stream function (4.209) which is extended up to the seventh-order terms is simplified as

$$\psi = x^2 y (y^2 + x^3). \tag{4.249}$$

The dividing streamline is figured in Fig. 4.62.

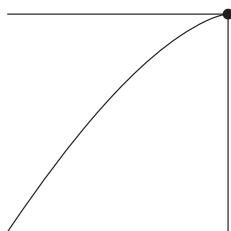


Figure 4.62: The dividing streamlines for the degenerate case (4.249).

The unfolding for the degenerate case (4.249) is simplified by applying series of transformation. In the end, the following theorem arises:

THEOREM 4.17 *Let $a_{3,1}$, $a_{4,1}$ and Γ be small parameters. Assuming the non-degeneracy conditions $a_{5,1} \neq 0$ and $a_{2,3} \neq 0$, the normal form is in the form*

$$\begin{aligned} \psi = x^2 y (3 c_{1,0} c_{2,1} y + c_{1,0} x + y^2 + 4 c_{2,0} c_{2,1} x y \\ + c_{2,0} x^2 + 5 c_{2,1} x^2 y + x^3) \end{aligned} \tag{4.250}$$

where $c_{1,0}$, $c_{2,1}$ and $c_{2,0}$ are sufficiently small parameters.

The velocity field of (4.250) is

$$\begin{aligned} u &= x(6c_{1,0}c_{2,1}y + c_{1,0}x + 3y^2 + 8c_{2,0}c_{2,1}xy \\ &\quad + c_{2,0}x^2 + 10c_{2,1}x^2y + x^3), \\ w &= -y(6c_{1,0}c_{2,1}y + 3c_{1,0}x + 2y^2 + 12c_{2,0}c_{2,1}xy \\ &\quad + 4c_{2,0}x^2 + 20c_{2,1}x^2y + 5x^3). \end{aligned} \quad (4.251)$$

The critical points on the wall can be obtained by substituting $x = 0$ into the velocity field

$$u = 0, \quad w = -2y^2(3c_{1,0}c_{2,1} + y). \quad (4.252)$$

The critical points are $(0, 0)$ and $(0, -3c_{1,0}c_{2,1})$. Since the physical plane is in the below of the interface, we are looking for the negative solutions for y and x . Therefore the solution of $w = 0$ exists when $c_{1,0}c_{2,1} \geq 0$.

On the interface, the critical points are the solutions of

$$u = x^2(x^2 + c_{2,0}x + c_{1,0}) = 0, \quad (4.253)$$

which vary according as the sign of its discriminant $\Delta = c_{2,0}^2 - 4c_{1,0}$.

About the finding the critical points away from the boundaries, we use "resultant" command to eliminate firstly "x" from the velocities u and w , secondly y from the equation obtained from first resultant and its derivative. It includes too much terms hence we do not need to emphasize it here, please see details in [36]. In the figure, the dashed curve denotes the local bifurcation curve for the critical points away from the boundaries.

It is worth pointing out that there is no global bifurcation for this case.

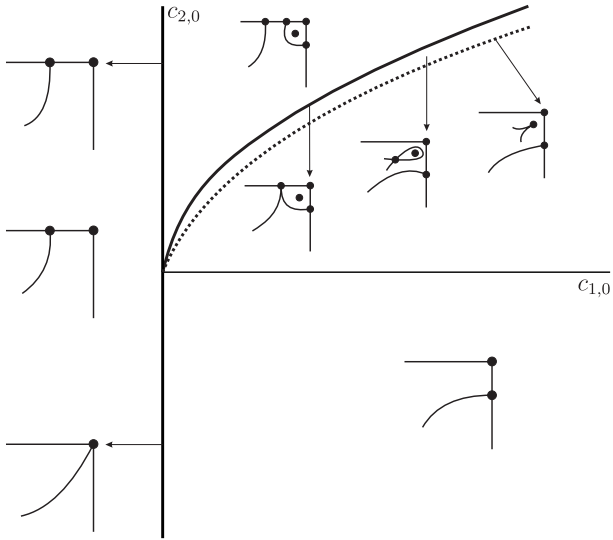


Figure 4.63: Bifurcation diagram for $c_{2,1} > 0$.

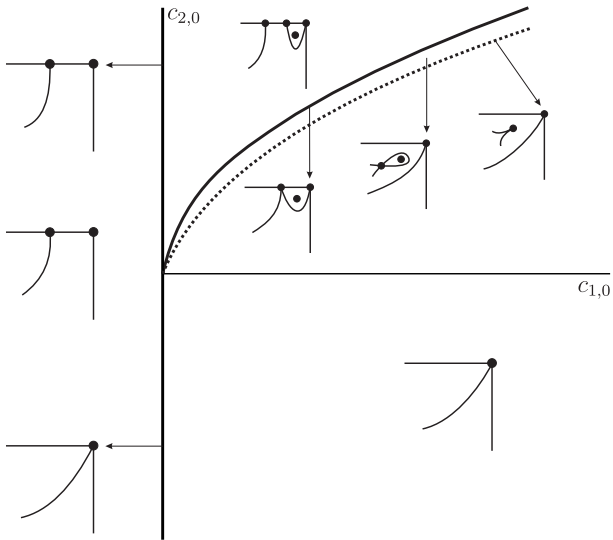


Figure 4.64: Bifurcation diagram for $c_{2,1} = 0$.

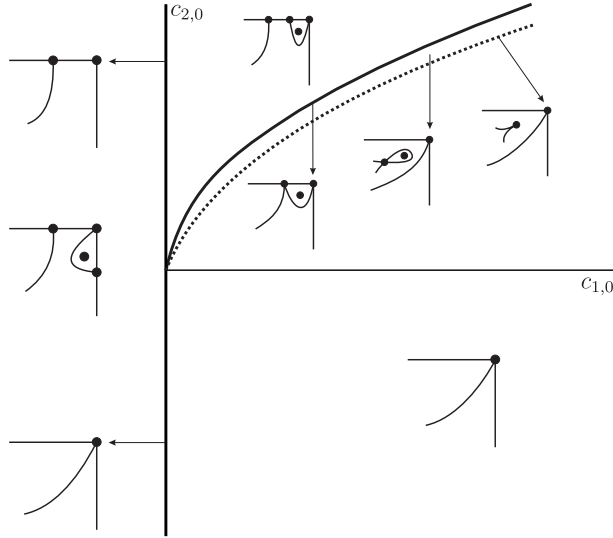


Figure 4.65: Bifurcation diagram for $c_{2,1} < 0$.

Until now, we consider the interface not flat, hence the coefficients of its expansion is considered as a bifurcation parameter. From now on, we will make an analysis for a flat interface, or creeping flow.

4.5 Flow Topology Close to a Stationary Wall with a Flat Interface

Assuming the interface is flat, that means all $k_i = 0$, we firstly follow the same process in the section 4.3 which is called as "Flow topology away from the axis". Next, we apply the stationary wall (4.208) conditions which are $u = w = 0$ and simplify the stream function. The lowest ordered term is

$$\psi = a_{2,1}s^2z + \mathcal{O}(|s, z|^4), \tag{4.254}$$

and the velocity field for the stream function (4.254) is (multiplied by $(s + r_0)$ and scaled time by dividing s)

$$u = a_{2,1}s, \quad w = -2a_{2,1}z. \tag{4.255}$$

4.5.1 Regular Case

The linearised system matrix of (4.254) is (by scaling time by dividing s)

$$\begin{pmatrix} u \\ w \end{pmatrix} = \begin{pmatrix} a_{2,1} & 0 \\ 0 & -2a_{2,1} \end{pmatrix} \begin{pmatrix} s \\ z \end{pmatrix}. \quad (4.256)$$

The eigenvalues for this matrix are $-a_{2,1}$ and $3a_{2,1}$. Firstly, we assume that $a_{2,1} < 0$, the origin is a saddle with the stable direction on the interface, which is the eigenvector $(1, 0)$ and unstable direction on the wall, which is the other eigenvector $(0, 1)$. For $a_{2,1} > 0$, only the stable and unstable direction reversed. (see Fig. 4.3)

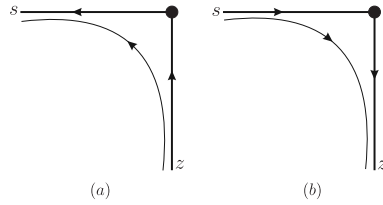


Figure 4.66: Streamlines in the vicinity of origin for the non-degenerate critical point with $a_{2,1} \neq 0$ (a) $a_{2,1} > 0$ (b) $a_{2,1} < 0$.

4.5.2 Co-dimension 1 bifurcation

If $a_{2,1} = 0$, higher order terms must be investigated in order to determine the flow topology. With this assumption, the extended stream function becomes (truncated after the fourth ordered terms)

$$\psi = a_{3,1}s^2z + a_{4,1}s^3z + (-6a_{4,1}d_1^2 + 3a_{3,1}d_2 + a_{2,3})z^3s, \quad (4.257)$$

where d_i is the coefficients of the expansion of wall (4.208). Note that the stream function scaled by dividing s . This stream function can be simplified by applying the non-linear transformation (which preserves the boundary conditions)

$$s = \xi + m_{2,0}\xi^2 + m_{1,1}\xi\eta, \quad z = \eta + l_{0,2}\eta^2 + l_{1,1}\xi\eta. \quad (4.258)$$

into the given stream function. Choosing

$$m_{2,0} = l_{0,2} = m_{1,1} = 0, \quad l_{1,1} = -\frac{a_{4,1}}{a_{3,1}}, \quad (4.259)$$

the stream function becomes

$$\psi = a_{3,1}\xi^2\eta + \tilde{a}_{2,3}\xi\eta^3, \tag{4.260}$$

where $\tilde{a}_{2,3} = -6a_{4,1}d_1^2 + 3a_{3,1}d_2 + a_{2,3}$. Further simplification is possible by scaling the stream function by dividing $a_{3,1}$ and scaling the coordinate system (ξ, η) as $\xi \rightarrow A\xi$ and $\eta \rightarrow B\eta$ (where $A, B > 0$ to make the transformation into given region), we have

$$\psi = A^2B\xi^2\eta + AB^3\frac{\tilde{a}_{2,3}}{a_{3,1}}\xi\eta^3. \tag{4.261}$$

Choosing $B = \frac{1}{A^2}$ and $A = \left(\frac{\tilde{a}_{2,3}}{a_{3,1}}\right)^{1/5}$, the stream function becomes

$$\psi = \xi\eta(\sigma\eta^2 + \xi). \tag{4.262}$$

where $a_{3,1} \neq 0$ and $\tilde{a}_{2,3} \neq 0$ are the new non-degeneracy conditions and

$$\sigma = \frac{\tilde{a}_{2,3}}{a_{3,1}} \left| \frac{a_{3,1}}{\tilde{a}_{2,3}} \right| = \pm 1. \tag{4.263}$$

Since $A > 0$, σ depends on the sign of $\frac{\tilde{a}_{2,3}}{a_{3,1}}$. The dividing streamline can be found by solving $\psi = 0$, which are in the direction $\xi = -\sigma\eta^2$, $\xi = 0$ and $\eta = 0$ figured as Fig. 4.67.

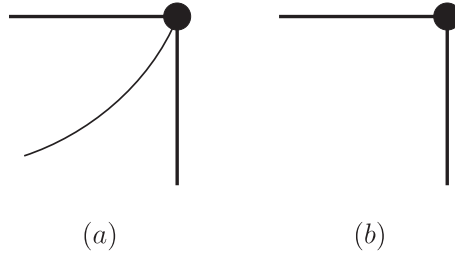


Figure 4.67: The dividing streamline for the degenerate case (4.262) with the non-degenerate conditions $a_{3,1} \neq 0$ and $\tilde{a}_{2,3} \neq 0$ (a) $\sigma = 1$ and (b) $\sigma = -1$.

Introducing the small parameter $a_{2,1} = \epsilon_1$, the unfolding of the degenerate case (4.262) is given by

$$\psi = \epsilon_1sz + a_{3,1}s^2z + a_{4,1}s^3z + (-6a_{4,1}d_1^2 + 3a_{3,1}d_2 + a_{2,3})z^3s. \tag{4.264}$$

By using the same transformation and scales in the degenerate case, the next theorem arises:

THEOREM 4.18 *Let $a_{2,1}$ be a small parameter. Assuming the non-degeneracy conditions $a_{3,1} \neq 0$ and $\tilde{a}_{2,3} \neq 0$, the normal form is written as*

$$\psi = xy(c_{0,0} + x + \sigma y^2), \quad (4.265)$$

where

$$\sigma = \begin{cases} +1 & \text{for } \tilde{a}_{2,3}/a_{3,1} > 0 \\ -1 & \text{for } \tilde{a}_{2,3}/a_{3,1} < 0 \end{cases},$$

and $c_{0,0}$ is sufficiently small parameter.

The velocity field of (4.265) is

$$\begin{aligned} u &= x(3\sigma y^2 + x + c_{0,0}), \\ w &= -y(\sigma y^2 + 2x + c_{0,0}). \end{aligned} \quad (4.266)$$

The critical points on the wall can be obtained by substituting $x = 0$ into the velocity field

$$u = 0, \quad w = -y(c_{0,0} + \sigma y^2). \quad (4.267)$$

The critical points are $y_{1,2} = \pm\sqrt{-\sigma c_{0,0}}$. Considering the physical plane, below interface, the critical point exist when $\sigma c_{0,0} < 0$ which is $(0, -\sqrt{-\sigma c_{0,0}})$.

On the interface, the critical points are the solutions of

$$u = x(x + c_{0,0}) = 0, \quad (4.268)$$

which vary depending on the sign of $c_{0,0}$. Hence, $c_{0,0} = 0$ is a bifurcation point for the critical points on the interface and wall.

Away from the boundaries, the critical points can be found by eliminating x from the velocity field

$$5\sigma y^2 + c_{0,0} = 0, \quad (4.269)$$

which has the same bifurcation point $c_{0,0} = 0$. The bifurcation diagram is seen in Fig. 4.68.

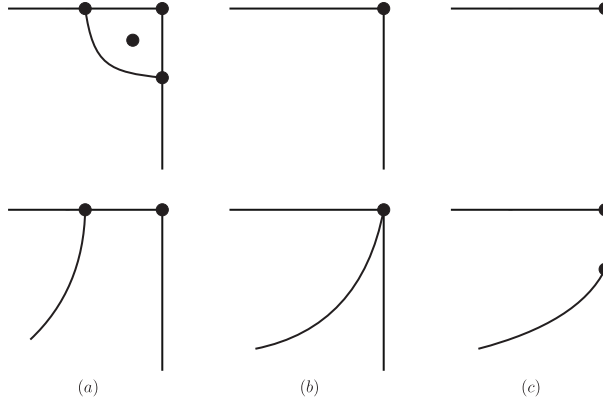


Figure 4.68: The streamline patterns for the normal form (4.265) with (a) $c_{0,0} > 0$ (b) $c_{0,0} = 0$ (c) $c_{0,0} < 0$.

If we break the one of the non-degeneracy conditions $a_{3,1} \neq 0$ and $\tilde{a}_{2,3} \neq 0$, we need to examine the higher order terms to determine the flow topology. These cases will be analysed in the following section.

4.5.3 Co-dimension 2 bifurcations

In this section, we break the non-degeneracy conditions $a_{3,1} \neq 0$ and $\tilde{a}_{2,3} \neq 0$ and create the new one as,

- (a) $a_{2,1} = 0, a_{3,1} = 0, \tilde{a}_{2,3} \neq 0$ and $a_{4,1} \neq 0$,
- (b) $a_{2,1} = 0, \tilde{a}_{2,3} = 0, a_{3,1} \neq 0$ and $\tilde{a}_{2,4} \neq 0$ where $\tilde{a}_{2,4} = -20 a_{5,1} d_1^3 + 3 a_{3,1} d_3 + 3 a_{3,3} d_1 + a_{2,4}$.

4.5.3.1 Case (a)

Applying the given assumptions and extended the stream function up to the fifth ordered term, the stream function is written as

$$\psi = a_{4,1} s^3 z + \tilde{a}_{2,3} z^3 s. \tag{4.270}$$

Scaling the stream function by dividing $a_{4,1}$ and the coordinates $s \rightarrow \left(\frac{\tilde{a}_{2,3}}{a_{4,1}}\right)^{1/2} s$, we simplify the stream function as

$$\psi = sz(s^2 + \sigma z^2), \tag{4.271}$$

where $\sigma = \frac{a_{4,1}}{\tilde{a}_{2,3}} \left| \frac{\tilde{a}_{2,3}}{a_{4,1}} \right| = \pm 1$. Depending on the sign of σ , the dividing streamline is figured in Fig. 4.69.

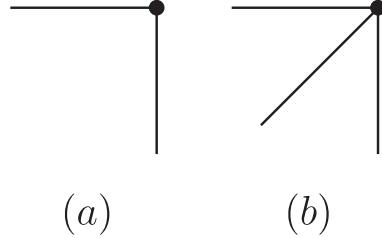


Figure 4.69: The dividing streamlines for the degenerate case (4.271) with (a) $\sigma = 1$, (b) $\sigma = -1$.

A small perturbation by considering $a_{2,1} = \epsilon_1$ and $a_{3,1} = \epsilon_2$ can effect the structure. Unfolding the degenerate case and using the same scaling as the degenerate case, the following theorem arises:

THEOREM 4.19 *Let $a_{2,1}$ and $a_{3,1}$ be small parameters. Assuming the non-degeneracy conditions $a_{4,1} \neq 0$ and $\tilde{a}_{2,3} \neq 0$, the normal form is in the form*

$$\psi = xy(c_{0,0} + c_{1,0}x + x^2 + \sigma y^2), \quad (4.272)$$

where

$$\sigma = \begin{cases} +1 & \text{for } a_{4,1}/\tilde{a}_{2,3} > 0 \\ -1 & \text{for } a_{4,1}/\tilde{a}_{2,3} < 0 \end{cases},$$

$c_{0,0}$ and $c_{1,0}$ are small parameters.

The velocity field of (4.272) is

$$\begin{aligned} u &= x(3\sigma y^2 + x^2 + c_{1,0}x + c_{0,0}), \\ w &= -y(\sigma y^2 + 3x^2 + 2c_{1,0}x + c_{0,0}). \end{aligned} \quad (4.273)$$

The critical points on the wall can be obtained by substituting $x = 0$ into the velocity field

$$u = 0, \quad w = -y(c_{0,0} + \sigma y^2). \quad (4.274)$$

The critical points are $y_{1,2} = \pm\sqrt{-c_{0,0}\sigma}$.

On the interface, the critical points are the solutions of

$$u = x(x^2 + c_{1,0}x + c_{0,0}) = 0, \quad (4.275)$$

which vary depending on to the determinant of given equation, which is $c_{1,0}^2 - 4c_{0,0}$. This discriminant is local bifurcation curve for the critical points on the interface.

Away from the boundaries, the local bifurcation curve for the critical points can be found by eliminating y from the velocity field

$$8x^2 + 5c_{1,0}x + 2c_{0,0} = 0, \tag{4.276}$$

and obtaining the discriminant of the previous equation, which is $25c_{1,0}^2 - 64c_{0,0} = 0$. The bifurcation diagram is figured in Fig. 4.70 and 4.71.

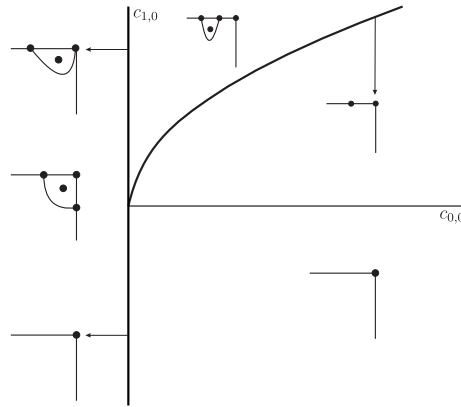


Figure 4.70: Bifurcation diagram and streamline patterns for the normal form (4.272) with $\sigma = 1$.

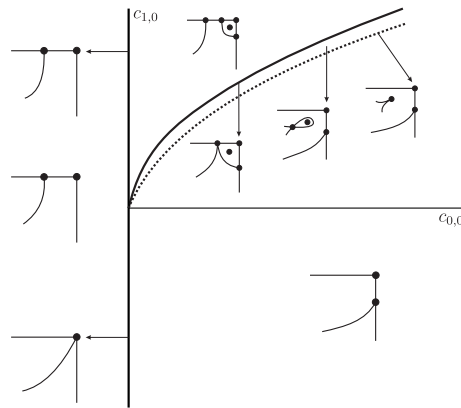


Figure 4.71: Bifurcation diagram and streamline patterns for the normal form (4.272) with $\sigma = -1$.

4.5.3.2 Case (b)

Applying the given assumptions and extended the stream function up to the fifth ordered term, the stream function is written as

$$\psi = a_{3,1}s^2z + a_{4,1}s^3z + a_{5,1}s^4z + \tilde{a}_{3,3}z^3s^2 + \tilde{a}_{2,4}z^4s, \quad (4.277)$$

where $\tilde{a}_{3,3} = -10a_{5,1}d_1^2 + 4a_{4,1}d_2 + a_{3,3}$ and $\tilde{a}_{2,4} = -20a_{5,1}d_1^3 + 3a_{3,1}d_3 + 3a_{3,3}d_1 + a_{2,4}$. Using the non-linear transformation (4.258) including third order terms, one can simplify the stream function as

$$\psi = a_{3,1}\xi^2\eta + \tilde{a}_{2,4}\xi\eta^4, \quad (4.278)$$

by choosing

$$m_{2,0} = l_{0,2} = m_{1,1} = m_{3,0} = m_{2,1} = m_{1,2} = l_{1,2} = 0, \quad l_{1,1} = -\frac{a_{4,1}}{a_{3,1}}, \quad (4.279)$$

$$l_{2,1} = \frac{-a_{3,1}a_{5,1} + a_{4,1}^2}{a_{3,1}^2}, \quad l_{0,3} = \frac{10a_{5,1}d_1^2 - 4a_{4,1}d_2 - a_{3,3}}{a_{3,1}}.$$

Scaling the stream function by dividing $a_{3,1}$ and the coordinates $\xi \rightarrow A\xi$ and $\eta \rightarrow B\eta$ (where $A, B > 0$), the stream function is written

$$\psi = AB\xi\eta(A\xi + B^3\frac{\tilde{a}_{2,4}}{a_{3,1}}\eta^3). \quad (4.280)$$

Choosing $B = \frac{1}{A^2}$ and $A = \left(\frac{\tilde{a}_{2,4}}{a_{3,1}}\right)^{1/7}$, the stream function becomes

$$\psi = \xi\eta(\sigma\eta^3 + \xi). \quad (4.281)$$

where $a_{3,1} \neq 0$ and $\tilde{a}_{2,4} \neq 0$ are the new non-degeneracy conditions and

$$\sigma = \frac{\tilde{a}_{2,4}}{a_{3,1}} \left| \frac{a_{3,1}}{\tilde{a}_{2,4}} \right| = \pm 1. \quad (4.282)$$

Since $A > 0$, σ depends on the sign of $\frac{\tilde{a}_{2,4}}{a_{3,1}}$. The dividing streamlines of the critical point occurs when $\psi = 0$, or

$$\xi = 0, \quad \eta = 0, \quad \xi = -\sigma\eta^3. \quad (4.283)$$

The degenerate case for this non-simple critical point is seen in Fig. 4.52.

A small perturbation by considering $a_{2,1} = \epsilon_1$ and $\tilde{a}_{2,3} = \epsilon_2$ can effect the structure. Unfolding the degenerate case, applying the same non-linear transformation with IFT, and using the same scaling as the degenerate case, the following theorem arises:

THEOREM 4.20 *Let $a_{2,1}$ and $\tilde{a}_{2,3}$ be small parameters. Assuming the non-degeneracy conditions $a_{3,1} \neq 0$ and $\tilde{a}_{2,4} \neq 0$, the normal form is in the form*

$$\psi = xy(c_{0,0} + c_{0,2}y^2 + x + y^3), \quad (4.284)$$

where

$$\sigma = \begin{cases} +1 & \text{for } \tilde{a}_{2,4}/a_{3,1} > 0 \\ -1 & \text{for } \tilde{a}_{2,4}/a_{3,1} < 0 \end{cases},$$

$c_{0,0}$ and $c_{0,2}$ are small parameters.

The velocity field of (4.284) is

$$\begin{aligned} u &= x(4\sigma y^3 + 3y^2c_{0,2} + x + c_{0,0}), \\ w &= -y(\sigma y^3 + y^2c_{0,2} + 2x + c_{0,0}). \end{aligned} \quad (4.285)$$

The critical points on the wall can be obtained by substituting $x = 0$ into the velocity field

$$u = 0, \quad w = -y(c_{0,0} + c_{0,2}y^2 + \sigma y^3). \quad (4.286)$$

The local bifurcation curve can be obtained by eliminating y from w and its derivative with respect to y , which is

$$-c_{0,0}(-4c_{0,2}^3 - 27c_{0,0}) = 0. \quad (4.287)$$

On the interface, the critical points are the solutions of

$$u = x(x + c_{0,0}) = 0, \quad (4.288)$$

which is $x = -c_{0,0}$, hence $c_{0,0} = 0$ is a bifurcation point on the interface.

Away from the boundaries, the local bifurcation curve for the critical points can be found by eliminating x from the velocity field

$$7\sigma y^3 + 5y^2c_{0,2} + c_{0,0} = 0, \quad (4.289)$$

and eliminating y from this equation and its derivative with respect to y , which gives

$$7c_{0,0}(500c_{0,2}^3 + 1323c_{0,0}) = 0. \quad (4.290)$$

The bifurcation diagram is figured in Fig. 4.72 and 4.73.

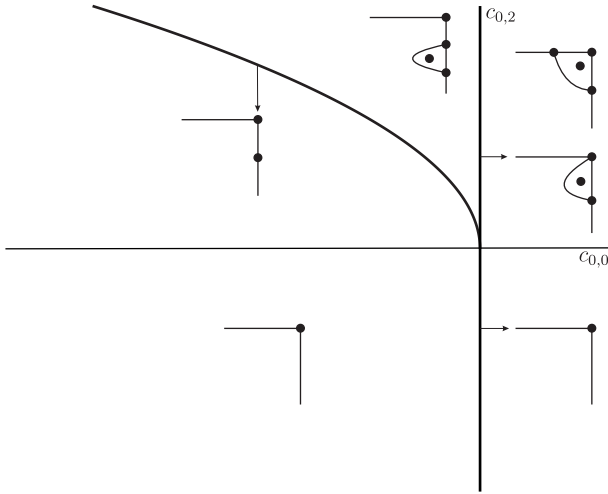


Figure 4.72: Bifurcation diagram and streamline patterns for the normal form (4.284) with $\sigma = 1$.

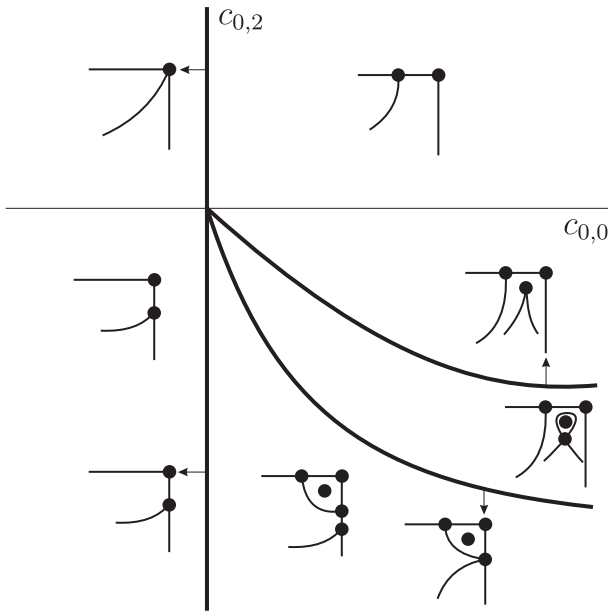


Figure 4.73: Bifurcation diagram and streamline patterns for the normal form (4.284) with $\sigma = -1$.

4.6 Conclusion

The axisymmetric steady flow is analysed on the interface using the cylindrical coordinate (r, θ, z) by considering the existence of azimuthal velocity. Firstly, in the vicinity of the intersection of interface and center axis, then away from the axis, and finally close to a stationary wall, we expand the stream function in a Taylor series. The normal form theory is used to simplify the given stream function and the unfolding theory is used to create a small bifurcation points. Up to the co-dimension three, we observed the bifurcation diagrams and the streamline patterns.

In the analysis, we see that the tangential stress condition makes some differences while obtaining the normal form of the stream function. Especially, in the bifurcation analysis close to center axis, even though the normal form which is obtained by Brøns [30] is different from our normal form, the streamline patterns and the bifurcation diagrams give us the same results. That makes us to ask the tangential stress boundary condition is important or not. However, in the following process we see that its effect can be visible somehow, in co-dimension three cases.

The existence of azimuthal velocity seems not very useful to sketching meridional plane, however, elimination process of the radial and axial velocities' coefficients by using the Navier-Stokes equations is provoked due to its existence. For example, in [37] the coefficient $a_{0,4}$ is eliminated by using vorticity transport equation. However, in our cases it is impossible to eliminate the coefficients, because it depends on the coefficients of azimuthal velocity.

This study can be helpful to see all possible streamline patterns if one have the same flow properties. In a different shape, that can be cylindrical container see in Fig. 4.74, conical container or spherical container, if there are a rotation and a free surface with the kinematic, tangential and normal stress boundary conditions, this study will give a brief bifurcation process depending on the parameter.

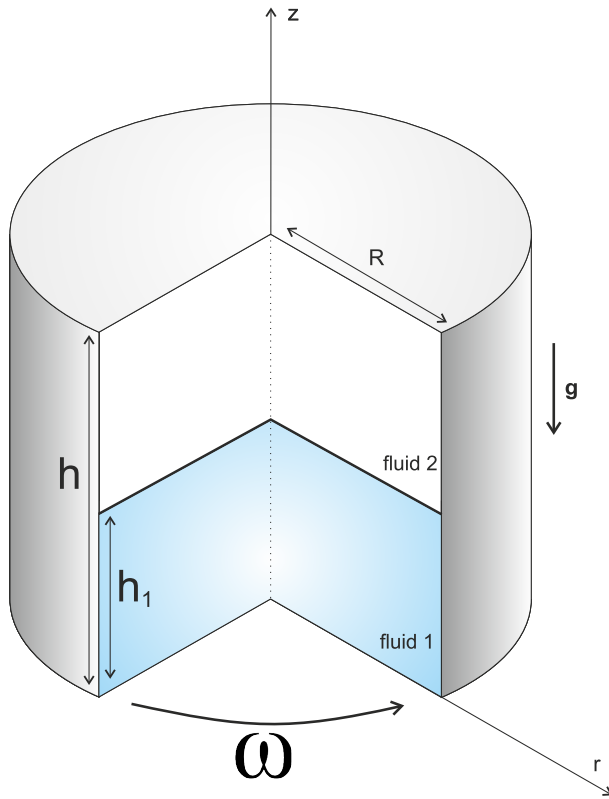


Figure 4.74: Two immiscible fluids in a lid-driven cylinder.

CHAPTER 5

Topology of axisymmetric flow near a viscous surface

In Chapter 4, we considered an axisymmetric flow close to a free surface, by neglecting the stresses of upper fluid $z > F(r)$. In this chapter, we consider the axisymmetric flow of two immiscible fluids, by revisiting [17], where a similar situation in $2D$ flow is studied.

Using the tangential stress (2.55) and normal stress (2.57) boundary conditions, the flow field can be patched together across the interface. To make easier to read, let us introduce again the dynamic boundary conditions in here for axisymmetric flow in cylindrical coordinate (r, θ, z) with corresponding velocity field (u, v, w)

$$\mathbf{t}_1 \cdot (u_1, w_1) = \mathbf{t}_1 \cdot (u_2, w_2), \quad (5.1)$$

$$\mathbf{t}_2 \cdot v_1 = \mathbf{t}_2 \cdot v_2, \quad (5.2)$$

$$\mathbf{n}\Upsilon_1\mathbf{t}_1 = \mathbf{n}\Upsilon_2\mathbf{t}_1, \quad (5.3)$$

$$\mathbf{n}\Upsilon_1\mathbf{t}_2 = \mathbf{n}\Upsilon_2\mathbf{t}_2, \quad (5.4)$$

$$\mathbf{n}\Upsilon_1\mathbf{n} + \sigma \left(\frac{1}{R_1} + \frac{1}{R_2} \right) = \mathbf{n}\Upsilon_2\mathbf{n}, \quad (5.5)$$

where \mathbf{t}_1 is tangential vector (4.6b), \mathbf{t}_2 is tangential vector (4.6c), \mathbf{n} is normal vector (4.6a), Υ_i is the stress tensor (4.8) and the radii of curvature is eq. (4.7).

Note that the notation i ($i = 1, 2$) means fluid 1 and fluid 2. For example, u_1 is the radial velocity in fluid 1.

The continuity and *steady* Navier-Stokes equations is in the form for axisymmetric flow

$$\frac{1}{r} \frac{\partial(ru_i)}{\partial r} + \frac{\partial w_i}{\partial z} = 0, \quad (5.6a)$$

$$\rho_m \left(u_i \frac{\partial u_i}{\partial r} + w_i \frac{\partial u_i}{\partial z} - \frac{v_i^2}{r} \right) = \mu_i \left(\nabla^2 u_i - \frac{u_i}{r^2} \right) - \frac{\partial p_i}{\partial r}, \quad (5.6b)$$

$$\rho_m \left(u_i \frac{\partial v_i}{\partial r} + w_i \frac{\partial v_i}{\partial z} + \frac{u_i v_i}{r} \right) = \mu_i \left(\nabla^2 v_i - \frac{v_i}{r^2} \right), \quad (5.6c)$$

$$\rho_m \left(u_i \frac{\partial w_i}{\partial r} + w_i \frac{\partial w_i}{\partial z} \right) = \mu_i \nabla^2 w_i - \frac{\partial p_i}{\partial z}, \quad (5.6d)$$

where $\nabla^2 = \frac{1}{r} \frac{\partial}{\partial r} \left(r \frac{\partial}{\partial r} \right) + \frac{\partial^2}{\partial z^2}$.

As a first step, we expand the stream function (4.2), pressure (4.4) and azimuthal velocity (4.5) in each fluid as

$$\psi_i = \sum_{m+n=0}^{\infty} a_{m,n}^{(i)} (r - r_{00})^m (z - z_{00})^n, \quad (5.7)$$

$$p_i = \sum_{m+n=0}^{\infty} p_{m,n}^{(i)} (r - r_{00})^m (z - z_{00})^n, \quad (5.8)$$

$$v_i = \sum_{m+n=0}^{\infty} b_{m,n}^{(i)} (r - r_{00})^m (z - z_{00})^n. \quad (5.9)$$

As the previous chapter, we divide this chapter into three parts:

- (a) close to the center axis,
- (b) away from the center axis, and
- (c) close to a stationary wall.

The process for obtaining the stream function and bifurcation diagrams are similar as in the previous chapter. For example, let us consider case (a). For this case, after applying the boundary conditions we obtain the stream function for the physical region $z < F(r)$. One can also observe the same stream function for the physical region $z > F(r)$. The difference between them is just the

coefficients. For instance, for physical region $z < F(r)$, we will say $a_{m,n}^{(1)}$ instead of $a_{m,n}$ and for physical region $z > F(r)$, $a_{m,n}^{(2)}$.

In the following section, we will give the relations among the coefficients of the stream function by applying boundary conditions (5.1)-(5.4). The following process can be summarize by giving an example:

- 1 For free surface, the stress of fluid in region $z > F(r)$ is neglected. Therefore the tangential stress (5.3) for case (a) yields (4.19),

$$a_{2,2} - 2k_2 a_{2,1} = 0. \quad (5.10)$$

- 2 If the stress of fluid in region $z > F(r)$ exists, we can write the tangential stress (5.3) for case (a) as

$$\mu_1(a_{2,2}^{(1)} - 2k_2 a_{2,1}^{(1)}) = \mu_2(a_{2,2}^{(2)} - 2k_2 a_{2,1}^{(2)}). \quad (5.11)$$

5.1 Flow topology of The Viscous Surface Close To Axis

The dynamic boundary conditions (5.1)-(5.5) yield the following relations between two immiscible fluids

$$a_{2,1}^{(2)} = a_{2,1}^{(1)}, \quad (5.12)$$

$$a_{2,2}^{(2)} = \frac{\mu_1}{\mu_2} a_{2,2}^{(1)} + \mu_R a_{2,1}^{(1)}, \quad (5.13)$$

$$a_{4,1}^{(2)} = a_{4,1}^{(1)} + 2k_2 \mu_R a_{2,2}^{(1)} + 4\mu_R k_2^2 a_{2,1}^{(1)}, \quad (5.14)$$

$$\begin{aligned} a_{2,3}^{(2)} = & \frac{\mu_1}{\mu_2} a_{2,3}^{(1)} - \frac{64a_{2,1}^{(1)} k_2^2 \mu_R}{3} + \left(\frac{\rho_1 - \rho_2}{\mu_2} \right) \left(\frac{b_{1,0}^{(1)2} - a_{2,1}^{(1)2}}{6} \right) \\ & - 2k_2 \mu_R a_{2,2}^{(1)} - 8\mu_R a_{4,1}^{(1)} - 4\mu_R a_{2,1}^{(1)} k_2^2 - 16\sigma k_4, \end{aligned} \quad (5.15)$$

where

$$\mu_R = 1 - \frac{\mu_1}{\mu_2}, \quad (5.16)$$

and σ is the surface tension. Remember that origin is a regular point for the free surface flow (fluid 1) close to axis when $a_{2,1} \neq 0$, called "regular case". Eq. (5.12) yields that the same holds in fluid 2. Hence the streamlines in the vicinity of origin for the non-degenerate critical point are figured as in Fig. 5.1. We kindly refer to [31] to see the tangential stress and normal stress boundary conditions.

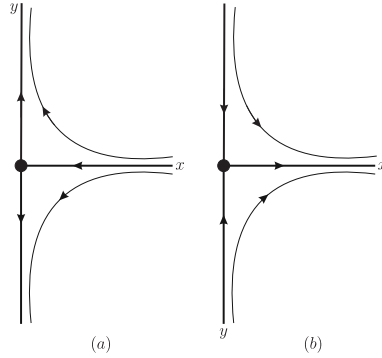


Figure 5.1: Streamlines in the vicinity of origin for the non-degenerate critical point with $a_{2,1} \neq 0$ in both fluids (a) $a_{2,1} < 0$ (b) $a_{2,1} > 0$.

5.1.1 Co-dimension 1 bifurcation on viscous surface

When $a_{2,1} = 0$, we said that co-dimension 1 bifurcation occurs, see section 4.2.2. For fluid 1 (in chapter 4 co-dimension 1 case), we observe two kinds of degenerate streamline patterns depending on σ (not surface tension, just parameter and it will be used as a parameter from now on, unless explicitly stated) which is

$$\sigma = \frac{a_{4,1}}{a_{2,3}} \left| \frac{a_{2,3}}{a_{4,1}} \right| = \begin{cases} +1 & \text{for } a_{2,3}/a_{4,1} > 0 \\ -1 & \text{for } a_{2,3}/a_{4,1} < 0 \end{cases} ,$$

In here, let us define it as σ_1 for fluid 1 and σ_2 for fluid 2. Using the phase portraits of Fig. 4.4, we can patch the flows across the interface as in fig. 5.2. When $\sigma_1 = -1$ and $\sigma_2 = -1$ fig. 5.2(a), when $\sigma_1 = 1$ and $\sigma_2 = -1$ fig. 5.2(b), when $\sigma_1 = -1$ and $\sigma_2 = 1$ fig. 5.2(c) and when $\sigma_1 = 1$ and $\sigma_2 = 1$ fig. 5.2(d) are seen.

As one see from eq. (5.14), $a_{4,1}$ for both fluids have the same sign when $a_{2,2}^{(1)} = 0$, and from eq. (5.15) the sign of $a_{2,3}$ for both fluids may vary depending on

$$\gamma = \left(\frac{\rho_1 - \rho_2}{\mu_2} \right) \left(\frac{b_{1,0}^{(1)2}}{6} \right) - 4a_{4,1}^{(1)} \frac{\mu_R}{k_2} - 16\sigma k_4. \quad (5.17)$$

If γ is "zero" or sufficiently small, the sign of $a_{2,3}$ for both fluids are same, and different when γ is larger. In conclusion, these results yield that σ_1 and σ_2 can have the same or different signs. This gives to us different streamline topologies as shown in Fig. 5.2.

The unfolding of the degenerate case is analysed by assuming $a_{2,1} = \epsilon$. From

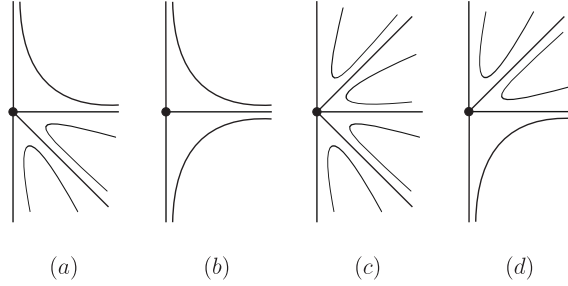


Figure 5.2: Degenerate streamline patterns near the viscous interface with $a_{2,1} = 0$. (a) $\sigma_1 = -1$ and $\sigma_2 = -1$, (b) $\sigma_1 = 1$ and $\sigma_2 = -1$, (c) $\sigma_1 = -1$ and $\sigma_2 = 1$ and (d) $\sigma_1 = 1$ and $\sigma_2 = 1$.

eq. (5.12), we can say that ϵ in fluid 1 is equal to ϵ in fluid 2. As a conclusion of this, we can sketch the co-dimension 1 bifurcation diagram as in fig. 5.5. For a free surface, one can see the streamlines in fig. 4.5.

5.1.2 Co-dimension 2 bifurcation on viscous surface

Following the same idea as in the previous section, we can break the non-degeneracy conditions which are $a_{4,1} \neq 0$ and $a_{2,3} \neq 0$, one by one. Like the case for free surface, we can divide this case into two sub-cases as in 4.2.3;

- (a) $a_{2,1} = 0$, $a_{2,3} = 0$, $a_{4,1} \neq 0$ and $a_{2,5} \neq 0$,
- (b) $a_{2,1} = 0$, $a_{2,3} \neq 0$, $a_{4,1} = 0$ and $-3a_{2,3}k_2^2 + a_{6,1} \neq 0$.

5.1.2.1 Case (a)

In fact, there is no big difference on the process obtaining the degenerate streamline patterns and unfolding for this case. From 4.2.3.1, one can see that the sign of σ determines the flow topology, which is

$$\sigma = \frac{a_{2,5}}{a_{4,1}} \left| \frac{a_{4,1}}{a_{2,5}} \right| = \begin{cases} +1 & \text{for } a_{2,5}/a_{4,1} > 0 \\ -1 & \text{for } a_{2,5}/a_{4,1} < 0 \end{cases} ,$$

This again yields the possibility of four kind of dividing streamline patterns as the co-dimension 1 case. If the sign of σ for two fluids are same, there is a

symmetric vision of the streamline patterns as in Fig. 5.2 (b) and (c), and in Fig. 5.5 (a) and (b). Therefore, we will just consider which streamlines can be seen when $\sigma_1 = -1$ and $\sigma_2 = 1$. The degenerate streamline pattern for this choices can be sketched by considering 4.6 as in Fig. 5.3. And from fig. 4.8 and 4.9, one can obtain the bifurcation diagram 5.4.

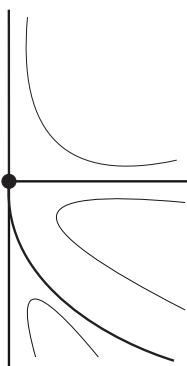


Figure 5.3: Degenerate streamline patterns for viscous surface with $\sigma_1 = -1$ and $\sigma_2 = 1$ for case (a).

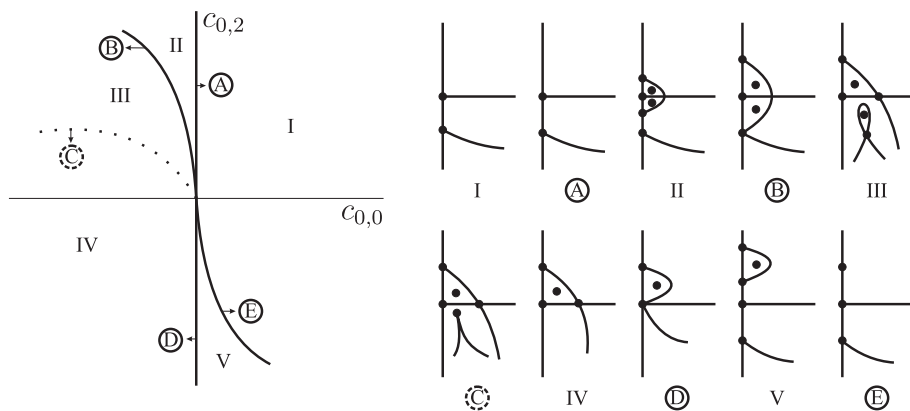


Figure 5.4: Bifurcation diagram for case (a) with $\sigma_1 = -1$ and $\sigma_2 = 1$.

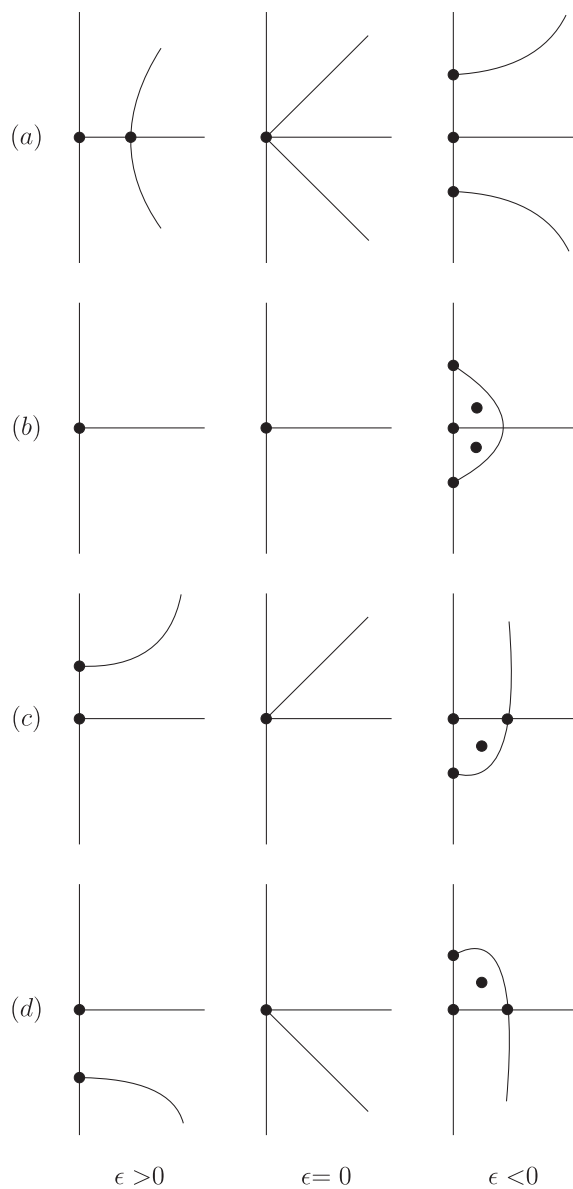


Figure 5.5: Bifurcation diagrams for the normal form (4.45) for viscous surface. (a) $\sigma_1 = -1$ and $\sigma_2 = -1$, (b) $\sigma_1 = 1$ and $\sigma_2 = 1$, (c) $\sigma_1 = 1$ and $\sigma_2 = -1$, (d) $\sigma_1 = -1$ and $\sigma_2 = 1$.

5.1.2.2 Case (b)

From 4.2.3.2, one can see that the sign of σ determines the flow topology again.

$$\sigma = \frac{a_{2,3}}{\tilde{a}_{6,1}} \left| \frac{\tilde{a}_{6,1}}{a_{2,3}} \right| = \begin{cases} +1 & \text{for } \tilde{a}_{6,1}/a_{2,3} > 0 \\ -1 & \text{for } \tilde{a}_{6,1}/a_{2,3} < 0 \end{cases} ,$$

One can observe four kinds of degenerate streamline patterns and bifurcation diagrams depending on the sign of σ . Again, we will just show the degenerate streamline patterns and bifurcation diagrams for $\sigma_1 = -1$ and $\sigma_2 = 1$. The combination of fig. 4.10 (a) and fig. 4.10 (b) creates the degenerate streamline for viscous surface as in fig. 5.6. And the combination of fig. 4.11 and fig. 4.12 creates the bifurcation diagram for viscous surface as in fig. 5.7

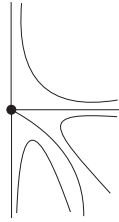


Figure 5.6: Degenerate streamline patterns for viscous surface with $\sigma_1 = -1$ and $\sigma_2 = 1$ for case (b).

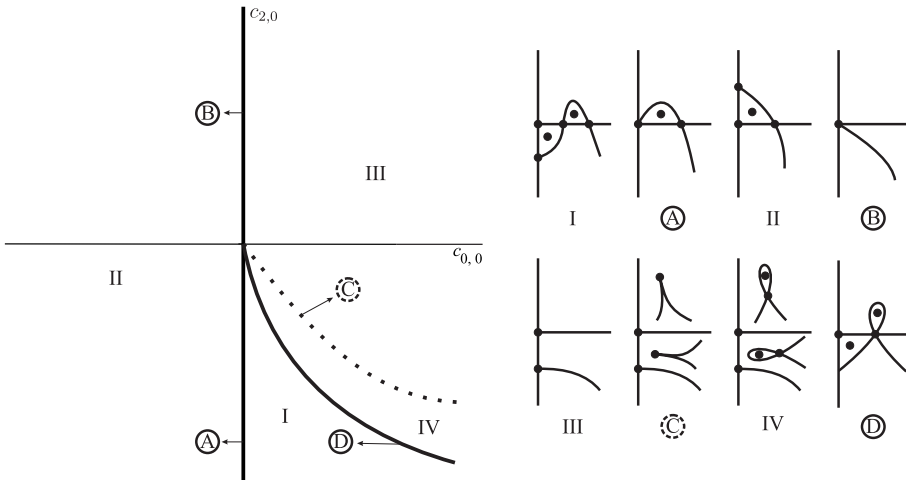


Figure 5.7: Bifurcation diagram for case (b) with $\sigma_1 = -1$ and $\sigma_2 = 1$.

5.2 Flow topology of The Viscous Surface Away From Axis

The dynamic boundary conditions (5.1)-(5.4) yield the following relations between two immiscible fluids (see for one fluid in [35])

$$a_{0,1}^{(2)} = a_{0,1}^{(1)}, \quad (5.18)$$

$$a_{1,1}^{(2)} = a_{1,1}^{(1)}, \quad (5.19)$$

$$a_{2,1}^{(2)} = a_{2,1}^{(1)}, \quad (5.20)$$

$$a_{0,2}^{(2)} = \frac{\mu_1}{\mu_2} a_{0,2}^{(1)} \quad (5.21)$$

$$+ \mu_R((k_1^2 - 1)2r_0 a_{0,1}^{(1)} k_2 + (k_1^2 + 1)(2r_0 a_{1,1}^{(1)} k_1 - a_{0,1} k_1)), \quad (5.22)$$

$$a_{0,3}^{(2)} = \frac{\mu_1}{\mu_2} a_{0,3}^{(1)} \quad (5.23)$$

$$+ h(a_{0,2}^{(1)}, a_{2,1}^{(1)}, a_{1,2}^{(1)}, b_{0,0}^{(1)}, r_0, k_1, k_2, k_3, \sigma, \rho_1, \rho_2), \quad (5.24)$$

where

$$\mu_R = 1 - \frac{\mu_1}{\mu_2}, \quad (5.25)$$

and σ is the surface tension. Remember that origin is a regular point for the free surface flow (fluid 1) away from the axis when $a_{1,1} \neq 0$. Eq. (5.19) yields that the same holds in fluid 2. The regular cases and the bifurcation diagrams are similar as in paper Brøns [17]. Therefore, there is no need to analyse this section. The difference is that the regular point for this section is $a_{1,1} \neq 0$, and in his study $a_{1,0} \neq 0$. Even though the calculations are different, one can consider section 4.3 to see the similarities.

5.3 Flow topology of The Viscous Surface Close To Wall

In chapter 4, we obtain all possible streamline patterns on a free surface for the flow close to a stationary wall. Introducing $\Gamma = \frac{k_1}{k_1^2 + 1}$ which is slope of the interface, we analyse the flow topologies in two ways; the interface is flat $\Gamma = 0$ and not flat $\Gamma \neq 0$.

Firstly, we assume the interface is not flat. We see that the effect of the slope of interface in a topological way. We analyse how a small perturbation on the slope create a difference on the streamline patterns. Secondly, assuming the

interface is completely flat the flow is analysed on the free surface and obtained the bifurcation diagrams. In here, we will just consider a flat interface, because the idea is completely same.

The dynamic boundary conditions (5.1)-(5.4) yield the following relations between two immiscible fluids

$$a_{2,1}^{(2)} = a_{2,1}^{(1)}, \quad (5.26)$$

$$a_{3,1}^{(2)} = a_{3,1}^{(1)}, \quad (5.27)$$

$$a_{4,1}^{(2)} = a_{4,1}^{(1)}, \quad (5.28)$$

$$a_{2,2}^{(2)} = \frac{\mu_1}{\mu_2} a_{2,2}^{(1)}, \quad (5.29)$$

$$a_{2,3}^{(2)} = \frac{\mu_1}{\mu_2} a_{2,3}^{(1)} + h(a_{2,1}^{(1)}, a_{3,1}^{(1)}, a_{4,1}^{(1)}). \quad (5.30)$$

Remember that origin is a regular point for the free surface flow (fluid 1) away from the axis when $a_{2,1} \neq 0$ in section 4.5. Eq. (5.26) yields that the same holds in fluid 2. Hence the streamlines in the vicinity of origin for the non-degenerate critical point is seen in Fig. 5.8.

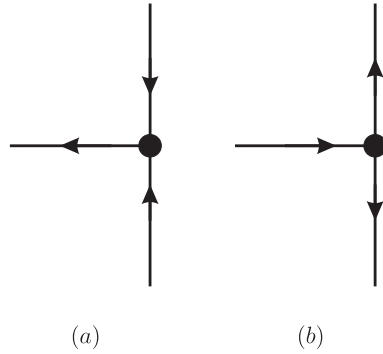


Figure 5.8: The dividing streamline patterns for the regular case with (a) $a_{2,1} > 0$ and (b) $a_{2,1} < 0$.

5.3.1 Co-dimension 1 bifurcation

When $a_{2,1} = 0$, co-dimension 1 bifurcation occurs. For fluid 1, we observe two kinds degenerate streamline patterns depending on σ which is

$$\sigma = \frac{a_{2,3}}{a_{3,1}} \left| \frac{a_{2,3}}{a_{3,1}} \right| = \begin{cases} +1 & \text{for } a_{2,3}/a_{3,1} > 0 \\ -1 & \text{for } a_{2,3}/a_{3,1} < 0 \end{cases},$$

Let us define σ as σ_1 for fluid 1 and σ_2 for fluid 2. Using the phase portraits of Fig. 4.67, we can patch the flows across the interface as in fig. 5.9. When $\sigma_1 = -1$ and $\sigma_2 = 1$ fig. 5.9(a), when $\sigma_1 = 1$ and $\sigma_2 = 1$ fig. 5.9(b), when $\sigma_1 = -1$ and $\sigma_2 = -1$ fig. 5.9(c) and when $\sigma_1 = 1$ and $\sigma_2 = -1$ fig. 5.9(d) are seen.

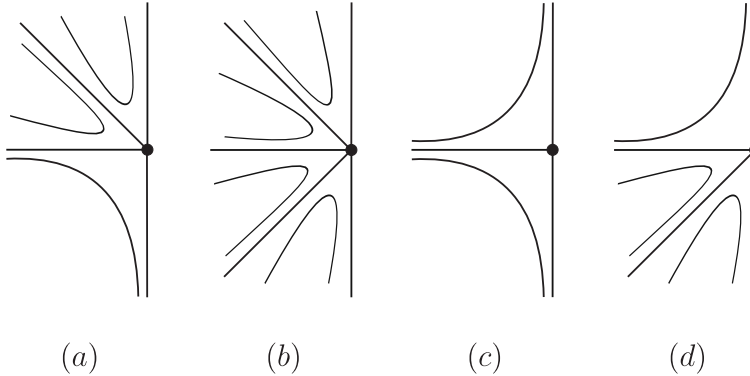


Figure 5.9: Degenerate streamline patterns near the viscous interface with $a_{2,1} = 0$.

The unfolding of the degenerate case, can be analysed by assuming $a_{2,1} = \epsilon$. From eq. (5.26), we can say that ϵ in fluid 1 is equal to ϵ in fluid 2. The bifurcation process and the possible streamline patterns are seen in Fig. 5.10.

5.3.2 Co-dimension 2 bifurcation

Following the same idea as in the previous section, we can break the non-degeneracy conditions which are $a_{3,1} \neq 0$ and $a_{2,3} \neq 0$, one by one. Like the case for free surface, we can divide this case into two sub-cases;

- (a) $a_{2,1} = 0$, $a_{2,3} \neq 0$ and $a_{3,1} = 0$,
- (b) $a_{2,1} = 0$, $a_{2,3} = 0$ and $a_{3,1} \neq 0$.

The degenerate streamline patterns for cases (a) and (b) are same as in fig. 5.9. It is possible to obtain four different bifurcation diagrams for both cases. Let us just unfold one degenerate case from the cases, which is (d) in fig. 5.9. The bifurcation diagram 5.11 for case (a) and 5.12 for case(b) are obtained as we did in section 5.1.2.

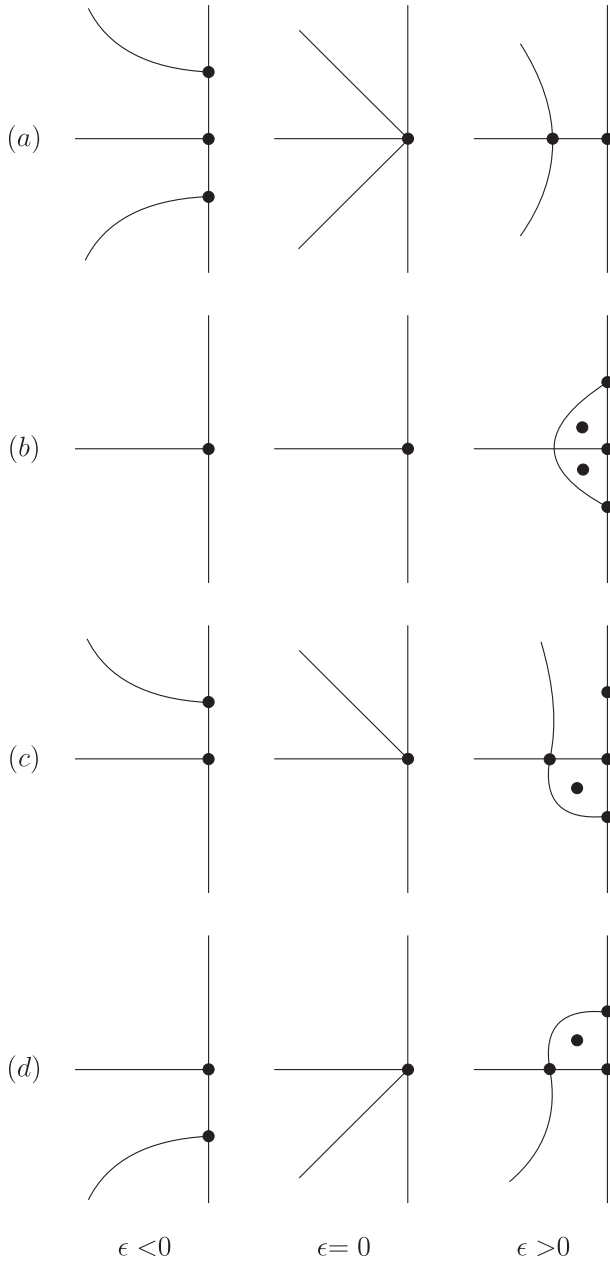


Figure 5.10: Bifurcation diagrams for the normal form blabalbal (a) $\sigma_1 = -1$ and $\sigma_2 = -1$, (b) $\sigma_1 = 1$ and $\sigma_2 = 1$, (c) $\sigma_1 = 1$ and $\sigma_2 = -1$, (d) $\sigma_1 = -1$ and $\sigma_2 = 1$.

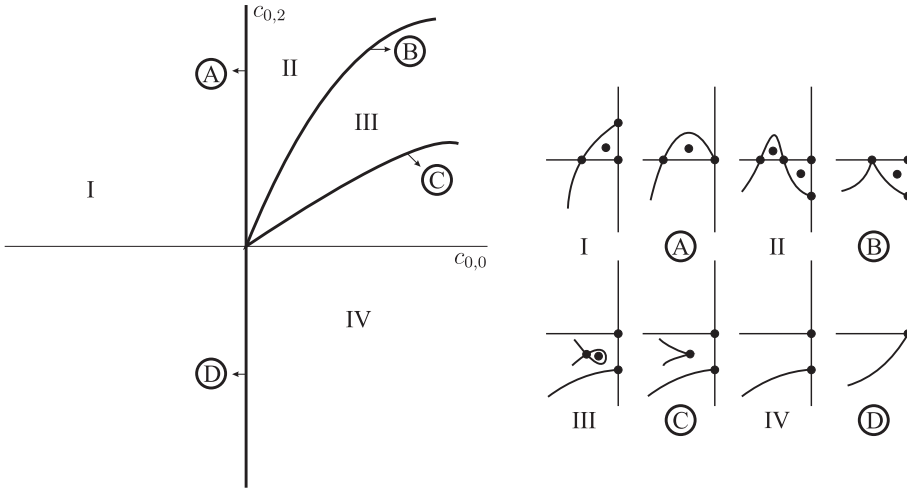


Figure 5.11: Bifurcation diagrams for case (a) by unfolding the degenerate streamline pattern in fig. 5.9 (d) for $\sigma_1 = 1$ and $\sigma_2 = -1$.

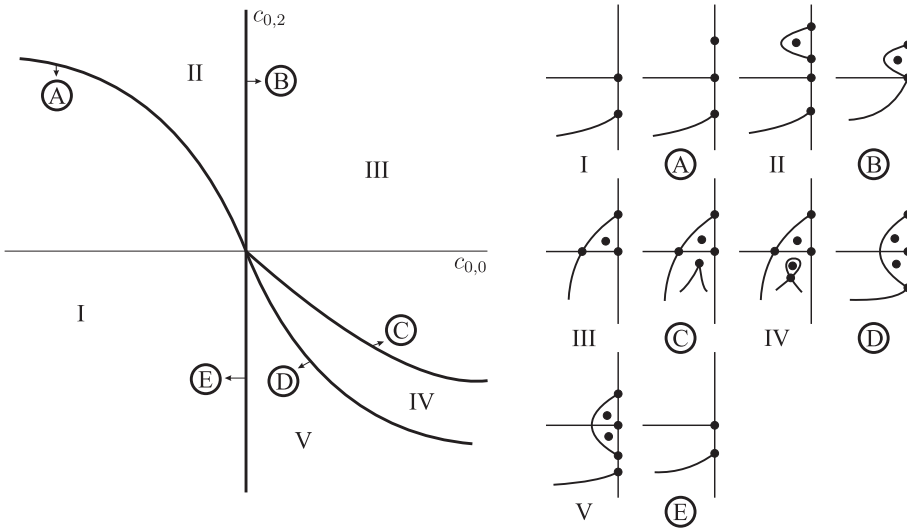


Figure 5.12: Bifurcation diagrams for case (b) by unfolding the degenerate streamline pattern in fig. 5.9 (d) for $\sigma_1 = 1$ and $\sigma_2 = -1$.

CHAPTER 6

Topology of 3D flow near a free surface

In Chapters 4 and 5, we consider the axisymmetric flow in the cylindrical coordinate to reduce dimension 3D to 2D. From now on, we will break the symmetry and considering the Cartesian coordinate system (x, y, z) , three dimensional viscous flow on the free surface is going to be analysed.

Obtaining the streamline patterns of three-dimensional flow is much more difficult than the two-dimensional one. Since the stream function does not exist for 3D flow, we consider the expansion of all velocities.

Three dimensional flow has been considered close to a fixed surfaces by many authors, see pioneering works Legendre [10], Delery [12]. Perry and Fairlie [14] revisited their works and using the theory of finite dimensional dynamical systems. In this study, they have considered in the vicinity of a no-slip wall and with a free-slip wall, the linear terms of the velocity field. Hartnack [39], using the normal form and unfolding theory, have investigated the three-dimensional flow in-flow and in the vicinity of a stationary wall. However, the vicinity of a free surface has not been considered yet.

In this study, we consider a free surface $z = f(x, y)$ in the Cartesian coordinate system (x, y, z) . In the vicinity of a point on this surface, we expand the velocity field and applying the boundary conditions we reduce the number of coefficients

as we did before. The idea is same as in the previous chapters. Using the near-identity transformation, we obtain the normal form first for the degenerate case and then unfolding of degenerate case. Using bifurcation theory, we finalize the analysis of 3D flow in the vicinity of a free surface.

Prior to starting analysis, we present some preliminaries.

6.1 Prerequisites

The general form of the Navier-Stokes Equations are given in (2.38) and the continuity equation (2.39) in the Cartesian coordinate system (x, y, z) . The interface is given by $z = f(x, y)$ with two immiscible fluids. Assuming that the coordinate system translated and rotated such that $f(0, 0) = f_x(0, 0) = f_y(0, 0) = 0$, we expand the surface in a Taylor series as

$$z = f(x, y) = s_{2,0}x^2 + s_{1,1}xy + s_{0,2}y^2 + \mathcal{O}(|x, y|^3). \quad (6.1)$$

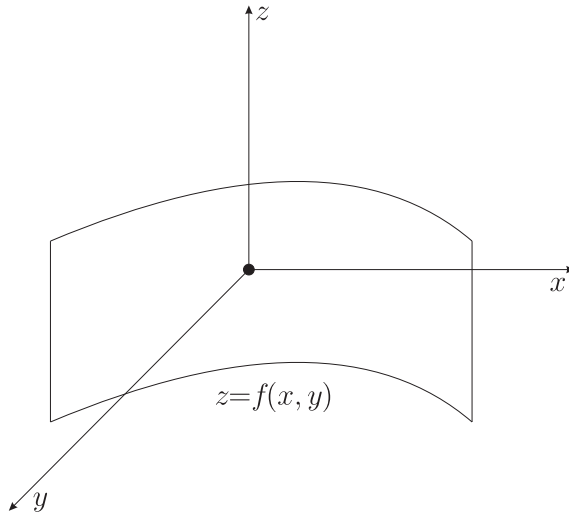


Figure 6.1: The surface is given by $z = f(x, y)$. In the following process, we will consider the fluid in $z > f(x, y)$ as a free surface.

The normal and tangential vectors on the free surface can be found in Chapter 2 as (2.43).

The kinematic (2.58), tangential stress (2.59) and normal stress (2.60) boundary conditions again can be found in Chapter 2 with the stress tensor (2.52) and the radii of curvature (2.47).

6.1.1 3D Flow Topology In One Fluid

To make a local analysis of the flow close to a free surface, we expand the fields as

$$\begin{aligned} u = \dot{x} &= \sum_{i+j+k=0}^{\infty} a_{i,j,k} x^i y^j z^k, & v = \dot{y} &= \sum_{i+j+k=0}^{\infty} b_{i,j,k} x^i y^j z^k, \\ w = \dot{z} &= \sum_{i+j+k=0}^{\infty} c_{i,j,k} x^i y^j z^k, & p &= \sum_{i+j+k=0}^{\infty} p_{i,j,k} x^i y^j z^k. \end{aligned} \quad (6.2)$$

The continuity equation (2.39),

$$\frac{\partial u}{\partial x} + \frac{\partial v}{\partial y} + \frac{\partial w}{\partial z} = 0, \quad (6.3)$$

gives us

$$c_{i,j,k} = -\frac{i+1}{k} a_{i+1,j,k-1} - \frac{j+1}{k} b_{i,j+1,k-1}, \quad k > 0. \quad (6.4)$$

From now on, we will apply the kinematic boundary condition (2.58) and tangential stress conditions (2.59) to the velocity field. Firstly, from the kinematic boundary condition (2.58)

$$\mathbf{n} \cdot \mathbf{V} = f_x u + f_y v - w = 0, \quad (6.5)$$

where $V = (u, v, w)$, we have

$$\begin{aligned} c_{1,0,0} = c_{0,1,0} &= 0, & c_{0,2,0} &= a_{0,1,0} s_{1,1} + a_{1,0,0} s_{0,2} + 3 b_{0,1,0} s_{0,2}, \\ c_{1,1,0} &= 2 a_{0,1,0} s_{2,0} + 2 a_{1,0,0} s_{1,1} + 2 b_{0,1,0} s_{1,1} + 2 b_{1,0,0} s_{0,2}, \\ c_{2,0,0} &= 3 a_{1,0,0} s_{2,0} + b_{0,1,0} s_{2,0} + b_{1,0,0} s_{1,1}, \dots \end{aligned} \quad (6.6)$$

Depending on the tangential vectors (2.43b) and (2.43c), we have two tangential stress boundary conditions which are

$$\begin{aligned} \mathbf{n} \cdot \Upsilon \cdot \mathbf{t}_1 &= (f_x^2 - 1)(w_x + u_z) + f_x f_y (v_z + w_y) \\ &+ 2 f_x (u_x - w_z) + f_y (v_x + u_y) = 0, \end{aligned} \quad (6.7)$$

$$\begin{aligned} \mathbf{n} \cdot \Upsilon \cdot \mathbf{t}_2 &= (f_y^2 - 1)(w_y + v_z) + f_x f_y (u_z + w_x) \\ &+ 2 f_y (v_y - w_z) + f_x (v_x + u_y) = 0. \end{aligned} \quad (6.8)$$

From tangential stress (6.8), we obtain some relations for $b_{i,j,1}$ as

$$\begin{aligned} b_{0,0,1} &= 0, & b_{0,1,1} &= -a_{0,1,0}s_{1,1} + 2a_{1,0,0}s_{0,2} + 2b_{0,1,0}s_{0,2} + b_{1,0,0}s_{1,1}, \\ b_{1,0,1} &= 2b_{0,1,0}s_{1,1} - 2b_{1,0,0}s_{0,2} + 2s_{2,0}b_{1,0,0} \dots \end{aligned} \quad (6.9)$$

and from tangential stress (6.7), we obtain some relations for $a_{i,j,1}$ as

$$\begin{aligned} a_{0,0,1} &= 0, & a_{0,1,1} &= 2s_{0,2}a_{0,1,0} - 2a_{0,1,0}s_{2,0} + 2a_{1,0,0}s_{1,1}, \\ a_{1,0,1} &= a_{0,1,0}s_{1,1} + 2a_{1,0,0}s_{2,0} + 2b_{0,1,0}s_{2,0} - b_{1,0,0}s_{1,1} \dots \end{aligned} \quad (6.10)$$

It is convenient to apply the transformation to make the surface flat

$$\tilde{z} = z - f(x, y), \quad \dot{\tilde{z}} = \dot{z} - f_x \dot{x} - f_y \dot{y}. \quad (6.11)$$

After the transformation, the new velocity field can be written as

$$\begin{pmatrix} \dot{x} \\ \dot{y} \\ \dot{\tilde{z}} \end{pmatrix} = \begin{pmatrix} a_{1,0,0} & a_{0,1,0} & 0 \\ b_{1,0,0} & b_{0,1,0} & 0 \\ 0 & 0 & -a_{1,0,0} - b_{0,1,0} \end{pmatrix} \begin{pmatrix} x \\ y \\ \tilde{z} \end{pmatrix} + \mathcal{O}(|x, y, \tilde{z}|^2). \quad (6.12)$$

The relations for the pressure, can be obtained from the Navier-Stokes equations, see details in [40]. If we apply the normal stress boundary condition (2.60) into the velocity field

$$\begin{aligned} \mathbf{n} \cdot \Upsilon \cdot \mathbf{n} - \sigma \left(\frac{1}{R_1} + \frac{1}{R_2} \right) &= \gamma^{\frac{1}{2}} (-p\gamma + 2\mu f_x f_y (v_x + u_y) - 2\mu f_x (w_x + u_z) \\ &\quad - 2\mu f_y (v_z + w_y) + 2\mu (f_x^2 u_x + f_y^2 v_y + w_z)) \\ &\quad - \sigma (2f_{xy} f_x f_y - f_{xx} (f_y^2 + 1) - f_{yy} (f_x^2 + 1)), \end{aligned} \quad (6.13)$$

where $\gamma = 1 + f_x^2 + f_y^2$ and σ is surface tension, we observe

$$\begin{aligned} x^0 y^0 &: -2\mu a_{1,0,0} - 2\mu b_{0,1,0} + 2\sigma s_{0,2} + 2\sigma s_{2,0} - p_{0,0,0} = 0, \\ x^1 y^0 &: -2\mu a_{0,0,2} - 2\mu a_{0,2,0} - 6\mu a_{2,0,0} - 2\mu b_{1,1,0} + 2\sigma s_{1,2} + 6\sigma s_{3,0} = 0, \\ x^0 y^1 &: -2\mu a_{1,1,0} - 2\mu b_{0,0,2} - 6\mu b_{0,2,0} - 2\mu b_{2,0,0} + 6\sigma s_{0,3} + 2\sigma s_{2,1} = 0. \end{aligned} \quad (6.14)$$

These equalities will give us just physical information. For example, whenever $a_{1,0,0} = -b_{0,1,0}$ the pressure at the origin is $2\sigma(s_{0,2} + s_{2,0})$.

The Hartman-Grobman Theorem can be applied for the velocity field (6.12). The characteristic polynomial of the given matrix which is linear part of velocity field is

$$(\tau - \lambda)(\text{Det}B + \tau\lambda + \lambda^2) = 0, \quad (6.15)$$

where

$$\tau = -a_{1,0,0} - b_{0,1,0}, \quad (6.16)$$

and

$$B = \begin{pmatrix} a_{1,0,0} & a_{0,1,0} \\ b_{1,0,0} & b_{0,1,0} \end{pmatrix}. \quad (6.17)$$

Equation (6.15) gives us

$$\lambda = \tau \quad (6.18)$$

is one of the eigenvalues of (6.15). From (6.14) we can express τ physically as

$$\tau = \frac{p_{0,0} - 2\sigma(s_{0,2} + s_{2,0})}{2\mu}. \quad (6.19)$$

Other eigenvalues are given by

$$\lambda^\pm = -\frac{\tau}{2} \pm \frac{\sqrt{\tau^2 - 4 \text{Det}B}}{2}. \quad (6.20)$$

Depending on the sign of $\text{Det}B$ and τ we can find the eigenvalues as the following:

1. $\lambda_3 = \tau > 0$
 - (a) If $0 < \text{Det}B < \frac{\tau^2}{4}$; the two remaining eigenvalues are $\lambda_1 < 0$ and $\lambda_2 < 0$. The origin is saddle for the xz and yz planes, and for the xy plane, origin is a stable node.
 - (b) If $\text{Det}B < 0$; the two remaining eigenvalues are $\lambda_1 > 0$ and $\lambda_2 < 0$. The origin is saddle for xy and yz planes, and for the xz plane, origin is a unstable node.
 - (c) If $0 < \frac{\tau^2}{4} < \text{Det}B$; the two remaining eigenvalues are complex with $\text{Re}\lambda_1 < 0$ and $\text{Re}\lambda_2 < 0$. The origin is stable focus.
2. $\lambda_3 = \tau < 0$
 - (a) If $0 < \text{Det}B < \frac{\tau^2}{4}$; the two remaining eigenvalues are $\lambda_1 > 0$ and $\lambda_2 > 0$. The origin is saddle for the xz and yz planes, and for the xy plane, origin is a unstable node.
 - (b) If $\text{Det}B < 0$; the two remaining eigenvalues are $\lambda_1 < 0$ and $\lambda_2 > 0$. The origin is saddle for xy and yz planes, and for the xz plane, origin is a stable node.
 - (c) If $0 < \frac{\tau^2}{4} < \text{Det}B$; the two remaining eigenvalues are complex with $\text{Re}\lambda_1 > 0$ and $\text{Re}\lambda_2 > 0$. The origin is unstable focus.

There exist six different eigenvalue regions in Fig. 6.2. This figure is also observed by Hartnack [39] for the stationary wall. On the boundaries between these six regions degenerate critical points can be observed.

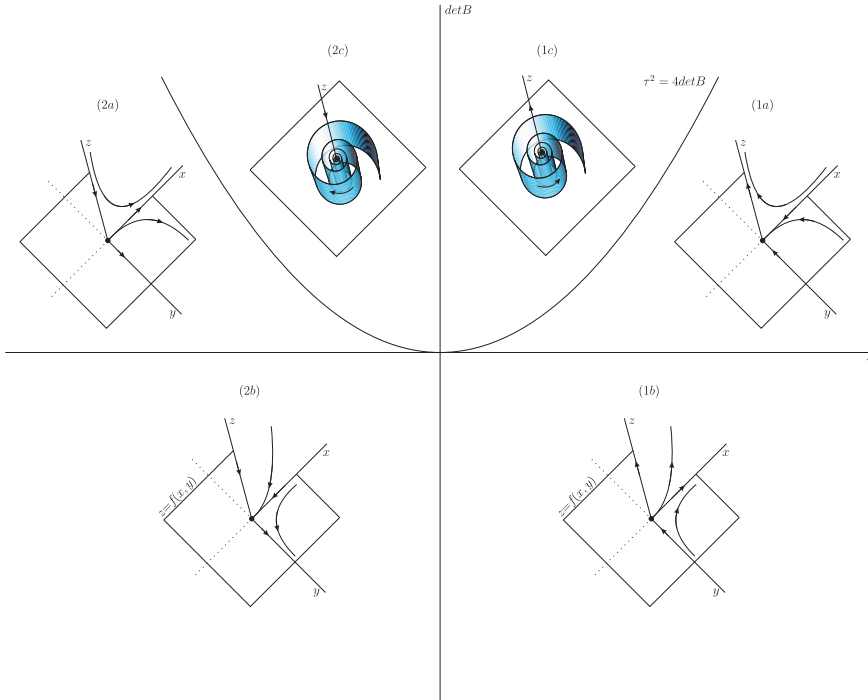


Figure 6.2: The classification of critical point on the free surface which is given by $z = f(x, y)$.

Whenever $trB = 0$ or $DetB = 0$, the algebraic multiplicity of eigenvalues is at least two. The geometric multiplicity is smaller or equal to algebraic multiplicity. Hence we need to examine the higher order terms to determine the flow topology.

The matrix B can be considered in real Jordan form since the solenoidal vector fields remain solenoidal under linear transformations. For a proof of this theorem please see in [39].

The matrix B can be investigated into three different cases, which are

1. $trB = 0$ and $DetB < 0$ with the real Jordan form $B = \begin{pmatrix} \tilde{a}_{1,0,0} & 0 & 0 \\ 0 & -\tilde{a}_{0,1,0} & 0 \\ 0 & 0 & 0 \end{pmatrix}$,
 where $\tilde{a}^2 = -DetB$, real solutions.

2. $trB = 0$ and $DetB > 0$ with the real Jordan form $B = \begin{pmatrix} 0 & -\tilde{a}_{0,1,0} & 0 \\ \tilde{a}_{0,1,0} & 0 & 0 \\ 0 & 0 & 0 \end{pmatrix}$,

where $\tilde{a}^2 = -DetB$, complex solutions.

3. $trB \neq 0$ and $DetB = 0$ with the real Jordan form $B = \begin{pmatrix} \tilde{a}_{1,0,0} & 0 & 0 \\ 0 & 0 & 0 \\ 0 & 0 & -\tilde{a}_{1,0,0} \end{pmatrix}$,

where $\tilde{a}_{1,0,0} = -\tau$.

6.2 Case 1: $trB = 0$ and $DetB < 0$

By using the given assumptions and removing tilde (\tilde{a}) from $a_{1,0,0}$, the velocity field (6.12) can be written as

$$\begin{pmatrix} \dot{x} \\ \dot{y} \\ \dot{\tilde{z}} \end{pmatrix} = \begin{pmatrix} a_{1,0,0} & 0 & 0 \\ 0 & -a_{1,0,0} & 0 \\ 0 & 0 & 0 \end{pmatrix} \begin{pmatrix} x \\ y \\ \tilde{z} \end{pmatrix} + \begin{pmatrix} f_{2,1} \\ f_{2,2} \\ f_{2,3} \end{pmatrix} + \begin{pmatrix} f_{3,1} \\ f_{3,2} \\ f_{3,3} \end{pmatrix} + \mathcal{O}(|x, y, \tilde{z}|^4), \quad (6.21)$$

where $f_{2,i}$ corresponds to second-order terms

$$f_{2,1} = 2a_{1,0,0}s_{1,1}yz + a_{2,0,0}x^2 + a_{1,1,0}xy + a_{0,2,0}y^2 + a_{0,0,2}z^2, \quad (6.22)$$

$$f_{2,2} = -2a_{1,0,0}s_{1,1}xz + b_{2,0,0}x^2 + b_{1,1,0}xy + b_{0,2,0}y^2 + b_{0,0,2}z^2, \quad (6.23)$$

$$f_{2,3} = (-2a_{2,0,0} - b_{1,1,0})xz + (-a_{1,1,0} - 2b_{0,2,0})yz, \quad (6.24)$$

and $f_{3,i}$ third-order terms. Using the near-identity transformation

$$\begin{pmatrix} x \\ y \\ \tilde{z} \end{pmatrix} = \begin{pmatrix} \xi \\ \eta \\ \zeta \end{pmatrix} + \begin{pmatrix} h_{2,1} \\ h_{2,2} \\ h_{2,3} \end{pmatrix} + \begin{pmatrix} h_{3,1} \\ h_{3,2} \\ h_{3,3} \end{pmatrix}, \quad (6.25)$$

where $h_{2,i}$ corresponds to second-order terms

$$\begin{aligned} h_{2,1} &= m_{0,2,0}\eta^2 + m_{1,1,0}\xi\eta + m_{0,1,1}\eta\zeta + m_{2,0,0}\xi^2 + m_{1,0,1}\xi\zeta + m_{0,0,2}\zeta^2, \\ h_{2,2} &= n_{0,2,0}\eta^2 + n_{1,1,0}\xi\eta + n_{0,1,1}\zeta\eta + n_{2,0,0}\xi^2 + n_{1,0,1}\xi\zeta + n_{0,0,2}\zeta^2, \\ h_{2,3} &= l_{0,1,1}\eta\zeta + l_{1,0,1}\xi\zeta + l_{0,0,2}\zeta^2, \end{aligned} \quad (6.26)$$

and $h_{3,i}$ third-order terms, the velocity field can be simplified. The new velocity field is in the form (2.20). Since the value for the coefficients $m_{i,j,k}$, $n_{i,j,k}$ and $l_{i,j,k}$ can be chosen to reduce the number of terms from velocity field. Please see the elimination process in [40]. It follows that the normal form of third order

system is given by

$$\begin{pmatrix} \dot{\xi} \\ \dot{\eta} \\ \dot{\zeta} \end{pmatrix} = \begin{pmatrix} a_{1,0,0} & 0 & 0 \\ 0 & -a_{1,0,0} & 0 \\ 0 & 0 & 0 \end{pmatrix} \begin{pmatrix} \xi \\ \eta \\ \zeta \end{pmatrix} + d_1 \begin{pmatrix} \xi^2 \eta \\ \xi \eta^2 \\ -2\xi \eta \zeta \end{pmatrix} + d_2 \begin{pmatrix} \xi \zeta^2 \\ \eta \zeta^2 \\ -\frac{\zeta^3}{3} \end{pmatrix}, \quad (6.27)$$

where the non-degeneracy condition $d_1 \neq 0$ and $d_2 \neq 0$. It is possible to simplify this normal form by scale time as

$$ta_{1,0,0} \rightarrow t \quad (6.28)$$

and then scaling ξ and ζ as

$$g_1 \xi \rightarrow \xi, \quad g_3 \zeta \rightarrow \zeta, \quad (6.29)$$

where

$$g_1 = \frac{a_{1,0,0}}{d_1}, \quad g_3 = \left| \frac{a_{1,0,0}}{d_2} \right|^{\frac{1}{2}}. \quad (6.30)$$

These scales yields the system as

$$\dot{\xi} = \xi(1 + \xi\eta + \sigma\zeta^2), \quad (6.31)$$

$$\dot{\eta} = -\eta(1 - \xi\eta - \sigma\zeta^2), \quad (6.32)$$

$$\dot{\zeta} = -\zeta \left(2\xi\eta + \sigma \frac{\zeta^2}{2} \right) \quad (6.33)$$

where

$$\sigma = \begin{cases} +1 & \text{if } a_{1,0,0}/d_2 > 0, \\ -1 & \text{if } a_{1,0,0}/d_2 < 0. \end{cases}$$

The flow topology can be sketched as in Fig. 6.3. If $d_1 = 0$ or $d_2 = 0$, the higher order terms need to be investigated.

As we know in previous chapters, degenerate critical points are structurally unstable. We can perturb the degenerate case by assuming $trB = 2\tilde{\epsilon}$. The velocity field with this assumption is written as (up to the fourth order terms)

$$\begin{pmatrix} \dot{x} \\ \dot{y} \\ \dot{z} \end{pmatrix} = \begin{pmatrix} a_{1,0,0} + \tilde{\epsilon} & 0 & 0 \\ 0 & -a_{1,0,0} + \tilde{\epsilon} & 0 \\ 0 & 0 & -2\tilde{\epsilon} \end{pmatrix} \begin{pmatrix} x \\ y \\ z \end{pmatrix} + \begin{pmatrix} f_{2,1;\tilde{\epsilon}} \\ f_{2,2;\tilde{\epsilon}} \\ f_{2,3;\tilde{\epsilon}} \end{pmatrix} + \begin{pmatrix} f_{3,1;\tilde{\epsilon}} \\ f_{3,2;\tilde{\epsilon}} \\ f_{3,3;\tilde{\epsilon}} \end{pmatrix}, \quad (6.34)$$

where $f_{2,i;\tilde{\epsilon}}$ corresponds to second-order terms

$$f_{2,1} = 2xz s_{2,0}\tilde{\epsilon} + 2a_{1,0,0}s_{1,1}yz + a_{2,0,0}x^2 + a_{1,1,0}xy + a_{0,2,0}y^2 + a_{0,0,2}z^2,$$

$$f_{2,2} = b_{2,0,0}x^2 + b_{1,1,0}xy + (2\tilde{\epsilon}s_{1,1} - 2a_{1,0,0}s_{1,1})xz + b_{0,2,0}y^2 + 2yz\tilde{\epsilon}s_{0,2} + b_{0,0,2}z^2,$$

$$f_{2,3} = (-2a_{2,0,0} - b_{1,1,0})xz + (-a_{1,1,0} - 2b_{0,2,0})yz + (-\tilde{\epsilon}s_{0,2} - s_{2,0}\tilde{\epsilon})z^2.$$

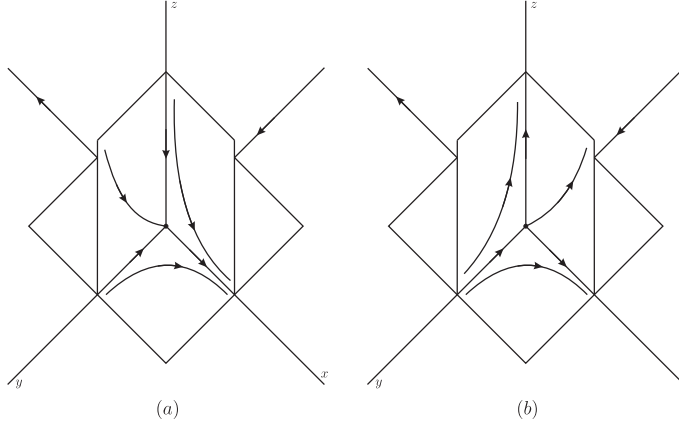


Figure 6.3: Degenerate critical point on the surface $z = f(x, y)$ with the assumptions $trB = 0$ and $DetB < 0$. (a) for $\sigma = 1$ and (b) for $\sigma = -1$.

and $f_{3,i;\tilde{\epsilon}}$ third-order terms. Again using the near-identity transformation (6.25) and similar scales for the degenerate case, we can simplify the velocity field as (please see the elimination process in [40]).

$$\dot{\xi} = \xi(1 + \epsilon + \xi\eta + \sigma\zeta^2), \quad (6.35)$$

$$\dot{\eta} = -\eta(1 - \epsilon - \xi\eta - \sigma\zeta^2), \quad (6.36)$$

$$\dot{\zeta} = -\zeta \left(2\epsilon + 2\xi\eta + \sigma\frac{\zeta^2}{2} \right), \quad (6.37)$$

where $\epsilon = \tilde{\epsilon}/a_{1,0,0}$. One can observe that this perturbation is just effect to the velocity $\dot{\zeta}$. Considering the dynamics on this velocity for $(x, y) = (0, 0)$, we have

$$\dot{\zeta} = -\zeta \left(2\epsilon + \sigma\frac{\zeta^2}{2} \right). \quad (6.38)$$

The critical points for this system are

$$\zeta = 0, \quad \text{and} \quad \zeta = \pm 2\sqrt{-\sigma\epsilon}, \quad (6.39)$$

The bifurcation type of this differential equation is called pitch-fork bifurcation. Note that one of the critical points is under the free surface. Since we are just considering one fluid, physically the critical point under the surface has no significance.

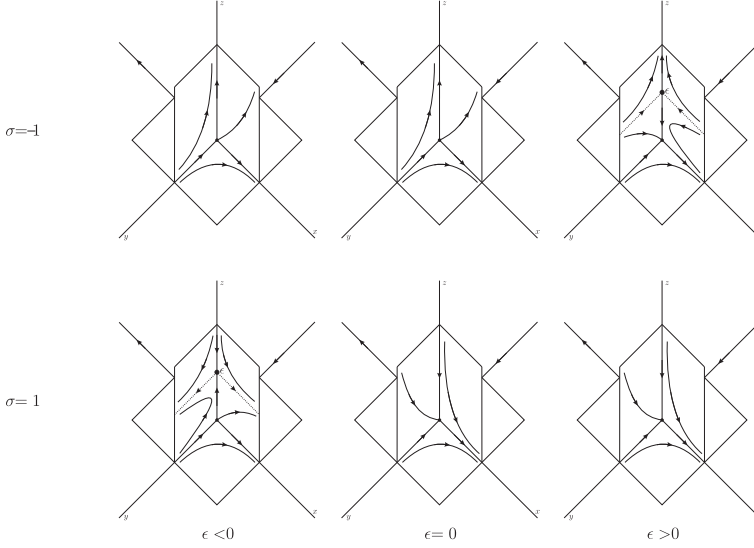


Figure 6.4: A small perturbation on the degenerate case with the assumptions $trB = \epsilon$ and $DetB < 0$.

6.3 Case 2: $trB = 0$ and $DetB > 0$

By using the given assumptions and removing tilde from $a_{1,0,0}$, the velocity field (6.12) can be written as

$$\begin{pmatrix} \dot{x} \\ \dot{y} \\ \dot{z} \end{pmatrix} = \begin{pmatrix} 0 & -a_{0,1,0} & 0 \\ a_{0,1,0} & 0 & 0 \\ 0 & 0 & 0 \end{pmatrix} \begin{pmatrix} x \\ y \\ z \end{pmatrix} + \begin{pmatrix} f_{2,1} \\ f_{2,2} \\ f_{2,3} \end{pmatrix} + \begin{pmatrix} f_{3,1} \\ f_{3,2} \\ f_{3,3} \end{pmatrix} + \mathcal{O}(|x, y, z|^4). \quad (6.40)$$

Using the linear transformation

$$x = \phi + \bar{\phi}, \quad y = -i(\phi - \bar{\phi}) \quad (6.41)$$

where the bar denotes complex conjugate, we can write the system as

$$\begin{pmatrix} \dot{\phi} \\ \dot{\bar{\phi}} \\ \dot{z} \end{pmatrix} = \begin{pmatrix} ia_{0,1,0} & 0 & 0 \\ 0 & -ia_{0,1,0} & 0 \\ 0 & 0 & 0 \end{pmatrix} \begin{pmatrix} \phi \\ \bar{\phi} \\ z \end{pmatrix} + \mathcal{O}(|\phi, \bar{\phi}, z|^2). \quad (6.42)$$

This system is in the form (6.21), hence we can write it as

$$\begin{pmatrix} \dot{\phi} \\ \dot{\bar{\phi}} \\ \dot{z} \end{pmatrix} = \begin{pmatrix} ia_{0,1,0} & 0 & 0 \\ 0 & -ia_{0,1,0} & 0 \\ 0 & 0 & 0 \end{pmatrix} \begin{pmatrix} \phi \\ \bar{\phi} \\ z \end{pmatrix} + d_{11} \begin{pmatrix} \phi^2 \bar{\phi} \\ \bar{\phi} \phi^2 \\ -2\phi \bar{\phi} z \end{pmatrix} + d_{21} \begin{pmatrix} \phi z^2 \\ \bar{\phi} z^2 \\ -\frac{z^3}{3} \end{pmatrix}. \quad (6.43)$$

We can apply the inverse transformation

$$\phi = x + iy \quad \bar{\phi} = x - iy, \quad (6.44)$$

to make the system real-valued, the normal form of (6.40) becomes

$$\begin{pmatrix} \dot{x} \\ \dot{y} \\ \dot{z} \end{pmatrix} = \begin{pmatrix} -a_{0,1,0}y \\ a_{0,1,0}x \\ 0 \end{pmatrix} + d_{11} \begin{pmatrix} x(x^2 + y^2) \\ y(x^2 + y^2) \\ -2z(x^2 + y^2) \end{pmatrix} + d_{21} \begin{pmatrix} xz^2 \\ yz^2 \\ -\frac{z^3}{3} \end{pmatrix}. \quad (6.45)$$

Under the non-degeneracy conditions

$$d_{11} \neq 0, \quad d_{21} \neq 0, \quad (6.46)$$

we can analyse the local topology of the velocity field. To make more simplification in the velocity field we can scale time

$$ta_{0,1,0} \rightarrow t \quad (6.47)$$

and scaling coordinate system as

$$\gamma_1 x \rightarrow x, \quad \gamma_2 y \rightarrow y, \quad \gamma_3 z \rightarrow z, \quad (6.48)$$

where

$$\gamma_1 = \gamma_2 = \left| \frac{d_{1,1}}{a_{0,1,0}} \right|^{\frac{1}{2}}, \quad \gamma_3 = \left| \frac{d_{2,1}}{a_{0,1,0}} \right|^{\frac{1}{2}}. \quad (6.49)$$

The velocity field becomes after the scales,

$$\begin{pmatrix} \dot{x} \\ \dot{y} \\ \dot{z} \end{pmatrix} = \begin{pmatrix} -y \\ x \\ 0 \end{pmatrix} + \sigma \begin{pmatrix} x(x^2 + y^2) \\ y(x^2 + y^2) \\ -2z(x^2 + y^2) \end{pmatrix} + \alpha \begin{pmatrix} xz^2 \\ yz^2 \\ -\frac{z^3}{3} \end{pmatrix}, \quad (6.50)$$

where

$$\sigma = \left| \frac{d_{1,1}}{a_{0,1,0}} \right| \frac{a_{0,1,0}}{d_{1,1}} = \pm 1, \quad \alpha = \left| \frac{d_{2,1}}{a_{0,1,0}} \right| \frac{a_{0,1,0}}{d_{2,1}} = \pm 1. \quad (6.51)$$

It is easy to obtain the phase portrait for (xy) plane by assuming $z = 0$ which is sketched in 6.5.

To find the relation between the (xy) plane and z plane, it is advantageous to transform the given coordinate system to cylindrical coordinate

$$x = r \cos(\theta), \quad y = r \sin(\theta), \quad z = z. \quad (6.52)$$

The system then becomes

$$\dot{r} = r(\sigma r^2 + \alpha z^2), \quad (6.53)$$

$$\dot{\theta} = 1, \quad (6.54)$$

$$\dot{z} = -z \left(2\sigma r^2 + \frac{\alpha z^2}{3} \right). \quad (6.55)$$

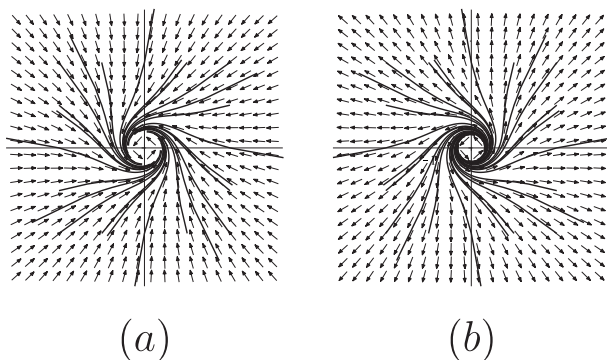


Figure 6.5: The degenerate critical points for the (xy) plane with the assumptions $trB = 0$ and $DetB > 0$. (a) $\sigma = -1$ (b) $\sigma = 1$.

The system has rotational symmetry about z - axis, since the velocity $\dot{\theta}$ is independent of θ . We can just consider the meridional plane to obtain local topology of flow which is sketched in Fig. 6.6.

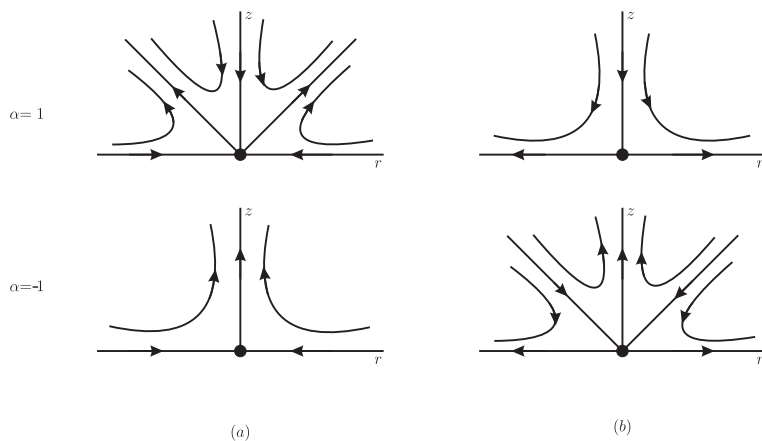


Figure 6.6: The degenerate critical points with the assumptions $trB = 0$ and $DetB > 0$ for meridional plane rz . (a) $\sigma = -1$ (b) $\sigma = 1$.

The degenerate case for the three-dimensional phase portrait with the given assumptions is sketched in Fig. 6.7 and 6.8.

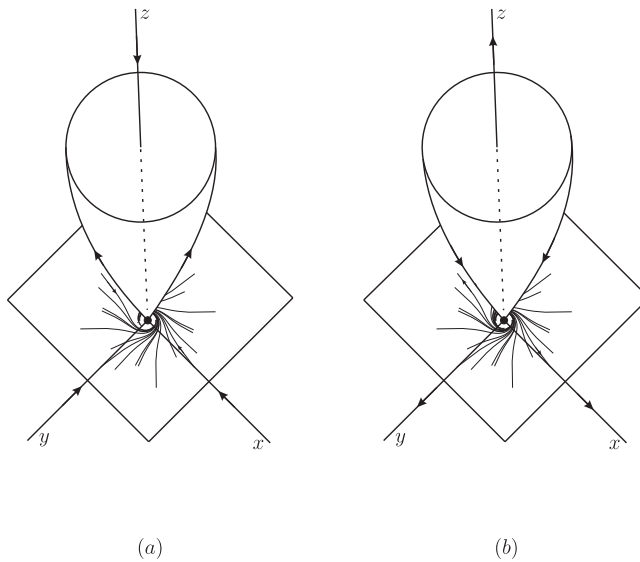


Figure 6.7: The degenerate critical points with the assumptions $trB = 0$ and $DetB > 0$. (a) $\sigma = -1$ and $\alpha = 1$ (b) $\sigma = 1$ and $\alpha = -1$.

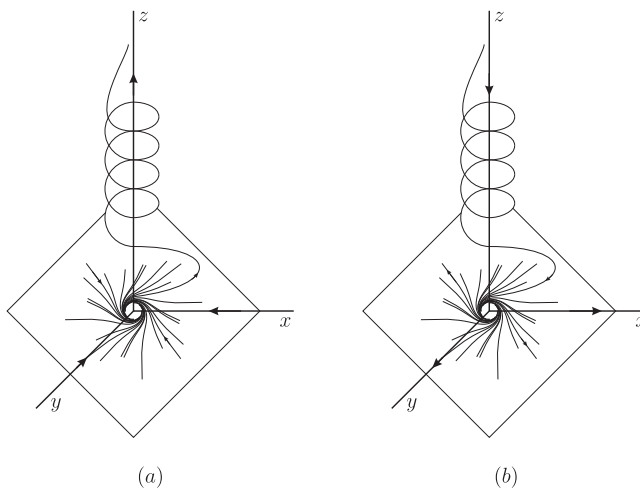


Figure 6.8: The degenerate critical points with the assumptions $trB = 0$ and $DetB > 0$. (a) $\sigma = -1$ and $\alpha = -1$ (b) $\sigma = 1$ and $\alpha = 1$

The unfolding of the degenerate case (6.50) is in the following form

$$\begin{pmatrix} \dot{\phi} \\ \dot{\bar{\phi}} \\ \dot{\tilde{z}} \end{pmatrix} = \begin{pmatrix} ia_{0,1,0} + \epsilon_1 & 0 & 0 \\ 0 & -ia_{0,1,0} + \epsilon_1 & 0 \\ 0 & 0 & -2\epsilon_1 \end{pmatrix} \begin{pmatrix} \phi \\ \bar{\phi} \\ \tilde{z} \end{pmatrix} + d_{11} \begin{pmatrix} \phi^2 \bar{\phi} \\ \phi \bar{\phi}^2 \\ -2\phi \bar{\phi} \tilde{z} \end{pmatrix} + d_{21} \begin{pmatrix} \phi \tilde{z}^2 \\ \bar{\phi} \tilde{z}^2 \\ -\frac{\tilde{z}^3}{3} \end{pmatrix}.$$

Applying the transformation (6.44) into the velocity field, one can obtain that

$$\begin{pmatrix} \dot{x} \\ \dot{y} \\ \dot{\tilde{z}} \end{pmatrix} = \begin{pmatrix} -a_{0,1,0}y + \epsilon x \\ a_{0,1,0}x + \epsilon y \\ -2\epsilon \tilde{z} \end{pmatrix} + d_{11} \begin{pmatrix} x(x^2 + y^2) \\ y(x^2 + y^2) \\ -2\tilde{z}(x^2 + y^2) \end{pmatrix} + d_{21} \begin{pmatrix} x\tilde{z}^2 \\ y\tilde{z}^2 \\ -\frac{\tilde{z}^3}{3} \end{pmatrix}. \quad (6.56)$$

To make more simplification in the velocity field we can scale time

$$ta_{0,1,0} \rightarrow t \quad (6.57)$$

and scaling coordinate system as

$$\gamma_1 x \rightarrow x, \quad \gamma_2 y \rightarrow y, \quad \gamma_3 \tilde{z} \rightarrow z, \quad (6.58)$$

where

$$\gamma_1 = \gamma_2 = \left| \frac{d_{1,1}}{a_{0,1,0}} \right|^{\frac{1}{2}}, \quad \gamma_3 = \left| \frac{d_{2,1}}{a_{0,1,0}} \right|^{\frac{1}{2}}. \quad (6.59)$$

The velocity field becomes after the scales,

$$\begin{pmatrix} \dot{x} \\ \dot{y} \\ \dot{z} \end{pmatrix} = \begin{pmatrix} -y + \tilde{\epsilon}x \\ x + \tilde{\epsilon}y \\ -\tilde{\epsilon}z \end{pmatrix} + \sigma \begin{pmatrix} x(x^2 + y^2) \\ y(x^2 + y^2) \\ -2z(x^2 + y^2) \end{pmatrix} + \alpha \begin{pmatrix} xz^2 \\ yz^2 \\ -\frac{z^3}{3} \end{pmatrix}, \quad (6.60)$$

where

$$\sigma = \left| \frac{d_{1,1}}{a_{0,1,0}} \right| \frac{a_{0,1,0}}{d_{1,1}} = \pm 1, \quad \alpha = \left| \frac{d_{2,1}}{a_{0,1,0}} \right| \frac{a_{0,1,0}}{d_{2,1}} = \pm 1, \quad (6.61)$$

and $\tilde{\epsilon}$ is transformed small parameter. It is advantageous to use polar coordinate transformation (6.52) into the system, which gives

$$\dot{r} = r(\tilde{\epsilon} + \sigma r^2 + \alpha z^2), \quad (6.62)$$

$$\dot{\theta} = 1, \quad (6.63)$$

$$\dot{z} = -z \left(2\tilde{\epsilon} + 2\sigma r^2 + \frac{\alpha z^2}{3} \right). \quad (6.64)$$

The system has rotational symmetry about z - axis, since the velocity $\dot{\theta}$ is independent of θ . We can just consider the meridional plane to obtain local topology of flow which is sketched in Fig.

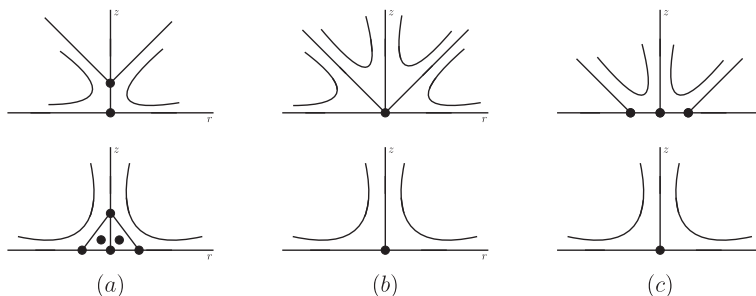


Figure 6.9: The meridional plane with the assumptions $trB = 0$ and $DetB > 0$. Top panel is for the different sign of σ and α , (a) $\sigma = 1$, $\alpha = -1$ and $\epsilon > 0$; or $\sigma = -1$, $\alpha = 1$ and $\epsilon < 0$ (b) $\epsilon = 0$ (c) $\sigma = 1$, $\alpha = -1$ and $\epsilon < 0$; or $\sigma = -1$, $\alpha = 1$ and $\epsilon > 0$. The bottom panel is for the same sign of σ and α , (a) $\sigma = 1$, $\alpha = 1$ and $\epsilon < 0$; or $\sigma = -1$, $\alpha = -1$ and $\epsilon > 0$ (b) $\epsilon = 0$ (c) $\sigma = 1$, $\alpha = 1$ and $\epsilon > 0$; or $\sigma = -1$, $\alpha = -1$ and $\epsilon < 0$.

The three dimensional version of Fig. 6.9 is sketched in Fig. 6.10 and 6.11.

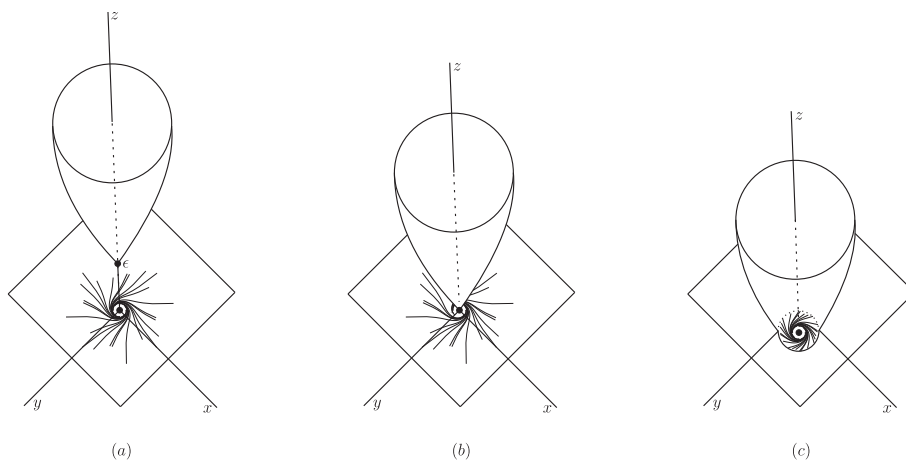


Figure 6.10: Bifurcation diagram of (6.60) with the different sign of σ and α . The three dimensional version of the top panel of Fig. 6.9.

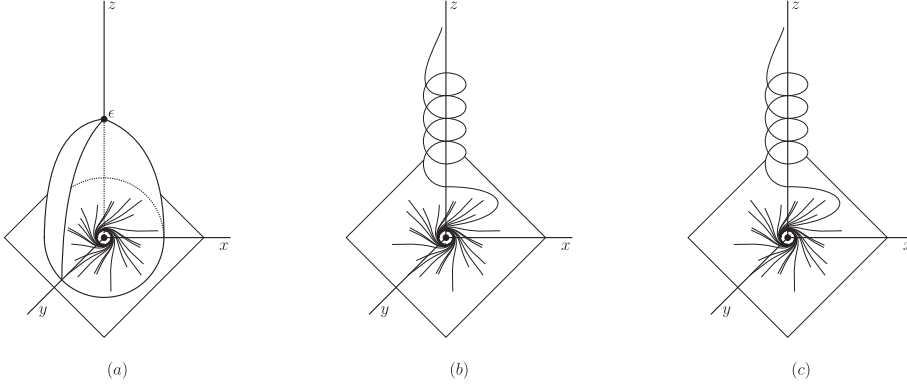


Figure 6.11: Bifurcation diagram of (6.60) with the same sign of σ and α . The three dimensional version of the bottom panel of Fig. 6.9.

6.4 Case 3: $trB \neq 0$ and $DetB = 0$

By using the given assumptions, the velocity field (6.12) can be written as

$$\begin{pmatrix} \dot{x} \\ \dot{y} \\ \dot{z} \end{pmatrix} = \begin{pmatrix} a_{1,0,0} & 0 & 0 \\ 0 & 0 & 0 \\ 0 & 0 & -a_{1,0,0} \end{pmatrix} \begin{pmatrix} x \\ y \\ z \end{pmatrix} + \begin{pmatrix} f_{2,1} \\ f_{2,2} \\ f_{2,3} \end{pmatrix} + \mathcal{O}(|x, y, z|^3), \quad (6.65)$$

where $f_{2,i}$ corresponds to second-order terms

$$\begin{aligned} f_{2,1} &= 2a_{1,0,0}s_{2,0}xz + 2a_{1,0,0}s_{1,1}yz + a_{2,0,0}x^2 + a_{1,1,0}xy + a_{0,2,0}y^2 + a_{0,0,2}z^2, \\ f_{2,2} &= 2a_{1,0,0}s_{0,2}yz + b_{2,0,0}x^2 + b_{1,1,0}xy + b_{0,2,0}y^2 + b_{0,0,2}z^2, \\ f_{2,3} &= (-2a_{2,0,0} - b_{1,1,0})xz + (-a_{1,1,0} - 2b_{0,2,0})yz + (-a_{1,0,0}s_{0,2} - a_{1,0,0}s_{2,0})z^2. \end{aligned} \quad (6.66)$$

Using the near-identity transformation (6.25), we simplify the velocity field as

$$\begin{pmatrix} \dot{\xi} \\ \dot{\eta} \\ \dot{\zeta} \end{pmatrix} = \begin{pmatrix} a_{1,0,0} & 0 & 0 \\ 0 & 0 & 0 \\ 0 & 0 & -a_{1,0,0} \end{pmatrix} \begin{pmatrix} \xi \\ \eta \\ \zeta \end{pmatrix} + d_1 \begin{pmatrix} \xi\eta \\ \eta^2 \\ -3\eta\zeta \end{pmatrix}. \quad (6.67)$$

Under the non-degeneracy condition

$$d_1 \neq 0, \quad (6.68)$$

we can analyse the local topology of the velocity field. To make more simplification in the velocity field we can scale time

$$ta_{0,1,0} \rightarrow t \quad (6.69)$$

and scaling coordinate system as

$$\frac{a_{1,0,0}}{d_1} \eta \rightarrow \eta. \quad (6.70)$$

The velocity field becomes after the scales,

$$\begin{pmatrix} \dot{\xi} \\ \dot{\eta} \\ \dot{\zeta} \end{pmatrix} = \begin{pmatrix} \xi \\ 0 \\ -\zeta \end{pmatrix} + \begin{pmatrix} \xi\eta \\ \eta^2 \\ -3\zeta\eta \end{pmatrix}. \quad (6.71)$$

The flow topology can be sketched as in Fig. 6.12.

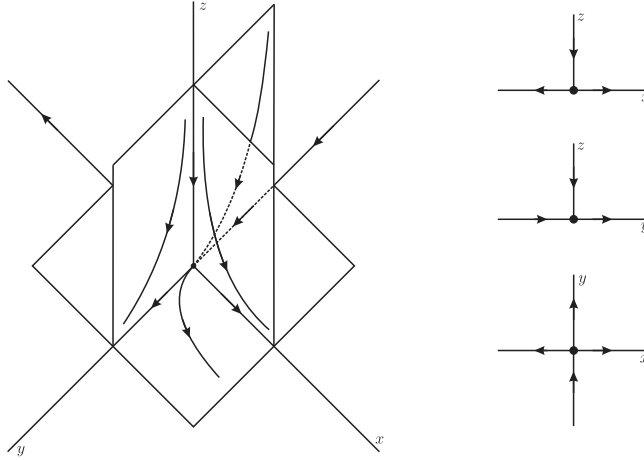


Figure 6.12: The degenerate critical points with the assumptions $trB \neq 0$ and $DetB = 0$.

A small perturbation for $DetB$ can change the streamline patterns of the given degenerate system. Hence, assuming that $DetB = \epsilon$ the unfolding of the system (6.65) is written as

$$\begin{pmatrix} \dot{x} \\ \dot{y} \\ \dot{z} \end{pmatrix} = \begin{pmatrix} a_{1,0,0} - \epsilon & 0 & 0 \\ 0 & \epsilon & 0 \\ 0 & 0 & -a_{1,0,0} \end{pmatrix} \begin{pmatrix} x \\ y \\ z \end{pmatrix} + \begin{pmatrix} f_{2,1,\epsilon} \\ f_{2,2,\epsilon} \\ f_{2,3,\epsilon} \end{pmatrix} + \mathcal{O}(|x, y, z|^3), \quad (6.72)$$

where $f_{2,i,\epsilon}$ corresponds to second-order terms

$$f_{2,1,\epsilon} = a_{2,0,0}x^2 + a_{1,1,0}xy + 2a_{1,0,0}s_{2,0}xz + a_{0,2,0}y^2 + (-2\epsilon s_{1,1} + 2a_{1,0,0}s_{1,1})zy + a_{0,0,2}z^2, \quad (6.73)$$

$$f_{2,2,\epsilon} = 2\epsilon s_{1,1}xz + 2a_{1,0,0}s_{0,2}yz + b_{2,0,0}x^2 + b_{1,1,0}xy + b_{0,2,0}y^2 + b_{0,0,2}z^2,$$

$$f_{2,3,\epsilon} = (-2a_{2,0,0} - b_{1,1,0})xz + (-a_{1,1,0} - 2b_{0,2,0})yz + (-a_{1,0,0}s_{0,2} - a_{1,0,0}s_{2,0})z^2.$$

Using the near-identity transformation (6.25) and same scales as in the degenerate case, we obtain the new system as

$$\begin{pmatrix} \dot{\xi} \\ \dot{\eta} \\ \dot{\zeta} \end{pmatrix} = \begin{pmatrix} 1 - \tilde{\epsilon} & 0 & 0 \\ 0 & \tilde{\epsilon} & 0 \\ 0 & 0 & -1 \end{pmatrix} \begin{pmatrix} \xi \\ \eta \\ \zeta \end{pmatrix} + \begin{pmatrix} \xi\eta \\ \eta^2 \\ -3\zeta\eta \end{pmatrix}, \tag{6.74}$$

where $\tilde{\epsilon} = \frac{\epsilon}{a_{1,0,0}}$. From now on, we will use (x, y, z) labels instead of (ξ, η, ζ) .

The critical points on the surface can be found by substituting $z = 0$ into (6.74)

$$\begin{pmatrix} \dot{x} \\ \dot{y} \\ \dot{z} \end{pmatrix} = \begin{pmatrix} (1 - \tilde{\epsilon})x + xy \\ \tilde{\epsilon}y + y^2 \\ 0 \end{pmatrix}. \tag{6.75}$$

Since the critical point exist when $\dot{x} = \dot{y} = 0$, we observe that $(0, 0)$ and $(0, -\tilde{\epsilon})$ are critical points on the surface. For $\tilde{\epsilon} < 0$, $(0, -\tilde{\epsilon})$ is a saddle point which is stable on z -axis and unstable on y -axis. For $\tilde{\epsilon} > 0$, $(0, -\tilde{\epsilon})$ is again a saddle point but the stability reversed. It can be observed a transcritical bifurcation in that process.

The bifurcation diagram can be figured in Fig. 6.13.

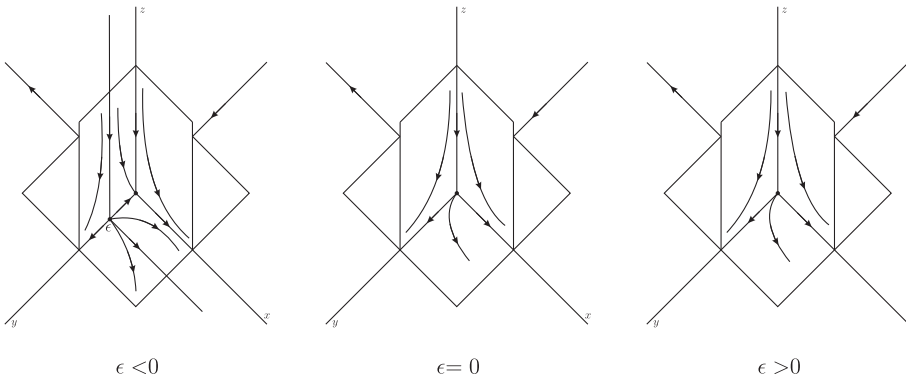


Figure 6.13: The unfolding with the assumptions $trB \neq 0$ and $DetB = \epsilon$.

6.5 Conclusion

In this chapter, three dimensional steady flow is considered close to a free surface. Using the normal form and unfolding theory, we observed the streamline patterns and bifurcations.

As boundary conditions, the kinematic, tangential stress and normal stress boundary conditions are used. The streamline patterns which we obtain, look similar to Hartnack's [39] streamline patterns for the flow close to a stationary wall. Although the streamline patterns have an exact match, occurring bifurcations are different. The differences of the streamline patterns can be visualized when the higher order terms are investigated.

Numerical Investigations of creeping vortex breakdown flows

In this chapter, we will make a numerical analysis to describe the eddy emergence and transformations in a slow steady axisymmetric air-water flow, driven by a rotating top disk in a three different shaped containers, which are shown in Fig. 7.1. They are a vertical truncated conical container (left picture will be called *LP*), a vertical conical container (middle picture will be called *MP*) and a sealed semispherical container (right picture will be called *RP*).

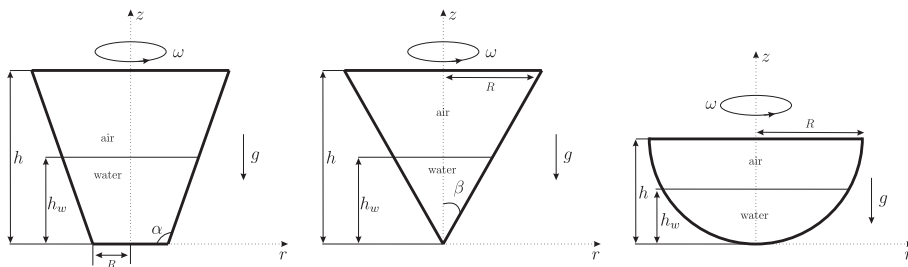


Figure 7.1: Schematic of the problems.

In a swirling flow, the emergence of a local circulation region, or vortex breakdown, has a great importance in last decades. For example, in nature (tornadoes, trapped wave, typhoons), in technological applications (heat exchange, aeronautics, delta-wing aircraft, combustion, vortex reactors, etc.) vortex breakdown can be observed. Recently, it has been seen that the vortex breakdown occurs in a creeping flow which is significant for bio-reactors.

The recent study by Herrada and Shtern [41] revealed a non-trivial topology of a creeping air-water flow in a vertical sealed cylinder driven by the rotating top disk. As the volume fraction of water increases, a number of eddies develop and multiple topological changes occur in both air and water motions despite the fact that the flow being extremely slow. Such paradoxical complexity of a creeping flow is caused by competing effects of the swirl and meridional motions. This makes the fluid mechanics of aerial bio-reactors, which are rapidly developing technology and employ air-water flows for the efficient growth of tissue culture, of fundamental interest. In this study, nine topological changes is revealed as the water volume fraction, H_w , increases. (This number is in fact larger, as we will show in the section 7.3.)

In the rest of this thesis, we formulate the problem, describe the numerical technique, explore the flow pattern for small H_w , investigate how the pattern changes as H_w grows in containers converging and diverging from the rotating lid to the stationary bottom disk, study the effect of increasing rotation, summarize the results and compare them with analytical ones.

This chapter summarizes the results in

- * A. Balci, M. Brøns, M. A. Herrada and V. Shtern : Bifurcations of a creeping air-water flow in a conical container. Submitted for publication. 2015.
- * A. Balci, M. Brøns, M. A. Herrada and V. Shtern : Vortex breakdown in a conical bioreactor. Submitted for publication. 2015.
- * A. Balci, M. Brøns, M. A. Herrada and V. Shtern : Vortex breakdown in a semispherical bioreactor. Submitted for publication. 2015.

7.1 Problem Formulation

In the containers, the lower part, $0 < z < h_w$, of the conical container is filled with water, the upper part, $h_w < z < h$, is filled with air; h is the height of the

containers, which serves as a length scale; g is the gravitational acceleration. The interface is depicted by the thin horizontal line, $z = h_w$. The rotation strength can be characterized by the Reynolds number, $Re = \omega h^2 / \nu_w$ which will be used a control parameter, ν_w is the kinematic viscosity of water and ω is the angular velocity. The other control parameters are aspect ratio $H = h/R$ and the water volume fraction characterized by $H_w = h_w/h$. The motion is creeping if $Re \ll 1$.

These are common properties for the containers in Fig. 7.1. Some properties are different hence problems need be investigated into three cases,

- (1) *LP*: α is the angle between the bottom and the side-wall. The top disk (at $z = h$) rotates with angular velocity ω . R is the bottom-disk radius. Additionally, α is a dimensionless control parameter.
- (2) *MP*: β is the angle between the axis and the side-wall. The top disk of radius $R = h \tan \beta$ is located at $z = h$ and rotates with angular velocity ω . Additionally, β is a dimensionless control parameter.
- (3) *RP*: The disk lid, located at $z = R$, rotates with angular velocity ω ; R is the disk and hemisphere radius, which serves as a length scale.

Our main goal is to study the flow transformations as H_w varies. It will be helpful to state the control parameters separately;

Control parameters

1. $Re = \frac{\omega R^2}{\nu_w}$: The rotation strength is characterized by Re .
2. $H = h/R$ aspect ratio.
3. $H_w = h_w/h$ water volume fraction.
4. α and β are the angle between the bottom and side wall.

In here we fixed $H = 1$ while H_w varies since the aspect ratio of aerial bio-reactors is typically close to one, see Liow et al. [42].

Governing Equations

The governing equations are the same as in the paper by Herrada and Shtern [41]. Using R , ωR and $\rho_w \omega^2 R^2$ as scales for length, velocity and pressure,

respectively, we consider a steady, viscous, incompressible axisymmetric flows governed by Navier-Stokes equations,

$$\frac{1}{r} \frac{\partial ru}{\partial r} + \frac{\partial w}{\partial z} = 0 \quad (7.1)$$

$$u \frac{\partial u}{\partial r} + w \frac{\partial u}{\partial z} - \frac{v^2}{r} = -\rho_n \frac{\partial p}{\partial r} + \nu_n Re^{-1} \left(\nabla^2 u - \frac{u}{r^2} \right) \quad (7.2)$$

$$u \frac{\partial v}{\partial r} + w \frac{\partial v}{\partial z} + \frac{uv}{r} = \nu_n Re^{-1} \left(\nabla^2 v - \frac{v}{r^2} \right) \quad (7.3)$$

$$u \frac{\partial w}{\partial r} + w \frac{\partial w}{\partial z} = -\rho_n \frac{\partial p}{\partial z} + \nu_n Re^{-1} (\nabla^2 w), \quad (7.4)$$

where $\nabla^2 = \frac{1}{r} \frac{\partial(r \frac{\partial}{\partial r})}{\partial r} + \frac{\partial^2}{\partial z^2}$, (u, v, w) are the velocity components in the cylindrical coordinate (r, θ, z) and p is pressure reduced by the hydrostatic contribution. The coefficients ρ_n and ν_n are 1 in water while $\rho_n = \rho_w/\rho_a$ and $\nu_n = \nu_a/\nu_w$. In air, $\nu_w = 10^{-6} m^2/s$ and $\nu_a = 15 \times 10^{-6} m^2/s$ are kinematic viscosities; and $\rho_w = 1000 kg/m^3$ and $\rho_a = 1.22 kg/m^3$ are the densities which are in the atmospheric pressure and the room temperature. Subscripts ‘‘a’’ and ‘‘w’’ are abbreviations for ‘‘air’’ and ‘‘water’’.

Boundary Conditions

The Navier-Stokes are solved under the following boundary conditions:

- (i) Regularity at the axis ($0 < z < 1, r = 0$). $u = v = 0, \frac{\partial w}{\partial r} = 0$,
- (ii) No-slip conditions at the rotating disk: the velocities $u = w = 0$ and $v = r$:
 for $LP, 0 < r < 1 - \cot \alpha, z = 1$;
 for $MP, 0 < r < \tan \beta, z = 1$;
 for $RP, 0 < r < 1, z = 1$.
- (iii) No-slip conditions at the side wall: the velocities $u = v = w = 0$:
 for $LP, 0 < z < 1, r = 1 - z \cot \alpha$;
 for $MP, 0 < z < 1, r = z \tan \beta$;
 for $RP, 0 < r < 1, z = 1 - (1 - r^2)^{1/2}$.
- (iv) No-slip condition at the still disk: the velocities $u = v = w = 0$ for $LP, 0 < r < 1, z = 0$.
- (v) Continuity of all the velocity and stress components at the interface $z = F(r)$. Since the interface is a streamline, the normal-to-interface velocity is zero: $w = 0$ at $z = H_w$ and the balance for the normal stress yields

$$p_w - p_a = We^{-1} \nabla \cdot \mathbf{n} - Re^{-1} \mathbf{n} \cdot (\tau_w - \mu_r \tau_a) \cdot \mathbf{n} - Fr^{-1} (1 - \rho_a/\rho_w) z + C, \quad (7.5)$$

where $We = \frac{\rho_w \omega^2 R^3}{\sigma}$ is the Weber number, characterizing the effect of surface tension σ , $Fr = \frac{\omega^2 R}{g}$ is the Froude number, which is a centrifugal-to-gravitational acceleration ratio, $g = 9.81 m^2/s$ being the gravitational acceleration magnitude; \mathbf{n} is the unit vector normal to the interface; τ_w and τ_a are tensors of the viscous stresses in water and air, respectively; μ_r is the air-to-water ratio of the dynamic viscosities; C is a constant which is determined by imposing the mass conservation of the liquid inside the container as the interface is deformed,

$$6 \int_0^a [F(r) - F(a)] r dr + F(a)(1 + a + a^2) = H_w(1 + r_w + r_w^2), \quad (7.6)$$

where $r_w = 1 - H_w \cot \alpha$ (for *LP*) and $r_w = H_w \tan \beta$ (for *MP*), a is the radial coordinate, where the interface meets the side-wall, and a root of the equation, $a = 1 - F(a) \cot \alpha$ (for *LP*) and $a = F(a) \tan \beta$ (for *MP*).

Reduced Problems

As $Re \rightarrow 0$, the motion becomes very slow and the interface deformation becomes negligible, $F(r) = H_w$. Hence, for equation (7.3), the non-linear terms become sufficiently small when we compare them with the linear ones. The reduced version of (7.3) becomes

$$\nabla^2 v - \frac{v}{r^2} = 0. \quad (7.7)$$

That means the swirl velocity becomes separated from the meridional motion. We first solve this linear problem for obtaining swirl velocity.

Secondly, we need to observe the meridional motion. Since the boundary conditions are uniform, the meridional motion is only driven by the centrifugal force ($\frac{v^2}{r}$) in equation (7.2). This term must be preserved and the other non-linear terms can be omitted when $Re \rightarrow 0$. Next, we scale u and w by dividing Re , the equations (7.1),(7.2) and (7.4) become

$$\frac{1}{r} \frac{\partial ru}{\partial r} + \frac{\partial w}{\partial z} = 0 \quad (7.8)$$

$$\rho_n \frac{\partial p}{\partial r} - \frac{v^2}{r} = \nu_n \left(\nabla^2 u - \frac{u}{r^2} \right) \quad (7.9)$$

$$\rho_n \frac{\partial p}{\partial z} = \nu_n (\nabla^2 w). \quad (7.10)$$

It is interesting that the entire problem formally is non-linear despite the motion is creeping, but can be reduced to the two linear problems: one for the swirl velocity (7.7) and the other for the meridional motion (7.8)-(7.10). After solving problem (7.7), the ‘‘source’’ term, v^2/r in equation (7.9), is prescribed, so the problem for the meridional motion also is linear.

7.2 Numerical Procedures

7.2.1 Transformation of Equations

The Navier-Stokes equations (7.1)-(7.4) are transformed into three equations for the Stokes stream function ψ , the meridional velocities $u = -\frac{1}{r}\frac{\partial\psi}{\partial z}$, $w = \frac{1}{r}\frac{\partial\psi}{\partial r}$, the azimuthal vorticity component, $\eta = \frac{\partial u}{\partial z} - \frac{\partial w}{\partial r}$ and the circulation, $\Gamma = rv$:

$$\nabla^2\psi - \frac{2}{r}\frac{\partial\psi}{\partial r} = -r\eta, \quad (7.11)$$

$$u\frac{\partial\eta}{\partial r} + w\frac{\partial\eta}{\partial z} - \frac{u\eta}{r} = \frac{2}{r^3}\Gamma\frac{\partial\Gamma}{\partial z} + \nu_n Re^{-1}\left(\nabla^2\eta - \frac{\eta}{r^2}\right), \quad (7.12)$$

$$u\frac{\partial\Gamma}{\partial r} + w\frac{\partial\Gamma}{\partial z} = \nu_n Re^{-1}\left(\nabla^2\Gamma - \frac{2}{r}\frac{\partial\Gamma}{\partial r}\right). \quad (7.13)$$

These equations are solved applying the boundary conditions for ψ , η and Γ , by using the given boundary conditions.

7.2.2 Linear Problem

In the limiting case as $Re \rightarrow 0$, scaling $\eta/Re \rightarrow \eta$ and $\Gamma/Re \rightarrow \Gamma$ reduces (7.11)-(7.13) to

$$\nabla^2\psi - \frac{2}{r}\frac{\partial\psi}{\partial r} = -r\eta, \quad (7.14)$$

$$\frac{2}{r^3}\Gamma\frac{\partial\Gamma}{\partial z} + \nu_n = -\left(\nabla^2\eta - \frac{\eta}{r^2}\right), \quad (7.15)$$

$$\nabla^2\Gamma = \frac{2}{r}\frac{\partial\Gamma}{\partial r}. \quad (7.16)$$

7.2.3 Discretization

A boundary-fitted coordinate system is used to calculate the problem. Both the water and air regions are mapped onto the fixed rectangular domains (a) $0 \leq \eta \leq 1$, $0 \leq \xi_w \leq H_w$, and (b) $0 \leq \eta \leq 1$, $H_w \leq \xi_a \leq 1$. To this end, we perform the coordinate transformations:

for LP ; $\xi_{w,a} = z$, $\eta = \frac{r}{1-z\tan\alpha}$,
 for MP ; $\xi_{w,a} = z$, $\eta = \frac{r}{z\tan\beta}$,
 for RP ; $\xi_{w,a} = z$, $\eta = \frac{r}{a\cos(1-z)}$.

These domains are discretized by using a set of n_{ξ_w} and n_{ξ_a} Chebychev spectral collocation points in the ξ direction. The η interval is discretized using a set of n_η Chebychev spectral collocation points. The rectangular domain has been investigated by Herrada and Shtern [41]. The code for the obtaining these points is developed by Herrada.

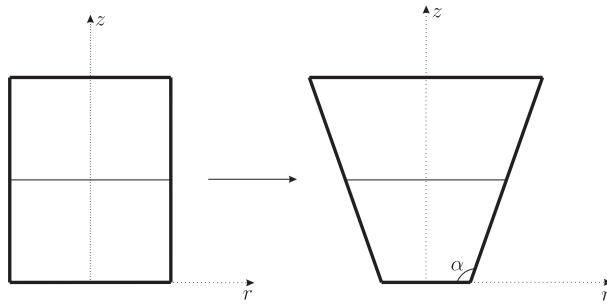


Figure 7.2: Mapping the fixed rectangular domains to LP .

The Chebyshev grid points concentrate on both sides of interface and near the walls. That helps to better resolve the Moffatt and other corner eddies, even using a moderate number of radial points. For the presented results, the simulations are done mostly with radial points $n_\phi = 50$, axial points for water $n_{\xi_w} = 40$ and axial points for air $n_{\xi_a} = 30$ (standard grid). We also run the program at $n_{\xi_a} = 40$, $n_{\xi_w} = 50$ and $n_\phi = 60$ (fine grid) to verify the grid independence.

Figure 7.3 verifies that the obtained results are grid-independent for spherical case. Note that the other cases look similar to spherical one, there is no need to mention them. The profiles of (a) radial, u , and (b) swirl, v , velocities at $Re = 0.1$ and $H_w = 0.8$ are plotted. The solid curves present the numerical results obtained with the standard grid, while the cross symbols present the numerical results obtained with the fine grid. The crosses merge with the curves within the accuracy of the drawing in Fig. 7.3 even for the radial velocity which is very small compared to the swirl velocity.

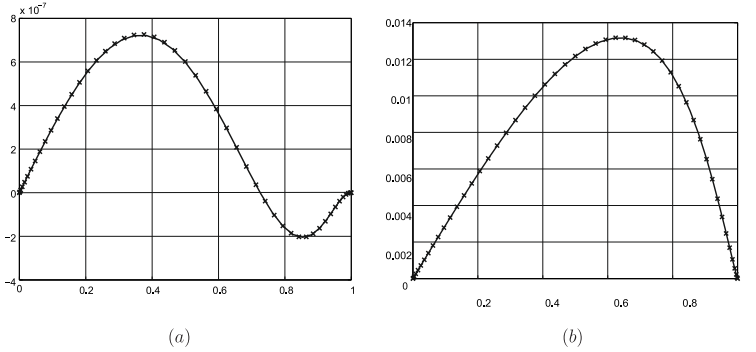


Figure 7.3: Profiles of (a) radial and (b) swirl velocities on the interface at $Re = 0.1$ and $H_w = 0.8$, obtained using the standard grid (solid curves) and fine (crosses) grids.

7.3 Bifurcation Analysis for LP

It is convenient to start with the cylindrical-container creeping flow and to discuss a topological transformation, as H_w decreases from 0.1 to zero, which was not described by Herrada and Shtern [41]. Figure 7.4 depicts the streamline patterns of meridional flow near the bottom-sidewall intersection at $\alpha = 90$, $H = 1$ and (left) $H_w = 0.1$ and (right) $H_w = 0.072$. In here, control parameter is H_w with fixed value of $\alpha = 90$. Recall that the flow is steady.

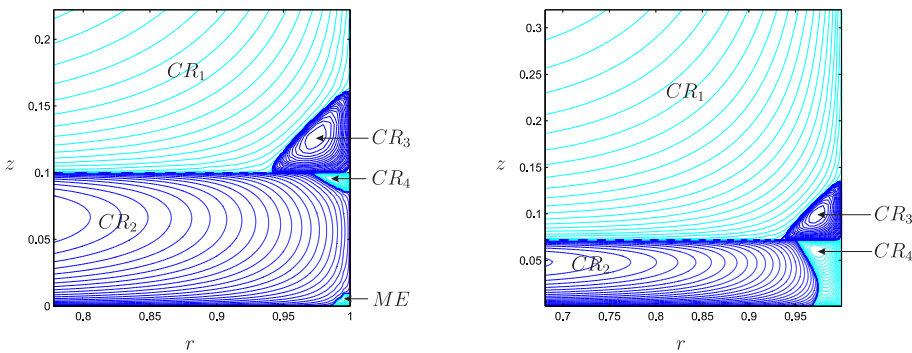


Figure 7.4: The streamline patterns for $H_w = 0.1$ (left pattern) and $H_w = 0.072$ (right pattern), for case LP , $\alpha = 90$.

As we mentioned before, Herrada and Shtern [41] revealed nine topological changes, we will not mention them. We said that the number is larger, because the following bifurcation progress 7.5 has not been observed by them. It is very hard to see this progress in numerical plot. However, the profile of the velocity field yields that as H_w decreases, the water circulation region CR_4 and the out-most ME (Moffatt eddy) merge into a circulation cell again marked as CR_4 by following the bifurcation progress 7.5. As H_w further decreases down to zero, no topological transformation occurs, just the water layer shrinks to the bottom. The arrows in figure 7.5 indicate the flow directions.

To give a brief explanation of Moffatt eddies, we copy the sentences from the book "Chebyshev and Fourier Spectral Methods" written by *John P. Boyd*: *The driven cavity flow has weaker singularities at the lower corners. Moffatt showed that as the corners are approached, the flow becomes more and more linear because the velocity tend to zero (relative to the walls). This near corner linearity allowed him to show that the flow consists of an infinite sequence of eddies of rapidly diminishing size and intensity - the so called "Moffatt eddies".*

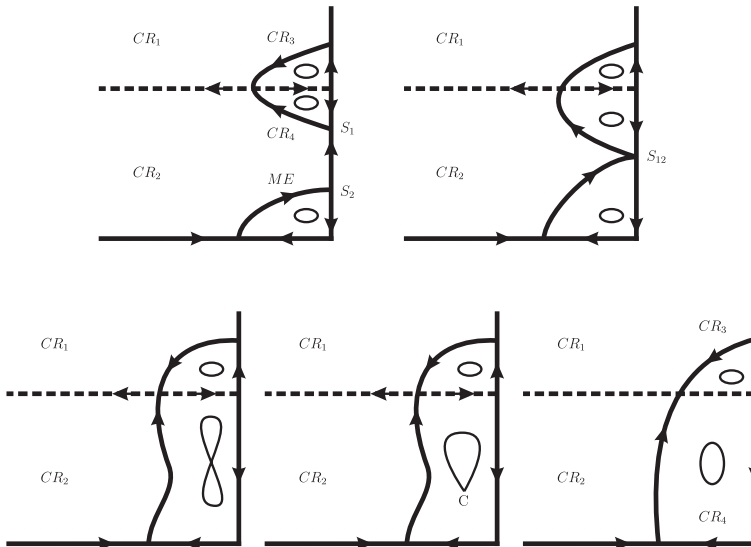


Figure 7.5: The bifurcation process between $H_w = 0.1$ and $H_w = 0.072$ for case LP, $\alpha = 90$.

7.3.1 Topological metamorphoses of air-water flow in the $\alpha = 120$ cone as H_w increases

At fixed value for $\alpha = 120$, we increase the value of H_w . When the value of H_w is between 0.52 and 0.58, a development of clockwise circulation near the bottom center is observed. As H_w increases again, region CR_3 enlarges. Initially, region CR_3 mostly extends in the radial direction and merges with the out-most Moffatt eddy; see ME in figure 7.6(a). Between $H_w = 0.608$ and $H_w = 0.61$, ME and CR_3 merge of near-bottom cells and then a figure eight shape can be observed. After that a cusp bifurcation occurs, and CR_3 extends to the wall.

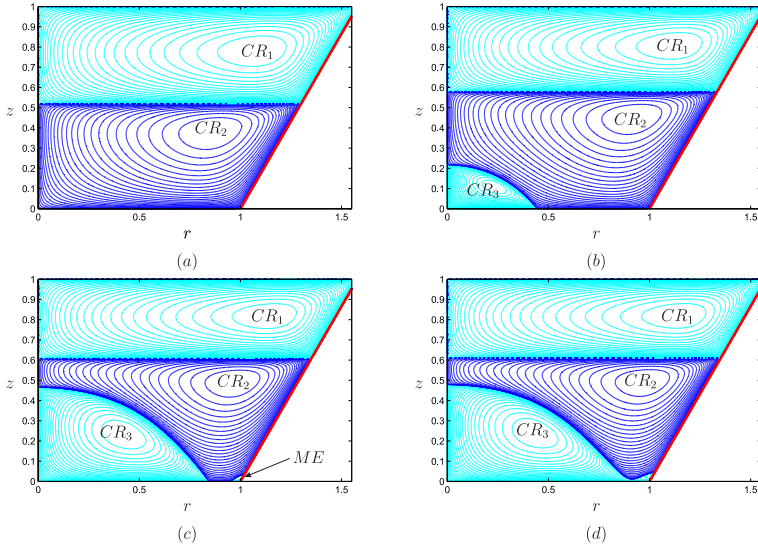


Figure 7.6: The topological changes near the bottom center when (a) $H_w = 0.52$ (b) $H_w = 0.58$ (c) $H_w = 0.608$ and (d) $H_w = 0.61$, for case LP , $\alpha = 120$.

Next, region CR_3 expands upward, reaches the interface at $H_w = H_{w,a} = 0.648$, and extends along the interface, reversing velocity u at the interface. The water flow near the interface-axis intersection, corresponding to the $u > 0$ range, drives the anticlockwise circulation of air in a thin circulation region, CR_4 . A corner bifurcation and bubble creation occur close to the axis.

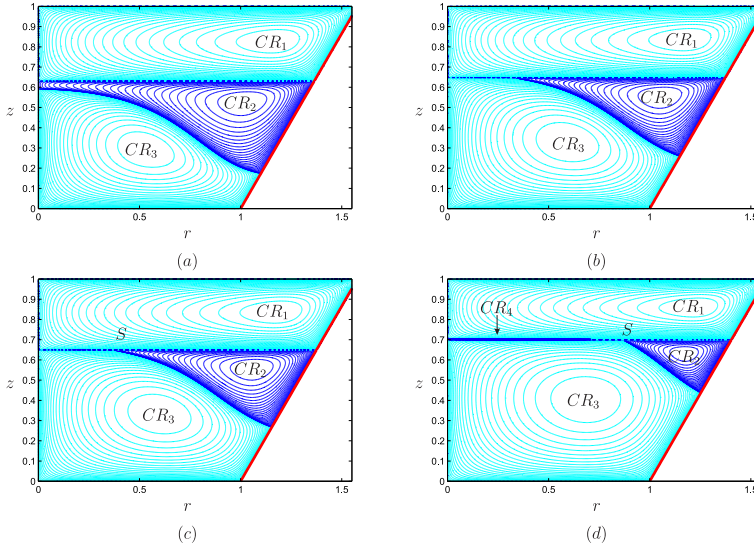


Figure 7.7: The topological changes near the interface when (a) $H_w = 0.63$ (b) $H_w = 0.648$ (c) $H_w = 0.65$ and (d) $H_w = 0.7$, for case LP , $\alpha = 120$.

Region CR_2 topologically is a bubble at $H_w = 0.63$ (figure 7.7 (a)), becomes a bubble-ring at $H_w = 0.648$ (figure 7.7 (b)), and is a ring in figures 7.7 (c) ($H_w = 0.65$) and 7.7 (d) ($H_w = 0.7$). Region CR_4 is very thin at $H_w = 0.65$ and clearly visible at $H_w = 0.7$. Regions CR_2 and CR_4 touch each other at the saddle point, S , where regions CR_1 and CR_3 also touch each other; S is a stagnation point of the meridional motion where $u = w = 0$, but $v \neq 0$. This bifurcation process has been observed analytically in fig. 5.5 (d).

As the expanding region CR_4 reaches the rotating top disk at $H_w = 0.867$, a corner bifurcation occurs. Region CR_1 separates from the axis and topologically becomes a ring as figure 7.8 illustrates depicting streamline patterns at $H_w = 0.86$ (a), $H_w = 0.867$ (b), $H_w = 0.87$ (c) and 0.94 (d). After the separation from the axis, region CR_1 shrinks toward the sidewall-top-disk corner as H_w further increases. No further changes in the flow topology occur as H_w approaches 1.

It is an interesting physical feature that the air mostly circulates in the anticlockwise direction (figure 7.8(d)) despite the fact that the centrifugal force, induced by the rotating disk, tends to move air in the clockwise direction. The feedback of the rotating water flow overcomes the direct effect of the centrifugal force which pushes the air to the periphery near the disk.

As H_w increases from 0 to 1, ten bifurcations occur in the conical (cylindrical) container LP . Vortex breakdowns in the water (at $H_w = 0.563$) and in the air (at $H_w = 0.648$) occur at smaller values of H_w than those in the cylindrical case. These features are due to the side-wall here converges from the rotating disk to the stationary disk and thus strengthens the effect of swirl on the water and air motions. Now we explore the effect of a diverging side-wall.

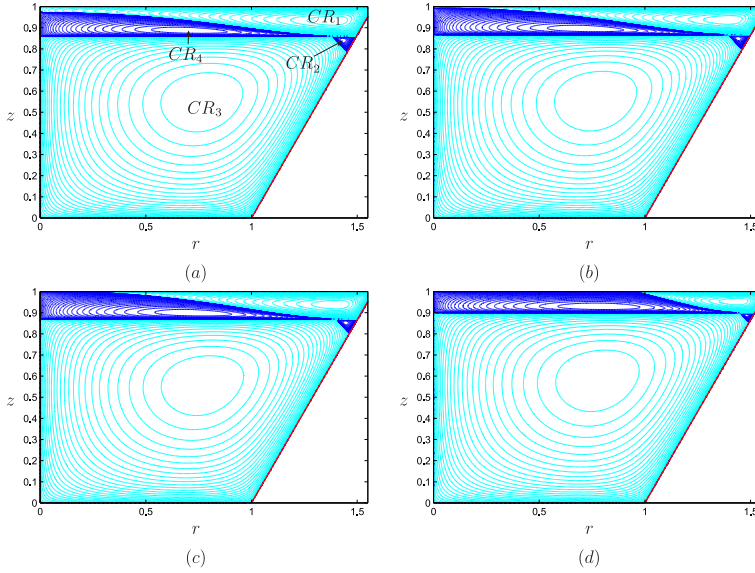


Figure 7.8: The topological changes near the interface when (a) $H_w = 0.86$ (b) $H_w = 0.867$ (c) $H_w = 0.7$ and (d) $H_w = 0.94$, for case LP , $\alpha = 120$.

7.3.2 Topological flow metamorphoses in the $\alpha = 60$ cone as H_w increases

No topological change occurs as H_w decreases from 0.15 down to zero. In contrast as H_w increases, numerous changes occur in the flow topology.

Figure 7.9(b) depicts streamlines at $H_w = 0.21$ near the bottom-sidewall intersection and reveals that the water flow has a figure-eight pattern in region CR_4 , as figure 7.10(c) schematically shows. Therefore as H_w increases and CR_4 shrinks to the side-wall, the figure-eight pattern emerges via a cusp bifurcation. Then saddle point moves to the side-wall, 7.10(d), and splits into two saddles

7.10(e). As a result, region CR_2 extends up to the side-wall and region CR_4 becomes divided as in 7.10(e). This occurs at $H_w = 0.219$ at $\alpha = 60$.

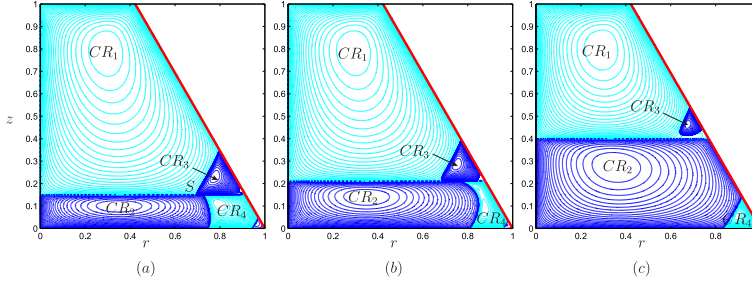


Figure 7.9: Expansion of CR_2 and separation of CR_3 from the interface whenever H_w increases (a) $H_w = 0.15$ (b) $H_w = 0.21$ (c) $H_w = 0.4$, for case LP, $\alpha = 60$.

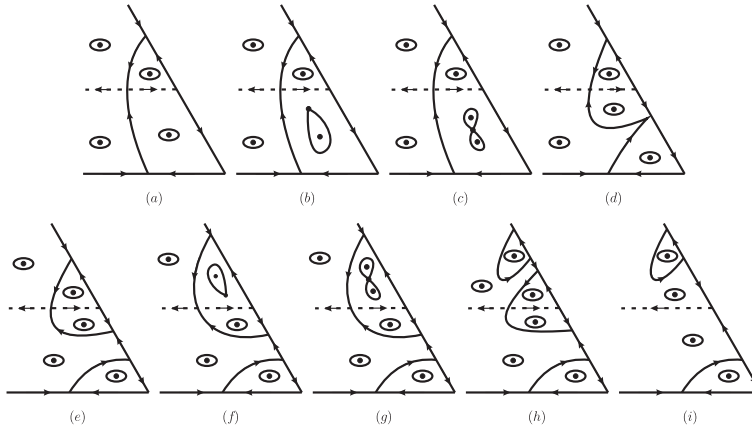


Figure 7.10: Bifurcation scenarios among (a) $H_w = 0.15$ (c) $H_w = 0.21$ (i) $H_w = 0.4$, for case LP, $\alpha = 60$.

The streamline pattern, depicted in figure 7.9(c), remains topologically invariant as H_w increases until it reaches a value around 0.81. At H_w slightly smaller than 0.81, a cell with clockwise circulation emerges near the axis-bottom intersection (region CR_4 in figure 7.11(a)), i.e., vortex breakdown occurs in the water flow.

Since region ME significantly expands as H_w increases from 0.4 to 0.81, regions CR_4 and ME merge just after CR_4 appears, as figure 7.11(b) illustrates. The merged region is again named CR_4 . Note that region CR_3 shrinks but remains observable in figure 7.11.

The transformations from figure 7.9(c) through the patterns shown in figure 7.11 consists of the following topological events: vortex breakdown emergence near the axis-bottom intersection, merging of the near-axis saddles at the bottom and followed by separation of the merged saddle from the bottom.

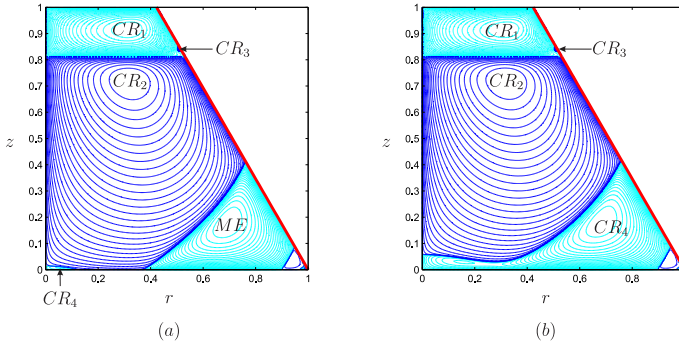


Figure 7.11: Creation of circulation CR_4 and its merging with eddy ME between (a) $H_w = 0.8115$ (b) $H_w = 0.8119$, for case LP , $\alpha = 60$.

Region CR_4 rapidly expands upward as H_w increases beyond 0.81. As the clockwise circulation in region CR_4 reaches the air, it reverses the radial velocity at the interface, which becomes positive, and drives an anticlockwise circulation in the thin air region CR_4 (figure 7.12(c)).

The physical reason for the vortex breakdown development in the air and the shrinking of region CR_2 in the water is the strengthening of water swirl as the interface approaches the rotating top disk. The growing centrifugal force intensifies the clockwise circulation in region CR_5 and suppresses the anticlockwise circulation in region CR_2 . The air flow is affected by the water flow feedback. This causes further topological metamorphoses in both water and air flows.

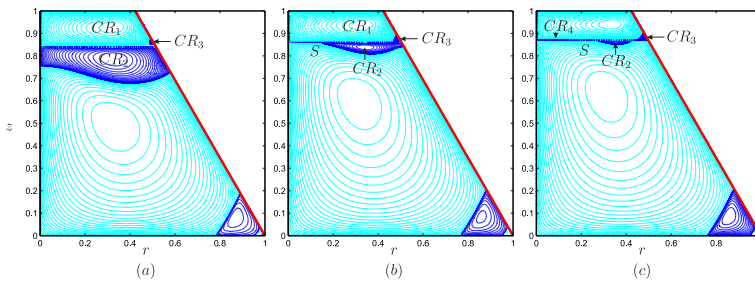


Figure 7.12: Streamline patterns for (a) $H_w = 0.84$ (b) $H_w = 0.86$ and (c) $H_w = 0.87$, for case LP , $\alpha = 60$.

Figures 7.13 schematically show the corresponding transformations of the flow pattern.

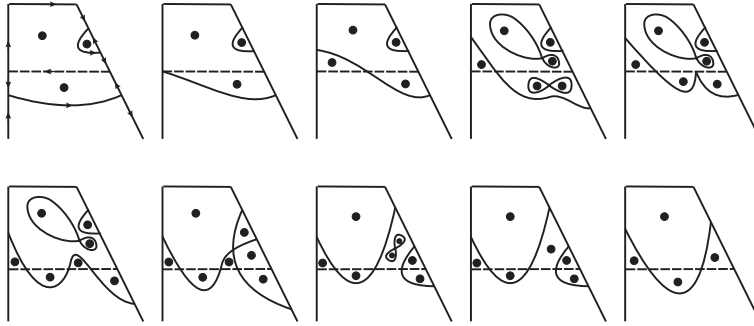


Figure 7.13: Bifurcations occurring between $H_w = 0.84$ and $H_w = 0.87$, for case LP , $\alpha = 60$.

Note that fig. 7.13 and 7.10 are created on the basis of profile of the velocity field. It is very hard to see these streamline patterns in numerical plot. However, we investigate the profile of the velocity field step by step and sketch these bifurcation process.

7.3.3 Conclusion

These analyses describe effects of a conical side-wall on an air-water motion, driven by the top rotating disk, in a bio-reactor and reveals a variety of flow patterns as the water level, H_w , grows from 0 to 1. In contrast to the single-fluid flow vortex breakdown and other topological metamorphoses occur in this two-fluid flow even if it is very slow. We revealed a new topological transformation in the shallow-water flow (see in fig. 7.9) in the sense that it does not occur in the cylinder case which is observed by Herrada and Shtern [41]). Similar to the corner eddies, unbounded sets of eddies develop near the side-wall above and below the interface. We found the effects of α on vortex breakdown occurrence in the water and air flows.

7.4 Bifurcation Analysis for MP

In this section, we will consider a conical container by fixing the angle between the wall and center axis and increasing H_w values.

7.4.1 Topological metamorphoses of air-water flow in the $\beta = 30$ cone as H_w increases

First, we explore the bifurcation scenario as the water height, H_w , increases in a conical container with $\beta = 30$.

Fig. 7.14 (a) shows two eddies in the air, Ca_1 and Ca_2 , and two eddies in the water, Cw_1 and Cw_2 , at $H_w = 0.1$; since Cw_1 and Cw_2 are very small in Fig. 7.14 (a) they are indicated in Fig. 7.14 (b). ‘C’, ‘a’ and ‘w’ are abbreviations for ‘cell’, ‘air’ and ‘water’, respectively. Contours, corresponding to the clockwise (anticlockwise) circulation are depicted hereafter by the light (dark) curves which are blue online.

As H_w increases, region Ca_2 shrinks and its upper boundary touches the interface at the axis as Fig. 7.14(b) illustrates at $H_w = 0.201$. Next, Ca_2 separates from the axis thus transforming from a bubble-like into a ring-like shape. At the same value of H_w , the clockwise air circulation in Ca_1 induces a new cell, Cw_3 , in the water as Fig. 7.14 (c) illustrates at $H_w = 0.205$. In the air flow, the destruction of bubble and in the water flow, creation of bubble occur.

As H_w further increases, region Cw_3 expands downward, as Fig. 7.14(d) shows at $H_w = 0.207$ and merges with region Cw_2 as Fig. 7.14(e) reveals at $H_w = 0.208$. Region Cw_1 becomes separated from the axis thus transforming from a bubble-like (Fig. 7.14(d)) into a ring-like (Fig. 7.14(e)) shape. In the region Cw_2 , a figure-eight shape is observed after separation of Cw_1 and a cusp bifurcation occurs to make it a center. For larger H_w , regions Ca_2 and Cw_1 shrink to the interface-sidewall intersection as in Fig. 7.14(f).

Fig. 7.15(a) depicts the flow pattern at $H_w = 0.33$, where three eddies are observed in the water: Cw_2 , Cw_3 , and Cw_4 ; Cw_4 is clearly seen in Fig. 7.15(b). Cw_3 mostly expands near the axis (because water moves up there) and reaches the interface at $H_w = 0.86$ as Fig. 7.15(c) illustrates. For large H_w , Cw_2 separates from the axis. The water flow in Cw_3 drives the adjacent air away from axis and thus generates cell Ca_3 . Regions Ca_1 , Ca_3 , Cw_2 and Cw_3 meet at a saddle point S located at the interface as shown in Fig. 7.15(d). Ca_3 is a very thin layer hardly visible in Fig. 7.15(d) at $H_w = 0.87$ and well observed in Fig. 7.15(e) at $H_w = 0.93$. As H_w increases, Ca_3 touches the lid and Ca_1 becomes separated from the axis as Fig. 7.15(f) illustrates at $H_w = 0.98$. Next, the saddle S reaches the sidewall at H_w around 0.98 and cell Ca_1 becomes separated from the interface. Finally, Ca_1 shrinks to the lid-sidewall intersection as $H_w \rightarrow 1$.

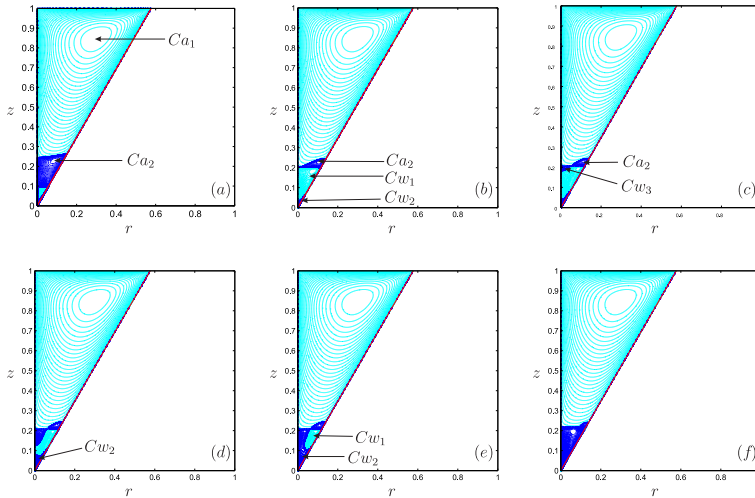


Figure 7.14: Streamline patterns of the meridional motion for (a) $H_w = 0.1$ (b) $H_w = 0.201$, (c) $H_w = 0.205$, (d) $H_w = 0.207$ (e) $H_w = 0.208$ and (f) $H_w = 0.22$ when $\beta = 30$.

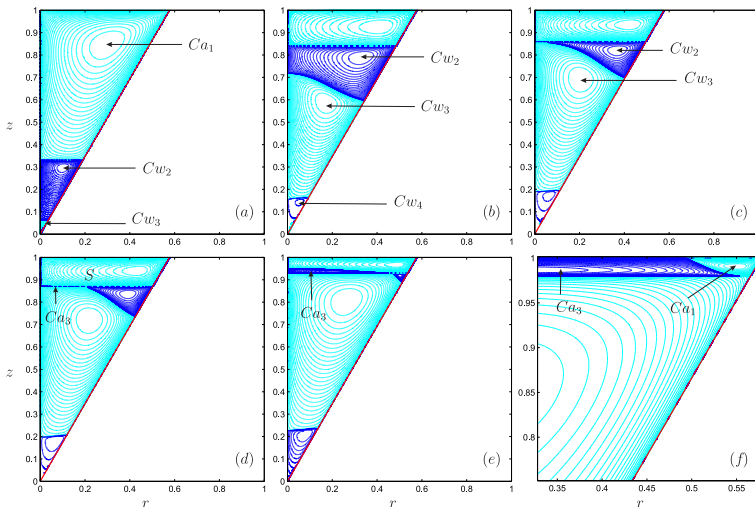


Figure 7.15: Streamline patterns of the meridional motion for (a) $H_w = 0.33$ (b) $H_w = 0.84$, (c) $H_w = 0.86$, (d) $H_w = 0.87$ (e) $H_w = 0.93$ and (f) $H_w = 0.98$ when $\beta = 30$.

7.4.2 Topological metamorphoses of air-water flow in the $\beta = 45$ and $\beta = 60$ cone as H_w increases

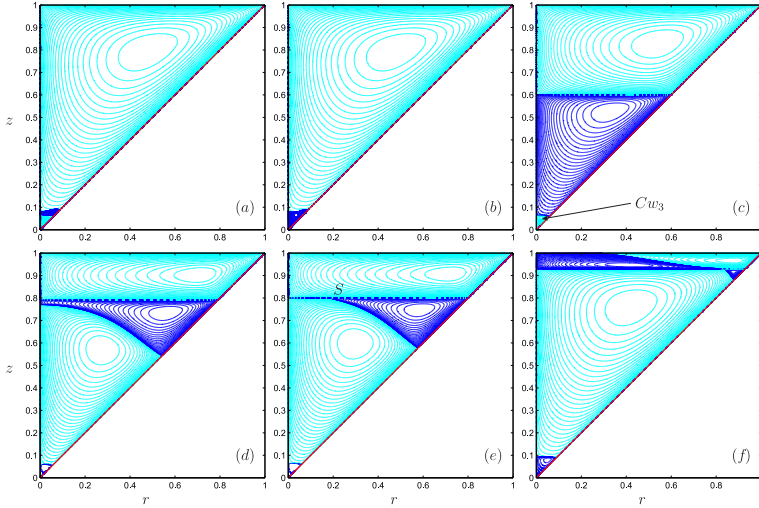


Figure 7.16: Streamline patterns of the meridional motion for (a) $H_w = 0.07$ (b) $H_w = 0.08$, (c) $H_w = 0.06$, (d) $H_w = 0.79$ (e) $H_w = 0.8$ and (f) $H_w = 0.93$ when $\beta = 45$.

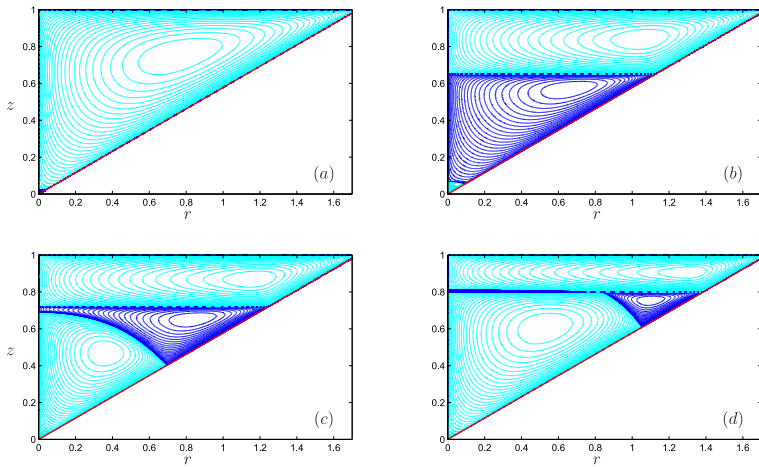


Figure 7.17: Streamline patterns of the meridional motion for (a) $H_w = 0.02$ (b) $H_w = 0.65$, (c) $H_w = 0.72$ and (d) $H_w = 0.8$ when $\beta = 60$.

The bifurcation sequence at $\beta = 45$ and $\beta = 60$ is similar to that at $\beta = 30$, but the topological changes occur for $\beta = 45$ at smaller H_w than for $\beta = 30$. For example, the flow pattern shown in Fig. 7.16(a) is similar to that in Fig. 7.14(b) and the pattern shown in Fig. 7.16(b) is similar to that in Fig. 7.14(f). In contrast to the cases where $\beta = 30$ and 45, the air flow is one-cellular for $\beta = 60$ even at $H_w = 0.02$ as Fig. 7.17(a) illustrates. Another difference is that no eddy is observed near the interface-sidewall intersection.

7.4.3 Conclusion

This section reveals and explains topological transformations in a slow steady axisymmetric air-water flow, driven by the rotating top disk, in a vertical conical container. There are five major flow bifurcations as the water height H_w varies at the cone half-angle $\beta = 30$. Most of the bifurcations occur at the interface. We observe same bifurcation sequence at $\beta = 45$ and 60 but for smaller H_w than at $\beta = 30$.

7.5 Bifurcation Analysis for RP

Fig. 7.18(a) depicts streamlines of the meridional motion, i.e., contours $\psi = \text{constant}$, at the water height $H_w = 0.66$. The arrows indicate the flow directions. The rotating disk generates a centrifugal force, which pushes the air to the periphery near $z = 1$ and thus develops the clockwise circulation in region CR_{a1} . Contours, corresponding to the clockwise (anticlockwise) circulation are depicted hereafter by the light (dark) curves which are blue online.

The air flow converges to axis near the interface, $z = H_w$, and drives the water anticlockwise circulation in region CR_{w1} . This flow topology remains invariant as H_w decreases down to zero. The physical reason for the anticlockwise circulation is a weak rotation of water for small H_w .

As H_w increases, the emergence of water clockwise circulation near the axis-bottom intersection (or vortex breakdown) is seen in region CR_{w2} shown in Fig. 7.18(b) at $H_w = 0.67$.

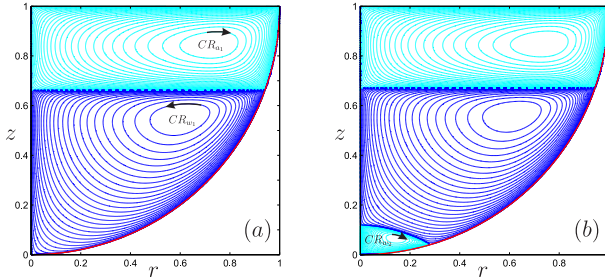


Figure 7.18: Emergence of counter-circulation CR_{w2} in water as H_w increases from 0.66 (a) to 0.67 (b), for case RP .

As H_w further increases, region CR_{w2} expands upward, reaches the interface-axis intersection point at $H_w = 0.732$ and then expands along the interface. This is known as a corner crossing bifurcation.

Region CR_{w1} is topologically a bubble in Fig. 7.19(a) at $H_w = 0.73$, becomes a bubble-ring at $H_w = 0.732H$, and then separates from the axis thus transforming in a ring as Figs. 7.19(b) at $H_w = 0.74$ and 7.19(c) at $H_w = 0.8$ depict. Region CR_{a2} , where air circulates anticlockwise, is very thin, extends up to point S being hardly visible in Fig. 7.19(b) at $H_w = 0.74$ and clearly visible in Fig. 7.19(c) at $H_w = 0.8$.

As H_w further increases, region CR_{a2} expands, reaches the axis-disk intersection point at $H_w = 0.935$ and expands along the rotating disk as Fig. 7.20(c) illustrates. The bifurcation at $H_w = 0.935$ is again a corner crossing bifurcation. Region CR_{a1} is topologically a bubble for $H_w < 0.935$, a bubble-ring at $H_w = 0.935$ and a ring for $H_w > 0.935$. As $H_w \rightarrow 1$, region CR_{a1} shrinks to the disk-wall. intersection.

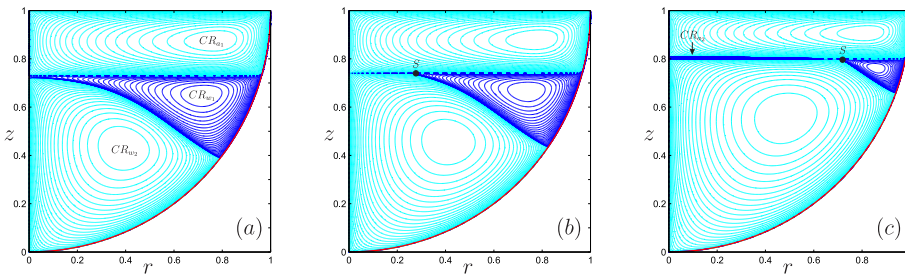


Figure 7.19: Emergence of counter-circulation CR_{a2} in air as H_w increases; from 0.73 (a), 0.74 (b) and 0.8 (c), for case RP .

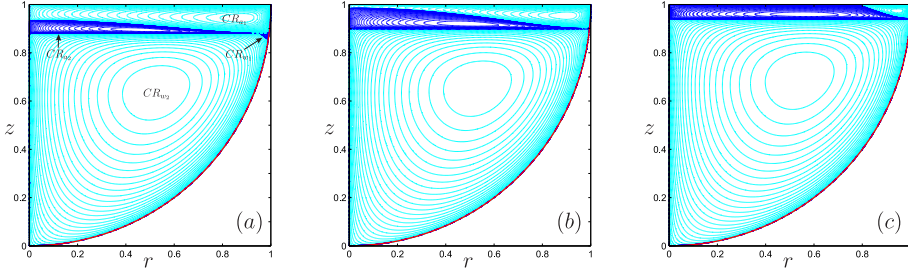


Figure 7.20: Collapse of region CR_{w1} and separation of region CR_{a1} from the axis as H_w increases; 0.88 (a), 0.9 (b) and 0.94 (c), for case RP .

7.5.1 Conclusion

The goal of this section is to explore the vortex breakdown (VB) development in a slow air-water flow with no interaction of VB regions with corner vortices. To this end, a hemispherical container is chosen, where the flow is driven by the a rotating lid. It is found that as the water height H_w increases, the VB region emerges in water near the axis bottom intersection at $H_w = 0.666$ (Fig. 7.18) and then in air near the axis-interface intersection $H_w = 0.732$ (Fig. 7.19). The air VB region is a thin layer adjacent to the interface. Next the water VB region occupies the entire water domain at $H_w = 0.898$ (Fig. 7.20). The air VB region expands up to the disk at $H_w = 0.935$.

The topological bifurcations we observe are simpler and fewer than those found in a cylindrical geometry where there is an interaction with the Moffatt corner vortices [43, 41]. This interaction gives rise to bifurcations where saddle stagnation points in the interior of the water are created, generating much more complex flow patterns. In the spherical container only corner bubble creation and corner crossing bifurcations are found. Consequently, the flow topology in a spherical container is much more robust with respect to changes in the parameters.

7.6 Conclusion

In Chapter 4 and 5, we analysed the axisymmetric flow close to free and viscous surfaces in a topological way. Now, we will give an explanation which bifurcations from the theoretical analysis we observe in numerical simulations.

In Fig. 7.5, in the region $z < F(r)$ (free surface) co-dimension 1 bifurcation occurs when $H_w < 0.1$. The creation of bubble $CR4$ is seen as in Fig. 4.68 (a), and for viscous flow one can observe the bifurcation progress as in Fig. 5.10 (b). Between $H_w = 0.1$ and $H_w = 0.072$, there is no changes for the flow in region $z > F(r)$. However, in the region $z < F(r)$ there exist two possibilities. One is the existence of co-dimension 1 bifurcation occurring by blowing up $CR4$ (means the saddle connection of S_1 and S_2 is not occurring close to interface). Second is the existence of co-dimension 2 bifurcation at that region. The streamline patterns for free surface is given in Fig. 4.73 by considering ME circulation separately, means that consider the figure-eight, if ME circulation does not exist this will look like the homo-clinic. In Fig. 7.10, same bifurcation can be seen but for both fluids.

In Fig. 7.7, we observe the corner crossing and corner creation bifurcations close to center axis. These bifurcations are observed for free surface in Fig. 4.5 and for viscous surface in Fig. 5.5 (d). These bifurcations are also seen in Fig. 7.8, but close to the wall.

Until now, we mention the bifurcations occurring for case LP . In the cases MP and RP , there exist no extra bifurcation except the case MP in Fig. 7.14 (d). Close to center axis, again we have two possibilities. If the saddle connection between Cw_2 and Cw_3 occurs close to the interface, this is co-dimension 2 bifurcation which is sketched in Fig. 4.9. If not, the bubble may blow up and co-dimension 1 bifurcation can be observed.

Bibliography

- [1] J. D. Meiss. *Differential Dynamical Systems*. Society for Industrial and Applied Mathematics, 2007.
- [2] Y. A. Kuznetsov. Elements of Applied Bifurcation Theory. *Applied Mathematical Sciences*, 112, 1995.
- [3] L. D. Landau and E. M. Lifshitz. *Fluid Mechanics*. Pergamon Press, 1987.
- [4] E. W. Weisstein. Normal and tangential vector, 1997. URL <https://www.mathworld.wolfram.com/NormalVector.html>.
- [5] C. E. Weatherburn. *Differential Geometry of Three Dimensions*. Cambridge University Press, 1961.
- [6] J. M. H. Peters. Total curvature of surfaces (via the divergence of the normal). *Int. J. Math. Educ. Technol.*, 32:795–810, 2001.
- [7] Patience Henson. A proof that the divergence of a surface normal is equal to the sum of the principal curvatures, 2000. URL http://willson.cm.utexas.edu/Research/Sub_Files/Surface_Phenomena/Spring%202000/surface_normal_proof.pdf.
- [8] W. R. Dean. Note on the Motion of Liquid Near a Position of Separation. *Proceedings of the Cambridge Philosophical Society*, 46(2):293–306, 1950.
- [9] R. Legendre. Lignes De Courant Dun Ecoulement Continu. *Recherche Aerospatiale*, (105):3–&, 1965.
- [10] R. Legendre. Separation of a Flow Along a Line of a Regular Surface. *Recherche Aerospatiale*, (5):213–219, 1978.

- [11] R. Legendre. Streamlines in a Permanent Flow - Separation and Division. *Recherche Aerospatiale*, (6):327–335, 1977.
- [12] JM Delery. Robert Legendre and Henri Werle: Toward the elucidation of three-dimensional separation. *Annual Review of Fluid Mechanics*, 33: 129–154, 2001.
- [13] M. Tobak and D. J. Peake. Topology Of 3-Dimensional Separated Flows. *Annual Review of Fluid Mechanics*, 14:61–85, 1982.
- [14] A. E. Perry and H. Hornung. Some Aspects of 3-Dimensional Separation, 2. Vortex Skeletons. *Zeitschrift fur Flugwissenschaften und weltraumforschung*, 8(3):155–160, 1984.
- [15] A. E. Perry and M. S. Chong. A Description of Eddyding Motions and Flow Patterns Using Critical-Point Concepts. *Annual Review of Fluid Mechanics*, 19:125–155, 1987.
- [16] P. G. Bakker. *Bifurcations in Flow Patterns*. Klüver Academic Publishers, 1991.
- [17] M. Brøns. Topological fluid-dynamics of interfacial flows. *Physics of Fluids*, 6(8):2730–2737, 1994.
- [18] M. Brøns and J. N. Hartnack. Streamline topologies near simple degenerate critical points in two-dimensional flow away from boundaries. *Physics of Fluids*, 11(2):314–324, 1999.
- [19] J. N. Hartnack. Streamline topologies near a fixed wall using normal forms. *Acta Mechanica*, 136(1-2):55–75, 1999.
- [20] M Brøns. Streamline Topology: Patterns in Fluid Flows and Their Bifurcations. *Advances in Applied Mechanics*, 41:1–42, 2007.
- [21] A. Deliceoglu. Topology of two-dimensional flow associated with degenerate dividing streamline on a free surface. *European Journal of Applied Mathematics*, 24:77–101, 2 2013.
- [22] A. Balci, M. Andersen, M. C. Thompson, and M. Brons. Codimension three bifurcation of streamline patterns close to a no-slip wall: A topological description of boundary layer eruption. *Physics of Fluids*, 27(5), 2015.
- [23] F. Gurcan, A. Deliceoglu, and P. G. Bakker. Streamline topologies near a non-simple degenerate critical point close to a stationary wall using normal forms. *Journal of Fluid Mechanics*, 539:299–311, 2005.
- [24] Morten Brøns, Bo Jakobsen, Kristine Niss, Anders V. Bisgaard, and Lars K. Voigt. Streamline topology in the near wake of a circular cylinder at moderate reynolds numbers. *Journal of Fluid Mechanics*, 584:23–43, 2007.

- [25] H. Kudela and Z. M. Malecha. Eruption of a boundary layer induced by a 2D vortex patch. *Fluid Dynamics Research*, 41(5), 2009.
- [26] H. Kudela and Z. M. Malecha. Investigation of unsteady vorticity layer eruption induced by vortex patch using vortex particles method. *Journal of Theoretical and Applied Mechanics*, 45(4):785–800, 2007.
- [27] M. Andersen. *Topology of streamlines and vorticity contours for two-dimensional flows*. PhD. Thesis DTU, 2013.
- [28] H. J. Lugt. Local flow properties at a viscous free-surface. *Physics of Fluids*, 30(12):3647–3652, 1987.
- [29] H. J. Lugt. Oblique vortices on a solid wall and on an interface between 2 immiscible viscous fluids. *Physics of Fluids a-Fluid Dynamics*, 1(8):1424–1426, 1989.
- [30] M. Brøns, L. K. Voigt, and J. N. Sorensen. Topology of vortex breakdown bubbles in a cylinder with a rotating bottom and a free surface. *Journal of Fluid Mechanics*, 428:133–148, 2001.
- [31] Adnan BALCI. Normal form and unfoldings analysis for the axisymmetric flow near-axis, 2015. URL <https://www.dropbox.com/s/517yvzchs2dr9p/Near%20Axis%20NormalForm%26Unfoldings.mw?dl=0>.
- [32] A. V. Bisgaard. *Structures and Bifurcations in Fluid Flows with Applications to Vortex Breakdown and Wakes*. PhD. Thesis DTU, 2005.
- [33] Adnan BALCI. Normal form and unfoldings analysis for the axisymmetric flow close to wall codimension-3 case 1, 2015. URL <https://www.dropbox.com/s/3qe2sd2h4a4x74o/Codimension3Case1.mw?dl=0>.
- [34] Adnan BALCI. Local analysis close to axis with three parameter space, 2015. URL <https://www.dropbox.com/s/w2s9pi091sq0j87/Bifurcation%20Analysis%20for%20Codimension%203%28a%29.mw?dl=0>.
- [35] Adnan BALCI. Normal form and unfoldings analysis for the axisymmetric flow away from axis, 2015. URL <https://www.dropbox.com/s/lzfnfcibue3yzc/0nInterface%20NormalForm%26Unfoldings%20%282%29.mw?dl=0>.
- [36] Adnan BALCI. Normal form and unfoldings analysis for the axisymmetric flow close to wall codimension-3 case 3, 2015. URL <https://www.dropbox.com/s/biw0zsh9tzv8qbd/Codimension3Case3.mw?dl=0>.
- [37] A. Deliceoglu. Topology of two-dimensional flow associated with degenerate dividing streamline on a free surface. *European Journal of Applied Mathematics*, 24:77–101, 2 2013.

-
- [38] Adnan BALCI. Normal form and unfoldings analysis for the axisymmetric flow close to wall, 2015. URL <https://www.dropbox.com/s/upkgiw36tio6zvv/CloseWall%20NormalForm%26Unfoldings.mw?dl=0>.
- [39] J. N. Hartnack. *Structural changes in incompressible flow patterns*. PhD. Thesis DTU, 1999.
- [40] Adnan BALCI. Normal form and unfoldings analysis for three dimensional flow, 2015. URL <https://www.dropbox.com/s/urim7q9nrbj8n9u/3DCase%28XYZCoordinate%29.mw?dl=0>.
- [41] M. Herrada and V. Shtern. Patterns of a creeping water-spout flow. *Journal of Fluid Mechanics*, 744:65–88, 2014.
- [42] K. Y. S. Liow, B. T. Tan, G. A. Thouas, and M. C. Thompson. CFD Modeling of the Steady-State Momentum and Oxygen Transport in a Bioreactor that is Driven by an Aerial Rotating Disk. *Modern Physics Letters B*, 23(2):121–127, 2009.
- [43] Miguel A. Herrada, Vladimir N. Shtern, and José María López-Herrera. Off-axis vortex breakdown in a shallow whirlpool. *Phys. Rev. E*, 87:063016, Jun 2013.